Impact of molecular structure on water vapour sorption properties in nanostructured polymeric films

By

Valeska Cloete

Thesis presented in partial fulfillment of the requirements for the degree of

PhD (Polymer Science)

at the

University of Stellenbosch

Promotor: Prof. H. Pasch

Co-promotor: Dr. P.C. Hartmann

December 2011

Declaration

I, the undersigned, hereby declare that the work contained in this dissertation is my own original work and that I have not previously in its entirety or in part submitted it at any university for a degree.

Signature: Date: 20 November 2011

Valeska Cloete

Abstract

In this study, the use of surfactants, plate-like clays, organophilic molecules and side-chain crystallinity was investigated for their impact on the transport mechanisms of water vapour through polymer films.

A model polymer latex, poly(styrene-co-butyl acrylate), was prepared using miniemulsion polymerization. Three different types of surfactants, sodium dodecyl benzene sulfonate (SDBS, an anionic surfactant), octyl phenol ethoxylate (OPE, a nonionic surfactant) and dodecyl ammonium-3-butenoate (DA3B, a reactive surfactant) were used to stabilize the latex. Films were prepared from the resultant latices and their water vapour sorption behaviour determined across a water vapour partial pressure range of 0.1 to 0.9. Sigmoidal kinetic behaviour was seen for all three films, with the DA3B stabilized film exhibiting high diffusion coefficients compared to films stabilized with SDBS and OPE. The thermodynamic behaviour of the films differed and was dependent on the reactivity of the surfactant. SDBS and OPE stabilized films exhibited Flory-Huggins behaviour, while the DA3B stabilized film followed Henry's Law. Despite significant differences in terms of these properties, the permeability coefficients were similar for the three films across the water vapour partial pressure range evaluated.

The impact of sodium montmorillonite (Na-MMT) clay and an organophilic modifier, 2-acrylamido-2-methylpropanesulfonic acid (AMPS), on the water vapour sorption properties of poly(styrene-co-butyl acrylate) was evaluated. These polymer clay nanocomposites (PCNs) were synthesized using miniemulsion polymerization. The resultant latex films were characterized and used for water vapour sorption analyses. It was shown that complete exfoliation of the Na-MMT was necessary to minimize the equilibrium water vapour uptake. Even when Na-MMT was completely exfoliated, the amount of water vapour sorbed by the PCN was high and this was attributed to the hydrophilic nature of the clay. Using a least squares regression fit, good correlation was obtained between the experimental isotherms and the sorption behaviour predicted by the Dual Mode Sorption model which was originally developed for polymers in their glassy state.

The impact of side chain crystallinity on the water vapour sorption properties of poly(methyl methacrylate-co-octadecyl acrylate) was evaluated. These random copolymers containing increasing amounts of octadecyl acrylate, and therefore increasing degrees of crystallinity, were synthesized using solvent polymerization. Although it could be expected that side chain crystallinity would be the main contributing factor resulting in a reduction in the diffusion coefficient, it was shown that the methyl group on the α-carbon of the vinyl group in the methacrylate reduced the diffusion to a greater extent through the increased stiffness of the polymer backbone. This was also reflected in poly(methyl methacrylate-co-octadecyl acrylate) having a greater activation energy for diffusion compared to polyoctadecyl acrylate.

Opsomming

In hierdie studie is die gebruik van sepe, plaatagtige kleie, organofiliese molekules en sy-kettingkristalliniteit ondersoek ten opsigte van die impak op transportmeganismes van waterdamp deur polimeerfilms.

'n Model polimeerlateks, polistireen-ko-butielakrilaat, is voorberei deur miniemulsiepolimerisasie. Drie verskillende tipes sepe, natriumdodekielbenseensulfonaat (NDBS, 'n anioniese seep), oktielfenoletoksilaat (OFE, 'n nie-ioniese seep) en dodekielammonium-3-butenoaat (DA3B, 'n reaktiewe seep) is gebruik om die lateks te stabiliseer. Films is van die resultante lateks voorberei en hul waterdampsorpsie –eienskappe oor die parsiële waterdampdrukreeks van 0.1 tot 0.9 bepaal. Sigmodale kinetiese gedrag is vir al drie films waargeneem, met die DA3B gestabiliseerde film wat hoër diffusiekoëffisiënte toon in vergelyking met die films wat met NDBS en OFE gestabiliseer is. Die termodinamiese gedrag van die films het verskil en was afhanklik van die reaktiwiteit van die seep. NDBS en OFE gestabiliseerde films het Flory-Huggins gedrag getoon, terwyl die DA3B gestabiliseerde film Henry se Wet gevolg het. Ten spyte van die beduidende verskille ten opsigte van hierdie eienskappe was die permitiewe koëffisiënte soortgelyk vir die drie films regoor die parsiële waterdampdrukreeks wat vir die evaluasie gebruik is.

Die impak van natriummontmorilloniet (Na-MMT) klei en 'n organofiliese modifiseerder, 2-akrielamido-2-metielpropaansulfoonsuur (AMPS), op die waterdampsorpsie-eienskappe van polistireen-ko-butielakrilaat is geëvalueer. Hierdie polimeer-klei-nanosaamgesteldemateriale (PKNe) is gesintetiseer deur van miniemulsiepolimerisasie gebruik te maak. Die resultante lateksfilms is gekarakteriseer en gebruik vir waterdampsorpsie analises. Daar is getoon dat algehele afskilfering van die Na-MMT nodig was om die ewewigswaterdampopname te minimaliseer. Selfs wanneer Na-MMT algeheel afgeskilfer was, was die hoeveelheid waterdamp gesorbeer deur die PKN hoog en kan dit toegeskryf word aan die hidrofiliese karakter van die klei. Deur 'n kleinste-kwadrate-regressie passing te doen, is 'n goeie korrelasie verkry tussen die eksperimentele isoterme en die sorpsie gedrag voorspel deur die Dubbelmodussorpsiemodel wat oorspronklik ontwikkel is vir polimere in hul glasagtige toestand.

Die impak van sykettingkristalliniteit op die waterdampsorpsie-eienskappe van poli(metielmetakrilaat-ko-oktadekielakrilaat) is ondersoek. Hierdie ewekansige kopolimere wat toenemende hoeveelhede oktadekielakrilaat, en dus toenemende grade van kristalliniteit bevat, is gesintetiseer deur van oplossingspolimerisasie gebruik te maak. Alhoewel dit te wagte was dat sykettingkristalliniteit die hoofbydraende faktor is in die redusering van die diffusiekoëffisiënte, is daar getoon dat die metielgroep aan die α-koolstof van die vinielgroep in die metakrilaat die diffusie tot 'n groter mate gereduseer het deurtoenemende styfheid van die polimeerrugraat. Dit is ook gereflekteer deur poli(metielmetakrilaat-ko-oktadekielakrilaat) wat 'n groter aktiveringsenergie vir diffusie het in vergelyking met polioktadekielakrilaat.

v

Acknowledgements

Firstly I would like to thank my husband and best friend Eugene Smit for his unwavering support and encouragement over a long period of time, without which it would not have been possible for me to complete my PhD. Thank you for believing in me. You are an inspiration and played a crucial role in me completing my studies.

Secondly, mom, thank you for the sacrifices you made to enable me to complete my studies. I sincerely appreciate it.

Ineke Tiggelman, you were my hands across a distance of more than 1500 km. You played a key role in this research project. Many thanks for your dedication and support.

Other acknowledgements:

Prof. R.D. Sanderson: Opportunity to further my studies; guidance; motivation

Prof. H. Pasch: Guidance in the completion of my thesis

Dr. Patrice Hartmann: SAXS analysis, guidance in the completion of my thesis

Prof. P.E. Mallon: Positron Annihilation Spectroscopy Analysis

Mohammed Jaffer (Electron Microscope Unit, UCT): TEM analysis

Jean McKenzie (NMR, US): NMR analysis

MPSA: Jeff Kirby-Smith, Theo van Breda, Mpact Limited R&D Centre at Stellenbosch

Carmen Swart: Synthesis and analyses

Lee-sa Harmse: Synthesis and analyses

Ineke Tiggelman: Synthesis and analyses

Pauline Skillington: Analyses

Dr. Matthew Tonge: Guidance

Eugene Smit and My Family: Support, motivation and encouragement

Table of Contents

List of Figures

List of Tables

LIST OF SYMBOLS

P	Permeation coefficient
D	Diffusion coefficient
S	Solubility coefficient
E_P	Activation energy of permeation
E_D	Activation energy of diffusion
ΔH_S	Heat of solution
γ	Surface tension or interfacial tension
η	Viscosity
T_g	Glass transition temperature
T_c	Crystallization temperature
M	Molar mass
d_p	depth of penetration

List of Acronyms

ACV	4,4-Azobis-4-cyanopentanoic acid
AIBN	2,2-Azo-bis-isobutyronitrile
AMPS	2-Acrylamido-2-methylpropanesulfonic acid
APS	Ammonium persulfate
BA	n-Butyl acrylate
BET	Brunauer, Emmet and Teller model
DDI water	Double deionised water
DLS	Dynamic light scattering
DMS	Dual Mode Sorption model
DMTA	Dynamic mechanical thermo analysis
GPC	Gel permeation chromatography
HCl	Hydrochloric acid
HD	Hexadecane
KOH	Potassium hydroxide
MeOH	Methanol
Na-MMT	Sodium montmorillonite
NMR	Nuclear magnetic resonance spectroscopy
PALS	Positron annihilation lifetime spectroscopy
PAS	Photoacoustic spectroscopy
PCNs	Polymer clay nanocomposites
PDI	Polydispersity Index
PMMA	poly(methyl methacrylate)
PODA	poly(octadecyl acrylate)
SDBS	Sodium dodecyl benzene sulfonate
SEC	Size exclusion chromatography
Sty	Styrene
TEM	Transmission electron microscopy
TGA	Thermal gravimetric analysis

CHAPTER 1

Introduction

1.1   General Introduction

Packaging materials, protective coatings and membrane separation processes are typical examples of applications where the transport of gases, vapours and liquids through polymeric films play a key role in functional properties. The study of the transport of penetrants through different classes of polymeric films is therefore not new. Various models have been developed to predict the transport of different types of penetrant molecules through polymer films; the impact of changes to the chemical or physical properties of films to the transport properties have been investigated; and transport coefficients have been determined.[1-4]

Although extensive information already exists in this specific field of materials science, the need to measure, understand and optimise the performance of such materials in terms of the transport of gases, vapours and liquids still remains, and is further driven by technical developments that enhance the performance of these materials.

The field of coatings used for controlled transport of penetrants have evolved significantly over the past couple of decades. Some of the key shifts in technology include: (1) The shift from solvent-based coatings to water-based coatings to overcome technical limitations and environmental concerns brought with it a host of challenges as a result of additives required to enhance the properties of the latexes. Reactive surfactants were one of the key developments to counter the negative attributes associated with conventional surfactants in latex coatings.[5, 6] (2) The development of miniemulsion polymerisation techniques for the

1

preparation of latexes enabled the incorporation of highly hydrophobic monomers in the polymer backbone by overcoming the limitations set by the migration of monomers from monomer droplets to micelles in conventional emulsion polymerisation techniques.[7, 8] This created new opportunities for the development of highly hydrophobic latexes for use as water vapour barrier coatings. (3) The use of intercalated or exfoliated plate-like nano clays in the production of polymer clay nanocomposites for use in latex and rigid plastics applications brought about significant changes in the properties of the final composite materials.[9-11]

Building on these recent developments, the possibility of obtaining a better understanding of the sorption behaviour of such modified polymer films was identified and forms the basis of this study.

1.2   Goals and Objectives

The goal of this study was to investigate the impact of surfactants, plate-like clays, organophilic molecules and side-chain crystallinity on the transport mechanism of water vapour, at a molecular level, through model polymeric films.

The specific objectives were:

- To evaluate the water vapour sorption behaviour of a model polymer latex film stabilized with different types of surfactants. Two conventional surfactants, sodium dodecyl benzyl sulfonate and octyl phenol ethoxylate, and one reactive surfactant, dodecylammonium-3-butenoate, were used to stabilize the model polymer latex poly(styrene-*co*-butyl acrylate) random copolymer.

- To determine the impact of the presence of a plate-like clay and a reactive organophilic clay modifier on the water vapour sorption properties of a model polymer. Sodium montmorillonite was used for this purpose and was incorporated into a poly(styrene-*co*-butyl acrylate) random copolymer with the aid of a reactive organophilic modifier 2-acrylamido-2-methylpropane sulfonic acid.

- To determine the impact of side-chain crystallinity on the water vapour sorption properties of a model polymer. Various poly(methyl methacrylate-*co*-octadecyl acrylate) random copolymers containing increasing degrees of crystallinity were synthesized for this purpose.

1.3   Layout of dissertation

This dissertation consists of the following sections:

A brief introduction is given in Chapter 1, including the goals and objectives of this study. Chapter 2 gives a broad outlook on the principles of permeation and sorption in polymers, from a brief historical overview, to looking at specific methods of evaluating permeation properties in terms of their kinetic and thermodynamic behaviour. Factors affecting the sorption behaviour of polymers are discussed in Chapter 3. These factors include the temperature at which sorption is determined, the type of penetrant used and the chemical and physical properties of polymers. Chapter 4 reviews the experimental procedures for the synthesis of the model polymers of this study. The methods used for the characterization of the films and the measurement of sorption properties are also given here. Chapter 5 explores the impact of the choice of surfactant on the water vapour sorption properties of poly(styrene-co-butyl acrylate) latex films. The impact of sodium montmorillonite and 2-acrylamido-2-methylpropane sulfonic acid on the water vapour sorption properties of poly(styrene-co-butyl acrylate) latex films are investigated in Chapter 6, with different theoretical models being considered to match the sorption behaviour measured experimentally. Chapter 7 evaluates the impact of increasing degrees of side-chain crystallinity in poly(methyl methacrylate-co-octadecyl acrylate) on water vapour sorption properties of these polymers. Chapter 8 gives final conclusions of this study as well as recommendations for future work.

The theoretical aspects of sorption in polymers are discussed in the next chapter.

References

1.   Crank, J. and Park, G.S., eds. *Diffusion in Polymers*. 1968, Academic Press Inc. (London) Ltd: London. 452.

2.   Neogi, P., ed. *Diffusion in Polymers*. 1996, Marcel Dekker Inc.: New York. 309.

3.   Comyn, J., ed. *Polymer Permeability*. 1986, Elsevier Applied Science Publishers Ltd: London. 383.

4.   George, S.C. and Thomas, S., *Transport phenomena through polymeric systems.* Progress in Polymer Science, 2001. **26**: p. 985-1017.

5.   Asua, J.M. and Schoonbrood, H.A.S., *Reactive surfactants in heterophase polymerzation.* Acta Polymerica, 1998. **49**(12): p. 671-686.

6.   Guyot, A., Tauer, K., Asua, A.M., Van Es, S., Gauthier, C., Hellgren, A.C., Sherrington, D.C., Montoya-Goni, A., Sjoberg, M., Sindt, O., Vidal, F., Unzue, M., Schoonbrood, H.A.S., Shipper, E., and Lacroix-Desmazes, P., *Reactive surfactants in heterophase polymerization.* Acta Polymerica, 1999. **50**(2): p. 57-66.

7.   Asua, J.M., *Miniemulsion Polymerization.* Progress in Polymer Science, 2002. **27**: p. 1283-1346.

8.   Landfester, K., *Polyreactions in Miniemulsions.* Macromolecular Rapid Communications, 2001. **22**: p. 896-936.

9.   Faucheu, J., Gauthier, C., Chazeau, L., Cavaillé, J.-Y., Mellon, V., and Bourgeat-Lami, E., *Miniemulsion polymerization for synthesis of structured clay/polymer nanocomposites: Short review and recent advances.* Polymer, 2010. **51**: p. 6-17.

10.   Asua, J.M., European FP6 Report No. IP 011844-2 *Nanostructured waterborne polymer films with outstanding properties*, 2010, http://www.ehu.es/napoleon/.

11.   Esfandiari, A., Nazokdast, H., Rashidi, A.-S., and Yazdanshenas, M.-E., *Review of Polymer-Organoclay Nanocomposites.* Journal of Applied Sciences, 2008. **8**(3): p. 545-561.

CHAPTER 2

Sorption in Polymers

Summary: The development of theories to describe the transport of gases and vapours through polymer films is discussed based on the solution-diffusion model. The migration of penetrants can be classified as either Fickian or non-Fickian and are dependent on the rate of mass uptake as a function of time. Non-Fickian kinetics is classified as sigmoidal, two-stage or case-2 sorption and occurs when the polymer relaxation rate is slower than the diffusion rate of the penetrant.

The equilibrium mass uptake of polymers at different penetrant partial pressures is dependent on the degree of polymer-polymer interaction, polymer-penetrant interaction and penetrant-penetrant interaction. Based on these interactions, the thermodynamic behaviour of a polymer film can be classified as obeying Henry's Law for the case where the diffusion is independent of polymer-penetrant interactions; the Langmuir sorption mode is normally followed by polymers with microvoids or polymers containing fillers; the Dual-Sorption mode is followed if a combination of Henry's Law and Langmuir's sorption mode are followed; the Flory-Huggins sorption model is typical of systems with strong penetrant-penetrant interactions; and the BET sorption mode is followed for systems with a combination of Langmuir and Flory-Huggins behaviour.

5

2.1   Introduction

Transport of molecules through polymer materials is not a novel concept. Membranes have been used extensively for the purification of water, the separation of gases and even in fuel cells. Similarly, continuous polymeric films have found many applications in industry as liquid and gas barriers.

The subject of diffusion of gases and vapours through polymeric films has already been studied extensively for almost two centuries. Initial studies focused only on natural polymers. These theories were extended to synthetic rubbers due to potential practical applications.[1]

The earliest research on the transport of gases and vapours in polymers dates back to 1829, when Thomas Graham observed that a wet pig bladder inflated to bursting point when placed in an atmosphere of carbon dioxide.[1-3] However, it was only in 1866 that an explanation of the method of transport of small molecules through polymer films was proposed by Graham.[4] At that stage it was referred to as "colloidal diffusion", but the general perception of the permeation process was then already graphically proposed in a similar fashion to the solution-diffusion model as we know it today (See Figure 2.1).

The permeation concept then evolved through various stages of development, where Wroblewski quantified steady-state permeation in 1879 by applying *Henry's Law of Solubility* and *Fick's Law of Diffusion*. This quantification was extended to the non-steady state by Daynes in 1919, where the time-dependent increase in pressure of specific gases through a membrane was measured[4]. Further developments by Barrer and others established the permeation theory of vapours and gases through polymeric films to the level as we know it today (See Table 2.1).

6

Table 2.1: Development of some of earlier theories for gas and vapour transport through polymers[1]

Year	Scientist	Discovery
1829	T. Graham	Inflation of wet pig bladder when placed in atmosphere of CO_2.
1831	J.K. Mitchell	Systematic study of rates of permeation of 10 different gases through natural rubber.
1855	A. Fick	Laws of mass diffusion: Fick's first law of diffusion refers to the steady state of diffusion, while Fick's second law of diffusion is applicable to the non-steady state.
1866	T. Graham	Developed test method for permeation through flat membranes with pressure gradient across membrane. Postulated the solution-diffusion model.
1875/1878	J. Exner / J. Stefan	Permeation of gases through soap films proportional to product of solubility of gas in water and Fick's law diffusion coefficient.
1879	S. Wroblewski	Solution of gases in rubber followed Henry's law, where J is the flux, D the diffusion coefficient, S the solubility coefficient, Δp the difference in partial pressure on either side of the membrane and l the thickness of the membrane. $$J = \frac{D \times S \times \Delta p}{l}$$
1891	H. Kayser	Further support for solution-diffusion model: validity of Henry's law for absorption of CO_2 over a wide range of pressures.
1900	Lord Rayleigh	Calculated relative permeabilities of oxygen, nitrogen and argon in rubber, based on permeation of air through rubber membrane.
1917, 1920	G.A. Shakespear	Permeability of a gas is independent of presence of other gases.
1918	J.D. Edwards	Found a highly nonlinear effect of temperature and slight effect of total pressure on measured permeabilities of H_2 in rubber.
1918	J. Dewar	Measured permeability of several gases in rubber at different temperatures.
1920	H.A. Daynes	Plot of log P vs. T for a given gas gave 2 straight lines intersecting at 0 ºC. The discontinuity was contributed to the presence of water in the membrane.
1939	R.M. Barrer	Steady-state permeability can only lead to the determination of D x S, and not their separate values. Development of "time lag" method, using air downstream.
1946	G.J. Van Amerongen	Developed "Time Lag" method further, using vacuum downstream. Proved that solubility coefficients measured directly for various gases in rubber were the same as those obtained by the quotient of the permeabilities and the time lag diffusivities.
1954	P. Meares	Extended the time lag method to cases where diffusion coefficients were concentration dependent. Demonstrated the break in Arrhenius plots at the T_g, and speculated about 2 modes of solution in glassy polymers.
1957-58	H.L. Frisch	Demonstrated that permeability and diffusivity followed the Arrhenius equation and that activation energies for both processes could be determined.

2.2   The Solution-Diffusion Model

The solution-diffusion model, originally proposed by Thomas Graham, describes the mechanism whereby gases and vapours move through a polymer film, from a region of high partial pressure, through the film, to a region of low partial pressure (See Figure 2.1). This mechanism is described in terms of five definite steps:[5]

- Diffusion through the limit layer of the side corresponding to the higher partial pressure;

- Absorption of the gas (by chemical affinity or by solubility) by the polymer;

- Diffusion of the gas inside the membrane polymer ;

- Desorption of the gas at the side of lower partial pressure; and

- Diffusion through the limit layer of the downstream side.

The magnitude of the sorption/desorption and diffusion steps in the solution-diffusion model are determined by specific chemical and physical properties of the polymer film, as well as external conditions such as the temperature and penetrant concentration.

The permeability of gases or vapours through polymers is consequently based on the solubility thereof into the polymer and its diffusion through the polymer layer. It is quantified as the product of the solubility coefficient and the diffusion coefficient (see Equation 2.1).[2, 5-8]

$$P = D \times S$$
(2.1)

Here P is the permeability coefficient, D is the diffusion coefficient and S is the solubility coefficient. For a given polymer-penetrant combination, the permeability can therefore be used to describe the steady-state transport of a specific penetrant through a polymer. The steady-state rate can be calculated by means of *Fick's First Law* (see Equation 2.2 below).[2]

$$\frac{\Delta M_x}{\Delta t} = \frac{P A \Delta p_x}{L}$$
(2.2)

Here $\frac{\Delta M_x}{\Delta t}$ represents the steady-state rate of permeation of penetrant x through a polymer film (ΔM_x is the increase in weight of the polymer film due to absorption of penetrant and Δt is the time period during which the increase in weight was measured), with area A and thickness L; P is the permeability and Δp_x is the difference in pressure of the penetrant on either side of the film.
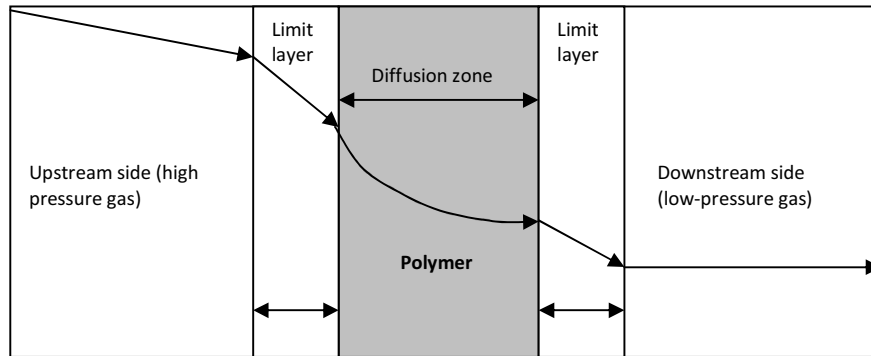
Figure 2.1: The Solution-Diffusion Model. [5]

2.3   Quantification of Transport Kinetics

The transport of gases through non-porous polymers can be quantified using different techniques. Two techniques exist today: permeation and sorption. The difference between these two methods is defined by the presence or absence of a pressure differential of the gas or vapour on either side of the polymer film. The kinetics of diffusion for a specific temperature and penetrant concentration differs between these two processes, resulting in either a sorption or permeation mechanism.

2.3.1   Sorption

Sorption kinetics require that a free film be exposed on both sides to a gas or vapour at the same specific penetrant activity (See Figure 2.2(a)). This measurement is done at accurately controlled conditions. Any traces of penetrant must be removed from the polymer film under high vacuum prior to starting the measurement. The amount of penetrant absorbed by the polymer film can be

9

measured either gravimetrically or volumetrically and is graphically represented by a sorption curve, where the relative mass uptake ($\frac{M_t}{M_\infty}$) is plotted as a function of time (t). The reduced sorption curve (See Figure 2.2(b)) is preferred for the determination of the diffusion coefficient, and is represented by the fractional mass uptake ($\frac{M_t}{M_\infty}$) of the penetrant by the polymer as a function of $\frac{t^{1/2}}{L}$, where t is the time and L the thickness of the polymer film. A state of equilibrium is reached after a period of time, where the polymer film is saturated by the penetrant, and is characterized by a constant maximum mass uptake (M_∞) which is independent of time.
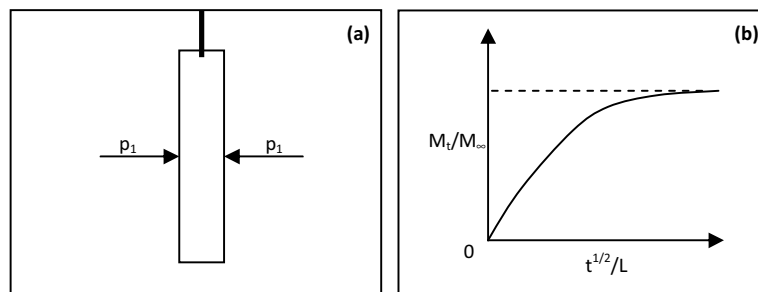
Figure 2.2: (a) Sorption technique and (b) Reduced sorption curve. [2, 7, 8]

Gravimetric determination: This method is very simple, requiring the direct weighing of a polymer sample at regular intervals. The polymer sample must have a known shape and size, and must be kept in an atmosphere of constant penetrant activity. This method evolved over time, from where the polymer was removed from its constant atmosphere for the purpose of weighing (which resulted in the formation of an air barrier at the surface of the film), to the use of a quartz spring for the direct measurement of increase in weight (thereby eliminating the formation of the air barrier). Today the quartz spring, which was difficult to handle and costly to replace, has been replaced by extremely accurate mass balances (6-decimal place measurement in grams) for the gravimetric

determination of the sorption of gases and vapours. Both sorption and desorption kinetics can be determined by means of this method.

Volumetric determination: At extremely low levels of absorbed penetrant, the accuracy of measured increase in mass becomes very dubious and gives very little information regarding the sorption kinetics. In this case, the direct measurement of the volume of absorbed gas or vapour by means of a manometer would generate the most accurate information regarding the sorption kinetics.[2, 9]

2.3.2   Permeation

The permeation method requires that a penetrant activity differential exists on either side of the film, resulting in a driving force for diffusion from the high activity side, towards the low activity side (See Figure 2.3(a)). Due to the initial activity gradient within the polymer film itself, the diffusion kinetics is first described according to the "time lag" method[1].[2] Only after the penetrant concentration in the polymer film is constant throughout the film thickness, can the "steady-state" method[2] be used to describe the transport kinetics. This phenomenon is illustrated by a permeation curve (See Figure 2.3(b)), where $\frac{LQ_t}{p_1}$ (where L is the thickness of the polymer film, Q_t is the total amount of penetrant that has permeated through the membrane, p_1 is the pressure of the gas or vapour that is introduced on the one side of the polymer film) is plotted against time (t). The initial non-linear increase in the rate of penetrant uptake represents the time lag period, where the x-intercept gives the time required for the penetrant to reach a constant concentration throughout

---

[1] Time lag method: At the outset of the permeation method when the penetrant is first admitted to one side of the polymer film, and prior to a steady state being reached, both the flow and concentration of the penetrant varies at any point in the polymer film as a function of time.

[2] Steady state method: The concentration and flow of the penetrant is constant at any point in the polymer film.

the polymer film. Once the steady-state is reached, the increase in weight (see weighed-cell method), or the increase in penetrant concentration (see partition-cell method) due to the diffusion of penetrant through the polymer film, is constant. This constant rate of permeation through the film is represented by the straight line region of the permeation curve.[8]

Permeation of the penetrant through the polymer film can be quantified either gravimetrically or volumetrically. In 1950 Newns classified these techniques as the weighed-cell and partition-cell methods respectively.[2]
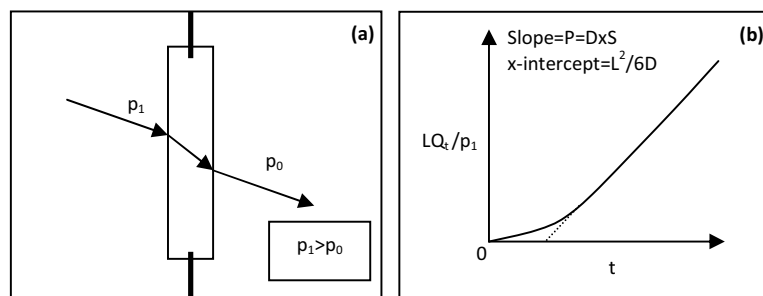
Figure 2.3: (a) Permeation technique and (b) Permeation curve. [2, 7, 8]

Weighed-cell method: The permeation of moisture vapour through a polymer film can be measured by sealing a shallow vessel containing either a humidifying solution or a dessicant with the polymer film, thereby creating a penetrant activity differential across the film, keeping the resulting cell at a fixed temperature in either a desiccator or a humidity cabinet and measuring the rate of water vapour transmission through the film by periodically weighing the cell. This method only gives the permeation rate for the steady-state. The diffusion coefficient can be determined by weighing the conditioned polymer film periodically. This method is subject to many errors, such as the formation of a diffusion barrier due to entrapped air, as well as sealing problems at the edges of the polymer film, and is therefore not very accurate. It is also restrictive in terms of the types of vapours and

gases that can be used. Industrial test methods such as TAPPI T464, ISO R1195:1970 and ASTM E96-66 for the determination of the water vapour transmission rate are based on this method.[2, 10]

Partition-cell method: This method was developed to circumvent the problems associated with the weighed-cell method. The equipment used for this determination typically consists of a diffusion cell, where the penetrant is introduced at a constant pressure on the one side of the polymer film or membrane, with an initial zero penetrant pressure on the other side. As the penetrant diffuses through the polymer film, the increase in pressure from zero is measured by a pressure gauge. It requires that the vapour pressure be controlled on either side of the membrane and allows for the independent measurement of the permeation rate. Both the time-lag and the steady-state flow rates can be determined with this method. Although this method was successful in addressing the diffusion barrier problem and the limitation in terms of the gases and vapours that could be analyzed, the problems associated with sealing the polymer film in the membrane cell largely remained.[2]

2.3.3   Suitability of penetrant transport mechanisms

The choice of analytical technique to be used is governed by the final application of the polymer film. Polymer films used in heterogeneous applications, i.e. where the film is applied to another surface, must be analyzed in terms of the permeation kinetics. Sorption kinetics is more appropriate in terms of homogeneous applications. Apart from final application, the relative magnitude of the solubility and diffusion coefficients also guides the method selection.[2] The permeation technique is preferred for films with a high diffusion coefficient, coupled with a low solubility coefficient. Low diffusion coefficients are determined more accurately by the sorption kinetic technique.

The sorption kinetic technique has many advantages over the permeation kinetic technique for the determination of the diffusion coefficient, mainly as a result of sample handling problems with the latter method.[2] Some of the advantages include: sealing efficiency, which is critical for permeation studies, is not required in sorption experiments; no complications arise from supporting grids, as the sample is exposed to equal pressures on either side of the film; small holes in the film under investigation is not detrimental to sorption experiments; and leakages and film distortion, which

13

cause serious errors in the determination of low diffusion coefficients, do not affect sorption determinations.

2.4   Diffusion Kinetics

The process whereby small molecules move through polymer materials is described in terms of the relative penetrant mass uptake as a function of time for a specific penetrant activity (chemical potential) and temperature, and is referred to as its diffusion kinetics. This process is classified as either Fickian or non-Fickian, where non-Fickian kinetics deviates from the ideal Fickian case. Three non-ideal kinetic types have been identified: two-stage sorption, sigmoidal sorption and case II sorption (See Figure 2.4). From the plot of relative mass uptake (*M)* versus (time)$^{1/2}$, the rate of penetrant uptake, as well as the time required to reach a constant relative mass uptake (the steady-state), can be determined.

2.4.1   Fickian Sorption

The Fickian absorption kinetics represent the ideal case, where the plot of relative mass uptake (*M*) versus (time)$^{1/2}$ is characterized by an initial linear region, followed by a levelling off of *M* with increasing time, and finally reaching saturation (*M*$_\infty$) (see Figure 2.4(a)). This behaviour is the result of free diffusion of the penetrant through the polymer without interference by polymer chain rearrangement or relaxation and is described by the following equation, also known as the general diffusion law or Fick's second law of diffusion:[6, 11]

$$\frac{\partial C}{\partial t} = \frac{\partial}{\partial x}\left(D(C)\frac{\partial C}{\partial x}\right) \tag{2.3}$$

Here C (kg.m^{-3}) is the penetrant concentration, t (s) the time, x (m) the position in the film in the direction of diffusion and D is the diffusion coefficient.

14
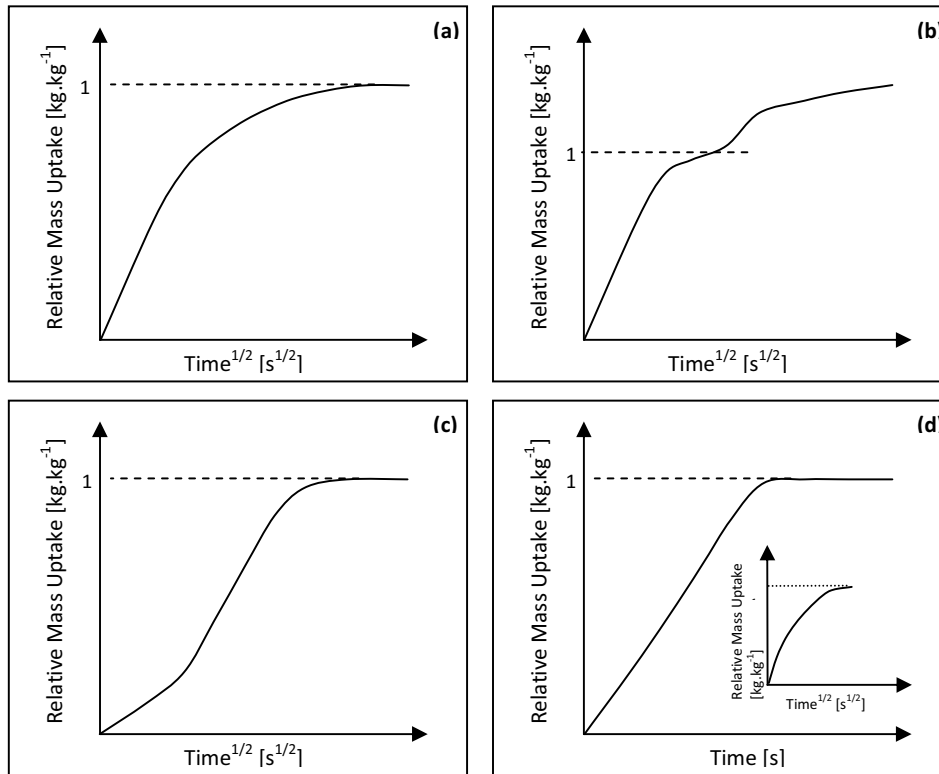
Figure 2.4: Different types of sorption kinetics: (a) Fickian sorption curve, (b) two-stage sorption curve, (c) sigmoidal (S-shaped) sorption curve, (d) Case II sorption curve (Inserted graph: Case II sorption curve where Time$^{1/2}$ is plotted against Relative Mass Uptake showing a significantly steeper gradient) [6]

2.4.2 Non-Fickian Sorption

Non-Fickian sorption behaviour is found where the rate of relaxation of the polymer is slower than the rate of diffusion. Three types of non-Fickian sorption have been defined: two-stage sorption, sigmoidal sorption and case II sorption and discussed in greater detail below.

2.4.2.1 Two-stage Sorption

The name "two-stage" sorption mode originates from the shape of its sorption curve, which appears to be a combination of two types of sorption curves, namely fast Fickian absorption followed by slow non-Fickian absorption. Berens and Hopfenberg proposed an explanation for this phenomenon in

15

1978.[12] Their diffusion-relaxation model described two independent processes: a concentration-gradient-controlled diffusion part $\left(M_F(t)\right)$ that follows Fick's laws, and a structural (relaxation-controlled swelling) part $\left(M_R(t)\right)$ resulting from polymer relaxations. The total increase in weight is then expressed as the sum of these contributions (refer to equation 2.4).

$$M(t) = M_F(t) + M_R(t) \qquad\qquad (2.4)$$

This model was originally developed for the uniform sphere model of diffusion[12], but later also applied to diffusion in polymer films.[13] Equation 2.5 below gives the detailed sorption equation, based on the proposed model of Berens and Hopfenberg, where M_t is the total amount of sorption per unit weight of polymeric microspheres, $M_{\infty,F}$ is the equilibrium amount of sorption in the unrelaxed polymer, k_F is the rate constant for the unrelaxed polymer and $k_F = 4\pi^2 D/d^2$ (with D the diffusion coefficient and d the particle diameter), t is time, $M_{\infty,i}$ represents the equilibrium sorption of the ith relaxation process and k_i the respective relaxation rate constant.

$$M_t = M_{\infty,F}\left[1 - \frac{6}{\pi^2}\sum_{n=1}^{\infty}\frac{1}{n^2}exp(-n^2 k_F t)\right] + \sum_i M_{\infty,i}[1 - exp(-k_i t)] \qquad (2.5)$$

2.4.2.2   Sigmoidal Sorption

The sigmoidal sorption curve is a typical S-shaped curve, showing a point of inflection. This non-Fickian sorption behaviour was explained by Long and Richman in the 1960s through the development of the "variable surface concentration" (VSC) model, where the initial slow absorption of penetrant is attributed to the slow establishment of equilibrium at the surface of the polymer film.[14] This is subsequently followed by normal Fickian behaviour. In some cases, it has also been shown that alternative non-Fickian kinetic behaviour, such as two-stage sorption effects, can follow the VSC model.[8]

16

2.4.2.3 Case II Sorption

This non-Fickian sorption model is completely different from the other two proposed non-Fickian models. While the other models focus on the movement of gases or vapours through polymer films, this case is also used to describe the movement of liquid through polymer films.

Alfrey and co-workers were the first group to classify the linear kinetics behaviour observed in a polystyrene-methanol system as Case II sorption. It was identified as a second limiting type of diffusion by linear kinetics, distinctly different to the Fickian (or Case I) type of kinetics.[15]

Further research by Thomas and Windle on the sorption of methanol on poly(methyl methacrylate) (PMMA) elucidated further aspects of Case II kinetics.[16-18] This study again confirmed the linear kinetics behaviour; it was also possible to visually follow a sharp front of penetrant moving at a constant velocity into the PMMA film; and it was shown that the weight gain due to sorption of the penetrant ended abruptly as the two opposing fronts meet in the centre of the film. The sharp penetrant front, evident of Case II sorption, was shown to be as a result of a difference in the rate of penetration of the penetrant in the glassy component of the polymer versus the rate of penetration in an already swollen component of the polymer. Due to the plasticization effect of the penetrant, the rate of diffusion of penetrant molecules in the already swollen section of the polymer is significantly faster than the diffusion of penetrant into the glassy section of the polymer. This results in the accumulation of penetrant molecules and the development of a sharp penetrant front.

Further development of theories for the Case II model included: the work of Crank[19] on the time dependence of the diffusion coefficient due to the effect of slow changes of polymer structure accompanying the diffusion, and internal stresses exerted by one part of the polymer while the other swells; the expansion of Crank's work by Petropoulos and Roussis;[20, 21] the introduction of an additional term to equation (2.3) to represent the constant velocity of the solvent front as developed by Peterlin;[22] Van Westling and co-workers[23] who found that, for the penetration of liquid water into an epoxy coating, the Case II sorption kinetics was preceded by Fickian-like kinetics; and Samus and Rossi[24] who proposed that, if geometric constraints of polymers were taken into consideration, initially perceived non-Fickian kinetics would actually comply to Fick's Law.

17

In summary, Case II kinetics can be described by the following key characteristics:[18]

- A linear increase in weight is observed with time until equilibrium is reached.

- An increase in sample volume is observed due to swelling of the polymer in the presence of the penetrant.

- An increase in temperature will enhance the rate of Case II sorption and may also in certain cases increase the equilibrium sorption value.

- For a sufficiently wide temperature range, systems exhibiting Case II sorption kinetics at ambient conditions will change to Fickian kinetics at elevated temperatures. At the elevated temperature the velocity of the front will decrease and will result in a steep penetrant concentration gradient behind the front. Based on this, equilibrium sorption cannot be achieved when the two opposing fronts meet.

- Case II sorption is often preceded by an induction period before the linear weight increase portion. This Fickian precursor is due to the viscous flow rate of the glassy polymer and is normally slow compared to the diffusion coefficient.

2.5   *Equilibrium Sorption Isotherms*

The equilibrium sorption isotherm for a specific polymer-penetrant system describes the equilibrium relative mass uptake $\left(\frac{M_t}{M_\infty}\right)$ of the penetrant by the polymer film as a function of different penetrant activities or partial pressures $\left(\frac{P}{P_0}\right)$, at a constant temperature.

The mode of sorption, and the quantity of gas or vapour molecules absorbed, is controlled by the thermodynamics of the specific polymer-penetrant system. The degree of interaction between the polymer and penetrant determines the actual mode of sorption. Types of interaction to be considered include: polymer-polymer, polymer-penetrant, and penetrant-penetrant interactions. Five types of equilibrium sorption isotherms have been defined, based on the type of interaction, or combination of interactions, that is dominant (See Figure 2.5):[5]

18

- Henry's law sorption: Polymer-polymer interactions;

- Langmuir-mode sorption: Polymer-penetrant interactions;

- Dual-mode sorption: Combination of Henry's law and Langmuir modes;

- Flory-Huggins mode sorption: penetrant-penetrant interactions; and

- BET mode sorption: Combination of Langmuir and Flory-Huggins modes.
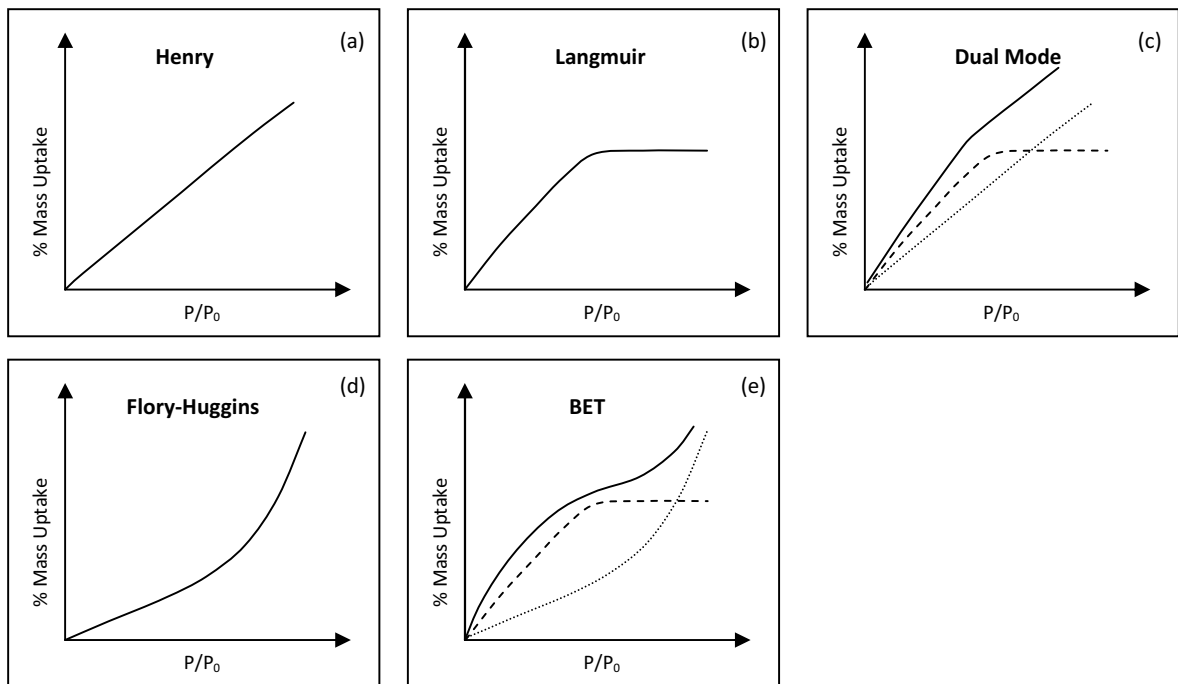
Figure 2.5: Equilibrium Sorption Isotherms: (a) Henry's Law, (b) Langmuir, (c) Dual Sorption Mode, (d) Flory-Huggins and (e) BET isotherm [6]

2.5.1   Henry's Law Sorption

This mode represents the simplest case of sorption, where a linear relationship exists between the penetrant concentration in the polymer film and its partial pressure $\left(\frac{P}{P_0}\right)$ (See Equation 2.6).[2, 6]

This mode is normally valid in the case of ideal gases where there is no interaction with the polymer and therefore also no saturation in the polymer film.[5, 25-27]

$$C = k_D p \qquad (2.6)$$

where C is the sorbed concentration of the penetrant, k_D is the solubility coefficient (S) and p is the partial pressure of the penetrant. The mode of sorption is often valid at low partial pressures where the polymer-penetrant and penetrant-penetrant interactions are insignificant.

2.5.2   Langmuir-Mode Sorption Isotherm

Polymers containing microvoids or inorganic fillers tend to behave according to this mode of sorption, where specific sites within the polymer matrix are occupied by the penetrant. Once all the sites are occupied, a small quantity of molecules may solubilise. The penetrant concentration is given by the following relationship:[5, 6, 27]

$$C_H = \frac{C'_H b p}{1 + b p} \qquad (2.7)$$

where C_H is the penetrant concentration, C'_H is the "hole saturation"[3] constant, b is the "hole affinity"[4] and p the partial penetrant pressure.

---

[3] Hole saturation: The hole saturation constant refers to the maximum concentration of a specific penetrant that can reside in the micro void sites of a polymer for which it has a specific affinity.

[4] Hole affinity: The hole affinity refers to the affinity of the penetrant for the micro voids in the polymer matrix, based on its chemical nature as well as relative size.

2.5.3   Dual-Mode Sorption Isotherm

This mode of sorption has been developed to describe the sorption of low-activity gases in micro-heterogeneous glassy polymers, where the model assumes that the penetrant molecules exist as two distinct populations in the polymer matrix.[28] The one group of penetrant molecules is sorbed into the polymer via a normal dissolution mechanism according to Henry's Law. The second group of penetrants is immobilized in pre-existing voids in the polymer and can be represented by Langmuir's expression. These two groups of molecules are in equilibrium throughout the polymer medium, with the immobilization process being a very rapid process compared to the rate of migration of the mobile phase. The diffusion process is therefore the rate-determining process and it is only these diffusive molecules that contribute to the diffusive flux, driven by a concentration gradient.[6, 29] This mode of sorption only occurs in cases where moderate partial pressures are used and where no swelling or plasticization of the polymer film occurs.

The solubility coefficient of the dual-mode sorption model is given by equation (2.8) where C is the solubility coefficient, C_D represents the diffusible species and C_H the sorption in micro voids or holes, k_D is Henry's law dissolution constant, b is the hole affinity constant, C'_H is the hole saturation constant and p is the pressure.

$$C = C_D + C_H = k_D p + C'_H \frac{bp}{1+bp} \tag{2.8}$$

When $bp \ll 1$, equation (2.8) is reduced to a linear form: $C = [k_D + C'_H b]p$

At sufficiently high pressures the micro voids will become saturated and $bp \gg 1$, resulting in equation (2.8) also being reduced to a linear form: $C = k_D p + C'_H$

At high pressures it would therefore be possible to determine k_D from the slope and the hole saturation constant (C'_H) from the intercept.[30, 31]

Vieth et al. developed an extension to the dual-mode sorption model, where they argued that there may be more than two sites with different penetrant affinities within the same polymer matrix.[29]

21

The total concentration of penetrant in the polymer is therefore expressed as the sum of the penetrant concentrations of the sub-populations at the different sites, namely:

$$C = C_1 + +C_2 + \cdots + C_n$$

Here C is the total penetrant concentration and $C_1 \dots C_n$ the penetrant concentrations of n sub-populations within the polymer matrix. Each penetrant concentration can be expressed by a sorption isotherm. In the case of the concentration being a linear function of pressure, Henry's law would apply: $C_j = k_j p$. By rearranging this relationship,, it was shown that the concentration of any species can be written in terms of the concentration of any other species:

$$p = \frac{C_1}{k_1} = \frac{C_2}{k_2} = \cdots = \frac{C_n}{k_n}$$

$$C_i = k_i C_j / k_j$$

For isotherms displaying non-linear sorption behavior, the concentration of the penetrant at each site was however expressed in terms of the nonlinear Langmuir expression. Two expressions were developed, one for a gas-phase penetrant (See equation 2.9), and the other for a dissolved penetrant (see equation 2.10):[29]

$$C_j = C_j' b_j p / (1 + b_j p) \tag{2.9}$$

$$C_j = C_j' b_j C_s / (1 + b_j C_s) \tag{2.10}$$

Here b is the affinity constant, C_j the hole saturation constant of the polymer, p the penetrant activity, bp a dimensionless number, C_s a measure of the penetrant activity (concentration) and bC_s a dimensionless number.

Through further mathematic manipulation a model was developed to describe the penetrant concentration in such a matrix. Equation (2.11) below is for the case of two different affinity levels,

where C is the total penetrant concentration, C_1 and C_2 the penetrant concentrations of two sub-populations within the polymer matrix, b_1 and b_2 are the hole affinities for the two different affinity regions and p the penetrant partial pressure:[29]

$$C = (C'_1 b_1 + C'_2 b_2)p/(1 + +b_1 p)(1 + b_2 p) \tag{2.11}$$

This equation is simplified for low pressure regions to a linear relationship where $b_1 p \ll 1$ and $b_2 p \ll 1$ (See equation (2.12)) and for high pressure regions a nonlinear relationship where $b_1 p \gg 1$ and $b_2 p \gg 1$ (See equation (2.13)).

$$C = (C'_1 b_1 + C'_2 b_2)p \tag{2.12}$$

$$C = (C'_1 b_1 + C'_2 b_2)/b_1 b_2 p \tag{2.13}$$

The values of b_1, b_2, C'_1 and C'_2 can be determined by means of a nonlinear regression analysis of experimental data using equation (2.11) for the entire pressure range.

2.5.4   *Flory-Huggins Mode Sorption Isotherm*

When the penetrant-penetrant interactions are dominant and the solubility coefficient increases continuously with increasing pressure, the Flory-Huggins sorption model is applied. This model is often applied in the case of hydrophobic polymer systems. The solubility coefficient can be calculated from the following relationship:[5, 6]

$$\ln(a) = \ln\frac{p}{p_0} = 1 - \varphi + \ln(\varphi) + \chi(1 - \varphi)^2 \tag{2.14}$$

where a is the thermodynamic activity of the penetrant in the polymer, p is the partial penetrant pressure, p_0 represents the saturation penetrant pressure, φ (unitless) is the volume fraction of the penetrant in the polymer and χ the enthalpic interaction parameter between the polymer and penetrant.

A deviation from the Flory Huggins model is seen with clustering of penetrants at higher penetrant activities.[32] Instead of only penetrant-penetrant interactions, the work of Perrin and Favre suggested that both penetrant-penetrant and penetrant-polymer interactions should be taken into consideration.[6, 33] An additional parameter (k_s) was therefore introduced to account for penetrant-penetrant interactions. This is referred to as the ENSIC model and is represented by equation (2.15) below, where φ is the volume fraction of dissolved penetrant, k_s the penetrant mutual interaction parameter and k_p the penetrant-polymer interaction parameter (similar to χ in equation (2.11)).

$$\varphi = \frac{e^{(k_s-k_p)^a}-1}{(k_s-k_p)/k_p} \qquad (2.15)$$

The ENSIC model may describe sorption behaviour across the full range of penetrant activity, while the Flory-Huggins model often fails at higher levels of penetrant activity.

2.5.5   *Brunauer, Emmett and Teller Mode Sorption Isotherm*

The Brunauer, Emmet and Teller (BET) sorption mode represents all three types of interactions (a combination of the Langmuir and Flory-Huggins sorption modes) and is characteristic of water sorption in highly hydrophilic polymers.[5] The classic BET equation is a two-parameter model and is based on certain assumptions of which the following two are important: (1) the number of sorbed layers is assumed to be infinite, and (2) the condensation-evaporation properties in the second and higher layers are assumed to be the same as that for the liquid state. This model is represented by equation (2.16), where C is the concentration of penetrant sorbed, a is a parameter of the BET model, $x = \frac{p}{p_0}$ (i.e. x is the relative pressure of the water vapour) and c_p is the internal partition function of the bound and liquid water. Equation (2.16) can be re-written into a linear format to allow for the determination of the values of the parameters of the BET model via the intercept and slope of the line. This model only gives a good fit for penetrant activities between 0 and 0.5.

$$C = \frac{a c_p x}{(1-x)(1-x+c_p x)} \qquad (2.16)$$

24

To overcome this shortcoming, the Guggenheim-Anderson-de Boer (GAB) sorption model was developed (See equation 2.17) where it was assumed that the heat of adsorption into the multilayer structure is less than the heat of liquefaction.[6, 34]

$$C = \frac{a_{GAB}c_{p,GAB}kx}{(1-kx)} \frac{1}{1+(c_{p,GAB}-1)kx}$$

(2.17)

Here C is the solubility, a_{GAB} is a parameter of the GAB model, $c_{p,GAB}$ is a parameter of the GAB model, k is a correction factor of the GAB model and x is the relative humidity.[34] This model is an effective model for fitting Type II and Type III water sorption in polymers across the full penetrant activity range from 0 to 0.95.

Factors affecting the sorption properties of polymers are discussed in the following chapter.

25

References

1.   Stannett, V., *The Transport of Gases in Synthetic Polymeric Membranes - An Historic Perspective.* Journal of Membrane Science, 1978. **3**: p. 97-115.

2.   Crank, J. and Park, G.S., eds. *Diffusion in Polymers*. 1968, Academic Press Inc. (London) Ltd: London. 452.

3.   Graham, T., *Notice of the singular inflation of a bladder.* Journal of Membrane Science, 1995. **100**: p. 9.

4.   Hopfenberg, H.B., *Permeability of Plastic Films and Coatings*. Polymer Science and Technology, ed. W.J. Bailey, Berry, J.P., DiBenedetto, A.T., Hoeve, C.A.I., Ishida, Y., Karasz, F.E., Solomon, O. Vol. 6. 1974, New York: Plenum Press.

5.   Klopffer, M.H. and Flaconneche, *Transport Properties of Gases in Polymers: Bibliographic Review.* Oil & Gas Science and Technology - Revue de L'Institut Français du Pétrole, 2001. **56**(3): p. 223-244.

6.   Van der Wel, G.K. and Adan, O.C.G., *Moisture in Organic Coatings - A Review.* Progress in Organic Coatings, 1999. **37**: p. 1-14.

7.   Comyn, J., ed. *Polymer Permeability*. 1986, Elsevier Applied Science Publishers Ltd: London. 383.

8.   Neogi, P., ed. *Diffusion in Polymers*. 1996, Marcel Dekker Inc.: New York. 309.

9.   Lomax, M., *Permeation of Gases and Vapours through Polymer Films and Thin Sheet - Part I.* Polymer Testing, 1980. **1**: p. 105-147.

10.   Lomax, M., *Permeation of Gases and Vapours through Films and Thin Sheet - Part II.* Polymer Testing, 1980. **1**: p. 211-242.

11.   Rogers, C.E., *Permeation of Gases and Vapours in Polymers*, in *Polymer Permeability*, J. Comyn, Editor. 1986, Elsevier Applied Science: London. p. 11-73.

12.   Berens, A.R. and Hopfenberg, H.B., *Diffusion and relaxation in glassy polymer powders: Separation of diffusion and relaxation parameters.* Polymer, 1978. **19**(5): p. 489-496.

13. Sun, Y.-M., *Sorption/desorption properties of water vapour in poly(2-hydroxyethyl methacrylate): 2. Two-stage sorption models.* Polymer, 1996. **37**(17): p. 3921-3928.

14. Long, F.A. and Richman, D., *Concentration Gradients for Diffusion of Vapors in Glassy Polymers and their Relation to Time Dependent Diffusion Phenomena.* Journal of the American Chemical Society, 1960. **82**(3): p. 513-519.

15. Alfrey, T.J., Gurnee, E.F., and Lloyd, W.G., *Diffusion in Glassy Polymers.* Journal of Polymer Science: Part C Polymer Symposia, 1966. **12**(1): p. 249-261.

16. Thomas, N.L. and Windle, A.H., *A theory of Case II diffusion.* Polymer, 1982. **23**(4): p. 529-542.

17. Thomas, N.L. and Windle, A.H., *Diffusion mechanics of the system PMMA-methanol.* Polymer, 1981. **22**(5): p. 627-639.

18. Windle, A.H., *Case II Sorption*, in *Polymer Permeability*, J. Comyn, Editor. 1986, Elsevier Applied Science Publishers: London.

19. Crank, J., *A theoretical investigation of the influence of molecular relaxation and internal stress on diffusion in polymers.* Journal of Polymer Science, 1953. **11**(2): p. 151-168.

20. Petropoulos, J.H. and Roussis, P.P., *Study of "Non-Fickian" Diffusion Anomalies through Time Lags. I. Some Time-Dependent Anomalies.* Journal of Chemical Physics, 1967. **47**(4): p. 1491-1497.

21. Petropoulos, J.H. and Roussis, P.P., *Anomalous Diffusion of Good and Poor Solvents or Swelling Agents in Amorphous Polymers.* Journal of Polymer Science Part C: Polymer Symposia, 1969. **22**(2): p. 917-926.

22. Peterlin, A., *Diffusion in a network with discontinuous swelling.* Journal of Polymer Science Part B: Polymer Letters, 1965. **3**(12): p. 1083-1087.

23. Van Westing, E.P.M., Ferrari, G.M., and De Wit, J.H.W., *The determination of coating performance with impedance measurements - II. Water uptake of coatings.* Corrosion Science, 1994. **36**(6): p. 957-977.

24.   Samus, M.A. and Rossi, G., *Methanol Absorption in Ethylene-Vinyl Alcohol Copolymers: Relation between Solvent Diffusion and Changes in Glass Transition Temperature in Glassy Polymeric Materials.* Macromolecules, 1996. **29**(6): p. 2275-2288.

25.   Stern, S.A. and Trohalaki, S., *Fundamentals of Gas Diffusion in Rubbery and Glassy Polymers*, in *Barrier Polymers and Structures*, W.J. Koros, Editor. 1993, American Chemical Society: Washington DC.

26.   Wijmans, J.G. and Baker, R.W., *The solution-diffusion model: A review.* Journal of Membrane Science, 1995. **107**: p. 1-21.

27.   Stern, S.A. and Frisch, H.L., *The selective permeation of gases through polymers.* Annual Review of Materials Science, 1981. **11**: p. 523-550.

28.   Frisch, H.L., *Sorption and Transport in Glassy Polymers - A Review.* Polymer Engineering and Science, 1980. **20**(1): p. 2-13.

29.   Vieth, W.R., Amini, M.A., Constantinides, A., and Ludolph, R.A., *Extension of the Dual Sorption Theory and Its Relation to Transport Phenomena in Biologically Active Membranes.* Industrial & Engineering Chemistry Fundamentals, 1977. **16**(1): p. 82-87.

30.   Green, T.K. and Selby, T.D., *Pyridine Sorption Isotherms of Argonne Premium Coals: Dual-Mode Sorption and Coal Microporosity.* Energy & Fuels, 1994. **8**(1): p. 213-218.

31.   Vieth, W.R., Howell, J.M., and Hsiesh, J.H., *Dual Sorption Theory.* Journal of Membrane Science, 1976. **1**: p. 177-220.

32.   Beck, M.I. and Tomka, I., *Effects of the degree of substitution in ethyl cellulose on the clustering of sorbed water.* Journal of Macromolecular Science. Part B Physics, 1997. **36**(1): p. 19-39.

33.   Perrin, L., Nguyen, Q.T., Sacco, D., and Lochon, P., *Experimental Studies and Modelling of Sorption and Diffusion of Water and Alcohols in Cellulose Acetate.* Polymer International, 1997. **42**: p. 9-16.

34.   Jonquières, A. and Fane, A., *Modified BET Models for Modeling Water Vapor Sorption in Hydrophilic Glassy Polymers and Systems Deviating Strongly from Ideality.* Journal of Applied Polymer Science, 1998. **67**(8): p. 1415-1430.

CHAPTER 3

Factors Affecting Sorption Behaviour

Summary: *Factors affecting the sorption behaviour of polymer films to vapours and gases are discussed. These factors can be classified as external factors such as the type of penetrant and the temperature of the environment surrounding the polymer film, as well as material-related factors referring to the properties of polymer films. The polymer properties discussed include: the nature of solvent-based and water-based coatings; its chemical composition; the role of the glass transition temperature, degree of crosslinking and crystallinity of the polymer; the impact of additives such as surfactants and fillers; and lastly the impact of multilayered structures on sorption behaviour.*

The impact of these factors on the sorption properties of the polymer film is largely interrelated, making it difficult to attribute changes in sorption behaviour to specific changes in specific properties of the polymer matrix, penetrant or temperature.

Key areas of research in the field of polymer properties identified for this study are summarised and include: the impact of surfactants on the water vapour sorption behaviour of a model polymer latex film poly(styrene-co-butyl acrylate); the impact of plate-like fillers on the water vapour sorption behaviour of latex films from the same model polymer, the impact of a low molecular weight hydrophilic additive, 2-acrylamido-2-methylpropanesulfonic acid, on the water vapour sorption behaviour of latex films from the model polymer; and lastly the impact of degree of crystallinity on the water vapour sorption behaviour of poly(octadecyl-co-methyl methacrylate).

3.1   The impact of penetrant type on sorption behaviour

The diffusion of penetrants through a polymer matrix is dependent on the size, shape and polarity of the penetrant. In order to understand the behaviour of penetrants in terms of its impact on the solubility and diffusion coefficients, it is necessary to classify penetrants into three categories, based on their nature. This classification is in terms of simple gases, organic vapours and water vapour.[1]

3.1.1 Simple gases

It is generally perceived that, for the diffusion of simple gases through polymer films, Henry's law is obeyed. This implies that the diffusion coefficient is independent of the gas concentration, resulting in a linear relationship between the percentage mass uptake and the partial pressure of the penetrant.[2] Such behaviour is due to the lack of interaction between the gas and polymer. The diffusion coefficient is therefore dependent on the nature of the penetrant (gas), the nature of the polymer and the temperature only.

Table 3.1: Diameters of simple gases [1]

Simple Gas	Diameter (Å)
H_2	2.34
He	2.65
Ne	2.80
O_2	2.92
NH_3	3.08
CO	3.12
CH_4	3.23

The diffusion coefficient of different gases through the same polymer film is dependent on the diameter of the specific gas molecules (refer to Table 3.1 for diameters of simple gases). According to the diffusion mechanism of Barrer, larger diameter gas molecules would require higher activation energy to form larger holes through which the diffusing molecules could move, therefore resulting in a smaller diffusion coefficient.[3]

3.1.2 Organic vapours

The molecular mechanism required for the diffusion of organic vapours through polymer films is different to the molecular mechanism of extremely small penetrants. This difference can be attributed to the large molecular size of organic vapours relative to the monomer unit within a specific polymer, compared to the smaller size of simple gases and water vapour relative to the

31

monomer unit within a specific polymer. The two molecular mechanisms of diffusion can be defined as follows:

Molecular mechanism for small penetrants: For small molecules with weak thermodynamic interaction between the penetrant and the polymer (typically simple gases such as hydrogen, argon, nitrogen and carbon dioxide, as well as water vapour in a hydrophobic polymer matrix), a limited rotational oscillation of one or two monomer units is sufficient to allow a cross-section that is large enough for a penetrant molecule to jump thermally from one position to an adjacent position.

Molecular mechanism for large penetrants: Penetrant molecules with a size comparable or larger than a monomer unit of the polymer requires the movement of an entire polymer segment (referred to as a cooperative movement by the micro-Brownian motion of several monomer units) before diffusion of the penetrant can take place.

The sorption and permeation process of organic vapours through polymer films is therefore a diffusion-controlled process. As polymer chain mobility is temperature dependent, an increase in temperature would result in increased micro-Brownian motion of polymer chain segments and consequently result in an increase in the diffusion coefficient. This process is markedly different below and above the T_g of the specific polymer film.

Apart from the relative size of the penetrant, its shape is also important. For the same molecular volume, elongated or flattened organic vapours such as n-alkanes have significantly high diffusion coefficients compared to spherical penetrants. Berens and Hopfenberg attributed this to the ability of elongated penetrants to move along the long dimension of glassy polymer chains during diffusion.[4]

In summary it can be said that the diffusion of organic vapours through polymers is dependent on the nature of the penetrant, the nature of the polymer, the temperature and the concentration of the penetrant.[2]

3.1.3 Water vapour

Water molecules are relatively small and have strong association through hydrogen bonding due to their highly dipolar nature. As a result, strong localized interactions would occur with suitable polar groups within a polar material, while clustering of sorbed water molecules may be found in non-polar materials where sufficient space is available between the polymer chains. In general it is said

that the solubility of water in a polymer is dependent both on the concentration and the type of polar groups in the polymer matrix. This phenomenon, together with the different molecular diffusion mechanisms due to the significantly smaller size of water vapour compared to other penetrants, distinguishes water vapour from other organic vapours in terms of its impact on the diffusion coefficient. Three types of mechanisms have been identified whereby the sorption of water molecules in a polymer matrix can be explained:[5]

Single water molecules are present in the polymer matrix, showing little affinity for neither other water molecules nor the environment of the polymer matrix. At low water vapour concentrations, this behaviour resembles Henry's Law.[1, 5]

Aggregated water molecules are observed where water molecules associate strongly with other water molecules to form clusters of water in the polymer matrix. This phenomenon is generally observed at higher water vapour concentrations with hydrophobic polymers, although some hydrophilic polymers can contain clusters of water where the concentration of water molecules exceeds the number of sites available on the polymer for polymer-penetrant interactions.[1, 5] This phenomenon is responsible for the deviation from Henry's Law.

Localized interactions are observed where water molecules can either associate with other water molecules, or with polar groups in the polymer matrix. These interactions are generally associated with hydrophilic polymers.[1, 5]

3.2   The impact of temperature on sorption behaviour

The external temperature in relation to the glass transition temperature of the polymer is an important factor to consider when determining the sorption behaviour of polymer films. The diffusion of small molecules in rubbery polymers, i.e. T>T_g, is a thermally activated process. The transport coefficients (*P*, *D* and *S*) are given by the Arrhenius relationship for a narrow temperature range (See equations 3.1-3.3):[6]

$$S(T) = S_0 exp\left(-\frac{\Delta H_S}{RT}\right) \qquad\qquad (3.1)$$

$$D(T) = D_0 exp\left(-\frac{E_D}{RT}\right) \qquad\qquad (3.2)$$

$$P(T) = P_0 exp\left(-\frac{E_P}{RT}\right) \qquad\qquad (3.3)$$

where S_0, D_0 and P_0 are the pre-exponential factors representing the solubility coefficient, diffusion coefficient and permeability coefficient at zero concentration of the penetrant, ΔH_S is the heat of solution needed for dissolution of a penetrant molecule in the polymer matrix and E_D and E_P are the apparent activation energies of the diffusion process and permeation process respectively, R is the universal gas constant (R=8.314472 J.K^{-1}.mol^{-1}) and T the temperature.[6, 7] From these relationships it follows that the apparent activation energy of permeation equals the sum of the apparent activation energy of diffusion and the heat of solution:

$$E_P = E_D + \Delta H_S \qquad\qquad\qquad\qquad\qquad (3.4)$$

Solubility coefficient

The heat of solution ΔH_S may be expressed as the sum of the molar heat of condensation, ΔH_{cond} (small negative term) and the partial molar heat of mixing, ΔH_1 (small positive term). Based on its heat of solution, gases and vapours will result in either an increase or a decrease of the solubility coefficient as a function of increasing temperature:

- For gases well above its critical temperature[1] (e.g. H_2, N_2, O_2 at room temperature) the heat of solution is governed by the partial molar heat of mixing. This results in a positive term and therefore an increase in the solubility coefficient with an increase in temperature.

- For more condensable gases and vapours (e.g. CO_2, SO_2, NH_3 and hydrocarbons), the heat of solutions is a negative term as it is largely governed by the molar heat of condensation. This results in a decrease in the solubility coefficient with an increase in temperature.

Diffusion coefficient

For the diffusion coefficient the activation energy is always a positive value as it represents the amount of energy required by a penetrant molecule to jump from one position to the next. The diffusion coefficient increases with an increase in temperature and can be related to an increase in free volume of a polymer as a result of increased segmental mobility. Due to the strong cohesive forces between the polymer chains, the activation energy is also increased.

---

[1] The critical temperature of a gas is the temperature above which a gas cannot be liquefied by application of pressure. A gas will remain as gas above this critical temperature, and in order to liquefy it by compression, the gas must be cooled to its critical temperature. The critical temperature is denoted by T_c.

The pre-exponential factor, D_0, is entropic by nature, taking the length of the jump of a molecule from one position to the next into consideration, and increases with an increase in penetrant size. It can be calculated from the following expression:[3, 6]

$$lnD_0 = aE_D + b \qquad\qquad (3.5)$$

Here a and b are coefficients dependent on the penetrant type for a given polymer. Although the activation energy is independent of temperature over small temperature ranges, it is dependent of temperature over larger temperatures range where it follows the *Activated Zone Theory* of Barrer[2]. The activation energy can be expressed as the sum of two terms:

$$E_D = E_D(C \rightarrow 0) - \gamma RT \qquad\qquad (3.6)$$

The first term ($E_D(C \rightarrow 0)$) represents the apparent activation energy for diffusion in a polymer matrix unaffected by the penetrant, while the second term (γRT) quantifies the amount by which the activation energy is reduced as a result of plasticization of the polymer matrix by the penetrant.[6, 7]

3.3   The impact of polymer properties on sorption behaviour

For a given penetrant and temperature, the gas or vapour sorption behaviour of a specific polymer is determined by its chemical and physical properties.[8] Due to the nature of polymers, it is almost impossible to view the impact of these factors on the sorption behaviour of polymers individually. Various characteristics of polymers, including the nature of solvent-based and water-based polymer coatings, its chemical composition and physical properties, the use of additives such as surfactants and fillers in polymers, and multilayer polymer films are discussed in this section and the role of these factors relative to sorption behaviour are highlighted.

3.3.1 Water-based versus solvent based coatings

During the past 60 years a movement from solvent-based coatings to water-based coatings, through the production of latexes, was driven largely by environmental concerns. Advantages of utilizing water as the reaction medium include a reduction of cost, elimination of working with large volumes of often hazardous solvents, the ability to achieve high molecular weight polymer latexes with high

---

[2] Activated Zone Theory of Barrer: Increase in temperature results in an increase in chain entropy. The activated zone is therefore larger and the chain mobility enhanced, resulting in an increase in E_D.

solids contents while maintaining a low viscosity, and excellent heat transfer properties. It also allows for better control of the polymer morphology, allowing for the synthesis of core-shell type morphologies through semi-batch polymerisations and high levels of polymerization control through living controlled polymerisation techniques.[9-12]

The classical emulsion polymerization process is defined as the polymerization of monomer dispersed in an aqueous solution of surfactant, using mostly water soluble initiator systems. It exhibits three distinct kinetic phases during polymerisation:[13, 14] Phase I represents the particle nucleation phase, where polymer particles can be formed by heterogeneous particle nucleation (entry of radicals into micelles), homogeneous particle nucleation (oligomer formation in the aqueous phase), or radical entry into monomer droplets. The relatively large size of monomer droplets (1-10 μm) compared to that of monomer-swollen micelles (10-20 nm) result in a relatively low specific surface area for monomer droplets in comparison with monomer-swollen micelles. As a result, the probability that particle nucleation will take place via free radical entry from the water continuous phase in the monomer droplets is low compared to monomer-swollen micelles. Particle nucleation therefore mainly occurs in the micelles. Phase II is characterized by a constant rate of polymerization due to migration of monomer through the water phase from monomer droplets to nucleation sites. Phase III in classical emulsion polymerization starts at the point where all monomer droplets have been depleted and the remaining monomer in the nucleation sites is consumed. A reduction in the conversion rate is associated with this phase.

Miniemulsion polymerization, initially studied by Ugelstad and co-workers during the 1970s, reduced the requirement for the diffusion of monomer from the monomer droplets to the nucleated monomer-swollen micelles by increasing the surface area of monomer droplets and therefore increasing the probability of monomer droplet nucleation. Many reviews have been published in which the kinetics and key applications of this technique are discussed.[15-19] Miniemulsions consist of monomer dispersed in an aqueous phase, with a surfactant and a co-stabilizer, and are prepared through a 2-step mechanical process, whereby the droplets are deformed and disrupted to increase the specific surface area of the emulsion.[15-17] This process results in submicron-sized monomer droplets (50-500 nm). Kinetics of the miniemulsion polymerization process is also described by three phases: phase I, where, in the ideal case, particle nucleation takes place solely in the monomer droplets due to its small particle size, although secondary nucleation has been seen in the non-ideal case where new particles form according to the same mechanism as in classical emulsion polymerization; phase III, representing the monomer consumption in the monomer droplets; and phase IV, which is referred to as the gel peak due to a viscosity increase.

The absence of phase II kinetics of the polymerization process can be attributed to the nucleation of all monomer droplets due its sub-micron particle size and therefore large surface area, as well as the critical stabilization of monomer droplets with a co-stabilizer, preventing the migration of monomer from one droplet to another. The consequence of this is that extremely hydrophobic monomers could easily be incorporated into polymers.

Miniemulsions have been shown to exhibit greater shear stability compared to classical emulsions; they have lower viscosities; and they exhibit greater salt stability. Several drawbacks are however also associated with the miniemulsion polymerization technique. The small size of the particles require the addition of a co-stabilizer as well as higher surfactant loadings compared to what is required for classical emulsion polymerization. These additives can adversely affect the final properties of latex films. This technique is also limited with respect to the range of particle sizes that can be achieved, and results in a broader particle size distribution.[17]

3.3.1.1 Film formation of coatings

The film formation mechanism for both solvent and aqueous based systems has been studied extensively due to its industrial importance in the paints and coatings industries.[20, 21] Physical and mechanical properties of films are influenced by (1) the nature of the polymer; (2) the method of preparation of the polymer; and (3) the method of preparation of the film and the conditioning thereof.[20] It is therefore important to understand the impact of these factors on the final film properties for different polymer systems investigated.

Water-based latex systems consist of two distinct phases: an aqueous carrier phase and a polymer phase which is stabilized with surfactant. Solvent-based systems, on the contrary, consist of a single phase where the polymer is truly dissolved in the solvent. Based on this, film formation differs in terms of the following key factors:

> *Evaporation of the carrier fluid:* The evaporation of water from of latex film initially happen at the same rate as water would evaporate on its own, after which the rate is significantly reduced. Contrary to this, the evaporation of solvent from solvent-based polymer systems follows a Fickian desorption behaviour as the solvent moves through the homogeneous solution to the surface. Removal of the final traces of solvent from the film can be challenging, as the solvent may plasticize the film. This can be overcome by drying the film at elevated temperatures, using vacuum, or by having long drying periods.[20, 22]

Dependence on the minimum film formation temperature (MFFT): While film formation of latex cast films are dependent on the T_g and MFFT of the polymer, solvent based systems are independent of these factors and can form films at any temperature as the solvent can act as a coalescing agent.[20]

3.3.1.2 Mechanism of film formation from latex

Latex film formation is a multistep process which is typically described by a water evaporation phase, followed by particle deformation and particle diffusion.[20, 21, 23, 24] This 3-step process has been established using mostly gravimetric methods to monitor the evaporation of water from the latex phase to the continuous film phase. These water evaporation phases are depicted by a sigmoidal curve and have been classified by Vanderhoff et al. as the three stages of the drying process (refer to Figure 3.1):[25, 26] Further research by Alig et al. Identified a fourth phase of film formation which will also be discussed here.[27]

Stage I: Water evaporation: During the first stage, water evaporates from the latex surface, resulting in a concentrating effect and an increase in the solids content. Stage I is the longest of the three stages and continues until the volume of the latex has been reduced by 60-70% of its original volume.[20] The rate of evaporation is independent of the solids contents of the latex, or the presence of additives such as surfactants and occurs at the same rate of water evaporation alone.

Stage II: Particle deformation: In the early 1950s already Dillon et al. developed the first theory to explain particle deformation, which stated that the main force leading to the formation of contact between two adjacent particles is the energetically favourable driving force to reduce the overall surface area.[28] It was however the theory of Brown in 1956 that laid the foundation for further developments in the theory of film formation. His theory contrasted with that of Dillon's in three key areas, with the following not taken into consideration by Dillon: (1) film formation only occurred as water progressively evaporated; (2) that films that formed below the minimum film formation temperature (MFFT) were different in appearance when compared to film that formed above the MFFT; and (3) slightly crosslinked latexes may still form a continuous film, even though a viscous flow is no longer possible. This leads to Brown's definition of film formation in terms of the three stages of film formation that are commonly known to today. Since this, several other theories have also been put forward to explain the deformation of particles during film formation.[29]

The particle deformation stage marks the point where particles first make irreversible contact with each other. During this stage the particle shape also changes to a hexagonal structure, thereby

maximizing the contact area between adjacent particles. The rate of water evaporation is significantly lower during the second stage.[20]
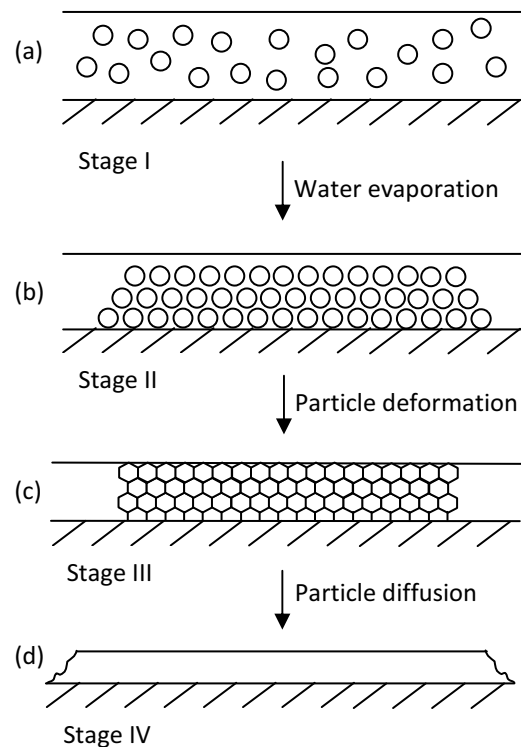
Figure 3.1: Schematic diagram of latex film formation: (a) Stage I, where the latex particles are dispersed in water, (b) Stage II, latex particles contact each other, (c) Stage III, latex particles deformation, and (d) Stage IV, coalesced latex film.[21]

Stage III: Particle diffusion: The formation of a continuous film only starts during the final stage of film formation. During this stage the remaining water will first evaporate from the film via inter-particle channels, after which the remainder will evaporate from the film through diffusion of the water vapour through the continuous polymer film. The rate of diffusion would be reduced by the presence of impermeable sections in the polymer film (e.g. platey additives), or the presence of hydrophilic components which would results in polar interactions.[20]

Stage IV: Viscoelastic changes: After the latex film has formed, further isothermal time dependent viscoelastic changes continue to take place within the polymer matrix. Alig et al. developed an ultrasonic shear wave reflection technique to monitor changes in the viscoelastic properties (storage modulus G' and loss modulus G") as a function of time.[30, 31] Apart from indicating the time when stage III is completed, this technique also indicates the time at which crystalline regions will form in semi crystalline polymers and as well as the concentration of these crystalline regions.

3.3.1.3 Key factors affecting latex film formation and final film properties

Several factors impact on the film formation and final film properties of specific latexes. These factors can either be internal to the latex itself, e.g. particle size, coalescing agents and type of surfactant, or it can be induced by external factors such as the temperature at which the film is formed and also the substrate onto which the film is cast.

Influence of temperature: Film formation is dependent on the minimum film formation temperature (MFFT) of the polymer in question and is unique to each polymer system. The MFFT is either slightly lower or slightly higher than the T_g of the specific polymer system in question. Film formation will only take place once the external temperature reaches the MFFT. At this temperature a sharp change in the elastic modulus of the polymer is observed.[13, 29]

Influence of particle size: Two aspects of the polymer particle size in latexes can have an impact on the film formation properties: (1) the absolute particle size of relatively monodisperse latexes; and (2) the use of bimodal latexes for enhanced film formation.[29]

Different models have been developed to describe the relationship between the particle diameter of latexes and its final film properties. These models all predicted a reversed proportionality between the extent of deformation and the particle size of the latex particles.[29]This is due to the greater inter-particle contact of small particles compared to larger particles during the water evaporation and particle deformation phases. Chain entanglement can therefore occur more effectively, resulting in good film integrity.

Bimodal distributions have shown to enhance film formation significantly. This could be attributed to greater deformation of large polymer particles as a result of the smaller polymer particles, or due to the placement of the smaller particles in the openings between large polymer particles.[29]

Influence of water: Several inconclusive theories have been formulated to describe the role of water during the film formation process.[29] The theory of Sperry et al. evaluated the role of water in both hydrophobic and hydrophilic polymer systems and was able to conclude that water played a key role in plasticizing the polymer, thereby enhancing chain entanglements in hydrophilic systems due to the interactions between the two phases.[32] This phenomenon is however limited or non-existent in hydrophobic polymer systems.

Influence of coalescing agents: The addition of volatile organic compounds (VOCs) into lattices is a common procedure in the paints and coatings industries to enhance film formation and improve film finishing.[20, 33] It reduces the elastic modulus of the polymer, provides temporary plasticization and promotes chain entanglement. The ease, with which the VOC is removed during film formation, is dependent on its molecular size and polarity. A more polar VOC would have a preference for the aqueous phase and would evaporate with the water phase, whereas a non-polar VOC would exhibit a preference to reside in the polymer matrix.[20]When choosing a coalescing agent, it is important to select a VOC that will penetrate into the polymer particle and not evaporate before the water evaporates, as the VOC must still be present during Stage II and III to enhance chain entanglement during the film formation process. VOCs typically used as coalescing agents include glycol derivatives, acetates and ethoxy alcohols. Due to environmental concerns and legislation limiting the emissions of VOCs, researchers such as Lahtinen et al. have now started developing reactive coalescing agents to reduce the risks associated with VOCs in paints and coatings.[33]

Influence of surfactants: The properties of a surfactant are of key importance in determining the final polymer film properties. The three main factors to consider are:[29]

The compatibility of the surfactant molecules with the polymer particles: Poor compatibility between the surfactant and the polymer would result in the migration of the surfactant to the film/air and film/substrate interfaces. Good compatibility would however have the opposite impact, where the surfactant is retained within the polymer matrix.

The degree of adsorption of the surfactant onto the polymer particle: Migration of the surfactant to the surface of the film, i.e. the film/air interface, is necessary to ensure good polymer chain entanglements between adjacent particles. Should the surfactant be grafted to the polymer chains, e.g. with reactive surfactants, it may hinder the diffusion of polymer chains and therefore also the chain entanglements. This could potentially result in poor film integrity.

The evaporation rate of water at the water/air interface: In cases where the evaporation of water at the film/air interface is slow compared to the diffusion of water between the polymer/polymer interfaces, a concentration effect of surfactant may occur at the film/air interface.

41

Based on the above factors, surfactants can migrate into the polymer particles, thereby reducing the elastic modulus; it can form concentrated areas of surfactant within the polymer film; it can migrate to the film/air and film/substrate interface; or it can be retained within the polymer matrix to form a hydrophilic network within the film.[29]

The position of the surfactant during film formation can be determined by a variety of Fourier Transform Infra-Red (FTIR) spectroscopy techniques. Amalvy and Soria [34] successfully used conventional FTIR spectroscopy, as well as Attenuated Total Reflectance (ATR) FTIR to determine the migration of sodium dodecyl sulfate to the film/air and film/substrate interfaces respectively. Studies were also conducted by Niu and Urban [21]to determine the impact of different substrates on the migration of surfactant to the film/air and film/substrate interfaces. They used both ATR-FTIR and Step Scan Photo-acoustic (S^2-PAS) FTIR spectroscopic techniques for this purpose.

Influence of substrates used for film preparation: When considering the industrial application of coatings, excellent adhesion properties to the substrate are required. However, free films are often required for the characterization of polymers in terms of properties such as diffusion and permeation, tensile strength, elasticity, etc. The adhesion requirements for free films are very different, as poor adhesion is required to ensure that films can be removed from the substrate they were prepared onto, without affecting the film integrity.[20, 35] A variety of substrates have been explored for this purpose: amalgamation of the substrate with mercury (tinfoil and silver-plated glass have typically been used), casting onto a glass surface and also poly-(tetrafluoroethylene) (PTFE).[21, 35, 36]

The surface tension of the substrate compared to that of the polymer can play a key role in determining the direction of surfactant exudation. Urban and Evanson evaluated films of poly(ethyl acrylate-*co*-methacrylic acid) copolymer stabilized with sodium dioctylsulfosuccinate cast onto different substrates (See Figure 3.2). Mercury resulted in the largest concentration of the surfactant at the film/substrate interface, while PTFE resulted in moderate exudation of surfactant to the film/substrate interface and glass resulted in little to no surfactant exudation.[21]
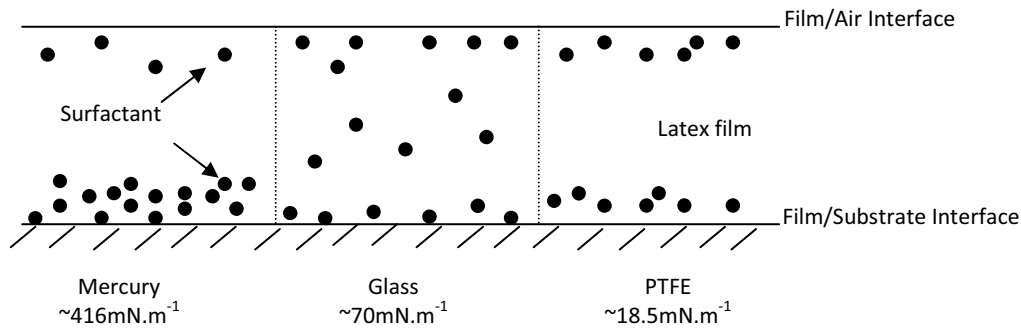
Figure 3.2: Schematic diagram of the surface tension effect on the surfactant exudation across the latex film when prepared on substrates with different surface energies (γ_{sv}).[21]

3.3.1.4 Relevance of solvent-based and water-based coatings to sorption properties

Several evaluations showed that solvent cast films have different barrier performance to latex cast films of the same polymer. Roulstone et al. found that latex and solvent-cast films from a poly(butyl methacrylate) surfactant-free latex exhibited two-sidedness in terms of water, water vapour and nitrophenol permeability.[37] This phenomenon was attributed to film asymmetry where latex-cast films have a higher surface roughness at the film-air interface and therefore a higher effective surface area resulting in higher permeability of penetrants at the film-air interface, while solvent-cast films have higher polymer density at the film-air interface due to the film formation process, resulting in lower permeability to penetrants at the film-air interface. The overall permeability of solvent-cast films was lower than that of latex-cast films. Similar observations were made by Okubo with respect to urea permeation for solvent-cast films.[38] Film orientation is therefore crucial in interpreting permeation properties of films.

Studies also showed that aging of latex-cast films result in improved permeability properties. This phenomenon could be attributed to further coalescence of the polymer chains, resulting in an increase in the polymer density along particle interfaces. This phenomenon was not evident for solvent-cast films.[37]

3.3.2 Surfactants used in heterophase polymerisations

The change from solvent-based coatings to water-based coatings required various low molecular weight additives to ensure good performance of films cast from emulsion, e.g. pigment dispersants, rheology modifiers, leveling additives, antifoams, coalescing agents and surfactants.[39] Extensive

43

studies in the field of paints and coatings (including edible coatings for preservation of food) have been done to elucidate more on the impact of these additives on the final properties, including barrier properties, of the latexes and films.[40-44]

Surfactants are used to stabilize immiscible phases in heterophase polymerization and are defined as surface active agents consisting of both a hydrophobic and hydrophilic moiety. The hydrophobic moiety is normally a long alkyl chain, whereas the hydrophilic section constitutes a functional group.[45] Surfactants can be classified in terms of their ionic charge as anionic, non-ionic, cationic or ampholytic[3] in nature.[46] Anionic, cationic and nonionic surfactants have successfully been used in miniemulsion polymerization.[47] The concentration of surfactant required however varies, with ionic surfactants requiring less surfactant to prevent coagulation than non-ionic surfactants. The surfactant concentration is furthermore directly influencing the monomer droplet size and would therefore also impact on the particle nucleation, polymerization rates and particle size.

3.3.2.1 Latest research trends in surfactants for heterophase polymerisation

During the past two decades surfactant research for heterophase systems largely shifted from conventional surfactants to focus on reactive surfactants.[48-55] Reactive surfactants, also referred to as non-migratory surfactants, contain a functional group that can act as initiators (inisurfs), chain transfer agents (transurfs) or polymerizable surfactants (surfmers) in a free radical polymerization process, resulting in them being incorporated into the polymer chain.

Reactive surfactants have several advantages over conventional surfactants in terms of both latex and final film properties:[48, 55] (1) surfactant-related problems with latex stability arising from factors such as particle concentration, temperature, electrolyte concentration and pH are minimized; (2) destabilization of the adsorption-desorption equilibrium of surfactant in a latex is reduced when the latex is blended with additives, such as a clay slurry containing a different surfactant or dispersing agent; (3) migration of surfactant to the air-film and air-substrate interfaces are reduced with reactive surfactants, as the surfactant is incorporated into the backbone of the polymer; (4) reactive surfactant buried in the bulk of the polymer particles may act as coalescing agents, improving film forming properties; (5) and the oxygen demand in water used to flocculate lattices in e.g. the rubber industry is reduced.

---

[3]An ampholytic surfactant is also known as an amphoteric surfactant. It contains dual functional groups in the same molecule, which, depending on the pH allows it to exist either in its cationic, anionic or nonionic state.

A significant amount of research was done in the field of reactive surfactants in the program "Human Capital and Mobility" sponsored by the European Union during the 1990s. This program, called "Reactive surfactants in heterophase polymerization for high performance polymers", was executed across 7 research institutes and covered various challenges of reactive surfactants. Due to the extensive nature of this project, the work published in this regard was viewed as being representative of typical research done in the field of reactive surfactants for heterophase polymerizations during that time.[49]

The reactivity of anionic surfmers was evaluated using a model copolymer system consisting of styrene, butyl acrylate and acrylic acid. Acrylate, maleate and crotonate-based surfmers were evaluated in terms of their reactivity and it was found that the maleate-based surfmer exhibited the preferred reactivity, achieving high conversions with high stability and no homopolymerisation of the surfmer. This research did however not lead to the identification of a surfmer with ideal surfmer behaviour, namely being unreactive at low conversions and reactive at the end of the reaction. It was found that the reactivity of surfmers can be controlled by changing the reactivity of the main monomers through the addition of less reactive main monomers towards the end of the polymerization or by inducing a change in the reactivity of main monomers based on the reactivity of the monomers. A key outcome of this research program was the development of a mathematical model that can be used for the exploration of surfmer reactivity in emulsion polymerization.

Polymerization of the surfactant in the water phase, the relative reactivity of the reactive surfactants compared to the main monomers, and the contribution to coalescence by the reactive surfactants were evaluated.[55] The relative position of the reactive group was also studied, comparing a maleate based surfactant with a crotonate-based surfactant, and changing the relative position of the reactive group from the hydrophilic moiety to the hydrophobic moiety or in between the two moieties.

Another field of surfmer research is that of surfmers containing a counterion. One such development was a surfmer with an organic polymerizable counterion located either in the cation component or the anion component.[56] Key benefits of this type of surfmer include ease of preparation, low cost and effective copolymerization of the surfmer with model monomers such as styrene to ensure good stability of the final latex. Cationic and zwitterionic polymerizable surfactants were also developed by Abele et al. where the surfmer consisted of a maleic anhydride derivative with an inorganic counterion (hydrogen sulfate, allyl or halogen group).[57] It was found that for cationic surfactants hydrogen sulfate and allyl groups were more effective than a halogen counterion as very low

conversions were achieved with the latter. The particle size was very small, although it had a large particle size distribution. On the other hand the zwitterionic surfactants had a larger particle size and performed overall better than the cationic reactive surfactants.

3.3.2.2 Impact of low molecular weight additives on sorption behaviour of polymers

The impact of low molecular weight additives on the sorption properties of liquids into latex films have been reported in the literature. Significant focus has been given to the sorption of water into films containing conventional or reactive surfactants. Some of the key findings include:

Butler et al. compared the water sensitivity of poly(butyl acrylate-*co*-methyl methacrylate) latex films stabilized with ionic, polymeric and electrosteric surfactants. Although limited information was generated on the transport mechanism, the study showed that properties such as the surfactant mobility, its crystallinity and polarity are key factors that would contribute to increased water absorption.[24] In another study, the impact of latex stabilization on water absorption was evaluated by comparing sodium dodecyl sulfate (SDS), a conventional anionic surfactant, with a maleate diester surfmer. Both surfactants resulted in Sigmoidal kinetic behaviour, with the surfmer resulting in a higher diffusion coefficient compared to the conventional surfactant. It was suggested that this phenomenon was due to the immobilization of the surfmer throughout the film which facilitated rapid penetration of the water molecules through the film. Conventional surfactants migrate during film formation to form surfactant aggregates in the film and at the film-air and film-substrate interfaces. Diffusion is therefore more difficult as the water molecules must diffuse from one surfactant aggregate region to another, passing through regions of hydrophobic polymer. Despite this, the overall water uptake of the SDS stabilized film was higher.[51] Steward et al. evaluated the transport mechanism of various penetrants using films that contained low levels of leachable additives such as surfactants or plasticisers.[58] They found that (1) the transport mechanism could occur via the normal activated solution-diffusion model described earlier; (2) it could take place through aqueous pathways that form a porous structure due to leaching of additives or due to the interaction between hydrophilic polymer components with the aqueous phase; or (3) transportation could take place via a combination of both mechanisms.

Gas and vapour sorption studies have also been done to quantify the impact of low molecular weight additives on latex film sorption and permeation properties. Limited information is however available. A series of experiments were done by Roulstone et al. to determine the impact of 3 different types of conventional surfactants (anionic, cationic and nonionic surfactants) on permeation properties of poly(butyl methacrylate) films.[59] Surfactants chosen had the same

hydrocarbon chain, differing only with respect to its head group. Weight loss curves were used to determine the water vapour permeability coefficients for the different configurations, comparing the coefficients for the film-air interface and the film-substrate interface. It was found that the type and concentration of surfactant used impacted significantly on the water vapour permeability. The film-air interface facing the high humidity side generally exhibited greater permeability coefficients compared to when the film-substrate interface was exposed to the high humidity side. In general permeability increased for increasing concentrations of SDS due to phase separation and surfactant exudation during film formation; incompatibility of the cationic surfactant dodecylethyldimethyl ammonium bromide with the polymer resulted in high permeability values; and the nonionic surfactant dodecyl tetraoxyethylene glycol monoether resulted in high permeability values due to its hydrophilic nature and plasticising effect on the polymer.

Very little information regarding the water vapour sorption or permeation properties of films prepared from latexes stabilized with surfmers is available. In a study by Aramendia et al. the water uptake, water vapour uptake and water vapour permeability of poly(methyl methacrylate-*co*-butyl acrylate) polymers were evaluated by comparing a nonionic conventional surfactant (NP30, a nonyl phenol ethoxylate surfactant containing 30 ethylene oxide units) with nonionic reactive surfactants (alkenyl succinic anhydride condensates containing 34 and 35 ethylene oxide units respectively) and an anionic surfactant (sodium dodecyl diphenyloxide disulfonate).[60] The surfmer stabilized latex films gave intermediate water absorption, with the NP30 giving the lowest water absorption due to desorption and migration of the surfactant into the water phase. Water vapour permeability was significantly higher for latex films stabilized with conventional surfactants where the film-air interface faced the high humidity, suggesting that the migration of these surfactants resulted in defects that promoted water vapour absorption. NP30 stabilized latex films had the lowest water vapour permeability where the film-substrate interface faced the high humidity. Limited information was however supplied in terms of the water vapour transport mechanisms through the latex films.

Surfactants have also been used extensively to increase the hydrophobicity of edible coatings used to maintain the quality of both fresh and processed fruits and vegetables, where films are used to prevent water loss, thus extending the shelf-life of the products.[41, 42] These edible films are normally manufactured using e.g. proteins and polysaccharides with additives such as fatty acids, natural waxes or surfactants to impart the water barrier properties. Gravimetric methods have been used to quantify the permeability of these edible films to water vapour.

3.3.3 Polymer properties

The monomers selected for the synthesis of polymers determine key properties such as polarity, degree of crystallinity, ability to crosslink, and its thermal properties. The impact of these properties on the sorption behaviour of polymers is discussed.

3.3.3.1 Chemical composition of polymers

The chemical composition of a polymer determines its polarity and therefore the solubility of penetrants in the polymer film, its density, the degree of hydrogen bonding between adjacent polymer chains and its free volume. Typical polar functional groups that could be incorporated to enhance hydrogen bonding within a polymer are summarized in Figure 3.3.

The nature of the functional groups may also impact on other properties of the polymer, resulting in a restriction in the mobility of the polymer chains. As a result, both the solubility and diffusion coefficients are affected by the chemical composition of the polymer.
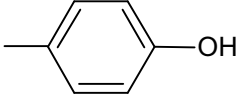
Figure 3.3: Typical polar functional groups to enhance hydrogen bonding

a)   Solubility coefficient

The solution-diffusion model requires that the penetrant absorbs into the polymer film through chemical affinity or through solubility of the penetrant in the polymer film. The extent to which this process takes place is quantified by means of the solubility coefficient.

Simple gases generally show no interaction with the polymer and are generally diffusion-driven. For vapours that interact with the polymer, however, the solubility coefficient is especially significant.

This is seen by the deviation from Henry's law due to the penetrant concentration dependence when evaluating permeability of vapours through polymer films. Increased polarity would, for example, enhance the solubility of water vapour in the polymer film, resulting in increased permeability of the membrane.

The permeation of water vapour through polymer systems with different degrees of polarity varies greatly due to the varying degree of interaction between the polymer and the water vapour molecules. Polymers such as poly(vinyl alcohol) and cellulose acetate have high water absorptions due to their high polarity (permeability of 4200 cm^3(STP)(mmx10^8)/(cm^2.s)(cm Hg) and 550 cm^3(STP)(mmx10^8)/(cm^2.s)(cm Hg) respectively), while significantly lower water absorption is observed for hydrocarbon polymers such as polystyrene and poly(vinyl chloride) (permeability of 12 cm^3(STP)(mmx10^8)/(cm^2.s)(cm Hg)and 6.1 cm^3(STP)(mmx10^8)/(cm^2.s)(cm Hg), respectively).[7]

b)   Diffusion coefficient

The chemical composition of the polymer chains determines the chain mobility and therefore also affects the diffusion coefficient. Chain mobility is controlled through attractions between adjacent polymer chains, steric hindrance due to bulky functional groups, crosslinking (refer to 3.3.3.3) and also chain entanglements which are generally affected by the chain lengths of the polymers.

Inter-chain attractions: Low polarity would result in weak Van der Waals interactions between adjacent polymer chains, whereas increased polarity would result in stronger interactions between adjacent polymer chains, with hydrogen bonding being the strongest inter-chain interaction. An increase in attraction between polymer chains would therefore result in restricted chain mobility and therefore reduced diffusion of penetrants.

Steric hindrances and chain entanglement: Bulky side chain groups (e.g. long-chain functional groups or benzene rings) and stiff polymer backbones (e.g. methacrylates) restrict backbone mobility, resulting in minimal chain movement and therefore restricting the diffusion of penetrant molecules through the polymer matrix.[61] The bulky groups also result in poor chain packing and would therefore result in increased free volume in the polymer matrix. Apart from this, it would also result in chain entanglements, thus increasing the activation energy required to generate an opening between polymer chains that would be large enough to allow a penetrant molecule to pass through. A reduction in the diffusion coefficient at a specific temperature would therefore be seen if bulky functional groups are introduced into the polymer.[62]

3.3.3.2 Rubbery versus glassy polymers

The diffusion coefficient, and therefore also the permeability, are affected by the testing temperature relative to the glass transmission temperature (T_g) of the polymer film. The diffusion coefficient increases when the polymer film is exposed to temperatures above its T_g. As a result, different models are used to describe the transport phenomena at temperatures below and above the T_g of a polymer. To understand the marked difference in the diffusion coefficient below and above its T_g, it is necessary to understand the molecular structure of a thermoplastic polymer film.

Glassy polymers (T<T_g): For the case of T<T_g, the polymer is in its glassy state where chain mobility is largely restricted. The *dual-mode sorption model*, where two penetrant populations are assumed, is generally used to describe diffusion of penetrant molecules through the glassy polymer matrix.[6, 63] The principles of this model are discussed in Chapter 2. A second model used to describe penetrant diffusion in glassy polymers is the *gas-polymer matrix model*.[64] This model was developed by Sefcik and Raucher and, in contrast to the dual mode sorption model, this model assumes a single population of penetrant molecules interacting with the polymer matrix. It is assumed that this interaction reduces the intermolecular forces between the polymer chains and facilitates the penetrant jumps between the polymer chains.

Rubbery polymers (T>T_g): Various molecular models were developed to describe the transport of penetrants through rubbery polymers, taking into consideration the relative mobility of the penetrant molecules as well as the polymer chains. Two principles were considered in the development of these models: (1) thermal activation and (2) the redistribution of free volume in the polymer matrix.

Two models have been proposed to predict transport phenomena above and below the T_g of the polymer:

(1) ***Thermal activation models:*** Several models were developed to describe the thermal activation of molecules in polymers. The initial models were only able to predict the diffusion activation energy and not the actual diffusion coefficients. These theories evolved from the Activation Zone Theory proposed by Barrer[65], to the theory of Brandt[66] where the activation energy consisted of two components (the intermolecular energy E_i and the intramolecular energy E_b) and are dependent on the penetrant diameter, the chain length involved in diffusion and the length of the elemental jump, to the theories of DiBenedetto and Paul. Two approaches were proposed by them, one applied to diffusion in glassy polymers and the other to transport in rubbery zones. Pace

50

and Datyner[67-69] incorporated the theory of DiBenedetto and Paul and the theory of Brandt into a single diffusion theory where they proposed that two mechanisms of transport exist, i.e. diffusion along the chain direction and diffusion as perpendicular jumps to the main-chain direction. The jumps across chains are viewed as the rate determining step of the transport phenomena and this will determine the activation energy of diffusion.

The thermal activation for the sorption of penetrants in polymers is described in greater detail in Section 3.1 of this chapter.

(2) *Free volume models:* Polymer volume can be classified in terms of three categories: occupied volume[4], interstitial free volume[5] and hole free volume[6]. The total polymer volume is dependent on temperature as the hole free volume increases significantly when the glass transition temperature is exceeded. The interstitial free volume also increases with an increase in temperature, but this increase is limited. Figure 3.4 illustrates the temperature dependence of polymer volume when the T_g is exceeded (not drawn to scale).

Transportation of penetrant molecules can only occur in the hole free volume of the polymer matrix. The modes of transportation of the penetrant molecules in the hole free volume are described by different models for glassy and rubbery polymers.

For glassy polymers the dual mode sorption model, where two populations of penetrant molecules are assumed, best describes the transportation mechanism through the polymer matrix. Also refer to Chapter 2 for a detailed description of the model.

Fujita and Kishimoto[2, 70] developed one of the earliest models for molecular transport through a rubbery polymer matrix due to the redistribution of free volume. It was suggested that a diffusing molecule can only move from one position to a neighbouring position if the local free volume exceeds a certain critical value.

---

[4] Occupied volume: This is the volume of the material without any free volume and is also referred to as the "Van der Waals" volume.

[5] Interstitial free volume: This free volume is actually inaccessible and is a result of the vibrational energy of polymer bonds. It increases slightly with temperature.

[6] Hole free volume: This results from volume relaxation and plasticization of the polymer when being heated and cooled. This free volume is accessible by penetrant systems and may be altered due to the adsorption and desorption of penetrants in the polymer.
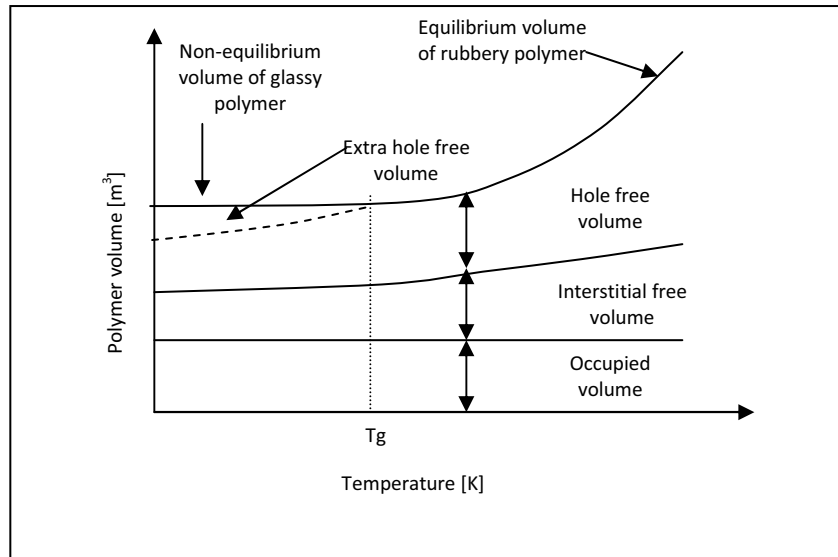
Figure 3.4: Polymer volume as a function of temperature [5]

3.3.3.3 Degree of crosslinking

Apart from secondary attraction between adjacent polymer chains through Van der Waals attraction and hydrogen bonding to restrict chain mobility, crosslinking of polymer chains through primary covalent bonds between adjacent polymer chains can further restrict chain mobility.

The impact of crosslinking on diffusion properties was first investigated by Barrer and Skirrow where they evaluated the impact of increased sulfur content on the diffusion coefficient of natural rubber.[1] It was found that for a given temperature, both the pre-exponential factor D_0 and the apparent activation energy E_D of the Arrhenius relationship for diffusion increased with increasing crosslinking (i.e. increased sulfur concentration). This increase in the activation energy required for diffusion of the penetrant molecule through the polymer matrix, would result in lower diffusion and permeation coefficients where crosslinking is introduced.

Contrary to this phenomenon, it has also been shown that an increase in crosslinking would not always result in a decrease in the diffusion coefficient, e.g. where other physical properties such as the density, fractional free volume, glass transition temperature and d-spacing (spacing between polymer chains as calculated using Bragg's Law) are independent of the crosslinking density.[71]

3.3.3.4 Degree of crystallinity

Crystalline domains in polymers result in unique physical and thermal properties, e.g. temperature dependent tackiness of films and temperature dependent sorption or permeation properties, which have resulted in specific applications in the field of agriculture, medicine and food packaging.[6, 61, 72-77]

Two types of crystallinity exist in polymers: main-chain crystallinity and side-chain crystallinity (See Figure 3.5).[61] Crystalline regions can originate from linear polymers where alignment of the polymer backbone results in main-chain crystallinity, e.g. polyethylene or polycaprolactone. Alternatively, crystallinity can be introduced into an atactic polymer matrix by incorporating vinyl monomers with linear side-chains in excess of 10-12 carbon atoms into the polymer, e.g. poly *n*-alkyl acrylates and methacrylates, poly(vinyl esters) and poly-*N*-*n*-alkylacrylamides. Due to the linear nature of these side-chains, crystallization occurs within these pendent groups and is referred to as side-chain crystallinity. A special case of polymer crystallinity is where a combination of backbone and side-chain crystallinity is obtained with highly crystalline isotactic poly-1-alkenes.[27, 78-81]
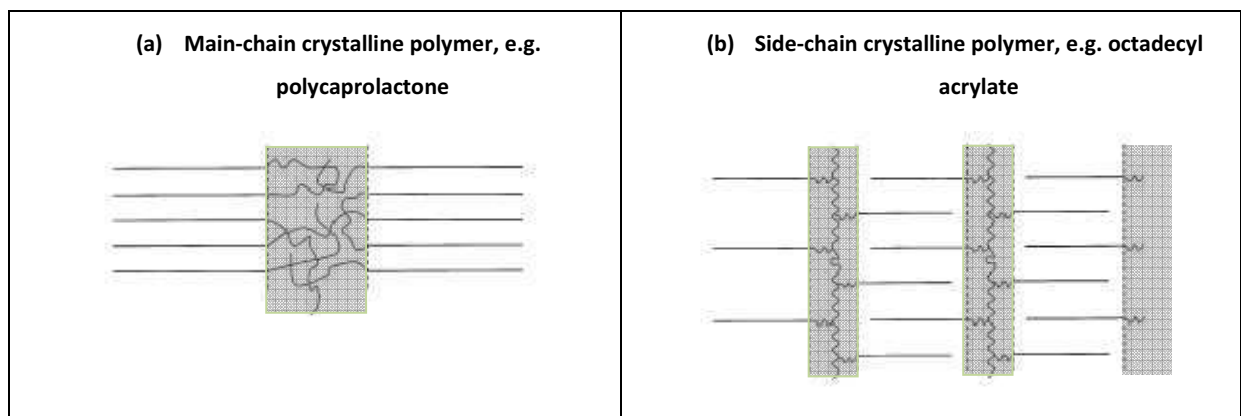
Figure 3.5: (a) Main chain crystallinity versus (b) side-chain crystallinity[61], where the grey areas indicate amorphous regions between the crystalline regions.

Sorption and diffusion are limited to amorphous areas within a polymer matrix when the temperature is well below the melting point of crystalline domains in a semi-crystalline polymer matrix. Crystalline regions in polymer matrices are therefore excluded from the polymer volume for sorption of gases or vapours and are consequently viewed as being impermeable.[7] Michaels and Bixler developed a 2-phase model for main chain semi-crystalline polymer systems such as polyethylene, assuming the crystalline regions to be impermeable.[82] Based on this model, the solubility coefficient is expressed as follows:[83-85]

53

$$S = S^* \alpha \qquad\qquad (3.7)$$

Here S is the solubility coefficient of the polymer, S^* is the solubility coefficient of the 100% amorphous polymer and α is the amorphous volume fraction. This model was applied successfully to other polymer systems such as polyethylene terephthalate, while polymer systems such as semicrystalline syndiotactic polystyrene showed evidence of sorption in both the amorphous and crystalline regions, thus disproving the 2-phase model from Michaels and Bixler.[84-89] Based on the findings for these and other polymer systems, it was deduced that there is not a clear distinction between the amorphous and crystalline regions and that the crystalline regions impact on the chain mobility of the polymer in the amorphous regions.[90]

The diffusion of gases or vapours is affected in two ways by the presence of crystalline areas. Firstly, crystalline areas increase the effective path length of the gas or vapour (also referred to as the tortuosity factor), and secondly the mobility of the amorphous phase is restricted by the presence of crystalline regions (referred to as the immobilization factor). This results in an increase in the activation energy of diffusion and would result in a reduced diffusion coefficient.[6] Michael and Bixler developed the following expression for the reduced diffusion coefficient:

$$D = D^*/\tau\beta \qquad\qquad (3.8)$$

D is the diffusion coefficient of the semicrystalline polymer, D^* is the diffusion coefficient of the completely amorphous polymer, τ represents the tortuosity and β the chain immobilization factor which represents the reduction in mobility of the polymer chains in the amorphous regions due to the presence of crystallites in the polymer matrix.

The changes in physical properties and thermal behaviour of semi crystalline polymers above and below its melting temperature (T_m) have been studied extensively by Jordan.[78-80] During the past decade, extensive permeation and sorption research was also done by the research group of Prof. D.R. Paul at the University of Texas at Austin [61, 72, 75-77, 91-93] evaluating poly(alkyl (meth)acrylate)s across a broad temperature range to include its crystalline and molten states. Some of their research findings are summarized below.

The studies of Paul et al. initially focused on homopolymers of poly(alkyl (meth)acrylates), where permeation and sorption properties were determined of (meth)acrylates with increasing carbon side chain lengths.[61, 77] For 14 carbon (C14) to 22 carbon (C22) side chain lengths, polyacrylates followed the Arrhenius temperature dependence, except in the region of the melting point. It was also found that penetrant permeability increased linearly for a range of gases (He, H_2, O_2, N_2, CH_4

and CO_2) evaluated with increasing number of carbons in the side chain of acrylates, when in its molten or rubbery state. This was attributed to an increase in free volume which resulted in an increase in diffusion. The permeability increase from methyl acrylate to ethyl acrylate did however not follow this linear trend. For the crystalline state this trend was also not observed. Increasing side chain lengths from C14 up resulted in an increase in crystallinity and therefore a reduction in permeability. The size of the crystalline regions and the arrangement of these crystals impacted on the permeability. Methacrylate homopolymers also exhibited a lower permeability to the test gases compared to acrylates of the same carbon side chain length, mainly due to increased stiffness of the backbone that required higher activation energy for diffusion to take place, although the temperature switch was comparable. The permeation properties of these side chain crystalline polymers were compared to polycaprolactone, a main chain crystalline polymer.

The evaluation of homopolymers was extended to include gas sorption and diffusion analyses of amorphous ethyl and decyl acrylate (PA-2 and PA-10) polymers, as well as semi-crystalline and molten octadecyl and behenyl acrylate (PA-18 and PA-22) polymers.[75] CH_4 and CO_2 were used as test gases and the sorption and diffusion properties were determined across a temperature range. It was found that the diffusion coefficient increased with increasing length of side chain. The solubility coefficient was dependent on the alkyl volume fraction and therefore the polarity of the polymer – an increase in alkyl volume reduces the polarity resulting in an increase in the solubility of CH_4. The opposite was shown for CO_2. Isotherms determined at 35 °C (for all four polymers) and 70 °C (for PA-18 and PA-22) obeyed Henry's law. Solubility and diffusion switch behaviour due to the melting point of the polymers under investigation, were also calculated.

Water vapour permeation studies were also conducted for the semi-crystalline and molten states of PA-18.[94] It was found that the water vapour permeability of PA-18 in its molten state was similar to shorter chain methacrylate polymers (poly ethyl-, propyl- and butyl methacrylates), while its water vapour permeability was similar to that of polyethylene when PA-18 was in its semi-crystalline state. It was furthermore found that the permeation switch for water vapour was between that of helium and hydrogen, in line with the dependence of penetrant size.

Their latest research focused on gas permeation studies (He, H_2, O_2, N_2, CH_4 and CO_2) of (poly(n-alkyl acrylate) copolymers consisting of crystalline/crystalline combinations as well as crystalline/non-crystalline combinations.[91, 92] This study revealed that for both crystalline/crystalline and crystalline/non-crystalline copolymer combinations there was a reduction in the heat of fusion; the

reduction in crystallinity manifested itself in increased permeability; and the permeation jump when traversing the melting point region was reduced.

3.3.4 Pigments and fillers used in polymers

The topic of polymer clay composites have been researched for many years, first with the aim of using fillers as extenders to reduce cost, but later on also to benefit from the unique properties that were achieved through the introduction of fillers with specific properties such as high aspect ratios into polymers. This has led to the field of polymer clay nanocomposites (PCNs) for which many review articles summarising the extensive research done in the field are available.[95-98]

Natural silicate clays such as sodium montmorillonite (Na-MMT) and synthetic silicate clays such as Laponite have been investigated extensively as fillers for polymer clay nanocomposite (PCN) materials.[96, 99-103] PCNs exhibit markedly improved properties compared to that of the virgin polymer or microcomposites of the virgin polymer with micro-sized mineral clays. Properties that are improved include increased strength, decreased gas permeation properties, increased resistance against heat and flammability, and increased biodegradability (for biodegradable polymers).[95, 96, 99, 104-107]

This section gives a brief summary of the preparation of modified fillers and its use in the synthesis of PCNs; the latest research trends in PCNs are also discussed, including the latest research done in the field of sorption behaviour of PCN films.

3.3.4.1 Modification of silicate clays

To ensure compatibility of hydrophilic inorganic clays with organic polymers, it is necessary to modify their surface properties. MMT, a smectite type clay, consists of a central octahedral sheet formed from $Mg(OH)_6^{4-}$ or $Al(OH)_6^{3-}$ sandwiched between two parallel tetrahedral sheets of continuous linkages of SiO_4 (see Figure 3.6). The individual sheets of the smectite structure are held together by electrostatic forces, resulting in an interlayer space repeat unit distance of 1 nm (for dry smectites) to more than 2 nm (for smectites swollen with water molecules).[108]

56
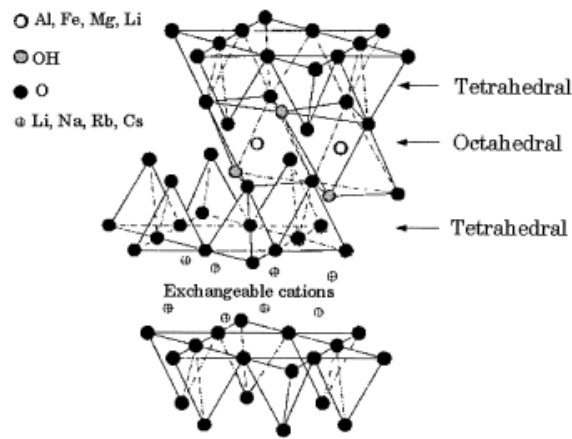
Figure 3.6: Typical 2:1 smectite structure [96, 107]

Several active sites on MMT allow for the modification of the clay surface: (1) Positive charges on the edges of the platelets can attract negatively charged molecules. Although this type of modification would not result in an intercalated structure, it would enhance the compatibility between MMT and the polymer. (2) Hydroxyl groups can allow for hydrogen bonding or covalent bonding. They are present along the edges of the platelets, bound to the octahedral ions. Oxygen atoms present on the surface of the platelets can also form hydrogen bonds for organic molecules. (3) Certain groups of the 2:1 phyllosilicates (smectites and vermiculites) have a negative charge density in its interlayer space, creating the potential to exchange the counterbalancing alkali or alkaline earth cations with other cations (see Figure 3.4). This potential is referred to as the cation exchange capacity (CEC) and is unique for each type of clay mineral. The ion exchange capacity is expressed in terms of the millimol equivalent cation concentration per 100 g of clay (meq/100g clay). The ion exchange effectiveness is affected by factors such as the interlayer space and the size of the organic cation.[109]

Today various organically modified clays are commercially available including *Somasif* from CO-OP Chemical Co. Ltd, *Cloisite* from Southern Clay products, *Nanomer* from Nanocor, and organoclays from Süd-Chemie and Rheox.[110]

Based on the active sites in clays, several methods of surface modification have been established to form intercalated organoclay particles. Some examples are discussed below:[109]

Modification by adsorption of small molecules onto fillers: The adsorption of molecules such as acids, bases, their salts and neutral compounds (including alcohols, ethers, aldehydes, ketones, nitriles, amides and amino acids) occurs by means of chemisorption to the mineral surface. The chemisorption process could involve different mechanisms including hydrogen bonding, proton transfer and coordination between the adsorbed species and the mineral surface.[109] As the surface of minerals is generally characterized by the presence of hydroxylic species capable of protonation, deprotonation and coordination with other metal ions, this is ideal for the chemisorption process.

Modification by adsorption of polymers: In contrast to the thin layer formed on clay surfaces as a result of the adsorption of small molecules, the adsorption of polymers via chemisorption or physisorption results in thick adsorbed layers onto dispersed layers of clay. Vaia and co-workers demonstated that Na-MMT or Li-MMT could be directly intercalated using polyethylene oxide to displace the water molecules in the interlayer and expand the interlayer distance.[111] Nanocor found that either a strong polar group (e.g. carbonyl, hydroxyl, carboxyl, amine, amide, etc.) or an aromatic ring that can form a metal-cation complex, are required to successfully modify clays.[110] The intercalation mechanism was shown to be due to hydrogen bonding to the surface hydroxyl groups, chelation of the clay metal cations, metal cation electrostatic bonding, or bonding between clay inorganic cations and intercalant aromatic rings. Water-soluble polymers and oligomers that were successfully incorporated into clays include poly(4-vinyl pyrrolidone), poly(4-vinyl pyridine), polyvinyl alcohol, polyethylene glycol, polypropylene glycol, polymeric quaternary ammonium salts, etc.

Modification by cation exchange: The preparation of intercalated clays using organic cations have been researched extensively over the past 70 years with quaternary ammonium ions probably the most researched type of organic cation for the preparation of organoclays.[98] The degree of intercalation, as measured by the increase in the interlayer distance, is dependent on the size of the organic cation used. The patent of Miyanaga et al. gives extensive information in this regard based on a study where four different clays were used.[112] Most commercially available organoclays are based on the modification of the clay via a quaternary ammonium salt.

Modification by covalent bonding: The hydroxyl groups on the surface of mineral fillers and pigments create the site for surface modification by means of covalently bound modifiers. Three classes of organic modifiers are used for this reaction: silanes, metal oxides and coordination complexes, and organic condensation compounds such as epoxides and isocyanates.

Modification by grafting and encapsulation polymerization: Surface initiated polymerization can occur by adsorption of radical initiators onto the clay surface. These initiators include azo initiators such as azobiscyanoisovaleric acid (ACV) or adsorbed persulfate initiators. This mechanism for surface modification is effective for both anionic (kaolin) and neutral (talc) minerals.[96, 109, 113] Grafting of RAFT agents onto MMT clays via cation exchange also yielded the capability of controlled polymerisation from the interlayer space of the clay.[114] Another method of grafting onto a mineral surface is through the adsorption of monomers onto the mineral surface. Monomers such as acrylic acid (for basic surfaces), vinylpyridine (for acidic surfaces), alkyl amino acrylates and acrylamide can effectively adsorb onto the mineral surface, followed by polymerization.[108, 109]

3.3.4.2 Polymer clay nanocomposite preparation

PCNs are a special class of composites, consisting of polymers containing filler particles which have at least one dimension in the nanometer range.[96] Three different types of structures can be distinguished based on the degree of interaction between the clay surface and the polymer as well as the strength of these interactions (See Figure 3.7):[95, 96] (A) Conventional or phase separated composites: This type of composite exhibits the same properties as the microcomposite, where no penetration or interaction occurs between the polymer and the mineral clay. (B) Intercalated nanocomposites: This structure exists because of the penetration and interaction of at least one polymer chain in interlayer space. This interaction results in an increase in the interlayer distance, although the ordered multilayer morphology remains. (C and D) Exfoliated nanocomposites: These PCNs can be ordered or disordered and depends on the orientation of the platelets. With the disordered PCN total disruption of the ordered multilayered structure occurs due to complete and uniform dispersion of the clay in the polymer matrix.

The preparation of nanocomposites is based on the ability of mineral clays to undergo modification of its surface and interlayer space. The type of polymer and its synthesis constraints determine the suitability of specific methods for the preparation of PCNs. Three main methods of synthesis exist: exfoliation-adsorption, in situ intercalative polymerization and melt intercalation. [95, 96]

Exfoliation-adsorption: This is a solvent-based process. The polymer (or prepolymer) is firstly dissolved in the solvent, after which the clay is dispersed and swollen in the solvent. Upon evaporation of the solvent, the polymer would be adsorbed onto the surface of the clay in the interlayer space. [96]

59

A: Conventional Composite

B: Intercalated Nanocomposite

C: Ordered Exfoliated
Nanocomposite

D: Disordered Exfoliated
Nanocomposite
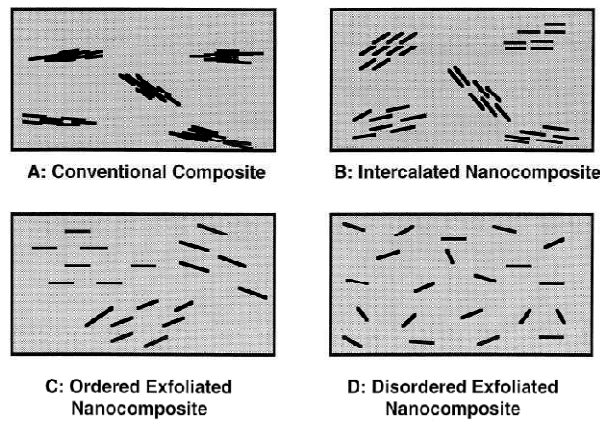
Figure 3.7: Schemes to illustrate the interaction between layered silicates with polymers: (a) phase-separated conventional microcomposites; (b) intercalated nanocomposites; (c) ordered exfoliated nanocomposites; and (d) disordered exfoliated nanocomposites[98]

In situ intercalative polymerisation: This method requires that the layered silicate be swollen by the monomer before polymerization through chemisorption. The formation of the polymer would then occur directly between the clay layers, resulting in intercalation or exfoliation of the clay. Depending on the type of polymerization mechanism being used, the polymerization can be initiated by heat or irradiation, or by the diffusion of the initiator into the interlayer. Alternatively, the initiator can be fixed to the clay surface by cationic exchange, or by adsorption onto the charged clay surface. [95, 96, 108, 109, 113-115] Free radical polymerization is classified as an *in situ* intercalative polymerisation method for the preparation of PCNs. Bulk, solution or emulsion-based polymerisation can be utilized. Examples of emulsion-based in situ polymerisation include: The preparation of polymethyl methacrylate/Na-MMT PCNs using pristine bentonite , and obtaining an intercalated structure[116]. Poly(styrene-*co*-methyl methacrylate)/MMT PCNs were synthesized using two types of MMT clays modified via a cation exchange mechanism to render a reactive and conventional organoclay. PCNs were synthesized via bulk, solution, suspension and emulsion polymerisation to give PCNs with varying degrees of intercalation and exfoliation.[117]

Melt intercalation: This is a solvent-free method, based on the blending of molten polymer with clay. The mineral clay can either be pristine clay, or organically modified clay, depending on the polymer properties and its requirements in terms of compatibility with a hydrophilic or hydrophobic clay surface. This method could result in either an intercalated or an exfoliated nanocomposite structure. [95, 96, 107]

60

Solution-based PCNs can be based on either hydrophilic or hydrophobic systems. In the case of hydrophilic polymer systems, pristine Na-MMT is used, as it is compatible with the solvent as well as the monomers or polymers. The incorporation of Na-MMT into hydrophobic polymer systems, however, requires that the pristine clay be modified with an organophilic modifier in order to make it compatible with the specific hydrophobic monomers or polymers. A variety of organophilic modifiers have been evaluated. The mechanism of modification has mainly focused on ion exchange by means of quaternary ammonium organophilic compounds. These organophilic compounds can either be unreactive, or it can contain a reactive group that would be incorporated into the polymer chain [118, 119].

3.3.4.3 Latest research trends in the use of fillers for heterophase polymerisation

Recently, the research focus has shifted from PCNs synthesized by solvent-based or bulk polymerization systems to that of emulsion-based polymerization systems. PCNs are prepared by means of *in situ* intercalation polymerization, where the interlayer distance of the pristine clay is increased by swelling the clay with water, followed by the modification of the clay surface through the adsorption of monomers [120-126] or initiators [117, 127, 128] and finally initiation of the free radical polymerization process by heating.

Emulsion polymerization, and more recently miniemulsion polymerization, received significant attention due to its environmental and commercial considerations. As a result heterophase polymerization for the synthesis of PCNs has become a major research focus.[100] Today two types of PCNs are produced: polymer particles with encapsulated clays and clay-armored polymer particles where the clays are found on the surface of the polymer particles. Initially conventional emulsion polymerization was explored using mainly sodium montmorillonite (Na-MMT). The possibility of encapsulating clays via miniemulsion polymerization resulted in a shift in research to PCN synthesis via miniemulsion instead of conventional emulsion polymerization. It also resulted in a shift from the very versatile sodium montmorillonite as model filler for heterophase PCN research to Laponite, a synthetic filler with a significantly smaller aspect ratio that would allow encapsulation into particles of smaller diameters. The encapsulation of Laponite into polystyrene particles was first reported by Sun et al.,[129] while MMT was incorporated successfully in polystyrene particles via Reversible Addition-Fragmentation Chain Transfer (RAFT) mediated miniemulsion polymerization.[115]

The functionalization of clays is critical to compatabilize the clays with the monomer phase. 3 Methods are available: cation exchange, silane grafting and adsorption of polar polymers such as poly-DADMAC.[100]

Heterophase PCN research largely focused on the synthesis of PCNs via conventional emulsion and miniemulsion processes, with limited attention given to properties of films produced from these PCN latexes. A key PCN research project entitled "Nanostructured waterborne polymer films with outstanding properties" (NAPOLEON), funded by the European Commission through its FP6 research programme, was executed from 2005 to 2009, contracting 19 research facilities to develop platform technology for the production of films with controlled nanostructure without the drawbacks of solvent removal and residual monomer in the final product normally associated with solvent-based and bulk polymerization.[100, 101] Alkyd-acrylic coatings and polyurethane-acrylic adhesives were used as model polymer systems for the synthesis of the polymer-clay nanocomposites. Three types of polymer-clay nanocomposite morphologies were investigated: (1) Laponite-armoured polymer particles where the Laponite clay particles were functionalized with a free radical initiator prior to dispersing it in an aqueous medium in the presence of a surfactant, followed by the formation of monomer droplets and finally polymerization of the monomer to form the PCN. (2) Polymer encapsulated clay platelets synthesized by organically modifying the clay platelets and dispersing them in the monomer mixture before miniemulsification and polymerization. (3) PCNs containing clay platelets both within the polymer particle and on the surface of the polymer particle were prepared by dispersing hydrophobically modified clay platelets in a nonionic surfactant and co-sonicating this with a monomeric miniemulsion stabilized with the same surfactant prior to polymerization of the PCN. The properties of the subsequent films were investigated. These studies led to various outputs including the development of a mathematical model for miniemulsification in high pressure homogenizers;[130] the development of techniques such as the quartz crystal microbalance, GARfield magnetic resonance profiling etc. to study drying and film formation of PCNs[131-133], including the development of a mathematical model to predict film morphology[134]; the synthesis of PCNs consisting of n-butyl acrylate, methyl methacrylate and Na-MMT at high solids contents (up to 45%) using either conventional polymerization or miniemulsion polymerization techniques.[135] The knowledge gained from the evaluation of film formation assisted in overcoming problems associated with controlling the rate of water loss from urethane/acrylic latex films which are normally very slow, lowering the water sensitivity of alkyd-acrylic coatings, avoiding wrinkling, poor wetting and heterogeneity in alkyd/acrylic coatings etc. This research project made a significant contribution to the knowledge base on PCNs with outputs including 9 PhD dissertations, 32 journal publications and 54 conference presentations.

3.3.4.4 The impact of fillers on the sorption behaviour of polymers

Transport of simple gases and vapours through polymers containing pigments or fillers are similar to that of transport of these penetrants through semicrystalline polymeric materials where the

polymer volume is assumed to be the permeable phase and the pigment or filler particles (similar to the crystalline regions) the impermeable phase. The aspect ratio of these plate-like clays, its orientation relative to the permeation direction and its volume relative to the polymer volume can impact on the solubility and diffusion coefficients and therefore the permeability properties of the PCN material. The increase in tortuosity of the path for the diffusing molecules, as determined by the shape of the clay and its degree of dispersion in the polymer matrix, is however viewed as the dominant factor, resulting in a reduction in the diffusion coefficient.[5, 136]

The latest research in the field of permeability of PCNs relates to the development of models to predict the transport of simple gases and vapours through these materials. Various review articles discuss these research trends in detail.[136-138]

Initial models for the transport of penetrants through composite materials containing plate-like materials have been developed many years ago and were based on the assumption that these materials were dispersed in a regular parallel manner in the polymer matrix. Barrer and Petropoulos,[139] were the first to develop such a method in the early 1960s, followed by Nielsen[140] who assumed that the direction of the plate-like filler particles were perpendicular to the direction of diffusion. These models were further developed by others to take into consideration the random spatial positioning of the parallel plates and also the possibility of having arrangements of the plate-like fillers at angles less than 90 ° to the direction of diffusion.

More recently it was recognized that the interface between the inorganic filler particle and the polymer could also impact on the diffusion properties due to the surfactant sorbed onto the surface of the filler or due to voids/ free volume that formed between the different phases in the PCN.[136] In this regard, Sorrentino et al. evaluated PCNs of polycaprolactone, polyurethane and polypropylene with Na-MMT using the gravimetric method to determine permeability, solubility and diffusion coefficients for different penetrants at 25 °C.[137] This investigation lead to the development of a new geometric model whereby the effective diffusivity of penetrants through the PCNs could be predicted based on the orientation of the clay platelets, the interaction between the clay and polymer and the aspect ratio of the clay. This model was an improvement on the models previously developed by Cussler and Aris where these models were only valid if the clay platelets were aligned either parallel or perpendicular to the polymer film surface.

3.3.5 Multilayer structures

Multilayered barrier films are a common phenomenon where barrier properties are required for more than one type of penetrant, where other properties such as heat sealability or printability is also required, or to optimize the cost to performance ratio of barrier materials, where a relatively cheap polymer film is used in combination with a more expensive functional coating to impart the required barrier function.[7, 141] In order to assess the barrier properties of the combined structure, the multi-layered structure can be viewed as a series of membranes, where the total barrier function is given by the following equation (see equation 3.9):

$$\frac{1}{P} = \frac{l_1}{lP_1} + \frac{l_2}{lP_2} + \cdots + \frac{l_n}{lP_n} \tag{3.9}$$

where P is the total permeability, $P_1, P_2 \cdots P_n$ are the permeabilities of the respective layers, and $l = l_1 + l_2 + \cdots + l_n$ where l represents the thickness of the total barrier and $l_1, l_2, \cdots l_n$ the thickness of the individual layers. The generalized relationship between the total permeability of a multi-layered structure and the contributions of the individual layers (where the separate layers have the same thickness) is represented by equation (3.10).

$$\frac{1}{P_t} = \frac{1}{P_1} + \frac{1}{P_2} + \cdots + \frac{1}{P_n} \tag{3.10}$$

where P_t is the permeability of the laminate and P_1, P_2 and P_n are the permeabilities of layers 1 ,2 up to layer n.[7]

3.4   Research focus for this study

The following aspects of sorption behaviour of polymers were identified for further investigation in this study:

(1) Although some research has already been published on comparing the water vapour permeation properties of latex films containing different surfactants, the role of these surfactants on the kinetics and thermodynamics of water vapour sorption in latex films are still not clearly understood. This was therefore explored in terms of the following three surfactants using poly(styrene-co-butyl acrylate) as model polymer latex: sodium dodecyl benzene sulfonate (an anionic surfactant), octyl phenol ethoxylate (a nonionic polymeric surfactant) and dodecylammonium-3-butenoate (a surfmer with polymerizable counterion).

64

(2) The synthesis of PCNs via in situ emulsion polymerization has been explored extensively and the properties of the resultant films understood. However, limited information is available in literature regarding the kinetics and thermodynamics of these emulsion-based films at different water vapour partial pressures. Poly(styrene-co-butyl acrylate) was therefore used as model polymer to explore the sorption behaviour of this polymer for increasing concentrations of Na-MMT and increasing concentrations of a reactive organophilic clay modifier (AMPS).

(3) The sorption behaviour in terms of its kinetics and thermodynamics of octadecyl acrylate copolymerized with a small-size comonomer such as methyl methacrylate is not available across the entire water vapour partial pressure range. It was therefore decided to determine these properties for the abovementioned films.

The next chapter describes the experimental procedures and analytical test methods used in this study.

References

1.   Crank, J. and Park, G.S., eds. *Diffusion in Polymers*. 1968, Academic Press Inc. (London) Ltd: London. 452.

2.   Fujita, H., *Organic Vapors above the Glass Transition Temperature*, in *Diffusion in Polymers*, J. Crank and G.S. Park, Editors. 1968, Academic Press: London.

3.   Stannett, V., *Simple Gases*, in *Diffusion in Polymers*, J. Crank and G.S. Park, Editors. 1968, Academic Press: London.

4.   Berens, A.R. and Hopfenberg, H.B., *Diffusion of organic vapors at low concentrations in glassy PVC, polystyrene, and PMMA.* Journal of Membrane Science, 1982. **10**(2): p. 283-303.

5.   Van der Wel, G.K. and Adan, O.C.G., *Moisture in Organic Coatings - A Review.* Progress in Organic Coatings, 1999. **37**: p. 1-14.

6.   Klopffer, M.H. and Flaconneche, *Transport Properties of Gases in Polymers: Bibliographic Review.* Oil & Gas Science and Technology - Revue de L'Institut Français du Pétrole, 2001. **56**(3): p. 223-244.

7.   Rogers, C.E., *Permeation of Gases and Vapours in Polymers*, in *Polymer Permeability*, J. Comyn, Editor. 1986, Elsevier Applied Science: London. p. 11-73.

8.   Lee, W.M., *Selection of Barrier Materials from Molecular Structure.* Polymer Engineering and Science, 1980. **20**(1): p. 65-69.

9.   Hayes, T., European FP6 Report No. 1771 *World Paints and Coatings*, 2004,

10.   Hayes, T., European FP6 Report No. 1813 *World Emulsion Polymers*, 2004,

11.   Van Herk, A.M. and Monteiro, M.J., *Heterogeneous Systems*, in *Handbook of Radical Polymerisation*, K. Matyjaszewski and T.P. Davis, Editors. 2002, John Wiley & Sons Inc.: New York.

12.   Monteiro, M.J. and Charleux, B., *Living Radical Polymerisation in Emulsion and Miniemulsion*, in *Chemistry and Technology of Emulsion Polymerisation*, A.M. Van Herk, Editor. 2005, Blackwell Publishing Ltd: Oxford.

13.   Lovell, P.A. and El-Aasser, M.S., eds. *Emulsion Polymerization and Emulsion Polymers*. 1st ed. 1997, John Wiley & Sons: West Sussex, England.

14.   Bechthold, N. and Landfester, K., *Kinetics of Miniemulsion Polymerization As Revealed by Calorimetry.* Macromolecules, 2000. **33**: p. 4682-4689.

15.   Landfester, K., *Polyreactions in Miniemulsions.* Macromolecular Rapid Communications, 2001. **22**: p. 896-936.

16.   Antonietti, M. and Landfester, K., *Polyreactions in miniemulsions.* Progress in Polymer Science, 2002. **27**: p. 689-757.

17.   Asua, J.M., *Miniemulsion Polymerization.* Progress in Polymer Science, 2002. **27**: p. 1283-1346.

18.   Cunningham, M.F., *Living/controlled radical polymerizations in dispersed phase systems.* Progress in Polymer Science, 2002. **27**: p. 1039-1067.

19.   Schork, F.J., Poehlein, G.W., Wang, S., Reimers, J., Rodrigues, J., and Samer, C., *Miniemulsion Polymerization.* Colloids and Surfaces A: Physiochemical and Engineering Aspects, 1999. **153**: p. 39-45.

20.   Steward, P.A., Hearn, J., and Wilkinson, M.C., *An overview of polymer latex film formation and properties.* Advances in Colloid and Interface Science, 2000. **86**: p. 195-267.

21. Niu, B.-J. and Urban, M.W., *Recent Advances in Stratification and Film Formation of Latex Films; Attenuated Total Reflection and Step-Scan Photoacoustic FTIR Spectroscopic Studies.* Journal of Applied Polymer Science, 1998. **70**: p. 1321-1348.

22. Holton-Andersen, J. and Hansen, C.M., *Solvent and water evaporation from coatings.* Progress in Organic Coatings, 1983. **11**: p. 219-240.

23. Park, Y.-J. and Kim, J.-H., *Film formation from reactive latex particles: influence of intraparticle crosslinking on mechanical properties.* Colloid Surface A, 1999. **153**: p. 583-590.

24. Butler, L.N., Fellows, C.M., and Gilbert, R.G., *Effect of Surfactant Systems on the Water Sensitivity of Latex Films.* Journal of Applied Polymer Science, 2004. **92**: p. 1813-1823.

25. Poehlein, G.W., Vanderhoff, J.W., and Witmeyer, R., *Drying of latex films.* Journal of Polymer Preprints, 1975. **16**(1): p. 268-273.

26. Vanderhoff, J.W., Bradford, E.B., and Carrington, W.K., *Transport of water through latex films.* Journal of Polymer Science: Polymer Symposia, 1973. **41**: p. 155-174.

27. Alig, I., Jarek, M., and Hellmann, G.P., *Restricted Segmental Mobility in Side-Chain Crystalline Comblike Polymers, Studied by Dielectric Relaxation Measurements.* Macromolecules, 1998. **31**(7): p. 2245-2251.

28. Dillon, R.E., Matheson, E.B., and Bradford, E.B., *Sintering of synthetic latex particles.* Journal of Colloid Science, 1951. **6**: p. 108-117.

29. Visschers, M., Laven, J., and German, A.L., *Current understanding of the deformation of latex particles during film formation.* Progress in Organic Coatings, 1997. **30**: p. 39-49.

30. Alig, I. and Tadjbakhsch, S., *Film formation and crystallization kinetics of polychloroprene studied by an ultrasonic shear wave reflection method.* Journal of Polymer Science Part B: Polymer Physics, 1998. **36**(16): p. 2949-2959.

31. Lellinger, D., Tadjbach, S., and Alig, I., *Determination of the elastic moduli of polymer films by a new ultrasonic reflection method.* Macromolecular Symposia, 2002. **184**(1): p. 203-214.

32. Sperry, P.R., Snyder, B.S., O'Dowd, M.L., and Lesko, P.M., *Role of Water in Particle Deformation and Compaction in Latex Film Formation.* Langmuir, 1994. **10**: p. 2619-2628.

33. Lahtinen, M., Glad, E., Koskimies, S., Sundholm, F., and Rissanen, K., *Synthesis of Novel Reactive Coalescing Agents and Their Application in a Latex Coating.* Journal of Applied Polymer Science, 2003. **87**: p. 610-615.

34. Amalvy, J.I. and Soria, D.B., *Vibrational spectroscopic study of distribution of sodium dodecyl sulphate in latex films.* Progress in Organic Coatings, 1996. **28**: p. 279-283.

35. Yaseen, M., Raju, K.V.S.N., *A critical analysis of various methods for preparation of free films of organic coatings.* Progress in Organic Coatings, 1982. **10**: p. 125-155.

36. Yaseen, M. and Ashton, H.E., *Effect of Free Film Preparation Method on Physical Properties of Organic Coatings.* Journal of Coatings Technology, 1977. **49**(629): p. 50-58.

37. Roulstone, B.J., Wilkinson, M.C., and Hearn, J., *Studies on polymer latex films. IV. Comparison of the permeability of latex and solvent-cast films.* Polymer International, 1992. **27**(4): p. 305-308.

38. Okubo, M., Takeya, T., Tsutsumi, Y., Kadooka, T., and Matsumoto, T., *Asymmetric porous emulsion film.* Journal of Polymer Science: Polymer Chemistry, 1981. **19**(1): p. 1-8.

39. Calbo, L.J., ed. *Handbook of Coatings Additives*. 1987, Marcel Dekker: New York.

40. Goossens, E.L.J., Van der Spoel, W.H., and Bancken, E.L.J., *Moisture transport in coated plaster.* HERON, 2001. **46**(3): p. 217-222.

41. Morillon, V., Debeaufort, F., Blond, G., Capelle, M., and Voilley, A., *Factors Affecting the Moisture Permeability of Lipid-Based Edible Films: A Review.* Critical Reviews in Food Science and Nutrition, 2002. **42**(1): p. 67-89.

42. Villalobos, R., Hernandez-Munoz, P., and Chiralt, A., *Effect of surfactants on water sorption barrier properties of hydroxypropyl methylcellulose films.* Food Hydrocolloids, 2006. **20**(4): p. 502-509.

43. Chen, C.-H., Kuo, W.-S., and Lai, L.-S., *Effect of surfactants on water barrier and physical properties of tapioca starch/decolorized hsian-tsao leaf gum films.* Food Hydrocolloids, 2009. **23**(3): p. 714-721.

44. Butler, L.N., Fellows, C.M., and Gilbert, R.G., *Effect of surfactants used for binder synthesis on the properties of latex paints.* Progress in Organic Coatings, 2005. **53**(2): p. 112-118.

45. Holmberg, K., Jonsson, B., Kronberg, B., and Lindman, B., *Surfactants and Polymers in Aqueous Solution*. 2nd ed. 2003, West Sussex: John Wiley & Sons Ltd.

46. Holmberg, K., Jönsson, B., Kronberg, B., Lindman, B., *Surfactants and polymer in aqueous solution*. 2nd ed. 2003, New York: John Wiley & Sons.

47. Landfester, K., Bechthold, N., Tiarks, F., and Antonietti, M., *Miniemulsion Polymerization with Cationic and Nonionic Surfactants: A Very Efficient Use of Surfactants for Heterophase Polymerization.* Macromolecules, 1999. **32**: p. 2679-2683.

48. Lam, S., Hellgren, A.C., Sjöberg, M., Homberg, K., Schoonbrod, H.A.S., Unzué, M.J., Asua, J.M., Tauer, K., Sherrington, D.C., and Goni, A.M., *Surfactants in Heterophase Polymerization: A Study of Film Formation Using Atomic Force Microscopy.* Journal of Applied Polymer Science, 1997. **66**(1): p. 187-198.

49. Asua, J.M. and Schoonbrood, H.A.S., *Reactive surfactants in heterophase polymerzation.* Acta Polymerica, 1998. **49**(12): p. 671-686.

50. Amalvy, J.I., Unzué, M.J., Schoonbrood, H.A.S., Asua, and J.M., *Reactive Surfactants in Heterophase Polymerizations. 11. Particle Nucleation.* Macromolecules, 1998. **31**: p. 5631-5638.

51. Amalvy, J.I., Unzue, M.J., Schoonbrood, H.A.S., and Asua, J.M., *Reactive Surfactants in Heterophase Polymerization: Colloidal Properties, Film-Water Absorption, and Surfactant Exudation.* Journal of Polymer Science Part A: Polymer Chemistry, 2002. **40**(17): p. 2994-3000.

52. Schoonbrood, H.A.S. and Asua, J.M., *Reactive Surfactants in Heterophase Polymerization. 9. Optimum Surfmer Behavior in Emulsion Polymerization.* Macromolecules, 1997. **30**(20): p. 6034-6041.

53. Schoonbrood, H.A.S., Unzué, M.J., Amalvy, J.I., and Asua, J.M., *Reactive Surfactants in Heterophase Polymerization. VIII. Emulsion Polymerization of Alkyl Sulfopropyl Maleate Polymerizable Surfactants (Surfmers) with Styrene.* Journal of Polymer Science Part A: Polymer Chemistry, 1997. **35**(13): p. 2561-.

54. Schoonbrood, H.A.S., Unzuè, M.J., Beck, O.-J., Asua, J.M., Gon, A.M., and Sherrington, D.C., *Reactive Surfactants in Heterophase Polymerization. 7. Emulsion Copolymerization Mechanism Involving Three Anionic Polymerizable Surfactants (Surfmers) with Styrene-Butyl Acrylate-Acrylic Acid.* Macromolecules, 1997. **30**(20): p. 6024-6033.

55.   Guyot, A., Tauer, K., Asua, A.M., Van Es, S., Gauthier, C., Hellgren, A.C., Sherrington, D.C., Montoya-Goni, A., Sjoberg, M., Sindt, O., Vidal, F., Unzue, M., Schoonbrood, H.A.S., Shipper, E., and Lacroix-Desmazes, P., *Reactive surfactants in heterophase polymerization.* Acta Polymerica, 1999. **50**(2): p. 57-66.

56.   Hartmann, P.C., *Preparation of polymer latexes*. Patent No: WO/2006/092736 A2 (2006).

57.   Abele, S., Zicmanis, A., Graillat, C., and Guyot, A., *Cationic and Zwitterionic Polymerizable Surfactants-Quaternary Ammonium Dialkyl Maleates. 2. Emulsion Polymerization of Styrene and Butyl Acrylate.* Langmuir, 1999. **15**(4): p. 1045-1051.

58.   Steward, P.A., Hearn, J., and Wilkinson, M.C., *Studies on permeation through latex films. I. Films containing no or only low levels of additives.* Polymer International, 1995. **38**(1): p. 1-12.

59.   Roulstone, B.J., Wilkinson, M.C., and Hearn, J., *Studies on polymer latex films. II. Effect of surfactant on the water-vapour permeability of polymer latex films.* Polymer International, 1992. **27**(1): p. 43-50.

60.   Aramendia, E., Barandiaran, M.J., Grade, J., VBlease, T., and Asua, J.M., *Improving water sensitivity in acrylic films using surfmers.* Langmuir, 2005. **21**(4): p. 1428-145.

61.   Mogri, Z., Paul, D.R., *Gas sorption and transport in poly (alkyl (meth)acrylate)s. I. Permeation properties.* Polymer, 2001. **42**: p. 7765-7780.

62.   Weinkauf, D.H. and Paul, D.R., *Effects of Structural Order on Barrier Properties*, in *Barrier Polymers and Structures*, W.J. Koros, Editor. 1993, American Chemical Society: Washington, DC.

63.   Frisch, H.L., *Sorption and Transport in Glassy Polymers - A Review.* Polymer Engineering and Science, 1980. **20**(1): p. 2-13.

64.   Raucher, D. and Sefcik, M.D., *Sorption and Transport in Glassy Polymers: Gas-Polymer-Matrix Model*, in *Industrial Gas Separations*, T.E. Whyte Jr., C.M. Yon, and E.H. Wagener, Editors. 1983, American Chemical Society: Washington DC.

65.   Barrer, R.M., *Some properties of diffusion coefficients in polymers.* Journal of Physical Chemistry, 1957. **61**(2): p. 178-189.

66.   Brandt, W.W., *Model Calculation of the Temperature Dependence of Small Molecule Diffusion in High Polymers.* Journal of Physical Chemistry, 1959. **63**(7): p. 1080-1084.

67.   Pace, R.J. and Datyner, A., *Statistical mechanical model of diffusion for simple penetrants in polymers. I. Theory.* Journal of Polymer Science Part B: Polymer Physics, 1979. **17**(3): p. 437-451.

68.   Pace, R.J. and Datyner, A., *Statistical mechanical model for diffusion of simple penetrants in polymers. II. Applications - nonvinyl polymers.* Journal of Polymer Science Part B: Polymer Physics, 1979. **17**(3): p. 453-464.

69.   Pace, R.J. and Datyner, A., *Statistical mechanical model for diffusion of simple penetrants in polymers. III. Applications-vinyl and related polymers* Journal of Polymer Science Part B: Polymer Physics, 1979. **17**(3): p. 465-476.

70.   Fujita, H. and Kishimoto, A., *Interpretation of Viscosity Data for Concentrated Polymer Solutions.* Journal of Chemical Physics, 1961. **34**: p. 393-398.

71.   Lin, H., Kai, T., Freeman, B.D., Kalakkunnath, S., and Kalika, D.S., *The Effect of Cross-linking on Gas Permeability in Cross-Linked Poly(Ethylene Glycol Diacrylate).* Macromolecules, 2005. **38**(20): p. 8381-8393.

72.   Mogri, Z. and Paul, D.R., *Water-Vapour Permeation in Semicrystalline and Molten Poly(octadecyl acrylate).* Journal of Polymer Science: Part B: Polymer Physics, 2001. **39**: p. 979-984.

73.   Stewart, R.F., *Temperature-Activated Adhesive Assemblies*. US Patent Patent No: 5,387,450 (1995).

74.   Reppe, W., Starck, W., and Voss, A., *Polymerization products from vinyl esters.* US Patent Patent No: 2,118,864 (1938).

75.   Mogri, Z. and Paul, D.R., *Gas sorption and transport in poly (alkyl (meth)acrylate)s: II. Sorption and diffusion properties.* Polymer, 2001. **42**: p. 7781-7789.

76.   Mogri, Z. and Paul, D.R., *Membrane formation techniques for gas permeation measurements for side-chain crystalline polymers.* Journal of Membrane Science, 2000. **175**: p. 253-265.

77.   Mogri, Z., Paul, D.R., *Gas sorption and transport in side-chain crystalline and molten poly(octadecyl acrylate).* Polymer, 2001. **42**: p. 2531-2542.

78.   Jordan, E.F., *Side-Chain Crystallinity. III. Influence of Side Chain Crystallinity on the Glass Transition Temperature of Selected Copolymers Incorporating n-Octadecyl Acrylate or Vinyl Stearate.* Journal of Polymer Science: Part A-1, 1971. **9**: p. 3367-3378.

79.   Jordan, E.F., Artymyshyn, B., Speca, A., and Wrigley, A.N., *Side-Chain Crystallinity. II. Heats of Fusion and Melting Transitions on Selected Copolymers Incorporating n-Octadecyl Acrylate or Vinyl Stearate.* Journal of Polymer Science: Part A-1, 1971. **9**: p. 3349-3365.

80.   Jordan, E.F., Feldeisen, D.W., and Wrigley, A.N., *Side-Chain Crystallinity. I. Heats of Fusion and Melting Transitions on Selected Homopolymers Having Long Side Chains.* Journal of Polymer Science: Part A-1, 1971. **9**: p. 1835-1852.

81.   Platé, N.A. and Shibaev, V.P., *Comb-Like Polymers. Structures and Properties.* Journal of Polymer Science: Macromolecular Reviews, 1974. **8**: p. 117-253.

82.   Michaels, A.S. and Bixler, H.J., *Flow of gases through polyethylene.* Journal of Polymer Science, 1961. **50**(154): p. 413-439.

83.   Michaels, A.S. and Parker Jr., R.B., *Sorption and flow of gases in polyethylene.* Journal of Polymer Science, 1959. **41**(138): p. 53-71.

84.   Michaels, A.S., Vieth, W.R., and Barrie, J.A., *Solution of Gases in Polyethylene Terephthalate.* Journal of Applied Physics, 1963. **34**(1): p. 1-12.

85.   Michaels, A.S., Vieth, W.R., and Barrie, J.A., *Diffusion of Gases in Polyethylene Terephthalate.* Journal of Applied Physics, 1963. **34**(1): p. 13-20.

86.   Lowell, P.N. and McCrum, N.G., *Diffusion mechanisms in solid and molten polyethylene.* Journal of Polymer Science Part A-2: Polymer Physics, 1971. **9**(11): p. 1935-1954.

87.   Puleo, A.C., Paul, D.R., and Wong, P.K., *Gas sorption and transport in semicrystalline poly(4-methyl-1-pentene).* Polymer, 1989. **30**(7): p. 1357-1366.

88.   Guadagno, L., Baldi, P., Vittoria, V., and Guerra, G., *Sub-T_g annealing of the clathrate δ form of syndiotactic polystyrene.* Macromolecular Chemistry and Physics, 1998. **199**(12): p. 2671-2675.

89.   Manfredi, C., Del Nobile, M.A., Mensitieri, G., Guerra, G., and Rapacciuolo, M., *Vapor sorption in emptied clathrate samples of syndiotactic polystyrene.* Journal of Polymer Science: Part B: Polymer Physics, 1997. **35**(1): p. 133-140.

90.   Flory, P.J. and Yoon, D.Y., *The Interphase in Lamellar Semicrystalline Polymers.* Macromolecules, 1984. **171**: p. 862-868.

70

91.   O'Leary, K.A. and Paul, D.R., *Physical properties of poly(n-alkyl acrylate) copolymers. Part 2. Crystalline/non-crystalline combinations.* Polymer, 2006. **47**(4): p. 1245-1258.

92.   O'Leary, K.A. and Paul, D.R., *Physical properties of poly(n-alkyl acrylate) copolymers. Part 1. Crystalline/crystalline combinations.* Polymer, 2006. **47**(4): p. 1226-1244.

93.   O'Leary, K. and Paul, D.R., *Copolymers of poly(n-alkyl acrylates): synthesis, characterisation, and monomer reactivity ratios.* Polymer, 2004. **45**(19): p. 6575-6585.

94.   Mogri, Z. and Paul, D.R., *Water-Vapor Permeation in Semicrystalline and Molten Poly(octadecyl acrylate).* Journal of Polymer Science Part B: Polymer Physics, 2001. **39**(10): p. 979-984.

95.   Ray, S.S. and Okamoto, M., *Polymer/layered silicate nanocomposites: a review from preparation to processing.* Progress in Polymer Science, 2003. **28**: p. 1539-1641.

96.   Alexandre, M. and Dubois, P., *Polymer-layered silicate nanocomposites: preparation, properties and uses of a new class of materials.* Materials Science and Engineering, 2000. **28**: p. 1-63.

97.   Lagaly, G., *Introduction: from clay mineral-polymer interactions to clay mineral-polymer nanocomposites.* Applied Clay Science, 1999. **15**(1-2): p. 1-9.

98.   LeBaron, P.C., Wang, Z., and Pinnavaia, T.J., *Polymer-layered silicate nanocomposites: an overview.* Applied Clay Science, 1999. **15**(1-2): p. 11-29.

99.   Gacitua, W., Ballerini, A., and Zhang, J., *Polymer Nanocomposites: Synthetic and Natural Fillers: A Review.* Maderas: Ciencia y Technología, 2005. **7**(3): p. 159-178.

100.   Faucheu, J., Gauthier, C., Chazeau, L., Cavaillé, J.-Y., Mellon, V., and Bourgeat-Lami, E., *Miniemulsion polymerization for synthesis of structured clay/polymer nanocomposites: Short review and recent advances.* Polymer, 2010. **51**: p. 6-17.

101.   Asua, J.M., European FP6 Report No. IP 011844-2 *Nanostructured waterborne polymer films with outstanding properties*, 2010, http://www.ehu.es/napoleon/.

102.   Esfandiari, A., Nazokdast, H., Rashidi, A.-S., and Yazdanshenas, M.-E., *Review of Polymer-Organoclay Nanocomposites.* Journal of Applied Sciences, 2008. **8**(3): p. 545-561.

103.   Chen, B., Evans, J.R.G., Greenwell, H.C., Boulet, P., Coveney, P.V., Bowden, A.A., and Whiting, A., *A critical appraisal of polymer–clay nanocomposites.* Chemical Society Reviews, 2008. **37**(3): p. 568-594.

104.   Biswas, M. and Ray, S.S., *Recent Progress in Synthesis and Evaluation of Polymer-Montmorillonite Nanocomposites.* Advances in Polymer Science, 2001. **155**: p. 170-221.

105.   Bourgeat-Lami, E., *Organic/Inorganic Nanocomposite Colloids.* Encyclopedia of Nanoscience and Nanotechnology, 2004. **8**: p. 305-332.

106.   Kickelbick, G., *Concepts for the incorporation of inorganic building blocks into organic polymers on a nanoscale.* Progress in Polymer Science, 2003. **28**: p. 83-114.

107.   Giannelis, E.P., Krishnamoorti, R., and Manias, E., *Polymer-Silicate Nanocomposites: Model Systems for Confined Polymers and Polymer Brushes.* Advances in Polymer Science, 1999. **138**: p. 107-147.

108.   Yariv, S. and Cross, H., *Organo-Clay Complexes and Interactions*. 2002, New York: Marcel Dekker, Inc.

109.   Solomon, D.H. and Hawthorne, D.G., *Chemistry of Pigments and Fillers*. 1982, New York: John Wiley & Sons.

110.   Utracki, L.A., *Clay-Containing Polymeric Nanocomposites*. Vol. Volume 1. 2004, Shawbury, UK: Rapra Technology Limited.

111.   Vaia, R.A., Vasudevan, S., Krawiec, W., Scanlon, L.G., and Giannelis, W.P., *New polymer electrolyte nanocomposites: melt intercalation of poly(ethylene oxide) in mica-type silicates.* Advanced Materials, 1995. **7**: p. 154-156.

112.   Miyanaga, S., Doi, Y., Nishimura, K., Nishi, I., and Sumida, Y., *Process for antistatic treatment of resin and antistatic resin composition*. Patent No: US 5,879,589 (1999).

113.   Bergaya, F. and Lagaly, G., *Surface modification of clay minerals.* Applied Clay Science, 2001. **19**: p. 1-3.

114.   Samakande, A., Juodaityte, J.J., Sanderson, R.D., and Hartmann, P.C., *Novel Cationic RAFT-Mediated Polystyrene/Clay Nanocomposites: Synthesis, Characterization, and Thermal Stability.* Macromolecular Materials and Engineering, 2008. **293**(5): p. 428--437.

115.   Samakande, A., Sanderson, R.D., and Hartmann, P.C., *Encapsulated Clay Particles in Polystyrene by RAFT Mediated Miniemulsion Polymerization.* Journal of Polymer Science: Part A: Polymer Chemistry, 2008. **46**(21): p. 7114-7126.

116.   Lee, D.C. and Jang, L.W., *Preparation and Characterization of PMMA-clay Hybrid Composite by Emulsion Polymerization.* Journal of Applied Polymer Science, 1996. **61**(7): p. 1117-1122.

117.   Wang, D., Zhu, J., Yao, Q., and Wilkie, C.A., *A Comparison of Various Methods for the Preparation of Polystyrene and Poly(methyl methacrylate) Clay Nanocomposites.* Chemistry of Materials, 2002. **14**: p. 3837-3843.

118.   Fu, X., Qutubuddin, S., *Polymer–clay nanocomposites: exfoliation of organophilic montmorillonite nanolayers in polystyrene.* Polymer, 2001. **42**: p. 807-813.

119.   Tyan, H.-L., Wei, K.-H., and Hsieh, T.-E., *Mechanical Properties of Clay-Polyimide (BTDA-ODA) Nanocomposites via ODA-Modified Organoclay.* Journal of Polymer Science: Part B: Polymer Physics, 2000. **38**: p. 2873-2878.

120.   Choi, Y.S., Wang, K.H., Xu, M., Chung, I.J., *Synthesis of Exfoliated Polyacrylonitrile/Na-MMT Nanocomposites via Emulsion Polymerization.* Chemistry of Materials, 2002. **14**: p. 2936-2939.

121.   Choi, Y.S., Kim, Y.K., Chung, I.J., *Poly(methyl methacrylate-co-styrene)/Silicate Nanocomposites Synthesized by Multistep Emulsion Polymerization.* Macromolecular Research, 2003. **11**(6): p. 418-424.

122.   Choi, Y.S., Choi, M.H., Wang, K.H., Kim, S.O., Kim, Y.K., Chung, I.J., *Synthesis of Exfoliated PMMA/Na-MMT Nanocomposites via Soap-Free Emulsion Polymerization.* Macromolecules, 2001. **34**: p. 8978-8985.

123.   Xu, M., Choi, Y.S., Wang, K.H., Kim, J.H., Chung, I.J., *Synthesis and Properties of Exfoliated Poly(methyl methacrylate-co-acrylonitrile)/Clay Nanocomposites via Emulsion Polymerization.* Macromolecular Research, 2003. **11**(6): p. 410-417.

124.   Choi, Y.S., Chung, I.J., *Poly(n-butyl acrylate-co-methyl methacrylate) and Poly(n-butyl acrylate-co-styrene)/Silicate Nanocomposites Prepared by Emulsion Polymerization.* Macromolecular Research, 2003. **11**(6): p. 425-430.

125.   Xu, M., Choi, Y.S., Kim, Y.K., Wang, K.H., and Chung, I.J., *Synthesis and characterization of exfoliated poly(styrene-co-methyl methacrylate)/ clay nanocomposites via emulsion polymerization with AMPS.* Polymer, 2003. **44**: p. 6387-6395.

126. Kim, Y.K., Choi, Y.S., Wang, K.H., and Chung, I.J., *Synthesis of Exfoliated PS/Na-MMT Nanocomposites via Emulsion Polymerization.* Chemistry of Materials, 2002. **14**: p. 4990-4995.

127. Choi, Y.S.H., H.T., Chung, I.J., *Polymer/silicate nanocomposites synthesized with potassium persulfate at room temperature: polymerization mechanism, characterization, and mechanical properties of the nanocomposites.* Polymer, 2003. **44**: p. 8147-8154.

128. Huang, X., Brittain, W.J., *Synthesis and Characterization of PMMA Nanocomposites by Suspension and Emulsion Polymerization.* Macromolecules, 2001. **34**: p. 3255-3260.

129. Sun, Q., Deng, Y., and Wang, Z.L., *Synthesis and Characterization of Polystyrene-Encapsulated Laponite Composites via Miniemulsion Polymerization.* Macromolecular Materials and Engineering, 2004. **289**(3): p. 288-295.

130. Manea, M., Chemtob, A., Paulis, M., De la Cal, J.C., Barandiaran, M.J., and Asua, J.M., *Miniemulsification in High-Pressure Homogenizers.* AIChE Journal, 2008. **54**(1): p. 289-297.

131. Bucking, W., Du, B., Turshatov, A., Konig, A.M., and Reviakine, I., *Quartz crystal microbalance based on torsional piezoelectric resonators.* Review of Scientific Instruments, 2007. **78**(7): p. 074903-1 - 074903-8.

132. Paulis, M., Bonnefond, A., Micusik, M., and Leiza, J.R., *New Agitated and Thermostatized Cell for In-Situ Monitoring of Fast Reactions by Synchrotron SAXS.* Journal of Synchrotron Radiation, 2009. **16**: p. 869-871.

133. Turshatov, A. and Adams, J., *A new monomeric FRET-acceptor for polymer interdiffusion experiments on polymer dispersions.* Polymer, 2007. **48**(26): p. 7444-7448.

134. Patel, M.J., Gundabala, V.R., and Routh, A.F., *Modeling Film Formation of Polymer-Clay Nanocomposite Particles.* Langmuir, 2010. **26**(6): p. 3962-3971.

135. Diaconu, G., Asua, J.M., Paulis, M., and Leiza, J.R., *High-Solids Content Waterborne Polymer-Clay Nanocomposites.* Macromolecular Symposia, 2007. **259**: p. 305-317.

136. Choudalakis, G. and Gotsis, A.D., *Permeability of polymer/clay nanocomposites: A review.* Europeaan Polymer Journal, 2009. **45**(4): p. 967-984.

137. Sorrentino, A., Tortora, M., and Vittoria, V., *Diffusion Behavior in Polymer–Clay Nanocomposites.* Journal of Polymer Science: Part B: Polymer Physics, 2006. **44**(2): p. 265-274.

138. Ku, B.-C., Froio, D., Steeves, D., Kim, D.W., Ahn, H., Ratto, J.A., Blumstein, A., Kumar, J., and Samuelson, L.A., *Cross-linked Multilayer Polymer-Clay Nanocomposites and Permeability Properties.* Journal of Macromolecular Science. Part A - Pure and Applied Chemistry, 2004. **41**(12): p. 1401-1410.

139. Barrer, R.M. and Petropoulos, J.H., *Diffusion in heterogeneous media: lattices of parallelepipeds in a continuous phase.* British Journal of Applied Physics, 1961. **12**(691-697).

140. Nielsen, L., *Models for the Permeability of Filled Polymer Systems.* Journal of Macromolecular Science. Part A - Pure and Applied Chemistry, 1967. **1**(5): p. 929-942.

141. Neogi, P., ed. *Diffusion in Polymers*. 1996, Marcel Dekker Inc.: New York. 309.

CHAPTER 4

Materials and Methods

Summary: The experimental methods used for the synthesis of model polymers are discussed, as well as the analytical test methods used to characterise the resultant polymer films.

Three experimental procedures are discussed: (1) The synthesis of poly(styrene-co-butyl acrylate) latex via miniemulsion polymerisation where the latexes are stabilized with three different types of surfactants: an anionic surfactant (sodium dodecyl benzene sulfonate, SDBS), a non-ionic surfactant (octyl phenol ethoxylate, OPE) and a surfmer with a reactive counterion (dodecylammonium-3-butenoate, DA3B). (2) The synthesis of poly(styrene-co-butyl acrylate)/sodium montmorillonite polymer clay nanocomposite with 2-acrylamido-2-methylpropanesulfonic acid (AMPS) as organophilic clay modifier via miniemulsion polymerisation. (3) The synthesis of poly(octadecyl acrylate-co-methyl methacrylate) polymer via solution polymerisation.

Three types of film preparation methods are discussed, namely casting of films, spin coating of films and pressing of films. The polymers synthesized were characterised in terms of chemical composition, molecular weight, particle sizes, thermal properties and free volume. The degree of exfoliation of clays was determined (for the polymer clay nanocomposites), crystal structure was determined, surface properties of films were characterised and sorption properties of films were determined. These methods and sample preparation procedures are discussed.

4.1   Background

Water vapour sorption behaviour of model polymers was evaluated in terms of the type of surfactant used to stabilize poly(styrene-*co*-*n*-butyl acrylate) (*p*(Sty-*co*-BA)) random copolymer latexes, the incorporation of sodium montmorillonite (Na-MMT) into the *p*(Sty-*co*-BA) matrix, and crystallinity of *poly(*octadecyl-*co*-methyl methacrylate) (*p*(ODA-*co*-MMA)) random copolymers. This was done by synthesizing the following polymers and measuring their water vapour sorption properties:

- *p*(Sty-*co*-BA) random copolymers stabilized with three different model surfactants (SDBS, OPE or DA3B);
- *p*(Sty-*co*-BA)/Na-MMT nanocomposites containing AMPS and Na-MMT
- *p*(ODA-*co*-MMA)

Although it is recognised that classical emulsion polymerization has successfully been used for the polymerization of homopolymers from water-insoluble monomers,[1] it was initially decided to use miniemulsion polymerization instead of classical emulsion polymerization for the synthesis of all the latexes for this study, as this would ensure comparable systems and it would also eliminate the impact of variability of mass transfer of monomers used for the preparation of the copolymers due to varying hydrophobicity of the monomers. During the execution of the project is was however decided to use solution polymerization for the synthesis of *p*(ODA-*co*-MMA) to eliminate the negative impact of surfactant on the water sensitivity of the resultant polymer films. The synthesis procedures, sample preparation and analytical methods used are described here.

4.2   Synthesis Procedures

4.2.1   Synthesis of poly*(*styrene-*co*-*n*-butyl acrylate) latex using different surfactants

The choice of surfactant system for the stabilization of emulsions (conventional or miniemulsion) will impact on the surface properties of the final film in terms of its surface tension and therefore its hydrophilicity.[2] This can be expected to further impact on the water vapour sorption properties of the final polymer film. Nonionic, cationic and anionic surfactant systems have been investigated for miniemulsion systems.[3] For the purpose of this investigation a model random copolymer, *p*(Sty-*co*-BA), was evaluated in terms of three different types of surfactant systems (See Figure 4.1 for chemical structures):

1.   Anionic surfactant: sodium dodecyl benzene sulfonate (SDBS)
2.   Nonionic surfactant: octyl phenol ethoxylate (OPE)

3. Reactive surfactant: Surfmer with organic polymerizable counterion: dodecylammonium-3-butenoate (DA3B)
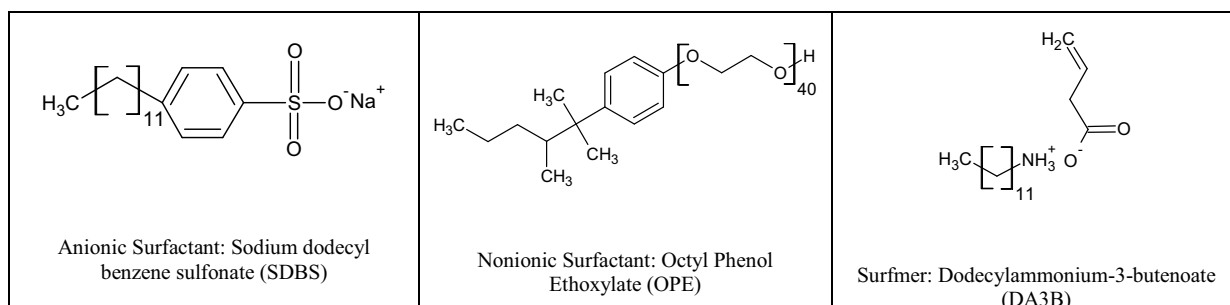
Figure 4.1: Chemical structures of surfactant systems.

4.2.1.1 Materials

n-Butyl acrylate (BA, Aldrich, 99%) and styrene (Sty, Aldrich, 99%) were washed with 0.3 M potassium hydroxide (KOH, Saarchem, 85%) to remove the inhibitor and distilled. Monomers were stored at 4 °C prior to use. Hexadecane (HD, Aldrich, 99% GC grade), methanol (Kimix, technical grade), sodium dodecyl benzene sulfonate (SDBS, Rhodacal SD-4, Rhodia, 25%), octyl phenyl ethoxylate (OPE, Igepal CA897, Rhodia, 70%), dodecylammonium-3-butenoate (DA3B, synthesized in-house), azobiscyanoisovaleric acid (ACV, Fluka, 98% puram.), methanol (MeOH, Saarchem, 98%) and hydrochloric acid (HCl, Saarchem, 37%) were used as received. Tetrahydrofuran (THF, Aldrich, HPLC grade) was distilled before being used. Distilled deionized water, produced by a Millipore Milli-Q water purification system, was used.

4.2.1.2 Experimental procedure

The model *p*(Sty-*co*-BA) copolymer was evaluated in terms of the 3 surfactants. In another study where the role of surfactants in latex films were evaluated, Butler et al. [4] used a seed polymer where the surfactant was removed via dialysis and the polymer stabilized through post addition of different surfactants to ensure particle size uniformity. Contrary to this, different surfactants and surfactant concentrations were used during polymerization of this model polymer as the low T_g of the polymer would have resulted in agglomeration at room temperature of the polymer particles after dialysis and removal of the original surfactant. (See Table 4.1).

Theoretical T_g calculations were based on the Fox equation (See Equation 4.1) for the determination of the ratio of co-monomers required to obtain a theoretical T_g value of 10 °C.[5]

$$\frac{1}{T_g} = \frac{m_1}{T_{g_1}} + \frac{m_2}{T_{g_2}} + \cdots + \frac{m_n}{T_{g_n}} \tag{4.1}$$

where T_g is the glass transition temperature (in Kelvin) of the copolymer, T_{g1}, T_{g2}, etc. refers to the glass transition temperatures (in Kelvin) of the homopolymers of the individual monomers incorporated into the copolymer, and m_1, m_2, etc. refers to the fractional mass of monomer (in gram/gram) that were used for the synthesis of the copolymer.

Example of calculations: p(Sty-*co*-BA) with a T_g of 10 °C

$$\frac{1}{T_g p(StyBA)} = \frac{\left[\frac{m(Sty)}{m(Sty + BA)}\right]}{T_g(Sty)} + \frac{\left[\frac{m(BA)}{m(Sty + BA)}\right]}{T_g(BA)}$$

$$= \frac{\frac{8.5}{15.5}}{373} + \frac{\frac{7}{15.5}}{219}$$

$$T_g p(StyBA) = 10.09°C$$

p(Sty-*co*-BA) random copolymers were synthesized by a miniemulsion batch polymerization reaction. Due to stability constraints of the reactive surfactant (DA3B), azobiscyanoisovaleric acid (ACV) was chosen as initiator, instead of a more conventional initiator such as ammonium persulfate (APS). The reactor charge was premixed magnetically for 10 minutes, after which it was sonicated with a Sonics & Materials Inc. Vibracell VCX 750 ultrasonicator equipped with a 19 mm solid probe (30 minutes sonication at 90% amplitude, using pulse mode and a cut-off temperature of 40 °C) (see Table 4.1). The samples were sonicated in a water-cooled jacketed vessel to prevent polymerization due to thermal self-initiation. After miniemulsification, the samples were transferred to a glass reactor equipped with a magnetic stirrer, condenser and a nitrogen purge inlet. The reactor was purged with ultra-high purity nitrogen gas for 30 minutes after which the glass reactor was submerged into a thermostated oil bath at 80 °C and the polymerization reaction started. Conversion levels varied significantly after 3 hours, depending on the type of surfactant used. At 1% SDBS addition level, a 98.0% conversion was achieved after 250 minutes. The nonionic surfactant required a significantly longer polymerization time (almost 24 hours) and a much higher surfactant concentration (6%) to reach 98.5% conversion level. A concentration of 1% DA3B was required for the reactive surfactant polymerization to achieve a 97.5% conversion after 300 minutes.

Table 4.1: Formulation and synthesis parameters

Reactor Charge	Conconcentration [% of total monomer, w/w]	Monomer Mol Fraction	Mass [g]
DDI water		-	50
Surfactant: SDBS	0.5%,1%,2%	-	Variable
: OPE	2%,4%,6%	-	Variable
: DA3B	0.5%,1%,2%	-	Variable
HD	4%	-	0.6
Sty		0.599	8.50
n-BA		0.401	7.00
Initiator: ACV	0.1%	-	0.015

4.2.2   Synthesis of poly(styrene-*co*-butyl acrylate)/Na-MMT composites

When incorporated into a polymer matrix, the high aspect ratio of plate-like fillers leads to an increase in the tortuosity of the path of penetrants through the resultant PCN film. This can impact on the diffusion of gases and vapours through the PCN film and therefore impact on its sorption properties. The purpose of this investigation was therefore to evaluate the impact of Na-MMT, a hydrophilic plate-like filler, on the water vapour barrier properties of a hydrophobic polymer. A series of PCNs were synthesized, based on the work of Choi et al. [6] and Greesh et al. [7, 8], using AMPS to incorporate pristine Na-MMT into *p*(Sty-*co*-BA) polymer. The impact of increasing amounts of Na-MMT on the diffusion coefficient, and therefore the sorption properties of the resultant PCN, was evaluated.

Different concentrations of AMPS were used as organophilic modifier for the Na-MMT clay. An increase in organophilic content should result in an increase in the solubility coefficient. The water vapour sorption properties were therefore evaluated in terms of the expected change in the solubility coefficient as well as the impact of increased tortuosity due to the presence of Na-MMT in the polymer matrix.

4.2.2.1 Materials

n-Butyl acrylate (BA, Aldrich, 99%) and styrene (Sty, Aldrich, 99%) were washed with 0.3 M potassium hydroxide (KOH, Saarchem, 85%) to remove the inhibitor and distilled. Monomers were stored at 4 °C prior to use. Hexadecane (HD, Aldrich, 98%), osmium tetroxide, methanol, ammonium hydroxide (NH$_4$OH, Saarchem), ammonium persulfate (APS, Saarchem), 4,4-azobis(4-cyanovaleric acid (ACV, Fluka, >97%), 2-acrylamido-2-methylpropanesulfonic acid (AMPS) and sodium dodecyl benzene sulfonate (SDBS, Fluka, 80%) were used without further purification. Sodium montmorillonite (Na-MMT, Cloisite Na$^+$, Southern Clay Products) was dried under vacuum at 40 °C for 24 hours and stored in a dessicator prior to use. Distilled deionized water produced by a Millipore Milli-Q water purification system, was used.

4.2.2.2 Experimental procedure: Modification of Na-MMT

Na-MMT was pre-dispersed in water containing different concentrations of AMPS, and stirred for a period of 24 hours at room temperature, allowing the water to swell the Na-MMT, thereby increasing the interlayer space and allowing the AMPS to be absorbed onto the clay surface. The clay surface was modified via hydrogen bonding between the amido group of the AMPS and the hydroxyl

groups from the octahedral sheets of the Na-MMT, and hydrogen bonding between the sulfate group of the AMPS and the hydroxyl groups of the clay surface.[8]

The work of Greesh et al. showed that for an AMPS concentration equal to 100% of the CEC of Na-MMT, approximately 5% of the initial amount of AMPS added to the clay dispersion was adsorbed onto the clay surface. The balance of the AMPS remained in solution. This is due to the type of mechanism whereby the clay is modified, namely hydrogen bonding instead of cation exchange. For the purpose of this study, different AMPS concentrations were used, namely 1.5%, 3.0%, 4.5% and 6.0% relative to the amount of monomer used in the synthesis of the PCN. These AMPS concentrations were significantly higher than the CEC for Na-MMT. It can therefore be assumed that a large proportion of the AMPS would remain in solution after the modification of Na-MMT and would be available for incorporation into the polymer backbone with styrene and *n*-butyl acrylate.

Organically modified Na-MMT was prepared for the synthesis of two series of p(Sty-co-BA)/Na-MMT PCNs: (1) 5% Na-MMT relative to the amount of monomer used for the polymerization of the PCN, modified with 0.225 g, 0.450 g, 0.675 g and 0.900 g AMPS respectively (refer to Table 4.2); and (2) 1%, 3%, 5% and 10% Na-MMT relative to the amount of monomer used for the polymerization of the PCN, modified with 0.675 g of AMPS (refer to Table 4.3).

Table 4.2: AMPS concentration used to modify 5% Na-MMT

AMPS concentration relative to monomer [wt%]	1.5	3.0	4.5	6.0
AMPS [g]	0.225	0.450	0.675	0.900
Na-MMT [g]	0.75	0.75	0.75	0.75
CEC: Equivalent moles of anionic charges on Na-MMT [meq/0.75g of Na-MMT]	0.6945	0.6945	0.6945	0.6945
AMPS added - percentage of CEC of Na-MMT [%]	156	312	469	625
Unbound AMPS-assuming 5% of CEC is bound to Na-MMT [mmol]	1.0509	2.1366	3.2222	4.3079

Table 4.3: 4.5% AMPS used to modify various quantities of Na-MMT

AMPS concentration relative to monomer [wt%]	4.5	4.5	4.5	4.5	4.5
AMPS [g]	0.675	0.675	0.675	0.675	0.675
Na-MMT [g]	0	0.15	0.45	0.75	1.5
CEC: Equivalent moles of anionic charges on Na-MMT [meq/x g of Na-MMT]	0	0.1389	0.4167	0.6945	1.389
AMPS - percentage of CEC of Na-MMT added [%]	0	17308	781	479	235
Unbound AMPS-assuming 5% is bound to Na-MMT [mmol]	3.257	3.250	3.236	3.222	3.188

4.2.2.3 Experimental procedure: PCNs with increasing amount of Na-MMT

PCNs, consisting of *p*(Sty-*co*-BA) random copolymers (styrene: *n*-butyl acrylate weight ratio was 1.21:1 for all PCNs) and organically modified Na-MMT clay, were synthesized by a miniemulsion polymerization reaction. A semi-batch process was used in order to maintain a starve-feed

polymerization mechanism, thereby controlling the rate of polymerization, minimizing the formation of coagulum and ensuring exfoliation of the Na-MMT clay.

The Na-MMT clay was organically modified before adding it to the kettle charge (see 4.2.2.2). The seed monomer (25% of the total monomer) was added to the pre-dispersed organically modified Na-MMT and was premixed magnetically for 30 minutes at room temperature, before it was sonicated with a Sonics & Materials Inc. Vibracell VCX 750 ultra-sonicator equipped with a 19 mm solid probe (90% amplitude; 2.5/1.0 seconds pulsing mode; 10 minutes duration; and 50 °C cut-off temperature). The samples were sonicated in a water-cooled jacketed vessel to prevent polymerization due to heating. After miniemulsification, the pH of the miniemulsion was adjusted to pH9 with ammonium hydroxide, and the sample was transferred to a glass reactor equipped with a magnetic stirrer, condenser and a nitrogen purge inlet. The glass reactor was submerged into a thermostated oil bath, purged with ultra-high purity nitrogen gas for 30 minutes after which the polymerization reaction was started through the addition of APS at 85 °C, whilst stirring at 100 rpm. The controlled addition of the remaining monomer started one hour after the initial polymerization started. The remaining monomer was fed into the reactor charge at a rate of 0.062 mL/min by means of a positive displacement pump. The monomer conversion was monitored gravimetrically. After 6 hours the polymerization reaction was completed, resulting in 88-98% monomer conversion levels. A detailed description of the polymerization setup is summarized in Table 4.4 below.

Table 4.4: PCN series using 4.5% AMPS as organophilic modifier with increasing amounts of Na-MMT

Synthesis parameters	[% of total monomer w/w	Mass [g]
Step 1: Na-MMT modification		
DDI water	-	52g
AMPS	4.5%	0.675g
Na-MMT	0%,1%,3%,5%,10%	0 g, 0.15 g, 0.45 g, 0.75 g, 1.5 g
Step 2: Initial reactor charge		
(Added to modified Na-MMT)		
SDBS (10% solution)	1%	1.52 g
HD	4%	0.60 g
Sty/n-BA monomer mix (1.21:1 weight ratio)	25%	3.75 g
Step 3: Initiator addition		
APS (1% solution)	0.15%	2.25 g
Step 4: Monomer feed		
Sty/n-Ba monomer mix (0.062 mL/min)	75%	11.29 g
Step 5: Initiator		
APS (1% solution)	0.02%	0.25 g

4.2.2.4 Experimental procedure: PCNs with increasing amount of AMPS

Refer to Section 0 for procedure and Table 4.5 for a detailed description of the experimental setup.

Table 4.5: PCN series using 5% Na-MMT with increasing amount s of AMPS as organophilic modifier

Synthesis parameters	Conc. [% of total monomer w/w]	Mass [g]
Step 1: Na-MMT modification		
DDI water	-	52g
AMPS	1.5%, 3.0%, 4.5%, 6.0%	0.225 g, 0.450 g, 0.675 g, 0.900 g
Na-MMT	5%	0.75 g
Step 2: Initial reactor charge		
(Added to modified Na-MMT)		
SDBS (10% solution)	1%	1.52 g
HD	4%	0.60 g
Sty/n-BA monomer mix (1.21:1 weight ratio)	25%	3.75 g
Step 3: Initiator addition		
APS (1% solution)	0.15%	2.25 g
Step 4: Monomer feed		
Sty/n-Ba monomer mix (0.062 mL/min)	75%	11.29 g
Step 5: Initiator		
APS (1% solution)	0.02%	0.25 g

4.2.3 Synthesis of poly(octadecyl acrylate-*co*-methyl methacrylate)

A 3-monomer system consisting of styrene, *n*-butyl acrylate and octadecyl methacrylate was initially considered for the evaluation of the impact of crystallinity on the sorption properties of the resultant polymer film. Due to the complexity of 3 monomers in a random batch polymerization, this was abandoned after a couple of failed attempts to achieve reproducibility in the incorporation of the 3 monomers, as well as the resultant properties of the final polymers. It was therefore decided to use only a 2-monomer system such as styrene and octadecyl methacrylate. Previous research however also showed that the incorporation of styrene monomer units increases the stiffness of the backbone, thus impeding the alignment of the alkyl chains of the alkyl (meth)acrylates, and limiting or preventing crystallization of the resultant polymer.[9] Furthermore, the greater rigidity of the alkyl methacrylate monomers resulted in a lower degree of crystallinity compared to the corresponding alkyl acrylate monomers.[10-12]

For the purpose of this investigation, it was therefore decided to evaluate the impact of side-chain crystallinity of an *n*-alkyl acrylate monomer on an amorphous polymer matrix by introducing increasing quantities of octadecyl acrylate (ODA) monomer to poly-methyl methacrylate (PMMA). These two monomers and their resultant homopolymers exhibit different degrees of hydrophobicity, with ODA being the most hydrophobic monomer and polymer.[13] A secondary impact of increased hydrophobicity on the water vapour sorption behaviour was therefore evaluated.

4.2.3.1 Materials

Methyl methacrylate (MMA, Aldrich, 99%) was washed with 0.3 M potassium hydroxide (KOH, Saarchem, 85%) to remove the inhibitor and was stored at 4 °C prior to use. Octadecyl acrylate

(ODA, Aldrich, 98%) was dissolved in hexane and the inhibitor removed using a column containing basic alumina (Sigma, type WB-2 Basic). 2,2-Azo-bis-isobutyronitrile (AIBN, Aldrich) was recrystallized 3 times from MeOH and dried under vacuum at room temperature before being used. Methanol (MeOH, Saarchem, 98%), heptane (Saarchem), toluene (Saarchem) and deuterated chloroform (CDCl$_3$, Aldrich) were used as received.

4.2.3.2 Experimental procedure

MMA-*co*-ODA random polymers were synthesized by a solvent batch polymerization reaction targeting a 35% polymer solution concentration. ODA and MMA were weighed off in a round bottomed flask and dissolved in heptane (Refer to Table 4.6) for reactor charge of the different copolymers). Thereafter the reactor charge was equipped with a magnet, connected to a condenser and purged with ultra-high purity nitrogen for 10 minutes while magnetically agitating the reactor charge. The initiator was added and the reactor charge purged further for another 10 minutes before submerging the reactor in a thermostated oil bath at 60 °C. The polymerization was stopped after a period of 24 hours.[14]

The resultant copolymer was recovered by precipitating the polymer in ice cold MeOH while stirring continuously. The polymer precipitate that formed was filtered off using Whatman Nr1 filter paper and dried in a fume hood at room temperature. The polymer was re-dissolved in heptane, re-precipitated in MeOH and dried three times before finally allowing it to dry at room temperature for a period of 24 hours.

Table 4.6: Reactor charge for the ODA series

Theoretical mol% ODA	ODA [g] Actual (Calculated)	MMA [g] Actual (Calculated)	AIBN [g] ±0.1% of [monomer]	Heptane [g]
0% ODA	0.0000 (0.000)	6.7924 (6.750)	0.0683	12.5
25% ODA	3.5121 (3.500)	3.2568 (3.250)	0.0680	12.5
50% ODA	5.2545 (5.250)	1.7219 (1.625)	0.0666	12.5
75% ODA	6.1457 (6.125)	0.6913 (0.625)	0.0652	12.5
100% ODA	6.7633 (6.750)	0.0000 (0.000)	0.0622	12.5

Films were prepared by dissolving the dried polymer in toluene (10% solution), casting it onto aluminium foil and allowing it to dry at room temperature for a period of 7 days. The combination of the brittle nature of PMMA and the crystalline nature of PODA resulted in the formation of fairly brittle films.

4.3   Film preparation methods

Contrary to the industrial requirements of films, where good adhesion to the substrate is a prerequisite, it is important that, for academic studies, polymer films can easily be removed from its substrate to allow for further characterization.[15] Films are therefore prepared by: casting onto surfaces such as photographic paper (and soaking it in warm water to dissolve the gelatin), aluminium foil, silanised plate glass, or PTFE surfaces where the film can be removed by gently peeling it from the substrate.

Different methods for the preparation of films were explored, looking at both film casting from emulsion and solvent. These included:

4.3.1   Casting films

Films were prepared by casting 2 mL of latex (20% solids) onto a glass microscope slide (size: 1 cm x 4 cm). The samples were left for approximately 24 hours at room temperature to allow for film formation, after which it was placed in a standard convection oven (110 °C) for 2 hours to remove any remaining water or volatiles.

Alternatively, the surfactant was removed from latex samples prior to preparing the film by destabilizing 15 mL of latex through the addition of 150 mL of methanol. Thereafter two drops of hydrochloric acid (37%) were added while stirring magnetically at 200 rpm. After the polymer had precipitated, the aqueous phase was decanted and the polymer washed with 5 aliquots of 200 mL of distilled water. The polymer was dried under vacuum at room temperature for 24 hours. A film was then prepared by (1) dissolving the polymer in a solvent such as THF and casting it from solvent onto a glass microscope slide; (2) spin coating the film; or (3) pressing the film.

Films were conditioned for a period of one week in a dessicator before analysis.

4.3.2   Spin coating films

Polymers were precipitated in the same manner as described above. Thereafter the precipitate was dissolved in THF and the dissolved polymer was spun from solvent using a spin coating machine. The spinning speed, the amount of polymer dissolved in THF and the spinning time were optimized for each sample. On average films were prepared using approximately 5 grams of latex, spinning the dissolved sample for approximately two minutes at a spinning speed range of 1000-2000 rpm.

4.3.3   Pressing films

Accurate control over the films thickness is limited with the above two film preparation methods. However, with the use of a sample mould designed to give controlled film thickness, it was possible to press samples at elevated temperatures to give films with accurately controlled film thicknesses. This was done on a Graseby Specac Press at 120 °C and varying pressure (depending on the type of polymer used). 0.2 g of precipitated dried polymer sample was placed into the sample mould. The method was only suitable for polymers with a high glass transition temperature as the high processing temperature would otherwise result in tackiness of the film. Unless otherwise specified, all films were conditioned at 50% relative humidity and 23 °C for a period of 1 week before being analyzed.

4.4   Analytical Methods

4.4.1   Chemical composition and molecular weight determination

4.4.1.1   Nuclear magnetic resonance spectroscopy

Nuclear magnetic resonance spectroscopy (NMR) was used to monitor the chemical composition of the synthesized copolymer.

1 mL of latex was precipitated in 50 mL of methanol containing 2 mL of HCl. The precipitated polymer was recovered by filtration through Whatman Nr1 filter paper. The resultant polymer was washed with 2 aliquots of distilled water and dried at room temperature, after which the polymer was dissolved in $CDCl_3$ (50 mg/5 mL) and analysed by ^{1}H NMR spectroscopy (Varian Inova 600MHz NMR spectrometer).

The signals integration methodology is described in Appendix A.

4.4.1.2   Size exclusion chromatography

Size exclusion chromatography (SEC) was used to determine the molecular weight of the synthesized polymers.

Sample preparation: The latex was precipitated in MeOH containing a few drops of 37% HCl and was stirred for 10 minutes. Thereafter the precipitated polymer was recovered by filtration through Whatman Nr1 filter paper and washed with distilled water to remove traces of HCl. The polymer was further purified by dissolving it in $CHCl_3$, precipitating it again with MeOH (without HCl) and

recovering the polymer via filtration. Thereafter the polymer was dried overnight under vacuum and used for the preparation of samples for SEC analysis.

The purified polymer was dissolved completely in THF (2 mg/mL), filtered with 0.22 μm syringe filter until completely clear.

Experimental setup: The SEC instrument used comprised of the following units: Waters 1515 isocratic HPLC pump; Waters 717 plus Autosampler; Waters 2487 Dual λ Absorbance detector; Waters 2414 Refractive index (RI) detector at 30 ^{o}C and data processing was performed using Breeze Version 3.30 SPA (Waters) software. Separation was achieved using two PLgel (Polymer Laboratories) 5μm Mixed-C (300×7.5 mm) columns connected in series along with a PLgel 5μm guard column (50×7.5 mm). The columns were kept at a constant temperature of 30 ^{o}C. THF Chromasolve HPLC grade solvent (0.125% BHT stabilised) was used as mobile phase at a flow rate of 1 ml/min and 100 μl injection volumes were used. The system was calibrated using polystyrene standards (Polymer Laboratories).

4.4.2   Particle size analysis

A variety of methods exist for the determination of latex particle sizes. [16] The effectiveness of these methods depends on the specific latex properties and is influenced by factors such as particle shape, particle size distribution and the degree of agglomeration or coagulation of adjacent latex particles. For this investigation, the latex particle size was determined by means of 2 techniques: dynamic light scattering (DLS) and transmission electron microscopy (TEM).

4.4.2.1 Dynamic light scattering

Dynamic light scattering (DLS), also known as photon correlation spectroscopy (PCS) or quasi-elastic light scattering (QELS), is an indirect and non-invasive technique whereby latex particle sizes are determined.[16] The principle of this method is based on the scattering of monochromatic light by small particles such as polymer particles, which will induce a shift in the frequency in the scattered light by particle diffusion under the influence of Brownian motion. When analyzed, the scattered beam can be related to an average diffusion coefficient of particles for a monodisperse sample, or to a distribution of diffusion coefficients for a polydisperse sample. The particle radius is determined from the diffusion coefficient, using the Stokes-Einstein relationship (See equation 4.2), where R_H is the radius, k is the Boltzmann constant, T is the temperature, η is the solvent viscosity and D is the diffusion coefficient:

$$R_H = \frac{kT}{6\pi\eta D} \tag{4.2}$$

A Malvern Zetasizer 1000HS was used for these analyses. The calibration was done using 10 mM NaCl solution and adding 2 drops of *Nanosphere*[1] standard into the solution, to give a count of 250-300 Kcps. The samples were prepared by adding the latex dropwise into 1 mM NaCl solution until a Tyndall effect[2] was observed. The particle size results were based on an average of 5 readings.

4.4.2.2 Transmission electron microscopy

Transmission electron microscopy (TEM) is a direct method of measurement. This method is especially valuable where latex particle agglomeration or fillers dispersed in the latex could distort the particle size when determined by means of indirect methods such as DLS. Emulsion-based PCNs consist of spherical latex particles with large aspect ratio clays attached to the sides of the latex particle. The largest dimension of the clay particle can be up to five times larger than the diameter of the latex particle. This discrepancy in size could result in a false particle size if determined by indirect methods such as the light scattering technique.

Sample preparation: Latex samples were diluted with DDI water until the latex appeared to be slightly transparent, after which it was mixed (ratio 1:1) with uranyl acetate staining agent. 20 µL of the mixture was placed on a Parafilm sheet, from which it was transferred to a copper grid for analysis. Excess water was removed with filter paper and the copper grid containing the emulsion particles was placed in a dessicator for 10 minutes to allow the remaining moisture to evaporate from the sample.

Experimental setup: A Leo transmission electron microscope (OMEGA 912) was used for the analysis.

4.4.3   Clay exfoliation measurements

The degree of exfoliation of clay in PCNs was measured both qualitatively (by means of transmission electron microscopy (TEM)) and quantitatively (by means of small angle X-ray spectroscopy (SAXS)).[17]

---

[1] Nanosphere: Polystyrene microspheres in water, supplied by Malvern.

[2] Tyndall effect: The Tyndall effect, more commonly known as Rayleigh scattering, refers to the effect of light scattering as a result of very small particles in colloidal systems such as suspensions or emulsions.

4.4.3.1 Transmission electron microscopy

Sample preparation: Films (of latexes) were cast at room temperature and allowed to dry for a minimum period of 48 hours. Thereafter it was sequentially stained with OsO_4, where after it was washed with water, dried and then embedded in an epoxy resin (Spurr's resin). The resin was cured for a minimum of 24 hours at 50 °C.

Experimental setup: A Reichert Ultracut S ultra microtome with a glass knife was used to microtome the embedded samples into sections of ± 100nm. This sections were transferred to 300-mesh copper grids and submitted to image recording with a JEM 200CX (JEOL Tokyo, Japan) TEM.

4.4.3.2 Small-angle X-ray scattering

Sample preparation: Films were cast onto a glass plate and allowed to dry at room temperature for a minimum period of 48 hours.

Experimental setup: Small angle X-ray scattering (SAXS) measurements were performed in a transmission configuration at 298 K. A copper rotating anode X-ray source (functioning at 4 kW), with a multilayer focusing "Osmic" monochromator giving high flux (10^8 photons/sec) and punctual collimation was used. An "image plate" 2D detector was used. Diffraction patterns were obtained, giving diffracted intensity as a function of the wave vector *q*. The wave vector is calculated using equation 4.3, where q is the wave vector, λ the radiation wavelength and θ the scattering angle.

$$q = (4\pi\lambda^{-1})\sin\frac{\theta}{2} \tag{4.3}$$

4.4.4   Crystal structure determination

X-Ray diffraction (XRD) is a useful tool to obtain structural information of polymers. At small angles structural information is obtained on larger structural properties, such as the lamellar structures within polymers due to self assembly of polymers, while at larger angles structural information related to small structural properties, such as crystalline regions in the polymer matrix, are obtained (see Figure 4.2).[18, 19]

Wide angle X-ray diffraction (WAXD) is generally used for the determination of crystal orientation within a polymer, while small angle X-Ray scattering (SAXS) is used to determine structures at lengths of approximately 10nm and also to determine electron density fluctuations occurring over larger distances as a result of structural inhomogeneities.
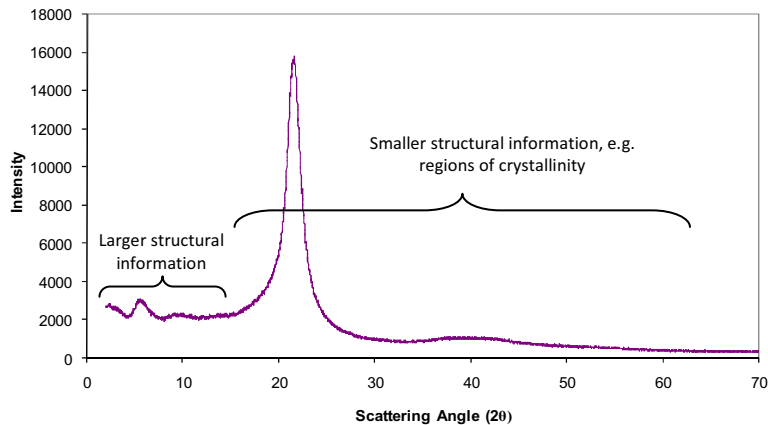
Figure 4.2: Illustration of regions where large and small structural information are obtained using XRD patterns

4.4.4.1 X-ray diffraction

In this study X-ray diffraction (XRD) in polymers is primarily used to confirm the crystal lattice pattern and the degree of crystallinity (as determined by DSC) through the integration of a 1-dimensional XRD pattern. The crystallinity is expressed as the volume fraction crystallinity of the polymer. Two approaches have been proposed in the literature:

- A two-phase model where it is assumed that the polymer consists of crystals and amorphous regions only with no semi-crystalline organization of the polymer.
- A para-crystalline model where interfacial zones between crystalline and amorphous regions are also taken into consideration.

For the purpose of determining the crystallinity, the two-phase model was assumed. The XRD integration methodology is described in Appendix H.

Sample preparation: The polymer was purified by dissolving it in heptane and precipitating it in cold methanol. This was repeated three times, after which the precipitated polymer was dried. The dried polymer was ground to a uniform size and analyzed in a powdered form.

Experimental setup: XRD scans were obtained using a Reflection-Transmission Spinner PW3064/60 sample stage from an X'PERT-PRO diffractometer. The samples were exposed to Cu Kα radiation with 45 kV and 40 mA. An angular range of 3 to 80 ° was scanned at a scan step of 0.0170 ° and a scan step time of 50.8 sec.

4.4.4.2 Small-angle X-ray scattering

SAXS was used to determine the lamellar structures of semicrystalline polymers.

Sample preparation: The polymer was purified by dissolving it in heptane and precipitating it in cold methanol. This was repeated three times, after which the precipitated polymer was dried. Films were cast from 10% solutions of the polymer in toluene and dried at ambient conditions for a minimum of 7 days before analysis.

Experimental setup: Refer to Section 4.4.3.2.

4.4.5 Polymer film surface characterization

A variety of techniques exist for the physical and chemical characterization of materials, e.g. electron microscopy, infra-red spectroscopy, surface energy (contact angle) measurement, high resolution electron energy loss spectroscopy, etc.[20, 21] Choosing the right method for the polymer surface characterization is largely driven by the type of information required, including:

- The visual appearance of the film,
- The elemental composition and the surface or interface of the film; or
- The molecules or chemical groups present at the surface or interface of the film.

Methods used in this study to characterize the surface of the polymer films are briefly described below.

4.4.5.1 FTIR transmission spectroscopy

Transmission Fourier Transform Infrared Spectroscopy (FTIR) was used to determine the relative ratio of different components within an entire polymer film.

Sample preparation: Latexes were cast onto a glass substrate and allowed to cure at ambient conditions for a minimum period of 3 days. Thereafter the formed films were removed from the support, heated slightly and stretched to a thickness of approximately 50 μm which is a suitable thickness for transmission FTIR.

Experimental setup: The films were placed in a screw-type demountable cell mount (suitable for analysis of films without a salt window support) and the samples analyzed using a Perkin Elmer Paragon 1000 FT-IR Spectrophotometer. 32 accumulations were performed at a resolution of 4 cm^{-1}.

4.4.5.2 FTIR-PAS spectroscopy

Photoacoustic spectroscopy (PAS) is an extension of the Fourier transform infrared spectroscopy (FTIR) technique and has been used extensively for depth profiling of materials to elucidate the potential chemical changes within the material at different depths.[21-28] FTIR-PAS is based on the evaluation of acoustic waves produced by thermal waves which are emitted when the sample absorbs infrared radiation.

The sampling depth, also referred to as the thermal diffusion length (μ_s), is dependent on both the wavenumber ($\bar{v}$) of the infrared radiation and the optical velocity (v) of the interferometer. The sampling depth of FTIR-PAS measurements is determined by calculating the thermal diffusion length, from equations 4.4-4.6.

$$\mu_s = \left(\frac{2k}{\rho c \omega}\right)^{1/2} \tag{4.4}$$

$$\omega = 2\pi f \tag{4.5}$$

$$f = v \cdot \bar{v} \tag{4.6}$$

Here k (cal.°C^{-1}s^{-1}cm^{-1}) denotes the thermal conductivity of the sample, ρ (gcm^{-3}) the density of the polymer, c (calg^{-1}°C^{-1}) the specific heat of the polymer, and ω (rads^{-1})the angular modulation frequency. The frequency (f) is the product of the optical velocity (v) of the interferometer and the wavenumber ($\bar{v}$) of the infrared radiation.[29]

In this study this method was used to determine the relative position of surfactants (Refer to Chapter 5) and filler particles (Refer to Chapter 6) to the rest of the polymer matrix in composite structures.

Sample preparation: Films were cast from emulsion at room temperature and allowed to dry at 55 °C.

Experimental setup: A Perkin Elmer Paragon 1000 FTIR equipped with a photoacoustic dector (MTEC300 chamber) was used.[28] Helium was used as transfer gas in the PAS detector. PAS spectra were collected over a spectral range of 400-4000 cm^{-1} by collecting 128 scans at a maximum source aperture setting with an optical velocity of 0.1cm.s^{-1} and resolution of 8 cm^{-1}. Carbon black was used as sample reference. The sample depth of FTIR-PAS measurements was varied by applying different mirror velocities: 4 different mirror velocities were used, namely 0.05 cm.s^{-1}, 0.15 cm.s^{-1}, 0.30 cm.s^{-1} and 0.75 cm.s^{-1}.

4.4.5.3 Contact angle goniometry

Contact angle measurements are used to quantify the wettability of solids by specific liquids at the three phase boundary (Point A in Figure 4.3). The angle, measured to the inside of the liquid droplet, can vary between 0 ° and 180 °. A small contact angle (θ < 90 °) indicates good wettability, with a contact angle of 0 ° showing complete wetting. Contact angles > 90 ° are indicative of poor wettability (see Figure 4.3 below).

The shape of the droplet is characteristic to the equilibrium between the liquid, solid and gas and can be described by Young's equation, where γ_{GS} is the interfacial tension between the gas and solid, γ_{LS} is the interfacial tension between the liquid and gas, γ_{LG} is the interfacial tension between the liquid and gas and θ is the contact angle at the three phase boundary (See equation 4.7):

$$\gamma_{GS} = \gamma_{LS} + \gamma_{LG} \times \cos\theta \qquad\qquad (4.7)$$
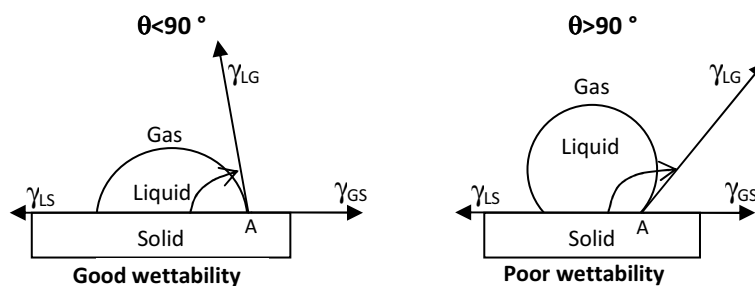
Figure 4.3: Contact angle measurement showing good and poor wettability.

The surface tension, and consequently the polarity, of solid polymers cannot be determined directly. As a result, a variety of indirect methods have been developed to determine the surface tension of solid polymers: the liquid homologue (molecular weight dependence) method, polymer melt (temperature dependence) method, equation of state method, harmonic-mean method, geometric-mean method, critical surface tension method, etc.[30] The accuracy with which the surface tension can be determined varies from one method to the next. The first 4 methods listed, are classified as being fairly accurate.

The Owens Wendt 2 component method was used for this study to determine the surface energy of a solid (γ_S), as well as its polar ($\gamma_S{}^P$) and dispersive ($\gamma_S{}^D$) components, where:

$$\gamma_S = \gamma_S^P + \gamma_S^D \tag{4.8}$$

This method requires that the contact angles of selected liquids, for which the surface tension (γ_L), the polar component (γ_L^P) and dispersive component (γ_L^D) are known, are measured for a specific solid. For each liquid a number of measurements must be made, and the average θ value is used for further calculations. The surface energy of the solid is calculated with the Owens-Wendt equation:

$$\gamma_L(1 + \cos\theta) = 2\sqrt{(\gamma_S^P \gamma_L^P)} + 2\sqrt{(\gamma_S^D \gamma_L^D)} \tag{4.9}$$

By dividing Equation 3.5 with $\sqrt{(\gamma_L^D)}$, a straight line equation is obtained, where $\sqrt{(\gamma_L^D)}$ is the y-intercept and $\sqrt{(\gamma_S^P)}$ is the slope of the straight line.

Sample preparation: The films were prepared using the spinning method (Refer to Section 4.3.2).

Experimental setup: The surface tension measurements were performed on a GBX DigiDrop contact angle analyzer, using the Sessile drop method[3]. Three liquids were used for the analysis: water (72.8 dynes.cm^{-1}), ethylene glycol (47.9 dynes.cm^{-1}) and methylene iodide (50.8 dynes.cm^{-1}). Measurements were done 10-fold under controlled environmental conditions (20 °C and 50% relative humidity). Liquid droplet size is 2 µL and is controlled via an automatic syringe.

4.4.5.4 Atomic force microscopy

Surface roughness of polymer films was determined by means of atomic force microscopy (AFM).

Sample preparation: Films were cast onto aluminium foil and allowed to cure for 7 days, conditioned at 23 °C, ±50% relative humidity prior to doing the AFM analysis. The films were removed from the aluminium foil after 2 days and turned daily thereafter to ensure homogeneity on both sides of the film.

Experimental setup: A Nanosurf EasyScan II AFM was used for the surface roughness measurements. The AFM was operated in contact mode using a 10 mm scan head and a Nanosensors PPP-contact silicone cantilever with a spring constant of k = 0.05 N.m^{-1}. The surface roughness was determined over a 20 µm x 20 µm area at 0 ° rotation, with a scan speed of 0.7

---

[3] Sessile drop method: For this method, a droplet of liquid is placed onto a solid surface using a vertically mounted software controlled syringe. A camera is used to capture the image of the droplet on the solid surface, and the contact angle is measured using sophisticated computer software.

lines/second. The average microscopic surface roughness was determined from a 256 x 256 pixel AFM image.

4.4.6   Sorption Measurements

The sorption of liquid water was determined gravimetrically, whereas the sorption of water vapour was determined by either gravimetrically or by using FTIR ATR spectroscopy.[31]

4.4.6.1 Water absorption: Gravimetry

The amount of water absorbed in the polymer films was determined gravimetrically. The amount of water absorbed is expressed as grams of water absorbed per gram of material (Refer to equation 4.10).

$$Water\ Absorbed\ [\%] = \frac{M_t - M_0}{M_0} \times 100 \tag{4.10}$$

where M_0 is the weight of the dry film and M_t is the weight of the film at time interval t.

Sample preparation: Films were prepared with and without surfactant (please refer to Section 4.3.1 for methodology). 2.5 cm x 2 cm sections (total surface area: 10 cm^2) were cut from the film and used for the water immersion tests.

Experimental setup: The films were weighed and immersed in water at 20 °C to allow the absorption of water. The amount of water absorbed was determined at specific time intervals by removing the film from the water, drying the surface water with filter paper and weighing the films with a 5-decimal balance (in grams). This process was repeated until no further change was observed in the weight of the film.

4.4.6.2 Water vapour sorption: Gravimetry

Water vapour sorption properties were determined by means of the gravimetric measurement of the amount of water vapour absorbed by the polymer film as a function of time (See Chapter 2). These measurements were performed using a Hiden Isochema gravimetric mass sorption analyzer (Intelligent Gravimetric Analyzer Model IGA 002). This equipment accurately measures the uptake of a gas or vapour by a polymer film (6-decimal places in grams) under accurately controlled conditions

(temperature and partial pressure[4] of the gas or vapour). It is a dynamic process whereby the mass uptake is measured in real time to allow for kinetic and thermodynamic studies.

Each point of the isotherm is generated by a real-time kinetic analysis, i.e. a mass sorption curve is generated at a specific temperature and partial pressure or chemical potential for the vapour. The end-point (equilibrium point) of each isotherm point is determined by the operating software. Also refer to Appendix I for more information regarding the real time analysis.

A sorption/desorption isotherm is generated from the real-time kinetic data. The determination of the solubility coefficient (S), diffusion coefficient (D) and the permeability (P) of the polymer film are calculated from this as set out below.

The diffusion coefficient for each kinetic curve is calculated using the IGA software if the following criteria are met: (1) the sample analyzed has a known thickness if its geometry is plate-like, or a known radius if it is spherical; and (2) the diffusion meets the criteria for Fick's Law and is confirmed by the linear plot of the fractional mass uptake of the penetrant versus time[1/2]. The equation for a plate-like geometry is depicted by equation 4.11 below, where M_t is the mass of penetrant sorbed at time t, M_∞ is the mass of penetrant sorbed at equilibrium, h is the thickness of the film and D the diffusion coefficient. The equation is solved via a least squares regression to yield the diffusion coefficient, D.[31, 32]

$$\frac{M_t}{M_\infty} = 1 - \sum_{n=0}^{\infty} \frac{8}{(2n+1)^2 \pi^2} exp \left[\frac{-D(2n+1)^2 \pi^2 t}{h^2} \right] \tag{4.11}$$

The diffusion coefficient can also be calculated from Fick's second law for gaseous diffusion in a planar sheet (Refer to equation 4.12 below), where M_t is the mass of penetrant sorbed at time t, M_∞ is the amount of penetrant sorbed at equilibrium, D is the diffusion coefficient and l the thickness of the sample.[33]

$$\frac{M_t}{M_\infty} = 4 \sqrt{\left(\frac{Dt}{\pi l^2} \right)} \tag{4.12}$$

The diffusion coefficient is determined from the initial gradient of plots of $\frac{M_t}{M_\infty}$ versus $\frac{\sqrt{t}}{l}$ for short times where $0.1 < \frac{M_t}{M_\infty} < 0.5$.

---

[4] Partial pressure (P/P$_0$) is defined as the ratio of actual vapour pressure (P) to the saturated vapour pressure (P$_0$) for a specific temperature. It therefore represents a fraction of the saturated vapour pressure at a specific temperature.

The solubility coefficient is calculated from the equilibrium penetrant concentration in the kinetic curve and is expressed as ratio between the equilibrium penetrant concentration (c) (in this case water vapour) and the vapour pressure (p) exerted by the water above the film (See equation 4.13 below).[33]

$$S = \frac{c}{p}$$ (4.13)

The equilibrium penetrant concentration (in this case water vapour) is calculated using equation 4.14 below, where M_0 and M_∞ are the initial and final mass of the film following the uptake of water vapour, V_P is the volume of the film, M_{H_2O} the molecular weight of water and V_m is the molar volume of the penetrant at STP[5] (in the case of water vapour $V_m = 22414$ cm^3.mol^{-1} at STP).[33]

$$c = \frac{M_\infty - M_0}{V_p M_{H_2O}} \times V_m$$ (4.14)

The units for the solubility coefficient S are [cm^3(STP).cm^{-3}] for water vapour with partial pressure p (cm Hg) having a molecular weight of 18.01 g.mol^{-1}. V_m is the molar volume (cm^3.mol^{-1}) at STP while V_p is the volume of the polymer film calculated from the density of the film and its dry mass.

For a specific gas or vapour, the permeability (P) of the polymer film is calculated from the product of the solubility coefficient (S) and diffusion coefficient (D) (Refer to equation 4.15 below).

$$P = D \times S$$ (4.15)

Sample preparation: Films were prepared using one of the methods detailed in Section 4.3.1. A sample size of 1.5 cm x 1.5 cm was used for analysis. The thickness of each film was measured with a micrometer.

Experimental setup: The Hiden Isochema Intelligent Gravimetric Analyzer (model: IGA002) was used for the water vapour sorption evaluations. All analyses were done in sorption mode using real time analysis mode F1 with water vapour as the penetrant. The samples were dried prior to starting the isotherm run using a manual Outgas program until a stable baseline was achieved. The partial

---

[5]STP: STP or **standard condition for temperature and pressure** and is standard sets of conditions for experimental measurements, to allow comparisons to be made between different sets of data. IUPAC's standard is a temperature of 0°C (273.15 K, 32 °F) and an absolute pressure of 100kPa (14.504 psi, 0.986 atm),[1] while NIST's version is a temperature of 20°C (293.15K, 68°F) and an absolute pressure of 101.325kPa (14.696 psi, 1 atm).

pressure was increased in intervals of 0.1 unless specified otherwise and specific temperatures were selected for different polymer films analyzed.

4.4.6.3 Water vapour sorption: FTIR-ATR spectroscopy

FTIR-ATR spectroscopy has been used extensively, not only for depth profiling, but also for monitoring the diffusion of liquids in a polymer matrix.[21, 24, 31, 34-39] The principle of monitoring the diffusion of liquid in a polymer film using FTIR-ATR was used as basis to determine the diffusion of water vapour into a film, while simultaneously monitoring the diffusion of surfactant towards the surface of the film.

Key constraints of FTIR-ATR spectroscopy include potential spectral distortions, band broadening at longer wavelengths and the relative absorption intensity changes caused by the ATR penetration depth dependence at different wavelengths for a specific sample.[39] As a result, quantitative FTIR-ATR spectroscopy utilizes FTIR transmission spectra for calibration purposes. The depth of penetration (d_p) of the analysis at a specific wavenumber is calculated using equation 4.16, where n_2 is the refractive index of the propagating medium or crystal in the ATR unit, n_1 is the refractive index of the polymer, θ the angle of incidence of the crystal and λ the wavelength (in nm).[40]

$$d_p = \frac{\lambda}{2n_2\pi\sqrt{sin^2\theta - \left(\frac{n_1}{n_2}\right)^2}} \tag{4.16}$$

Taking the Beer Lambert Law into consideration, equation 4.17 below is an adaptation of equation 4.11 used for the gravimetric determination of the diffusion coefficient, where A_t is the absorbance at time t, A_∞ the absorbance at equilibrium, $2L$ the thickness of the sample and D the diffusion coefficient.[40]

$$\frac{A_t}{A_\infty} = 1 - \frac{8\gamma}{\pi[1-exp(-2\gamma L)]} \times \left[\frac{exp\left(\frac{-D\pi^2 t}{4L^2}\right)\left(\frac{\pi}{2L}exp(-2\gamma L) + (2\gamma)\right)}{\left(4\gamma^2 + \frac{\pi^2}{4L^2}\right)}\right] \tag{4.17}$$

The above expression can be simplified if it is assumed that γ (the reciprocal of the penetration depth) remains constant and that $4\gamma^2 \gg \frac{\pi^2}{4L^2}$ and $1 \gg exp(-2\gamma L)$.

Equation 4.17 can then be reduced to:

$$\ln\left(1 - \frac{A_t}{A_\infty}\right) = \ln\left(\frac{4}{\pi}\right) - \frac{D\pi^2}{4L^2}t \tag{4.18}$$

From equation 4.18 the logarithm of the absorbance data is plotted as a function of time and the slope of a linear least squares regression will yield a value for the diffusion coefficient (D).

Sample preparation: Films cast from emulsion onto aluminium foil was dried at ambient conditions for a minimum period of 3 days. An average film thickness of 200 μm was targeted. Samples were conditioned under vacuum at 50 °C for 7 days prior to analysis. A series of samples of approximately 12 mm x 4 mm were also preconditioned at 93.2% relative humidity and used for FTIR-ATR analysis.

Experimental setup: The films were exposed to 93.2% relative humidity in the headspace above a saturated solution of K_2SO_4 at 25 °C. The films were removed at set time intervals and a FTIR-ATR spectrum taken using a Nicolette FTIR spectrophotometer equipped with a vertical ATR unit and a 45° ZnSe crystal (refractive index=2.4). The spectral range 440 cm^{-1} to 4000 cm^{-1} was selected, 50 scans were taken per spectrum and the background deducted.

The depth of penetration of the FTIR-ATR analysis was determined for each polymer using equation 4.15. The refractive index of the polymers was measured using an Abbe NAR-1T refractometer from Atago Co. Ltd. It was equipped with a D-line light source with average wavelength of 589.3 nm.

Sample preparation: Different quantities of dried polymer were dissolved in acetone at room temperature before applying it to the prism of the refractometer using a glass rod. The refractive index at different concentrations of styrene-*co*-butyl acrylate polymer was measured and plotted against the polymer concentration. The trend line indicated a linear relationship between polymer concentration and the refractive index. Extrapolated to 100% styrene-co-butyl acrylate polymer, the refractive index was calculated for each copolymer.

Polystyrene with a known refractive index was also evaluated using the same methodology to evaluate the feasibility of the test method. Please refer to Appendix F for the results of this evaluation.

Experimental setup: The temperature inside the refractometer was controlled at 25 °C with a thermostated water bath. The refractometer was calibrated with distilled water. Solutions of polymer were applied to the prism of the refractometer using a glass rod.

4.4.7   Thermal Analyses

4.4.7.1 Dynamic mechanical analysis

The glass transition temperature (T_g) of the synthesized copolymers was determined by means of dynamic mechanical thermoanalysis (DMTA) using a rheometer.[41] Typical results generated are depicted in Figure 4.4 below, where the storage modulus (G'), the loss modulus (G") and the damping factor (tan δ=G"/G') are plotted as a function of temperature.

Different interpretations of the actual T_g value exists. The T_g can be interpreted as being at the following points on these curves:

(1) The T_g coincides with the maximum of the tan δ curve (also known as the tan δ peak), where the maximum relative amount of energy is consumed;

(2) The maximum of the G" curve, indicating the temperature at which a maximum amount of deformation energy is consumed;

(3) The inflection point on the G' curve where the greatest change occurs in the storage modulus;

(4) The end-point of the freezing process, indicated by the intersection of a tangent running through the inflection point of the log G' curve and the second tangent running along the plateau of the log G' curve along the lower temperature range; and

(5) The beginning of the freezing point, indicated by the intersection of the tangent at the turning point of the log G' curve and the tangent along the higher temperature range.

For the purpose of this evaluation, method 2 was used to determine the T_g (See Figure 4.4).
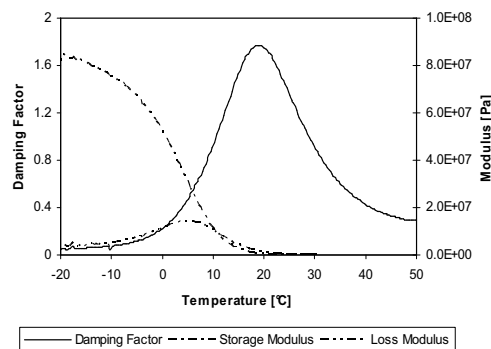
Figure 4.4: Typical temperature curves of an amorphous polymer

Sample preparation: Films were prepared from 15 mL of latex (20% solids) placed in an aluminium foil container. The samples were dried at 55 °C for 48 hours before being analyzed.

Experimental setup: An Anton Paar rheometer (model MCR501) was used equipped with 20 mm diameter plate/plate configuration geometry in oscillatory mode with a gap setting of 1 mm. The frequency setting was 1 Hz, the normal force 0 N and amplitude strain 1%. A temperature range of 50 °C to -20 °C (rate: 1 °C/min.) was evaluated.

4.4.7.2 Differential scanning calorimetry

The degree of crystallinity was determined by means of differential scanning calorimetry (DSC). This technique indicates thermal transitions within a polymer matrix, including its crystallization temperature (T_c), glass transition temperature (T_g) and its melting temperature (T_m). The crystallization temperature is indicated by a peak in the heat flow curve due to the absorption or release of energy during this transition phase.

This technique was used for (1) the qualitative determination of the presence of crystallinity in the films; and (2) the quantitative determination of the ratio of crystalline domains to amorphous domains in the polymer film.

The degree of crystallinity (x_c) of the copolymers was calculated by expressing the enthalpy of fusion (ΔH_f), as measured by DSC, as a fraction of the enthalpy of fusion of a crystal for corresponding alkyl side-chain polymers (ΔH_{f0} = 219.807 J.g^{-1}) (see equation 4.19).[12, 42-44]

$$x_c = \frac{(\Delta H_f)}{(\Delta H_{f0})} \tag{4.19}$$

Sample preparation: Polymer films were cast from solvent as described elsewhere in this chapter.

Experimental setup: The samples were analyzed with a TA Instruments (model Q100 V9.4 Build 287) differential scanning calorimeter. Aluminium pans were used for the analysis and the DSC was connected to nitrogen gas (flow rate: 5.0 mL/min). For the first heating cycle the temperature was increased from -40 °C to 150 °C at a ramp rate of 10 °C/min and was kept at 150 °C for 5 minutes. The mass flow was 50 mL/min. The cooling cycling went from a maximum temperature setting of 150 °C down to -40 °C at a temperature ramp rate of -10 °C and was kept at -40 °C for 5 minutes to equilibrate, followed by a second heating cycle from -40 °C to 150 °C at a ramp rate of 10 °C/min. The final equilibrium temperature was 25 °C.

4.4.7.3 Thermo gravimetrical analysis

Thermo gravimetrical analysis (TGA) was used as a tool to determine the amount of montmorillonite clay in polymer clay nanocomposites (PCNs) (Refer to Chapter 6). This method measures sample mass as a function of temperature. As the polymer component of the PCN will decompose at a lower temperature than the filler component, this method is ideally suited to determine filler loading in PCNs.

Sample preparation: Films were cast from emulsion as described elsewhere in the text. Approximately 15 mg of dried sample was used for the TGA analysis.

Experimental setup: Samples were measured using a TA Instrument, model TGAQ500. After the samples were placed in aluminium pans in the furnace chamber, the system was purged with nitrogen gas (30 mL/min flow rate). The temperature ramp rate was set at 25 °C/min, starting at 25 °C and going to a maximum of 600 °C.

4.4.8   Free volume analysis

Positron annihilation lifetime spectroscopy (PALS) was used to determine the localized free volume in polymers.[45-49] Information regarding free volume include the hole dimensions, number of holes, mean hole volume and fractional free volume.

Positrons emitted by a radioactive source such as [22]Na, annihilates from the positronium (Ps) bound state form, forming either a para positronium (p-Ps) or ortho positronium (o-Ps) in a ratio of 1:3.[49] The PALS spectra obtained are analyzed by means of a nonlinear least squares method using PATFIT-88 software.[47, 48] The spectra for polymers are normally best resolved into 3 or 4 lifetime components. These lifetime components represent the following positron annihilation behaviour:[47]

- τ_1: This component has the shortest lifetime (±0.125 ns) and is due to the self annihilation of a *para-positronium* (p-Ps) as a result of combining with an electron;

- τ_2: This intermediate lifetime component, with a mean lifetime of ± 0.3-0.5 ns, represents the annihilation of free *positrons* and *positron-molecule* species (i.e. the combination of p-Ps with an electron with opposite parallel spin);

- τ_3: The third component, an *ortho-positronium* (o-Ps) has a lifetime ≥0.5 ns and is the pick-off annihilation of o-Ps localized in the free volume of the crystalline regions of the polymer (i.e. combination of o-Ps with an electron with the same parallel spin); and

- τ_4: The longest living component has a lifetime >1.5 ns and is attributed to the pick-off annihilation of *ortho-positronium* (o-Ps) in the amorphous regions of the polymer matrix.

Two types of outputs are generated:

(1) Probability density function (PDF) of lifetime

(2) Probability density function (PDF) of free volume radius

These curves give a probability of finding a specific hole size within a polymer matrix. It does not give actual hole sizes. These results should therefore only be used in a comparative manner, where a series of polymers are compared to each other.

The free volume hole size (R, radius of hole) is deduced from the *o*-Ps lifetime (τ_4 in ns) according to the following relationship as developed by Tao et al. (See equation 4.20):[47]

$$\tau_4 = 0.5\left[1 - \frac{R}{R+0.166} + \frac{1}{2\pi}\sin\left(\frac{2\pi R}{R+0.166}\right)\right]^{-1} \tag{4.20}$$

The lifetime measurements are also used to estimate the fractional free volume of a material, based on the assumption that the total fraction of o-Ps formed (I_4) in the polymer is related to the number of free volume holes in the matrix according to the following relationship:[48]

$$f_v = CI_4\langle v_f(\tau_4)\rangle \tag{4.21}$$

Here f_v is the fractional free volume, *C* is an empirical scaling constant that reflects the probability of o-Ps formation independent of the free volume and is usually determined from specific pressure-volume-temperatures (PVT) measurements above and below glass transition temperature (T_g), and $\langle v_f(\tau_4)\rangle$ is the mean hole volume measured in ($Å^3$).

Sample preparation: Dried and purified polymer was heated to its melting temperature until all was melted. It was then cooled to room temperature to give smooth sample discs with a thickness of 2 mm.

Experimental setup: PALS experiments were performed at room temperature using a 20 µCi [22]NaCl positron source sealed in aluminium foil. For the spectra measurements, the source was sandwiched between two identical sample discs, wrapped in foil and placed between the two detectors of the spectrometer. The positron annihilation lifetimes were measured by detecting the prompt γ-ray (1.28 MeV) from the nuclear decay that accompanies the emission of a positron from the [22]Na radioisotope and the annihilation γ-ray (0.511 MeV). A fast-fast coincident circuit was used to measure the positron lifetime. Each spectrum was collected to at least 1 x 10^6 counts and 250 ps time resolution. The lifetime spectra were resolved to finite lifetimes using the PATFIT program.

The impact of different types of surfactants on the water vapour sorption behaviour of the model polymer p(Sty-co-BA) are discussed in the next chapter.

References

1. De Bruyn, H., Miller, C.M., Basset, D.R., and Gilbert, R.G., *Emulsion polymerization of vinyl neo-decanoate, a "water-insoluble" monomer.* Macromolecules, 2002. **35**: p. 8371-8377.

2. Métayer, M., Labbé, M., Marais, S., Langevin, D., Chappey, C., Dreux, F., Brainville, M., and Belliard, P., *Diffusion of water through various polymer films: a new high performance method of characterization.* Polymer Testing, 1999. **18**: p. 533-549.

3. Landfester, K., Bechthold, N., Tiarks, F., and Antonietti, M., *Miniemulsion Polymerization with Cationic and Nonionic Surfactants: A Very Efficient Use of Surfactants for Heterophase Polymerization.* Macromolecules, 1999. **32**: p. 2679-2683.

4. Butler, L.N., Fellows, C.M., and Gilbert, R.G., *Effect of Surfactant Systems on the Water Sensitivity of Latex Films.* Journal of Applied Polymer Science, 2004. **92**: p. 1813-1823.

5. Cameron, N.R. and Sherrington, D.C., *Preparation and glass transition temperatures of elastomeric PolyHIPE materials.* Journal of Materials Chemistry, 1997. **7**(11): p. 2209-2212.

6. Choi, Y.S., Ham, H.T., and Chung, I.J., *Polymer/silicate nanocomposites synthesized with potassium persulfate at room temperature: polymerization mechanism, characterization, and mechanical properties of the nanocomposites.* Polymer, 2003. **44**: p. 8147-8154.

7. Greesh, N., Hartmann, P.C., Cloete, V., and Sanderson, R.D., *Impact of the Clay Organic Modifier on the Morphology of Polymer–Clay Nanocomposites Prepared by In Situ Free-Radical Polymerization in Emulsion.* Journal of Polymer Science Part A: Polymer Chemistry, 2008. **46**(11): p. 3619-3628.

8. Greesh, N., Hartmann, P.C., Cloete, V., and Sanderson, R.D., *Adsorption of 2-acrylamido-2-methyl-1-propanesulfonic acid (AMPS) and related compounds onto montmorillonite clay.* Journal of Colloid and Interface Science, 2008. **319**(1): p. 2-11.

9. O'Leary, K. and Paul, D.R., *Copolymers of poly(n-alkyl acrylates): synthesis, characterisation, and monomer reactivity ratios.* Polymer, 2004. **45**(19): p. 6575-6585.

10. Platé, N.A. and Shibaev, V.P., *Comb-like Polymers. Structure and Properties.* Journal of Polymer Science: Macromolecular Reviews, 1974. **8**: p. 117-253.

11. Jordan, E.F., Feldeisen, D.W., and Wrigley, A.N., *Side-Chain Crystallinity. I. Heats of Fusion and Melting Transitions on Selected Homopolymers Having Long Side Chains.* Journal of Polymer Science: Part A-1, 1971. **9**: p. 1835-1852.

12. Mogri, Z., Paul, D.R., *Gas sorption and transport in side-chain crystalline and molten poly(octadecyl acrylate).* Polymer, 2001. **42**: p. 2531-2542.

13. Lide, D.R., ed. *CRC handbook of chemistry and physics*. 86th ed. 2005-2006, CRC Press, Taylor and Francis: Boca Raton, Florida.

14. Mogri, Z. and Paul, D.R., *Gas sorption and transport in poly (alkyl (meth)acrylate)s: II. Sorption and diffusion properties.* Polymer, 2001. **42**: p. 7781-7789.

15. Steward, P.A., Hearn, J., and Wilkinson, M.C., *An overview of polymer latex film formation and properties.* Advances in Colloid and Interface Science, 2000. **86**: p. 195-267.

16. Lovell, P.A. and El-Aasser, M.S., eds. *Emulsion Polymerization and Emulsion Polymers*. 1st ed. 1997, John Wiley & Sons: West Sussex, England.

17. Alexandre, M. and Dubois, P., *Polymer-layered silicate nanocomposites: preparation, properties and uses of a new class of materials.* Materials Science and Engineering, 2000. **28**: p. 1-63.

18.   Murthy, N.S., *Recent developments in polymer characterization using X-ray diffraction.* The Rigaku Journal, 2004. **21**(1): p. 15-24.

19.   Alexander, L.E., *X-Ray diffraction methods in polymer science*. 1969, New York: Wiley-Interscience.

20.   Stamm, M., *Polymer Interfaces on a Molecular Scale: Comparison of Techniques and Some Examples*, in *Macromolecules: Synthesis, Order and Advanced Properties*. 1991, Springer: Berlin. p. 357-400.

21.   Garbassi, F. and Occhiello, E., *Spectroscopic techniques for the analysis of polymer surfaces and interfaces.* Analytica Chimica Acta, 1987. **197**: p. 1-42.

22.   Zhao, Y. and Urban, M.W., *Phase Separation and Surfactant Stratification in Styrene/n-Butyl Acrylate Copolymer and Latex Blend Films. 17. A Spectroscopic Study.* Macromolecules, 2000. **33**: p. 2184-2191.

23.   Kumar, A., Commereuc, S., Gonon, L., and Verney, V., *Depth-profile of photo-oxidation of polyoctenamer.* Polymer Degradation and Stability, 2002. **75**: p. 509-516.

24.   Church, J.S. and Evans, D.J., *The Quantitative Analysis of Fluorocarbon Polymer Finishes on Wool by FT-IR Spectroscopy.* Journal of Applied Polymer Science, 1995. **57**: p. 1585-1594.

25.   Niu, B.-J. and Urban, M.W., *Recent Advances in Stratification and Film Formation of Latex Films; Attenuated Total Reflection and Step-Scan Photoacoustic FTIR Spectroscopic Studies.* Journal of Applied Polymer Science, 1998. **70**: p. 1321-1348.

26.   Gregoriou, V.G. and Rodman, S.E., *Quantitative Depth Profile Analysis of Micrometer-Thick Multilayered Thin Coatings Using Step-Scan FT-IR Photoacoustic Spectroscopy.* Analytical Chemistry, 2002. **74**: p. 2361-2369.

27.   Halttunen, M., Tenhunen, J., Saarinen, T., and Stenius, P., *Applicability of FTIR/PAS depth profiling for the study of coated papers.* Vibrational Spectroscopy, 1999. **19**: p. 261-269.

28.   McClelland, J.F., Jones, R.W., Bajic, S.J., *FT-IR Photoacoustic Spectroscopy*, in *Handbook of Vibrational Spectroscopy*, J.M. Chalmers and P.R. Griffiths, Editors. 2002, John Wiley & Sons, Ltd.: New York.

29.   Jurdana, L.E., Ghiggino, K.P., Leaver, I.H., and Cole-Clarke, P., *Application of FT-IR Step-Scan Photoacoustic Phase Modulation Methods to Keratin Fibers.* Applied Spectroscopy, 1995. **49**(3): p. 361-366.

30.   Wu, S., *Polymer Interface and Adhesion*. 1982, New York: Marcel Dekker Inc.

31.   Fieldson, G.T. and Barbari, T.A., *The use of FTIR-ATR spectroscopy to characterize penetrant diffusion in polymers.* Polymer, 1993. **34**(6): p. 1146-1153.

32.   Hiden-Isochema, *IGA Systems User Manual*. 2007, London: Hiden Isochema.

33.   Mwesigwa, E., Basit, A.W., and Buckton, G., *Moisture Sorption and Permeability Characteristics of Polymer Films: Implications for Their Use as Barrier Coatings for Solid Dosage Forms Containing Hydrolyzable Drug Substances.* Journal of Pharmaceutical Sciences, 2008.

34.   Sammon, C., Yarwood, J., and Everall, N., *A FTIR-ATR study of liquid diffusion processes in PET films: comparison of water with simple alcohols.* Polymer, 2000. **41**: p. 2521-2534.

35.   Linossier, I., Gaillard, F., Romand, M., and Feller, J.F., *Measuring Water Diffusion in Polymer Films on the Substrate by Internal Reflection Fourier Transform Infrared Spectroscopy.* Journal of Applied Polymer Science, 1997. **66**: p. 2465-2473.

36.   Ekgasit, S. and Ishida, H., *Optical Depth Profiling by Attentuated Total Reflection Fourier Transform Infrared Spectroscopy: A New Approach.* Applied Spectroscopy, 1996. **50**(9): p. 1187-1195.

37.   Shick, R.A., Koenig, J.L., and Ishida, H., *Theoretical Development for Depth Profiling of Stratified Layers Using Variable-Angle ATR.* Applied Spectroscopy, 1993. **47**(8): p. 1237-1244.

38.   Chu, A.P., Tebelius, L.K., and Urban, M.W., *Spectroscopic Studies of Surfactant Mobility and Stratification in Films from Homopolymer Latex Blends.* Technology for waterborne coatings, 1997. **663**: p. 212-225.

39.   Chen, J. and Gardella Jr., J.A., *Quantitative ATR FT-IR Analysis of Surface Seggregation of Polymer Blends of Polystyrene/Poly(dimethylsiloxane)-co-polystyrene.* Applied Spectroscopy, 1998. **52**(3): p. 361-366.

40.   Fieldson, G.T. and Barbari, T.A., *The use of FTi.r.-a.t.r spectroscopy to characterize penetrant diffusion in polymers.* Polymer, 1993. **34**(6): p. 1146-1153.

41.   Zorll, U., ed. *The Rheology Handbook*. 2002, Hannoprint: Hannover, Germany.

42.   Mogri, Z., Paul, D.R., *Gas sorption and transport in poly (alkyl (meth)acrylate)s. I. Permeation properties.* Polymer, 2001. **42**: p. 7765-7780.

43.   Platé, N.A. and Shibaev, V.P., *Comb-Like Polymers. Structures and Properties.* Journal of Polymer Science: Macromolecular Reviews, 1974. **8**: p. 117-253.

44.   Jordan, E.F., Feldeisen, D.W., and Wrigley, A.N., *Side-Chain Crystallinity. I. Heats of Fusion and Melting Transitions on Selected Homopolymers Having Long Side Chains.* Journal of Polymer Science: Part A-1, 1971. **9**: p. 1835-1852.

45.   Ito, K., Ujihira, Y., Yamashita, T., and Horie, K., *Positron Annihilation Lifetime Study of Continuous Volume Phase Transition of Poly (N-isopropylacrylamide) Gel Induced in Methanol-Water Mixed Solvent.* Journal of Polymer Science: Part B: Polymer Physics, 1998. **36**: p. 1141-1151.

46.   Wang, H., Ansems, P., Chum, S.P., Hiltner, A., Baer, E., *Free Volume Study in New Propylene-Ethylene Copolymers.* Polymeric Materials: Science & Engineering, 2004. **91**: p. 457-458.

47.   Danch, A. and Osoba, W., *Estimating the fractional free volume parameter in polyethylene by the positron annihilation method.* Fibres & Textiles in Eastern Europe, 2003. **11**(5(44)): p. 126-127.

48.   Jean, Y.C., Mallon, P.E., and Schrader, D.M., eds. *Principles and Applications of Positron & Positronium Chemistry*. 2003, World Scientific Publishing Co. Pte. Ltd.: New Jersey.

49.   Dlubek, G., Kilburn, D., Bondarenko, V., Pionteck, J., Krause-Rehberg, R., and Alam, M.A., *Positron Annihilation: A Unique Method for Studying Polymers.* Macromolecular Symposia, 2004. **210**: p. 11-20.

CHAPTER 5

Impact of surfactants on water vapour sorption properties of *p*(Sty-*co*-BA) polymer latex films

Summary: *The impact of the nature of the surfactants on the water vapour sorption behaviour of p(Sty-co-BA) random copolymer films are discussed (refer to Section 4.2.1, Chapter 4). Three model surfactants were used to prepare the respective latices: an anionic surfactant (sodium dodecyl benzene sulfonate, SDBS), a nonionic surfactant (octyl phenol ethoxylate, OPE) and a reactive surfactant with an organic polymerizable counterion (dodecylammonium-3-butenoate, DA3B).*

The resultant p(Sty-co-BA) polymer films were characterized in terms of their chemical composition and their surface properties. Their affinity for water and water vapour were also determined, using gravimetric and spectroscopic methods to determine the kinetics and thermodynamics of the sorption process.

This study showed a significant difference in the kinetics of water vapour sorption due to different surfactants used to stabilize the latex. SDBS and OPE exhibited similar sorption behaviour, following Sigmoidal kinetics and Flory Huggins thermodynamics for equilibrium mass uptake at increasing water vapour partial pressures. Contrary to this, DA3B stabilized latex films exhibited Sigmoidal sorption behaviour, while the diffusion was independent of the water vapour partial pressure, following Henry's Law. The permeability coefficients for all three films were however found to be similar across the water vapour partial pressure range evaluated.

5.1 Impact of type and concentration of surfactant on chemical composition of *p*(Sty-*co*-BA)

The type and concentration of surfactants used in this investigation could result in different monomer droplet sizes in the miniemulsion, which could result in different degrees of monomer droplet nucleation, different rates of monomer incorporation into the polymer backbone and therefore different polymerisation kinetics (refer to Appendix L for a brief summary regarding the monomer conversion for these polymerisations). This could ultimately result in significant differences in the final polymer properties such as differences in the degree of polymerisation, chain mobility and chemical composition. As the overall purpose was to determine the impact of the three model surfactants on the water vapour sorption properties of *p*(Sty-*co*-BA) films, it was necessary to understand potential variances in the chemical composition of the polymers and their potential impact on the water vapour sorption behaviour of the films.

The polymers synthesized were therefore characterized in terms of their chemical composition, molecular mass, thermal properties and free volume using ^{1}H NMR spectroscopy, SEC, DSC and PALS analytical techniques respectively.

Table 5.1: Chemical composition of polymers as determined by ^{1}H NMR spectroscopy

p(Sty-co-BA)	Theoretical content[1]				Experimental content			
	Mol %		Weight %		Mol %		Weight %	
Surfactant type	Sty	BA	Sty	BA	Sty	BA	Sty	BA
2% SDBS	60%	40%	55%	45%	63%	37%	58%	42%
2% DA3B	60%	40%	55%	45%	63%	37%	58%	42%
6% OPE	60%	40%	55%	45%	64%	36%	59%	41%

The chemical composition of the synthesized polymers was determined by means of quantitative ^{1}H NMR spectroscopy (See Chapter 4, Section 4.3.1, for sample preparation). The method of integration of the ^{1}H NMR spectra is summarized in Appendix A. Based on the integration results, it can be

---

[1]Theoretical content refers to the styrene:butyl acrylate composition that would be achieved should 100% of the styrene and butyl acrylate monomer added into the reactor charge be incorporated into the backbone of the polymer.

concluded that there is not a significant difference in the relative polymer composition of the different copolymers stabilized by the three model surfactants (See Table 5.1). The 1% variance in composition between the OPE stabilized polymer latex and the other two latexes can be attributed to the accuracy of the technique used to quantify the chemical composition.

The chemical composition of individual polymer chains is explained by looking at the reactivity ratios of the two monomers used, namely styrene and *n*-butyl acrylate (Refer to Table 5.2). Based on the reactivity ratios, it can be deduced that a styrene radical would react with either styrene or *n*-butyl acrylate monomers with little preference for a specific monomer. However, the probability of n-butyl acrylate propagating penultimate unit reacting with a styrene monomer is significantly higher than the probability for reacting with a *n*-butyl acrylate monomer. This would result in distinct polymer compositions, with polymer chains obtained at high conversion level containing slightly more *n*-butyl acrylate than polymer chains formed at the early stages of the polymerization reaction.

Table 5.2: Reactivity ratios of styrene and n-butyl acrylate monomers

Monomer 1	Monomer 2	$r_1=k_{11}/k_{12}$	$r_2=k_{22}/k_{21}$	r_1r_2
Styrene	n-butyl acrylate	0.79	0.25	0.20

The molar mass, T_g and free volume properties are summarized in Table 5.3 and Table 5.4 below. There was no significant difference in terms of these properties for *p*(Sty-*co*-BA) polymers stabilized with the three different surfactant systems.

Table 5.3: Molecular mass[2] and glass transition temperature of *p*(Sty-*co*-BA) polymers

Surfactant	Mn	Mw	PDI	T_g
	[g/mol]	[g/mol]		[°C]
1% SDBS	539,000	1,692,000	3.14	16°C
6% OPE	462,000	1,291,000	2.79	16°C
1% DA3B	597,000	1,632,000	2.73	14°C
2%DA3B	455,000	1,026,000	2.25	NA

NA: Not available

---

[2] Relative to polystyrene

Table 5.4: Free volume properties of *p*(Sty-*co*-BA) polymers

Surfactant	τ_4 [ns]	$\Delta\tau_4$ [ns]	I_3 [%]	ΔI_3 [%]	R [Å]	ΔR [Å]	F_v [Å^3]	ΔF_v [Å^3]
1% SDBS	2.7	0.1	22	5	3.45	0.07	172	11
6% OPE	2.62	0.08	21	3	3.36	0.04	159	6
1% DA3B	NA	NA	NA	NA	NA	NA	NA	NA
2%DA3B	2.8	0.2	20	5	3.50	0.08	180	12

NA: Not available

5.2 Impact of surface properties on surface energy of *p*(Sty-*co*-BA) films

It is well known that factors such as film thickness, surface roughness and chemical composition can impact on the surface energy of films.[1] The surface energy of a film could in turn impact on the solution of gases or vapours into the polymer matrix. Although the intention here was not to optimize surface energy in terms of these parameters, the evaluation of the impact of surface roughness and film thickness on the surface energy of the film could potentially shed further light on the sorption behaviour of the polymers studied here.

For the purpose of this investigation polymer films were prepared by casting ±10% solids latexes onto a glass substrate to eliminate the potential variance in surface properties caused by different substrates being used. The resultant films were analyzed in terms of (1) their physical properties (film thickness and surface roughness) and (2) their chemical properties.

5.2.1 Film topography

Films of two different thicknesses were prepared (±160 µm and ±400 µm) for each of the model surfactant stabilized films and their thickness measured with a micrometer. The surface topography of the films was determined by means of AFM analysis (see Chapter 4, Section 4.3.5.4). Three dimensional surface plots and line profiles were generated. At least three measurements were taken of each film to give a representative reflection of surface properties of the films analyzed. Advancing and receding contact angles of water were measured for each film. The contact angle hysteresis, $\Delta\theta$, was calculated as the arithmetic difference between the advancing contact angle, θ_a, and receding contact angle, θ_r.[1, 2] The results are summarised in Table 5.5, Figure 5.1, Figure 5.2 and Figure 5.3.

Table 5.5: Macroscopic films properties of *p*(Sty-*co*-BA) polymers stabilized with different surfactants.

Surfactant	Film Thickness	Roughness[3]	$\theta_a{}^4$ [°]	θ_r [°]	Δθ[°]
	[μm]	[nm]			
1% SDBS	430	164.21±2.52	67.02±13.27	43.05±19.36	23.97±17.62
1% SDBS	173	143.73±3.11	77.16 ±7.28	48.86 ±9.52	28.30 ±13.45
1% DA3B	365	237.47±39.07	85.24 ±8.17	52.58 ±4.26	32.68 ±10.15
1% DA3B	160	165.24±142.97	42.16 ±8.71	34.24 ±10.04	8.94 ±4.36
6% OPE	378	25.79±17.35	75.32 ±5.06	46.48 ±10.14	28.84 ±7.68
6% OPE	148	13.72±3.28	74.30 ±10.15	57.55 ±17.65	24.18 ±6.05

The OPE stabilized films gave the lowest surface roughness for both thick and thin films (Refer to Table 5.5), confirming the findings of Heldmann et al. who established that nonionic surfactants have a higher gloss than films stabilized with ionic surfactants due to relatively low surface roughness resulting from higher surfactant concentration with resultant smaller particle size and more efficient particle packing.[3] This is also confirmed by the line profile and three dimensional surface plots where the average peak-to-valley height is relatively small (refer to Figure 5.1). The OPE stabilized films have a characteristic overall topography consisting of many small peaks and valleys. The advancing contact angle was similar for both OPE stabilized films, while the receding contact angle for the thicker film was slightly higher than that for the thinner film indicating slightly better wettability for the thicker film. No significant difference could be seen in terms of the contact angle hysteresis for different film thicknesses of films stabilized with OPE.

---

[3]Roughness is based on the average of 4 measurements.

[4]Advancing and receding contact angles are based on average of 5 measurements.

6% OPE, 148µm film thickness

6% OPE, 378µm film thickness
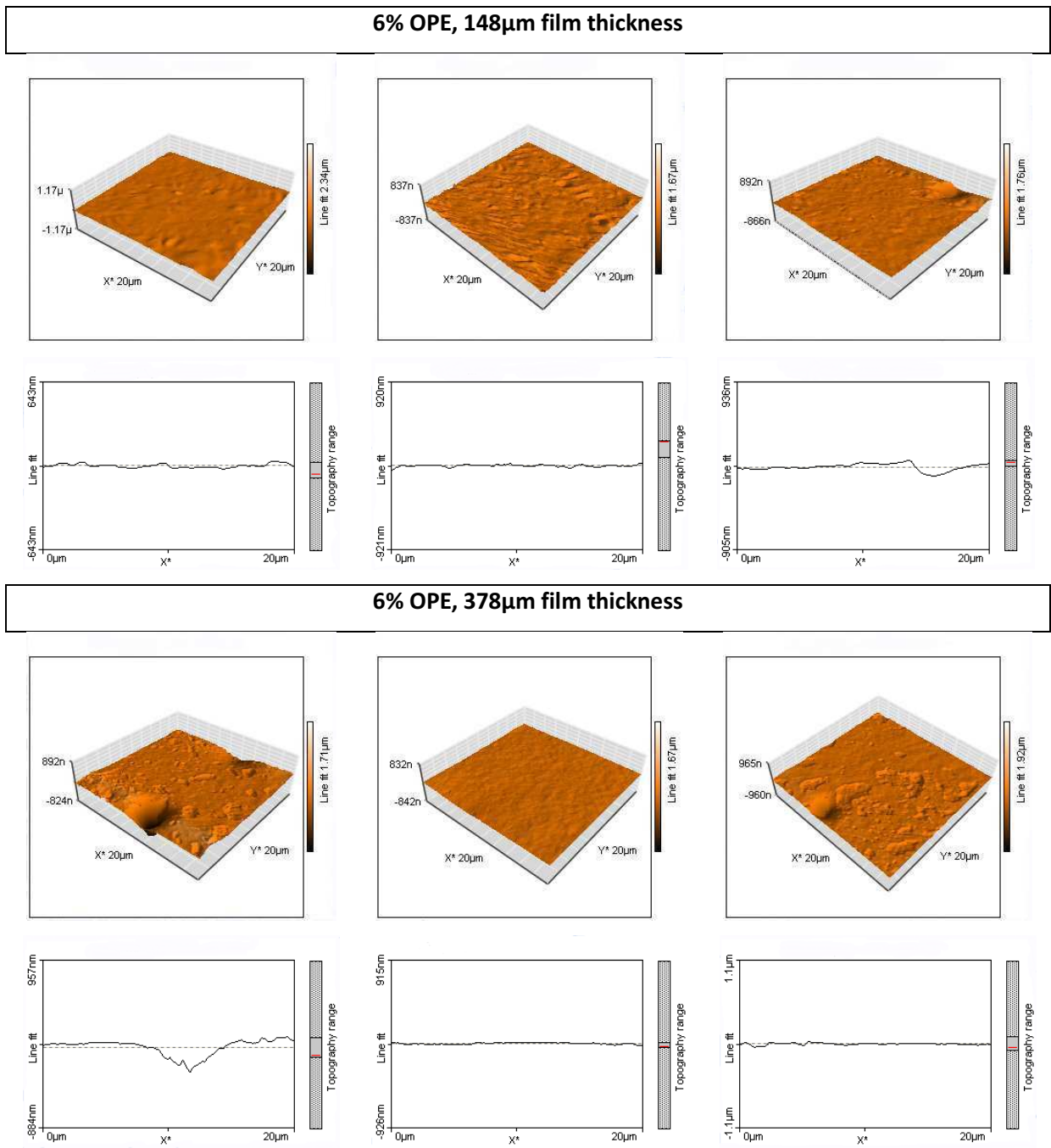
Figure 5.1: Typical AFM surface profiles of films cast *p*(Sty-*co*-BA) polymers stabilized with OPE surfactant

111

1% SDBS; 173µm film thickness

1% SDBS, 430µm film thickness
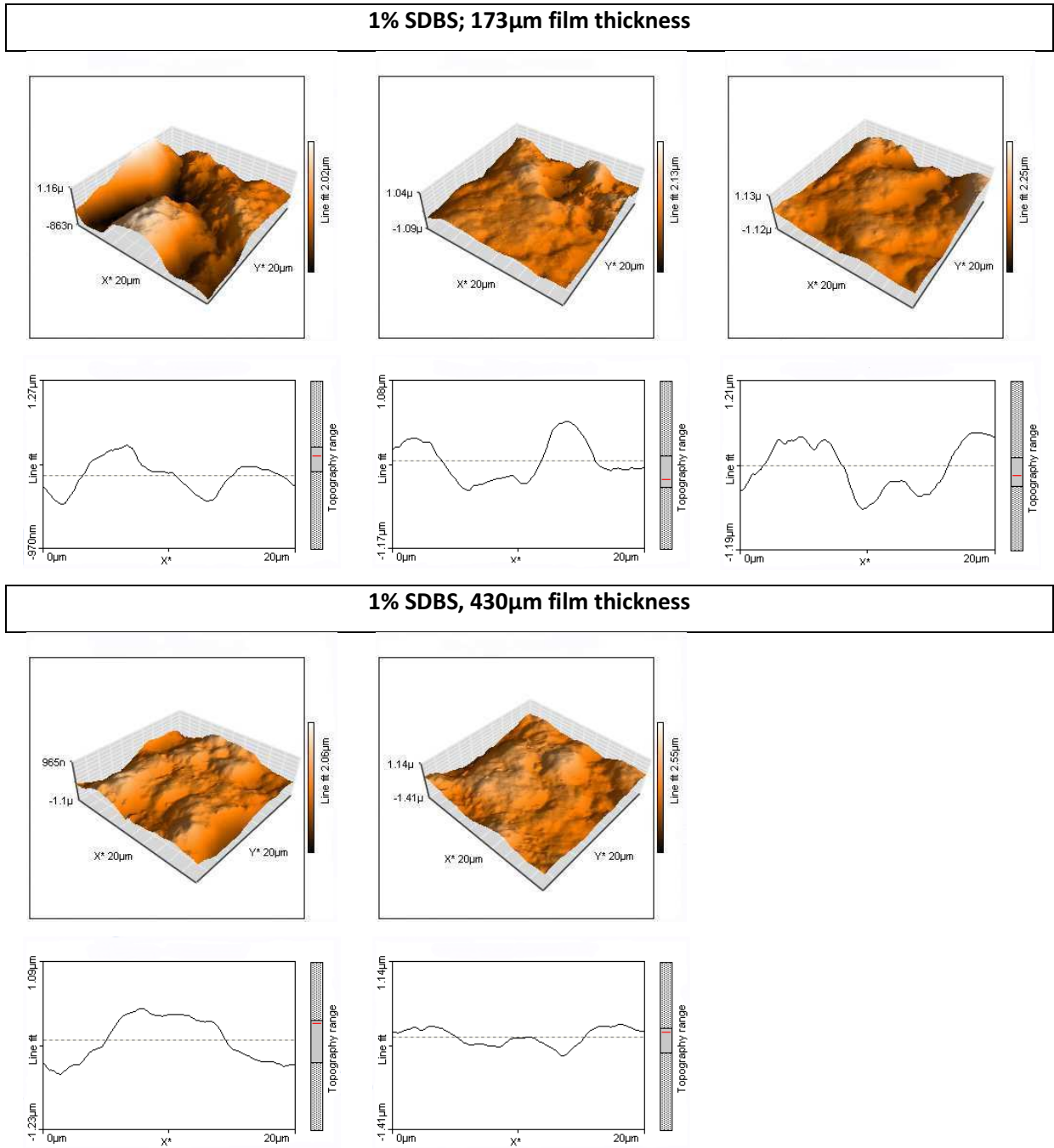
Figure 5.2: Typical AFM surface profiles of films cast *p*(Sty-*co*-BA) polymers stabilized with SDBS surfactant

112

1% DA3B, 160µm film thickness

1% DA3B, 365µm film thickness
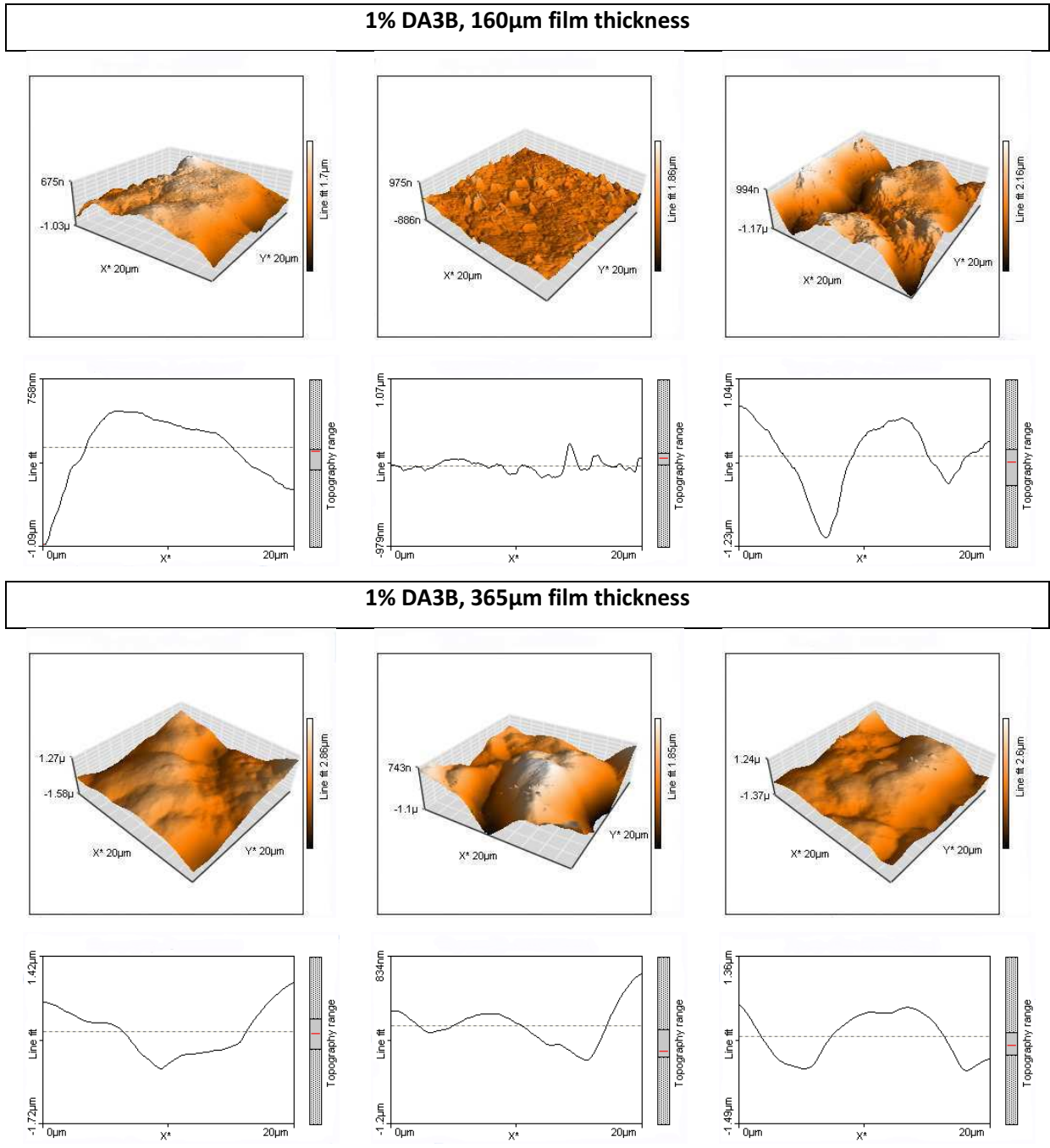
Figure 5.3: Typical AFM surface profiles of films cast *p*(Sty-*co*-BA) polymers stabilized with DA3B surfactant

SDBS stabilized films exhibited significantly higher surface roughness values, with the thicker film having a slightly higher roughness value. The general topography of the SDBS stabilized films differs significantly from that of the OPE stabilized films. The peak-to-valley height is significantly larger and

113

few peaks are visible in the 20 μm x 20 μm sample. The advancing and receding contact angles are similar to that of the OPE stabilized films.

The DA3B stabilized films have the highest surface roughness as well as the highest variance in surface roughness compared to the films stabilized with OPE or SDBS (see Figure 5.3). The topography of the thin film stabilized with DA3B was similar to that of OPE, while the thick film stabilized with DA3B resembled the topography of the SDBS stabilized films. A significant difference in wettability of the DA3B stabilized films were observed, with the thicker film exhibiting similar wettability to both the OPE and SDBS stabilized films, while the thin DA3B stabilized film had significantly lower advancing and receding contact angles and therefore much better wettability compared to any of the other films. The contact angle hysteresis of the thin DA3B stabilized film was extremely low, indicative of good wettability.

From these observations it is evident that, for *p*(Sty-*co*-BA) films stabilized with SDBS, OPE or DA3B, no correlation can be drawn between the measured surface topography and the resultant surface energy of the films.

5.2.2 Chemical composition

SDBS, DA3B and OPE differ in respect of their ***reactivity*** (DA3B is the only reactive surfactant able to copolymerize with ethylenic monomers) and their ***molecular size*** (SDBS is a small molecule that would have greater mobility than both OPE, a polymeric surfactant, and DA3B which would, due to their reactivity be incorporated into the polymer backbone and to some degree perhaps form homopolymers). Having distinctly different properties, it is expected that the 3 surfactant systems used for the stabilization of the *p*(Sty-*co*-BA) polymer latex will impact differently on the surface chemical properties of the polymer film. An increase in the surface polarity due to the presence of surfactant would enhance the solubility at the surface of the film for polar penetrants such as water vapour and would therefore impact on the sorption behaviour of *p*(Sty-*co*-BA).

Two methods were used to characterize the surface polarity: (1) FTIR spectroscopy to determine the chemical functionality through depth profiling; and (2) contact angle analysis and surface tension calculations to determine the surface energy of the film.

5.2.2.1 FTIR spectroscopy

Both FTIR-PAS and FTIR-ATR spectroscopy have been used extensively to determine the chemical composition of latex films at the air-film interface.[4-12] As only a 45° ZnSe crystal was available for use with the Golden Gate ATR unit, this would only allow for a single sampling depth at a specific wavenumber. More information regarding the chemical composition of the polymer matrix at different sampling depths could be obtained using FTIR-PAS at different mirror velocities. It was therefore decided to rather use FTIR-PAS for this evaluation to determine: (1) the relative position of different surfactants in the film by comparing the chemical composition of the waterborne films from different surfactant systems at specific sampling depths; and (2) the two-sidedness of these films by comparing FTIR spectra from the air-film interface and film substrate interface with each other.

FTIR spectroscopy of the pure surfactant, the *p(*Sty-*co*-BA) and the *p*(Sty-*co*-BA) containing the surfactant were recorded to identify unique surfactant bands that could be used as identification of the surfactant at various depths of analysis. The results of this investigation are summarised in Appendix C. In summary, this analysis indicated unique bands for SDBS (1043 cm^{-1} and 1012 cm^{-1} due to the symmetric vibration of the S-O functional groups) and DA3B (carboxylate functional groups resulted in absorption bands in the wavenumber region of 1622-1635 cm^{-1} and 1548 cm^{-1}). Significant overlap of absorption bands in the recorded spectra of OPE and *p*(Sty-*co*-BA), rendered it impossible to identify unique bands that could be used to identify the OPE surfactant at different sampling depths within the polymer film. From literature it is however known that OPE migrates to the surface of a polymer film.[13] This study therefore only focused in the polymers where SDBS and DA3B were used as surfactants.

SDBS Surfactant

Due to the ionic nature of SDBS, the compatibility of this surfactant with the hydrophobic *p*(Sty-*co*-BA) polymer matrix would be minimal. It is therefore expected that this would limit the surfactant from dissolving in the bulk of the polymer particles, rather allowing the surfactant to exude to the surface of the film, or to be present in the film as clusters of surfactant.[13] Its relatively low molecular mass would also allow for easy migration from the bulk of the film to the film-air or film-substrate interface.

115

The presence of the surfactant (at wavenumber=1046 cm^{-1} and 1013 cm^{-1}) at the air-film interface was confirmed using FTIR-PAS, where spectra were recorded at 4 different sampling depths in the film, namely 4.5 µm, 7.1 µm, 10.1 µm and 17.5 µm (Refer to Appendix B and Figure 5.4(a)). Bands at 1046 cm^{-1} and 1013 cm^{-1} appeared as shoulders to the right of the vibrational bands at 1066 cm^{-1} and 1029 cm^{-1} which are characteristic of the *p*(Sty-*co*-BA) polymer. These shoulders correlate well with the SDBS vibrational bands identified in the spectra in Appendix C (Figure 1). At deeper sampling depths these bands were not visible. This could be attributed to a significant reduction in the ratio of surfactant to polymer at greater sampling depths, resulting in quenching of the surfactant band by the high intensity polymer bands. From this it can be deduced that the surfactant is largely present at the film-air interface (within the first 4.5 µm) and to a lesser extent deeper into the polymer film. This corresponds with the findings of various other surfactant exudation studies.[5]
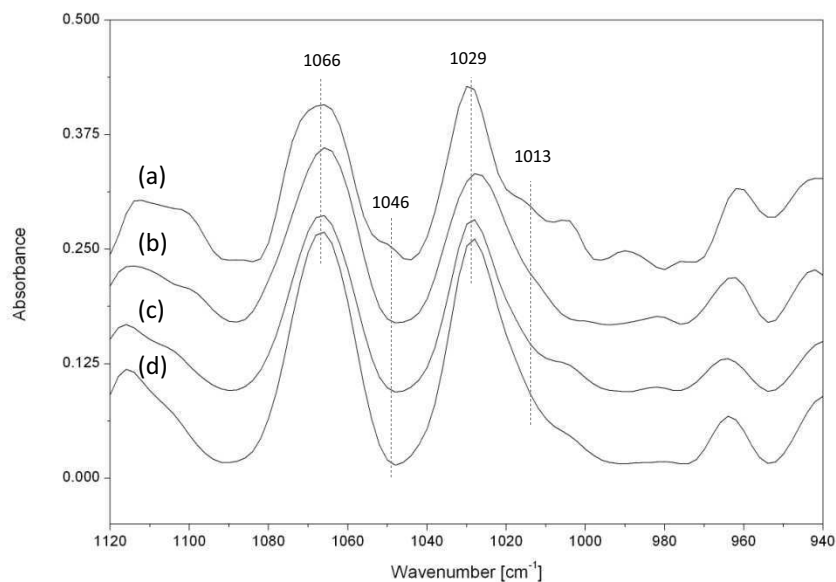
Figure 5.4: FTIR-PAS analyses at 4 depths of penetration at the film-air interface: (a) 4.5 µm, (b) 7.1 µm, (c) 10.1 µm and (d) 17.5 µm

FTIR-PAS spectra of the film-substrate interface indicated that stratification of SDBS to the film-substrate interface also took place, although to a lesser extent compared to the film-air interface as the absorption bands at 1046 cm^{-1} and 1013 cm^{-1} was evident up to a depth of 10.1 µm.

116
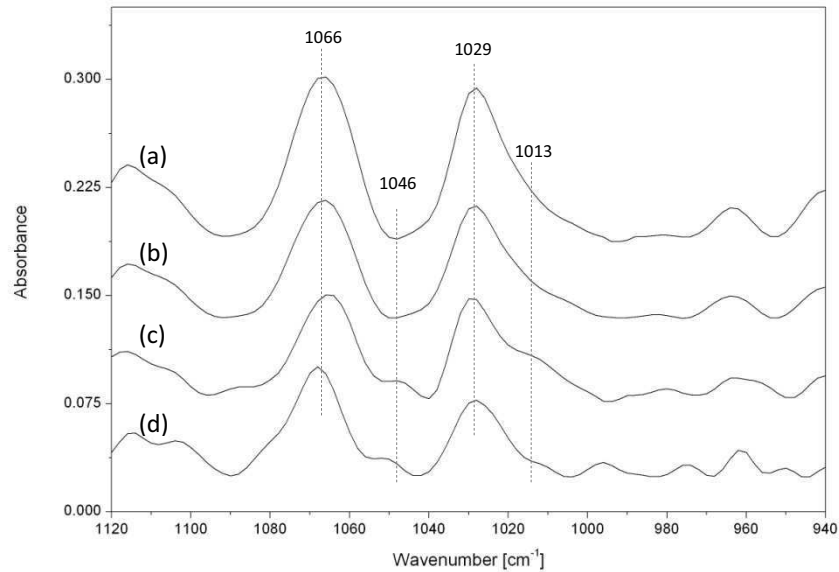
Figure 5.5: FTIR-PAS analysis at 4 depths of penetration at the film-substrate interface: a) 17.5 μm, (b) 10.1 μm, (c) 7.1 μm and (d) 4.5 μm

The difference in exudation of the surfactant to the air-film interface and film-substrate interface could be attributed to the surface energy of the glass substrate onto which the latex was cast initially.

DA3B Surfactant

FTIR-PAS was used to determine whether DA3B had reacted completely with the main monomers styrene and n-butyl acrylate. The presence of a vinyl functional group in DA3B has resulted in several unique infrared bands for unreacted DA3B which could be used to determine whether unreacted DA3B was present in the final polymer:

- The carbon-carbon stretching vibrational absorption band of a vinyl group is found in the region of 1640 cm^{-1}.[14, 15] This band is present in spectrum (b) of Figure 5.6 at 1635 cm^{-1}, but is absent in spectrum (a) due to the disappearance of the vinyl group.

- Mono substituted alkenes have 2 characteristic out-of-plane bending deformation bands at 910 cm^{-1} and 990 cm^{-1}.[15, 16] Both these bands are visible in spectrum (b) of Figure 5.6,

117

while only the band in the region of 910 cm^{-1} is visible in spectrum (a), thus indicating the absence of the mono substituted alkene.

- Carbon-carbon double bonds have stretching absorption bands in the region of 2000 to 1430 cm^{-1}. The position and intensity of these bands are very sensitive to substitution of this functional group with increasing levels of substitution resulting in a shift of this band to higher wavenumbers. The stretching absorption band of the mono substituted C-C double bond is visible at 2180cm^{-1} in spectrum (b) of Figure 5.6 while it is absent in spectrum (a) of the same figure.
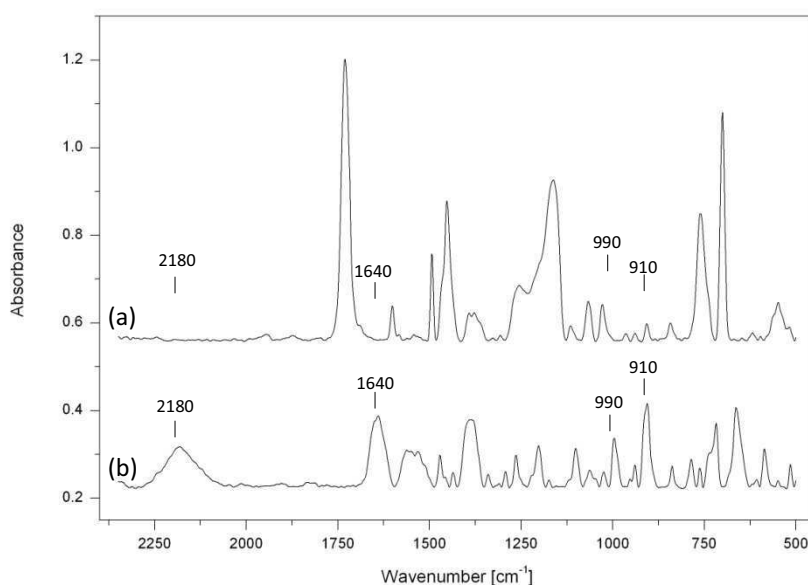
Figure 5.6: FTIR PAS spectra of (a) *p*(Sty-*co*-BA)polymer containing DA3B and (b) pure DA3B

Based on the above it can be said that DA3B was polymerized during the synthesis of the *p*(Sty-*co*-BA) polymer. The research of Schoonbrood et al. showed that oligomers of a surfmer may form, depending on the reactivity of the surfmer relative to the main monomers and that this may result in the migration of the oligomers to the surface of the latex film due to its relatively low molecular mass.[17] To confirm that DA3B was incorporated in the bulk of the polymer film and did not migrate to the film-air or film-substrate interface during film formation, FTIR-PAS was used to determine the presence of DA3B at these surfaces.

118

FTIR-PAS spectra were recorded at four depths of penetration: 3.8 μm, 6.0 μm, 8.4 μm and 14.6 μm at both the film-air and film-substrate interfaces. These spectra were normalized relative to the carbonyl band at 1730 cm^{-1}. Refer to Figure 5.7 and Figure 5.8 for the spectra. Similar trends were seen for the two surfaces analysed and are therefore discussed together. The following bands were identified in these spectra: the in-plane skeletal vibrations of the aromatic C=C functional groups of styrene were identified at 1601 cm^{-1}, 1493 cm^{-1} and 1453 cm^{-1}, while the asymmetric and symmetric bending deformations of the primary ammonium cation of DA3B were identified at 1540 cm^{-1} and 1470 cm^{-1}, respectively (Also refer to Appendix C). The intensity of the deformation bands of DA3B increased slightly with increasing depth of analysis. The very low intensity of the band at 1540 cm^{-1} and the overlap of the band at 1470 cm^{-1} with the in-plane skeletal vibration of the C=C functional group however made further interpretation difficult. It can however be said with certainty that there was not an accumulation of DA3B at the film-air or film-substrate interface.
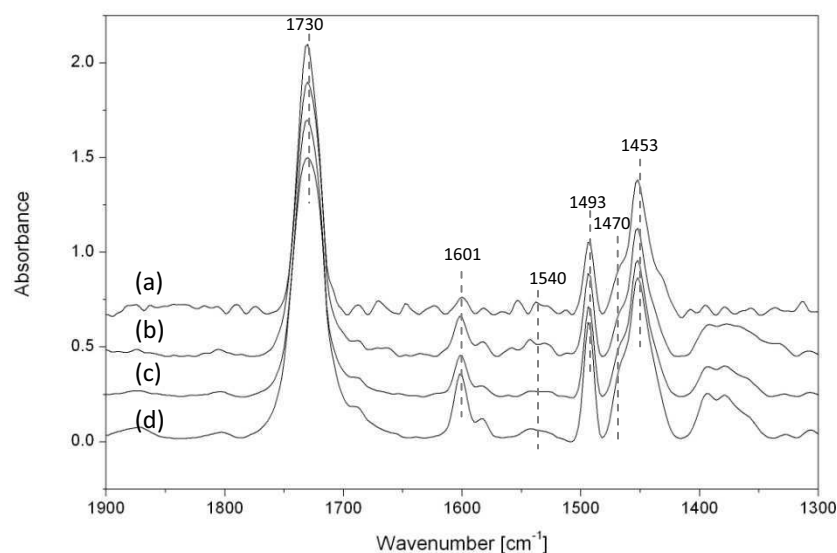
Figure 5.7: FTIR-PAS spectra of *p*(Sty-*co*-BA) latex film containing DA3B (film-air interface): (a) 3.8 μm, (b) 6.0 μm, (c) 8.4 μm and (d) 14.6 μm

119
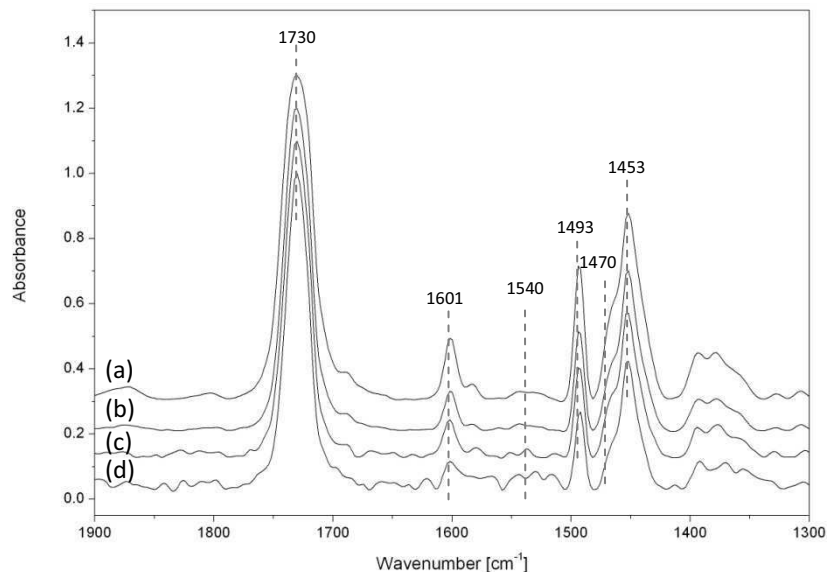
Figure 5.8: FTIR-PAS spectra of *p*(Sty-*co*-BA) latex film containing DA3B (film-substrate interface): (a) 14.6 μm, (b) 8.4 μm, (c) 6.0 μm and (d) 3.8 μm

5.2.2.2 Surface energy analysis

The surface energy properties of *p*(Sty-*co*-BA) films stabilized with different surfactants were determined using the 3-liquid harmonic method (Refer to Chapter 3, Section 3.6.3) and the results were reported in terms of contact angles with the different test liquids as well as surface energy (Refer to Table 5.6).

The results did not highlight significant differences in contact angle or surface energy properties between the 3 different surfactant systems. The film stabilized with 6% OPE, a polymeric surfactant containing hydrophilic ethylene oxide moieties, exhibited the highest contact angle with water and had the lowest polar surface energy component. Previous research has shown that, just like ionic surfactants, non-ionic surfactants typically migrate to the film-air interface.[3] The lower surface energy properties can therefore be attributed to the relative position of OPE at the film-air interface, as well as the lower polarity of the ethylene oxide moieties relative to that of the ionic groups.

120

Table 5.6: Surface energy properties of *p*(Sty-*co*-BA) polymer films stabilized with SDBS, DA3B or OPE

Surfactant	Contact angles for different surface tension liquids [°][5]			Free Surface Energy [mN/m]		
	Water	Diiodomethane	Ethylene glycol	Total	Dispersive	Polar
1% SDBS	90.3±1.26	55.9±3.49	70.3±0.45	30.3	28.3	2.0
1% DA3B	90.6±1.36	64.0±2.17	67.9±1.37	27.9	25.1	2.8
2% DA3B	93.8±0.82	69.4±1.65	70.7±1.26	25.2	22.6	2.6
6% OPE	96.4±1.05	59.1±1.10	79.1±0.45	27.1	26.1	1.0

5.3 Water sorption behaviour of *p*(Sty-*co*-BA) films stabilized with different surfactants

It was shown that the conventional surfactants SDBS and OPE migrated to the film-air and film-substrate interface of the film, while the reactive surfactant DA3B remained immobilized within the bulk of the polymer matrix (see Section 5.2). The presence of such hydrophilic components at the surface of the *p*(Sty-*co*-BA) film can influence the sorption of polar penetrants into the film as the solution of the penetrant into the film would be enhanced by the presence of the conventional surfactants. Although the overall aim of this study was to evaluate the water vapour sorption behaviour of *p*(Sty-*co*-BA) films stabilized with different surfactants, it was thought pertinent to also consider the sorption behaviour of these films to water. It was expected that similar behaviour would be seen for water sorption and for water vapour sorption at high P/P_0 values.

Water absorption of *p*(Sty-*co*-BA) films with the same monomer composition, but stabilized with different surfactant systems, were therefore evaluated. The amount of water absorbed by each film was determined gravimetrically (see Section 4.3.6.1) using films cast directly from emulsion to ensure the presence of the surfactant in the film. The water absorption of these films was compared to a polymer film containing no surfactant (prepared from the SDBS latex, where the polymer was precipitated from the latex with methanol, before being cast from solvent).

---

[5]Contact angles for different test liquids are given as the average contact angle (unit: degrees) of 10 measurements ± the standard deviation (unit: degrees).

The data presented here was for a period of seven days. The accuracy of the results became questionable after an extended period of time as the films began to disintegrate, making an accurate measurement of the increase in mass due to the absorption of water difficult. The amount of water absorbed over a fixed period of time varied significantly between the different types of surfactants used (See Figure 5.9). The rate of water absorption for all 4 films evaluated was fast initially, but slowed down after 24 hours. Although the kinetic curves for these films did not reach equilibrium, it followed the typical Fickian sorption behaviour. After seven days the DA3B stabilized film absorbed the least water, followed by *p*(Sty-*co*-BA) without any surfactant. The OPE stabilized film absorbed the most water over the seven day period.
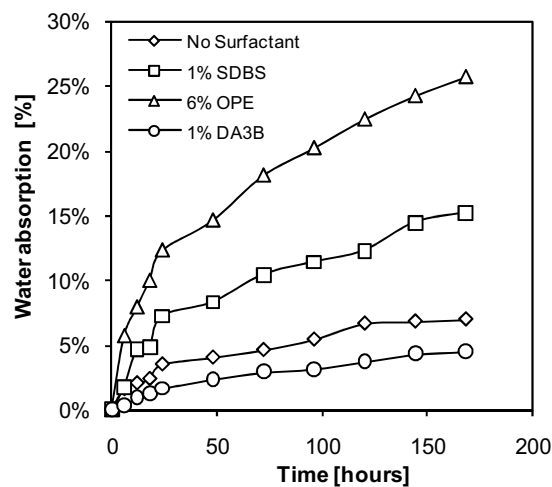
Figure 5.9: Water absorption of *p*(Sty-*co*-BA) stabilized with different types of surfactants

This observed trend can be explained in terms of the chemical composition of the films, taking into consideration the type and concentration of surfactant relative to the polymer in the emulsion.

- **DA3B versus SDBS:** Both DA3B and SDBS have a dodecyl group as part of their nonpolar moiety, thus introducing significant hydrophobicity to the surfactant. Despite this similarity in the chemical structure and the equal quantities of surfactant used during the polymerization, the water absorption evaluation indicated a significant difference in the tendency of the polymer film to absorb water. After 168 hours, the SDBS stabilized film absorbed 15.3% water (w/w) compared to a mere 4.5% of water absorbed by the DA3B stabilized film. This variance can be attributed to the reactive nature of the DA3B surfactant

resulting in the immobilization of the surfactant at the polymer particle/aqueous medium interface (refer to Figure 5.10). SDBS on the contrary will migrate to the surface, where the anionic groups in the surfactant will have an affinity for the water molecules, resulting in higher water absorption values. A further contributing factor is the lower polarity of the organic polar head of the DA3B surfactant compared to the inorganic polar head of SDBS.

- **DA3B versus No Surfactant:** Despite the absence of any surfactant, *p*(Sty-*co*-BA) polymer film resulted in a higher level of water absorption than the DA3B stabilized film. This unexpected behaviour can be attributed to the incorporation of the hydrophobic component (dodecyl ammonium group) of the DA3B surfactant into the backbone of the polymer, which will contribute to the overall hydrophobicity of the polymer structure.
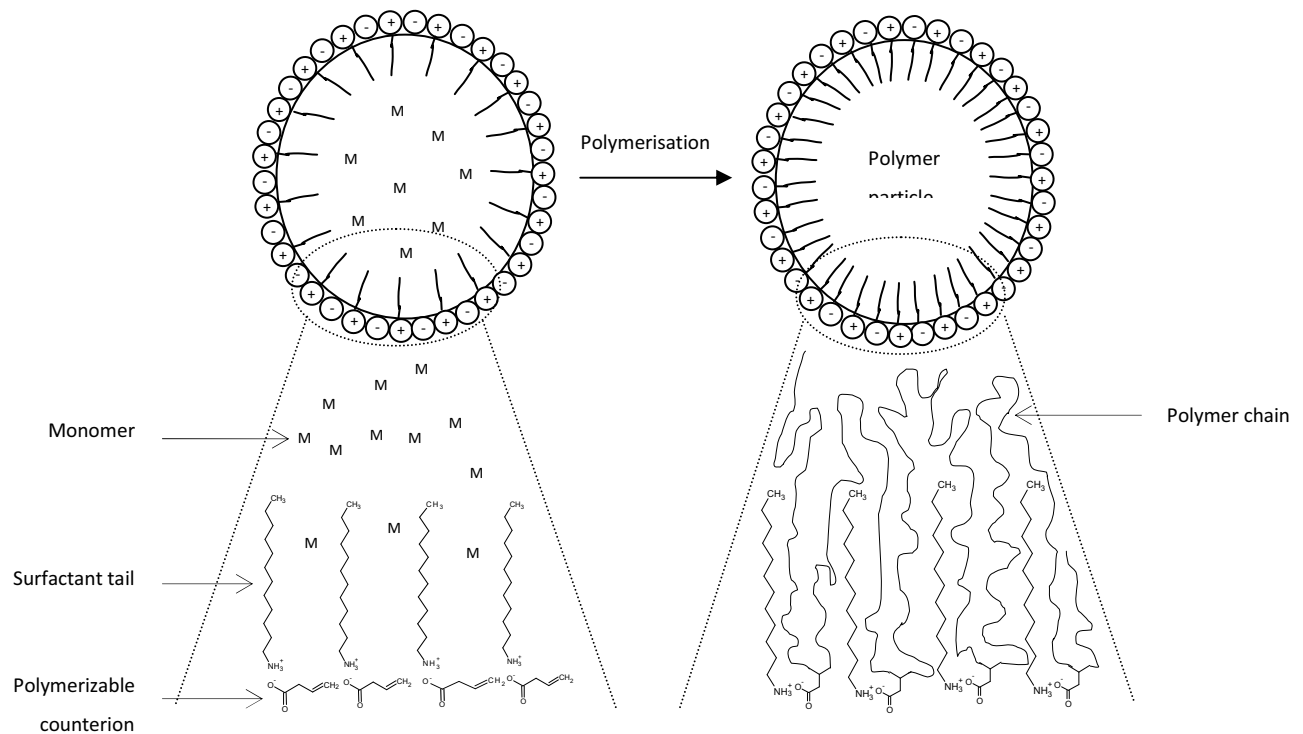
Figure 5.10: Reactive surfactant polymerization mechanism

123

- ▪ **SDBS versus OPE:** Both SDBS and OPE are conventional surfactants that will migrate to the surface of the polymer film. However, the OPE polymer film gave the highest water absorption results. This could be attributed to the relatively high OPE concentration (6%) relative to polymer compared to the SDBS (1%) that was required to ensure a stable emulsion system. The significant difference in chemical composition of the two surfactants could be a further contributing factor, with OPE containing hydrophilic poly ethylene oxide moieties that would have a greater affinity for water.

5.4 Mobility of surfactants induced by high relative humidity

Several studies have evaluated the migration of water into films using FTIR-ATR spectroscopy. These studies have however never considered the simultaneous migration of small molecules such as surfactants to the film-air interface of the film when exposed to water. The objective was therefore to simultaneously monitor the migration of water into the *p*(Sty-*co*-BA) latex film, and the migration of surfactant towards the film-air interface of the film, comparing a conventional surfactant (SDBS) to a reactive surfactant (DA3B). The work of Fieldson and Barbari [18] was used as basis for this study.

A FTIR-ATR flow through liquid cell is normally used for spectroscopic determination of the diffusion and absorption of liquids into polymer films.[19-21] As this equipment was not available, it was decided to expose dried films to a controlled environment of high relative humidity and to perform FTIR-ATR analyses at set intervals to determine the increase in water in the polymer film as a function of time and to correlate that to the migration of surfactant as a result of the presence of water in the film.

The sample preparation and experimental setup are described in Chapter 4, Section 4.4.6.3 and the evaluations were done in triplicate. The depth of penetration of the analysis for the hydroxyl and surfactant bands is summarized in Table 5.7 below. (Also refer to Appendix F for refractive index and depth of analysis calculations).

Table 5.7: FTIR-ATR spectroscopy depth of analysis

	p(Sty-*co*-BA) with SDBS		*p*(Sty-*co*-BA) with DA3B	
Refractive index (n_D)	1.5262		1.5159	
d_p (O-H stretching vibration) @ 3500 cm^{-1}	0.61 µm		0.60 µm	
Wavenumber of surfactant bands	1012 cm^{-1}	1045 cm^{-1}	1493 cm^{-1}	1601 cm^{-1}
d_p at specified surfactant wavenumber	2.12 µm	2.05 µm	1.40 µm	1.30 µm

5.4.3 The mobility of SDBS surfactant

The following bands were integrated as a function of time: SDBS bands at 1043 cm^{-1} and 1012 cm^{-1} and the free water band at 2755-3800 cm^{-1}. The methodology is described elsewhere (refer to Section 4.4.6.3). The mobility of SDBS was evaluated relative to the migration of water vapour into the *p*(Sty-*co*-BA) film. Migration of the surfactant bands to a lower wavenumber was noted in the evaluation. This phenomenon is also explained below.

5.4.3.1 Diffusion of free water versus diffusion of surfactant

For this evaluation *p*(Sty-*co*-BA) films were prepared containing 10% SDBS. The SDBS concentration was increased from the original 1% concentration level to ensure good intensity of the symmetric vibrational bands at 1043 cm^{-1} and 1012 cm^{-1} for accurate quantitative determination of the SDBS concentration as a function of time. Figure 5.11 depicts the relative change in concentration of SDBS (wavenumber: 1043 cm^{-1}) and water vapour (wavenumber: 3450 cm^{-1}) as a function of time.
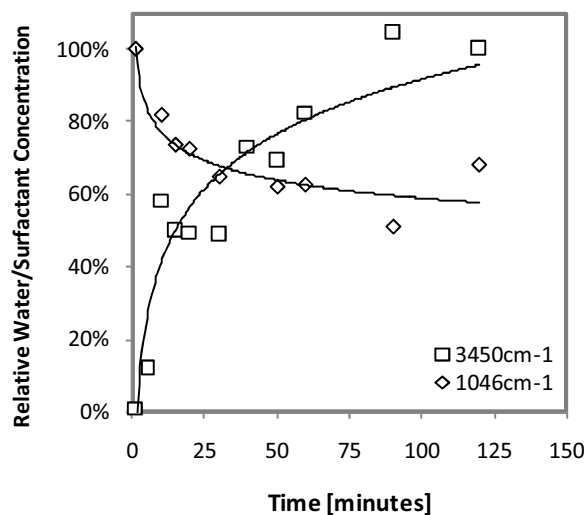
Figure 5.11: Relative change in concentration of SDBS and water vapour as a function of time

As the water vapour concentration increases in the outermost 0.6 μm of the latex film, a reduction in the SDBS concentration is observed. This reduction in SDBS concentration in the outer 2.05 μm of the latex film could be attributed to the migration of SDBS into the bulk of the film together with the water molecules. Approximately 40% of the original SDBS concentration found in the outer 2.05 μm of the latex film was found to be redistributed into the bulk of the film.

The diffusion coefficient for the migration of water and SDBS into the film were calculated using equation 4.18 (refer to Section 4.4.6.3) where $\ln(1 - \frac{A_t}{A_\infty})$ is plotted against time for water vapour and SDBS respectively (refer to Figure 5.12). From this calculation, a diffusion coefficient of 3.89E-06 cm^2/sec and 2.59E-06 cm^2/sec was found for the migration of water vapour and SDBS respectively when the partial pressure of water vapour was increased from 0% relative humidity to 93.2% relative humidity in the atmosphere surrounding the latex film. The diffusion coefficient for the diffusion of water vapour into p(St-co-BA) latex film stabilized with SDBS was found to be several orders of magnitude larger than the diffusion coefficient that was determined for the migration of water vapour into the bulk of this film using the gravimetric method (refer to Section 5.5 and Appendix K). This could be attributed to the presence of surfactant at the film-air interface resulting in higher hydrophilicity near the surface of the film compared to the bulk of the film. Diffusion of water vapour into the outer part of the latex film should therefore be faster than diffusion through the bulk of the polymer where the hydrophobic nature of styrene and n-butyl acrylate would result in a reduced rate of diffusion.
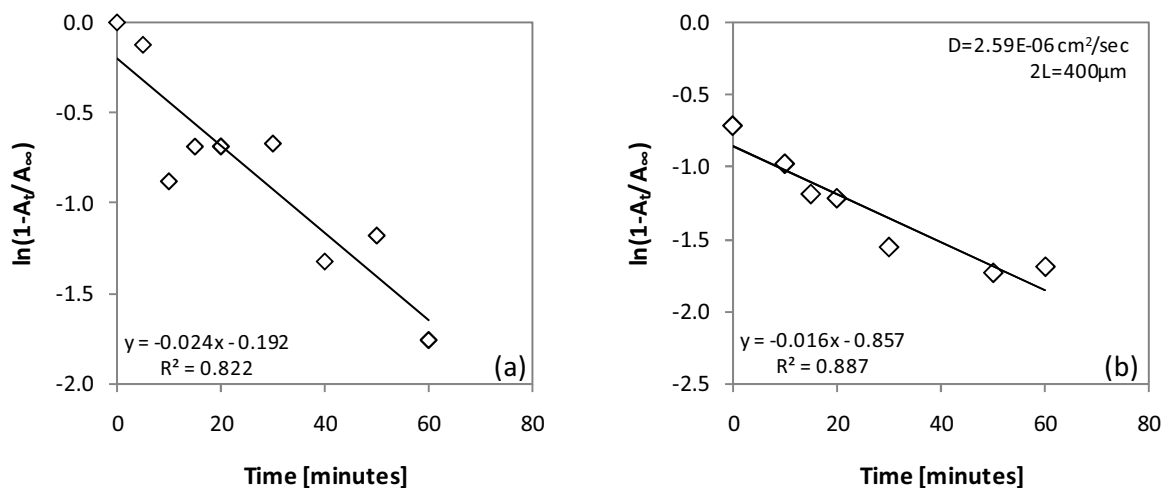
Figure 5.12: Kinetic plot of $\ln(1 - \frac{A_t}{A_\infty})$ vs. time for the diffusion of (a) water vapour and (b) SDBS

126

5.4.3.2 Shift in SDBS bands to lower wavenumber

It was noted that the surfactant bands at 1043 cm^{-1} and 1012 cm^{-1} shifted as a function of time, i.e. as more free water molecules penetrated the polymer film. To understand this shift in the surfactant vibrational bands, pure SDBS was subjected to different degrees of wetting by water molecules. 4 samples of SDBS were compared: (a) SDBS dried under vacuum; (b) dry SDBS exposed to ambient conditions for 6 hrs; (c) dry SDBS crystals exposed to a drop of water so that some surfactant crystals remained visible; and (d) SDBS completely dissolved in water (refer to Figure 5.13).
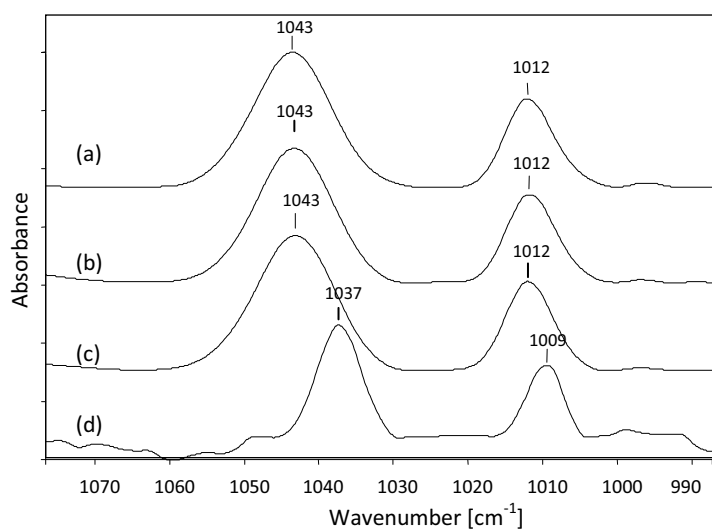
Figure 5.1: FTIR-ATR Absorbance spectra indicating the shift of surfactant bands due to interaction with water molecules: (a) SDBS dried under vacuum; (b) SDBS exposed to ambient conditions for 6hrs; (c) SDBS exposed to a drop of liquid water; and (d) SDBS dissolved completely in water

From this evaluation it was evident that the surfactant bands showed a significant shift when dissolved in water from 1043 cm^{-1} and 1012 cm^{-1} to 1037 cm^{-1} and 1009 cm^{-1}, respectively.

The shift in S-O vibrational bands could be attributed to the association of the water molecules with the sulfonate group of SDBS.[4, 6] The association of the H-atoms of the water molecules with the sulfonyl groups of the surfactant resulted in a shift of the symmetric stretching vibrations to lower wavenumbers as the redistribution of electrons strengthened the S-O bond. (Also refer to schematic representation of interaction below in Figure 5.14)
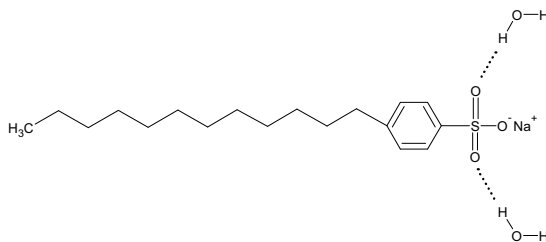
Figure 5.14: Chemical structure of SDBS denoting the association with free water molecules

5.4.4 The mobility of DA3B surfactant

For the purpose of this evaluation 2% (w/w) DA3B relative to the monomer was used. The following infrared absorption bands were integrated as a function of time: the asymmetric and symmetric bending deformation bands of the primary ammonium cation of DA3B at 1540 cm^{-1} and 1472 cm^{-1} and the stretching deformation band of the non-bonded hydroxyl group of free water at 2755-3800 cm^{-1}. The methodology is described elsewhere (Refer to Section 4.4.6.3).

Baseline correction and normalization relative to the carbonyl band of the ester at 1726 cm^{-1} were done prior to integrating the spectra. Due to significant overlap between the absorption bands of the primary ammonium cation and the C=C in-plane skeletal vibrations it was not possible to integrate the bands associated with the presence of DA3B. It was therefore decided to only monitor the increase in the intensity of the stretching deformation band of the non-bonded hydroxyl group of free water. Contrary to the observation made with the SDBS stabilized *p*(Sty-*co*-BA) film, no water absorption was detected. FTIR-ATR spectra of the *p*(Sty-*co*-BA) film showed that, over the wavenumber range 2750-3800 cm^{-1} and at different time intervals, there was no free water detected in the film (refer to Figure 5.15).

This may be attributed to the relatively low DA3B concentration of 2% compared to 10% of the SDBS. In another part of this study, where gravimetry was used to determine the absorption of water vapour in films (Refer to Section 5.5), it was however established that SDBS stabilized *p*(Sty-*co*-BA) absorbed 10 times more water vapour than the same polymer films stabilized with the same concentration of DA3B. It is therefore unlikely that a higher DA3B concentration would result in a significant increase in the absorption of free water at the air-film interface.

Another contributing factor for the lack of free water absorption of the film prepared from the latex stabilized by DA3B compared to the film prepared from the latex stabilized by SDBS is the methodology used to measure water vapour absorption. FTIR-ATR only detects the migration of small molecules (in this case water vapour) within the first 1.4 µm at the air-film interface. The gravimetric method however determines water vapour sorption throughout the entire film. Apart from this, the experimental setup for FTIR-ATR spectroscopy utilized a vertical ATR unit implying that the measurement was done on an extremely small surface area (±2 mm diameter circle) and that no attenuation of the signal was possible. In comparison to this, the gravimetric method utilized a 1.5 cm x 1.5 cm sample of approximately 350 µm film thickness. This methodology would therefore not be suitable for film with a low affinity to free water.
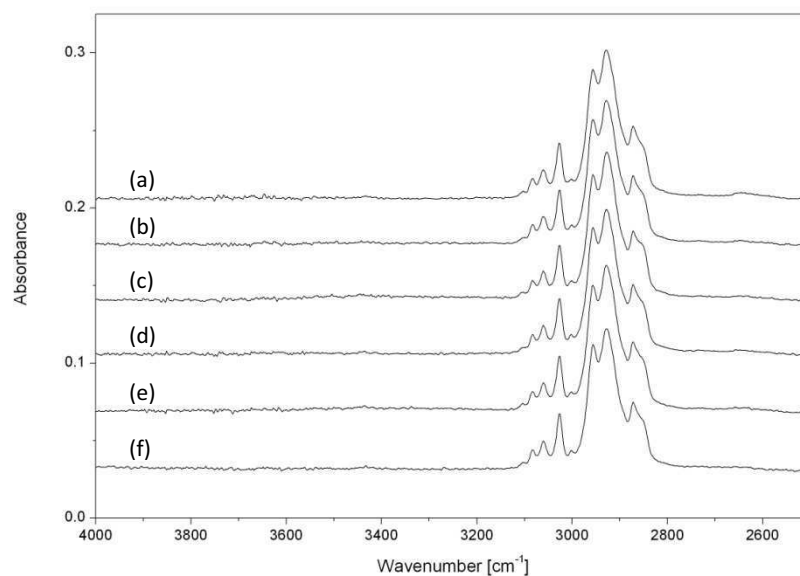
Figure 5.15: FTIR-ATR absorbance spectra of *p*(Sty-*co*-BA) polymer containing 1% DA3B at different time intervals: (a) 180 min, (b) 150 min, (c) 120 min, (d) 90 min, (e) 60 min and (f) 0 min

5.5 Gravimetric determination of water vapour sorption behaviour of *p*(Sty-*co*-BA) films stabilized with different surfactants

Sections 5.3 investigated the absorption of water into *p*(Sty-*co*-BA) films, while Section 5.4 considered the simultaneous migration of unbound polar components such as SDBS and DA3B to the film-air interface and water vapour from the film-air interface into the *p*(Sty-*co*-BA) films. Both

129

studies found that the film stabilized with DA3B surfactant exhibited the lowest affinity for water and water vapour, while the films stabilized with conventional surfactants (SDBS and OPE) had a significantly higher affinity for water and water vapour. Based on these findings, as well as the relative position of the surfactants in the film, a similar trend was expected for the gravimetric determination of water vapour sorption into p(Sty-co-BA) films stabilized with these surfactants.

The purpose of the evaluation discussed here was therefore to evaluate the impact of different types of surfactants on the water vapour sorption properties of p(Sty-co-BA) films. Each sample was evaluated at 25 °C and at a water vapour partial pressure range from 0.1 to 0.9. These isotherm evaluations were done well above the T_g of the polymers (Refer to Table 5.8 for T_g values of polymers). The water vapour sorption behaviour of the different p(Sty-co-BA) films was discussed in terms their kinetic behaviour and thermodynamic behaviour. The impact of film thickness on the water vapour sorption behaviour of p(Sty-co-BA) films stabilized with SDBS and DA3B were also explored.

Table 5.8: Properties of p(Sty-co-BA) films used for this evaluation

Sample Nr	Surfactant Type	Surfactant Concentration	T_g [°C]	Film thickness [μm]
1	SDBS	1%	16	173
2	SDBS	1%	16	420
3	OPE	6%	16	378
4	DA3B	1%	14	160
5	DA3B	1%	14	365

Reproducibility of the experimental procedure was determined using a 1% SDBS stabilized p(Sty-co-BA) film with a 365 μm thickness. The reproducibility evaluation considered two factors: (1) the reproducibility of the test method for a single film; and (2) the reproducibility of the sorption properties for different films prepared from the same p(Sty-co-BA) latex. The results are summarized in Appendix J. These results indicate good reproducibility for both scenarios evaluated.

5.5.5 Water vapour sorption kinetic behaviour of *p*(Sty-*co*-BA) stabilized with different surfactants

The kinetic behaviour of the different films was evaluated in terms of their sorption behaviour as a function of time. The reduced sorption curve was used to establish whether water vapour sorption followed the Fickian model, or whether an alternative model was more appropriate to describe the kinetic behaviour.

5.5.5.1 Conventional surfactants: SDBS and OPE

The mass sorption curves (Refer to Figure 5.16 and Figure 5.17) indicated similar kinetic behaviour for the SDBS and OPE stabilized systems, where, for increasing P/P_0 partial pressures, more water vapour was absorbed and longer times were required to reach equilibrium. This can be illustrated as follows: For an increase in partial pressure from 0.5 to 0.6, the OPE system absorbed 0.106 mg water vapour compared to the 0.101 mg for the SDBS stabilized system and both systems required approximately 200 minutes to achieve equilibrium. However, for an increase from 0.8 to 0.9 partial pressure, the OPE system absorbed 1.2 mg of water vapour compared to 1.1 mg for the SDBS system and significantly longer time was required to achieve equilibrium. Although not shown here, the desorption kinetic curves exhibited similar kinetic behaviour, where a reduction in partial pressure resulted in a reduction in the amount of water vapour desorbed from the sample as well as a reduction in the time required to reach equilibrium. The reduced sorption curves indicate Sigmoidal kinetics and therefore a deviation from Fickian sorption behaviour for both surfactants evaluated.
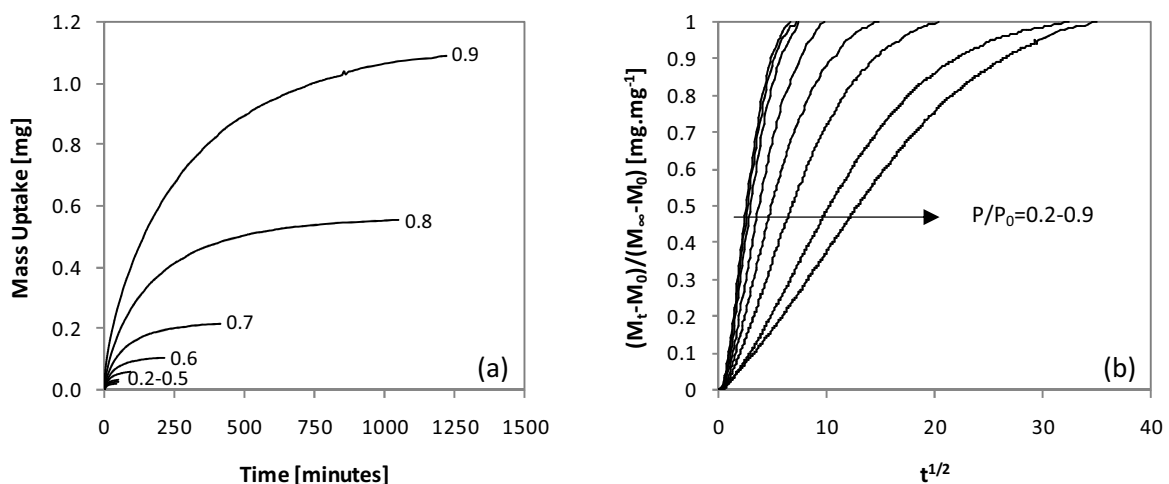
Figure 5.16: (a) Mass sorption curve of *p*(Sty-*co*-BA) polymer stabilized with SDBS and (b) reduced mass sorption curves at P/P$_0$ from 0.2 to 0.9 for *p*(Sty-*co*-BA) polymer stabilized with SDBS
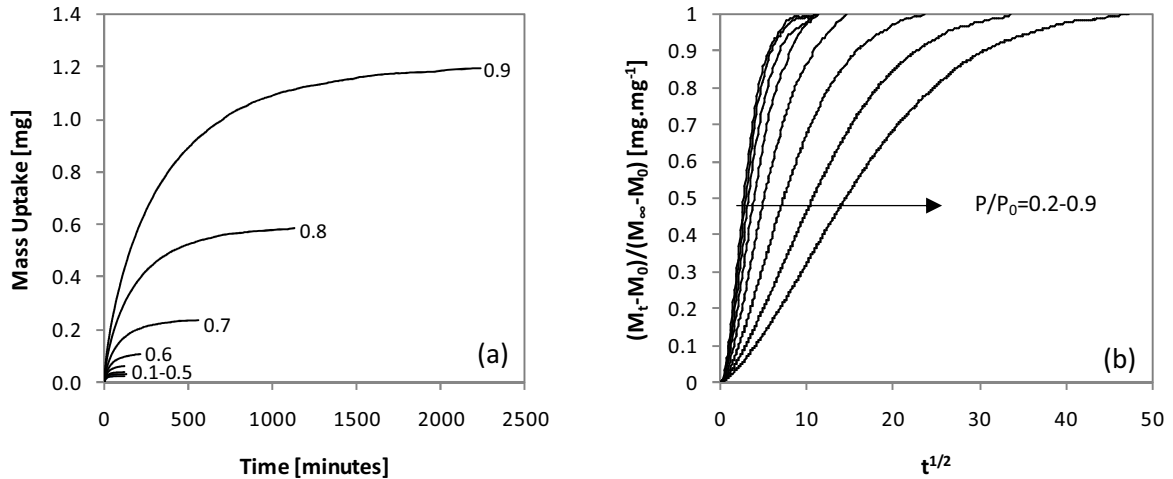
Figure 5.17: (a) Mass sorption curve of *p*(Sty-*co*-BA) polymer stabilized with OPE and (b) reduced mass sorption curves at P/P$_0$ from 0.2 to 0.9 for *p*(Sty-*co*-BA)polymer stabilized with OPE

The SDBS and OPE stabilized *p*(Sty-*co*-BA) films exhibited similar diffusion behaviour, with the OPE stabilized film having a slightly lower diffusion coefficient compared to the SDBS stabilized film (refer to Figure 5.18). This similar behaviour could be attributed to similar positions of the surfactant, i.e. more concentrated at the film-air and film-substrate interfaces, within the polymer matrix. The diffusion coefficient was not constant across the partial pressure range evaluated. For the adsorption curve, an initial increase in the diffusion coefficient was observed from P/P$_0$=0.1 to P/P$_0$=0.2, after which it decreased exponentially with an increase in water vapour partial pressure from P/P$_0$=0.3-0.9. This behaviour can be attributed to the tendency of the water molecules to associate with the surfactant molecules present close to the surface of the latex film. The water molecules will aggregate in this region due to strong cohesive forces with the surfactant as well as between the water molecules, leaving few water molecules available to diffuse freely in the polymer matrix. Where the diffusion of water vapour molecules initially took place from a high water vapour partial pressure (p$_1$) to a low water vapour partial pressure (p$_2$), the aggregation of water molecules at the surface of the film result in an intermediate water vapour partial pressure (p$_3$) being established, thus reducing the water vapour gradient between the atmosphere surrounding the film and the water vapour partial pressure immediately at the surface of the latex film (refer to Figure 5.19). This phenomenon reduces the rate of migration of the water vapour molecules from the atmosphere surrounding the film into the film. At low water vapour partial pressures this tendency is

not evident, but once a critical minimum amount of water molecules is present in the polymer matrix, the tendency of the water molecules to aggregate becomes the dominant behaviour.[22]
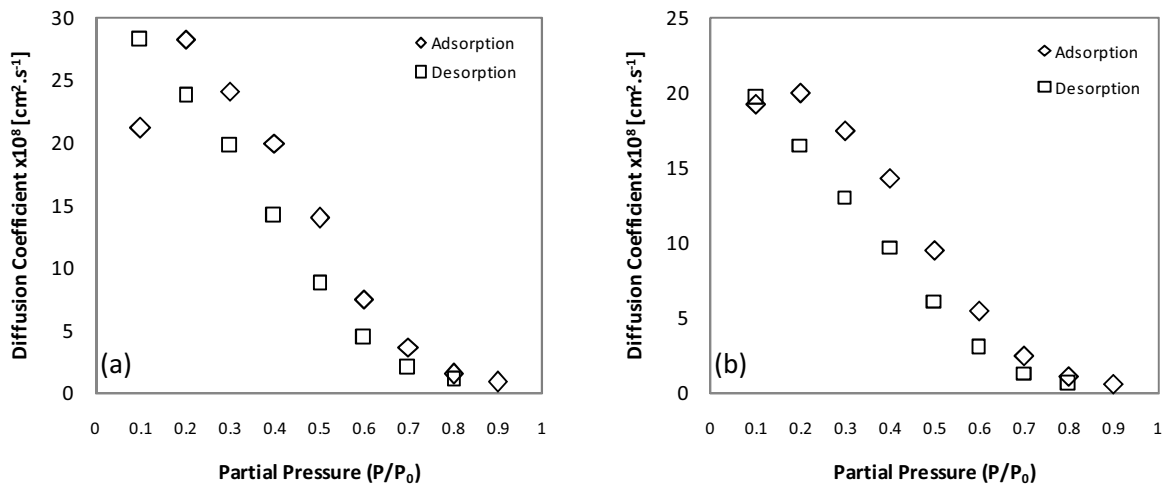
Figure 5.18: Adsorption and desorption diffusion coefficients for *p*(Sty-*co*-BA) latex films stabilized with (a) SDBS and (b) OPE
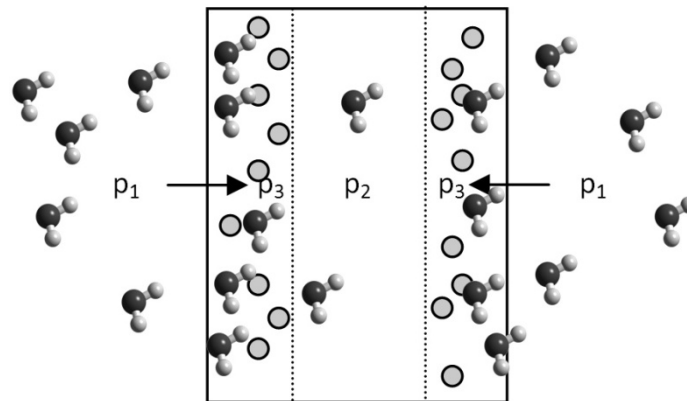
Figure 5.19: Illustration of pressure gradients in film due to relative position of surfactant (represents water molecules;◯ represents surfactant molecules)

The diffusion coefficient for desorption of water vapour was also not constant over the partial pressure range evaluated. As the water vapour partial pressure decreased, an increase in the diffusion coefficient was seen, in line with a reduction in the clustering of water molecules and an increase in the availability of unassociated water molecules that can diffuse freely in the polymer matrix. A hysteresis effect was seen between the diffusion coefficients for the adsorption and desorption curves, with the diffusion coefficient for desorption of water vapour being slightly lower

133

at low partial pressures compared to the diffusion coefficient for the adsorption of water vapour. This effect became more prominent al lower partial pressures. The hysteresis effect at low water vapour partial pressures can be attributed to the relative position of the surfactant at the surface of the latex film, resulting in an intermediate water vapour gradient forming between p_3 and p_1 (refer to Figure 5.19). This reduced gradient results in a reduction in the rate at which the water molecules migrate from the film to the atmosphere surrounding the film.

5.5.5.2 Reactive surfactant: DA3B

The mass sorption curve and reduced mass sorption curve for p(Sty-co-BA) latex film stabilized with DA3B indicated that the time required to reach equilibrium at each partial pressure setting remained constant, i.e. equilibrium was reached within approximately 30 minutes and was independent of the partial pressure (refer to Figure 5.20). This is much faster than the times required for reaching equilibrium with the conventional surfactants and is also reflected in the significantly higher diffusion coefficient for the DA3B stabilized polymer matrix (refer to Figure 5.21 and Appendix K). This confirms the findings from Amalvy[23] where it was shown that diffusion coefficients of a polymer stabilized with reactive surfactants were higher than for the same polymer stabilized with conventional surfactants. This behaviour is due to the uniform presence of the reactive surfactant throughout the polymer matrix, which facilitates fast migration of water vapour through the polymer matrix. Other factors such as free volume variances did not play a role as no significant difference in free volume could be found between films stabilized with the 3 different surfactants (refer to Table 5.4).
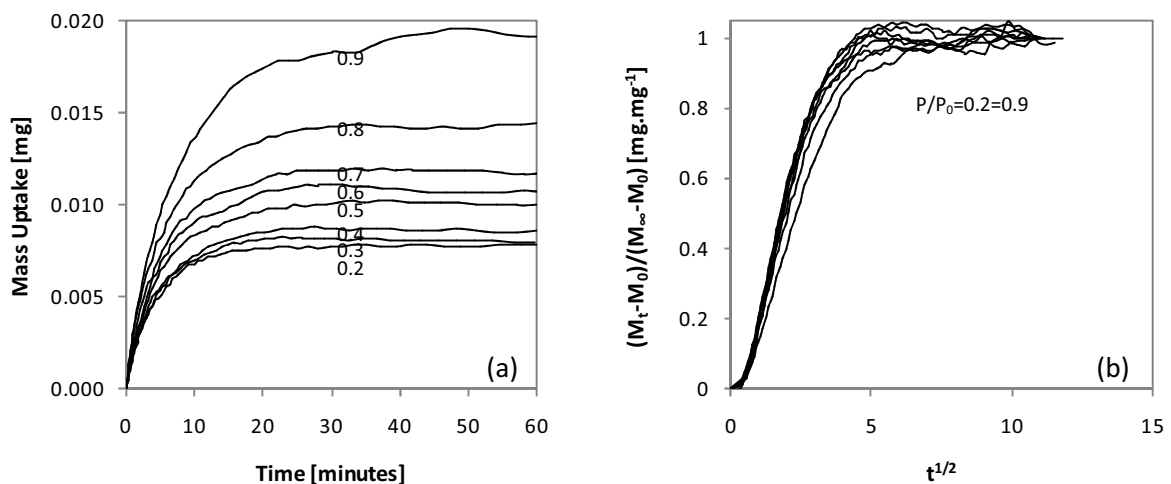
Figure 5.20: (a) Mass sorption curve of p(Sty-co-BA) polymer stabilized with DA3B and (b) Reduced adsorption curves at P/P$_0$ from 0.2 to 0.9 for p(Sty-co-BA)polymer stabilized with DA3B
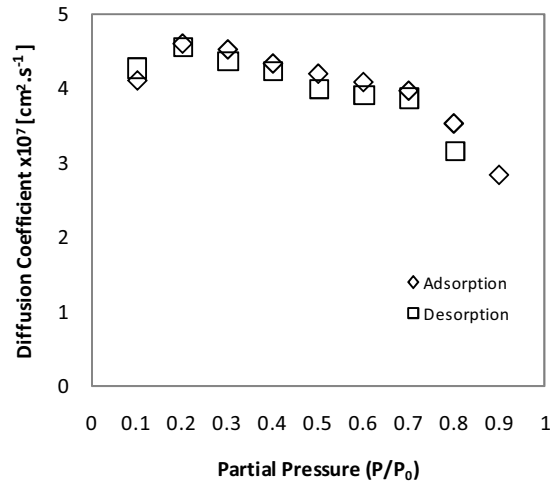
Figure 5.21: Adsorption and desorption diffusion coefficients for *p*(Sty-*co*-BA) films stabilized with 1% DA3B

In contrast to the change in diffusion behaviour of water vapour through *p*(sty-*co*-BA) films stabilized with SDBS or OPE, the diffusion coefficient D for the DA3B stabilized film showed a very different trend, where almost no change in D was observed over the partial pressure range investigated (refer to Figure 5.21). The hysteresis effect observed with the latex films stabilized with conventional surfactants was also not evident for the DA3B stabilized polymer.

5.5.5.3 Sigmoidal behaviour

The reduced sorption curves for all 3 types of surfactants showed Sigmoidal behaviour at short times, where the time required for reaching equilibrium at the surface of the polymer film was initially slow. An example of the Sigmoidal kinetic curves are given in Figure 5.22 for $P/P_0=0.6$.

Although it was initially thought that Sigmoidal behaviour could be caused by the clustering of conventional surfactants close to the film-air and film-substrate interfaces, Sigmoidal kinetic behaviour was also noted for *p*(Sty-*co*-BA) stabilized with the reactive surfactant DA3B. As DA3B is immobilized throughout the bulk of the film, the accumulation of surfactant near the surface of the film could not be the only reason for slow equilibrium of water vapour sorption close to the surface of the film. Even *p*(Sty-*co*-BA) containing no surfactant exhibited the same type of kinetic behaviour. It is therefore believed that the Sigmoidal kinetic behaviour is also a function of the polymer itself, and not only the surfactant.

135
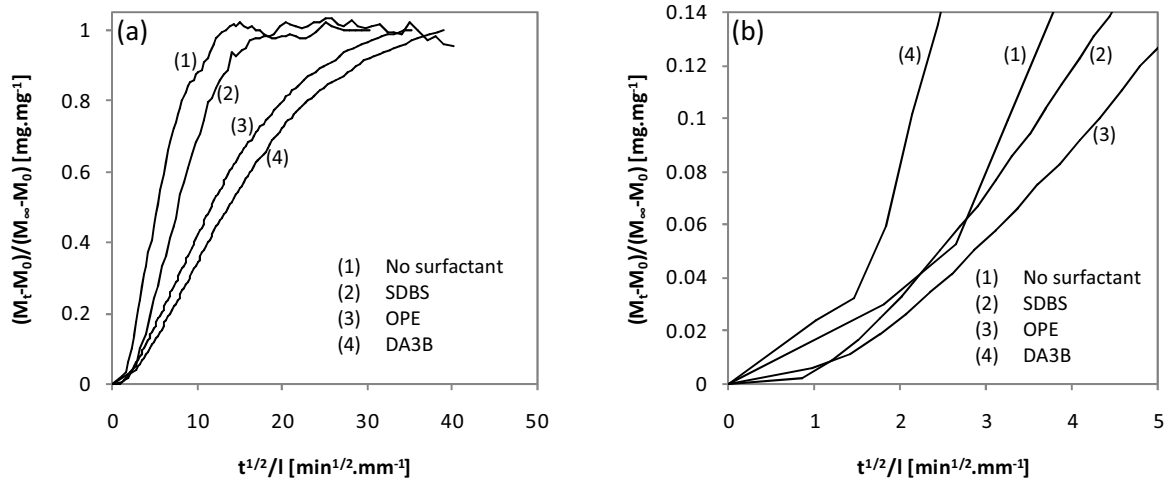
Figure 5.22: Reduced sorption curves showing Sigmoidal kinetic behaviour: (a) entire reduced kinetic curve; and (b) reduced kinetic curve reflecting the initial slow uptake of water vapour

When evaluating the initial part of the reduced sorption curve (see Figure 5.22(b)) it is interesting to note that the rate of sorption differs quite significantly for the four films evaluated. The initial retardation of the rate at which water vapour sorption equilibrium is reached appears to be the most significant for p(Sty-co-BA) stabilized with conventional surfactants, while p(Sty-co-BA) containing either DA3B or no surfactant at all showed less retardation. It can therefore be concluded that the type and mobility of the surfactant determines the degree or equilibrium retardation at the surface of the polymer latex film.

5.5.6 Thermodynamic behaviour of p(Sty-co-BA) stabilized with different surfactants

The thermodynamic behaviour of p(Sty-co-BA) latex films stabilized with different surfactants was evaluated in terms of their equilibrium isotherm plot at 25 °C and for a water vapour partial pressure range from 0.1 to 0.9 at 0.1 increments (refer to Figure 5.23 and Figure 5.25). Their solubility coefficients, across the water vapour partial pressure range, were also evaluated (refer to Figure 5.24 and Figure 5.26).

5.5.6.1 Conventional surfactants: SDBS and OPE

SDBS stabilized p(Sty-co-BA) latex film exhibited low water vapour sorption at low partial pressures, while higher partial pressures were characterized by significant mass increase due to the sorption of water vapour. The resultant equilibrium sorption isotherm indicated typical Flory-Huggins behaviour both for the adsorption and desorption isotherms (see Figure 5.23(a)). No hysteresis was seen during desorption of the water vapour molecules, indicating that the sorption was mainly due to penetrant-penetrant interaction, and not penetrant-polymer interactions. The OPE stabilized film exhibited similar thermodynamic behaviour to the SDBS stabilized system, where the equilibrium isotherm at 25 °C also followed the Flory-Huggins model (see Figure 5.23(b)). At P/P_0=0.9 the mass of both the SDBS and the OPE stabilized films increased by approximately 3.7% compared to the original dry sample mass.
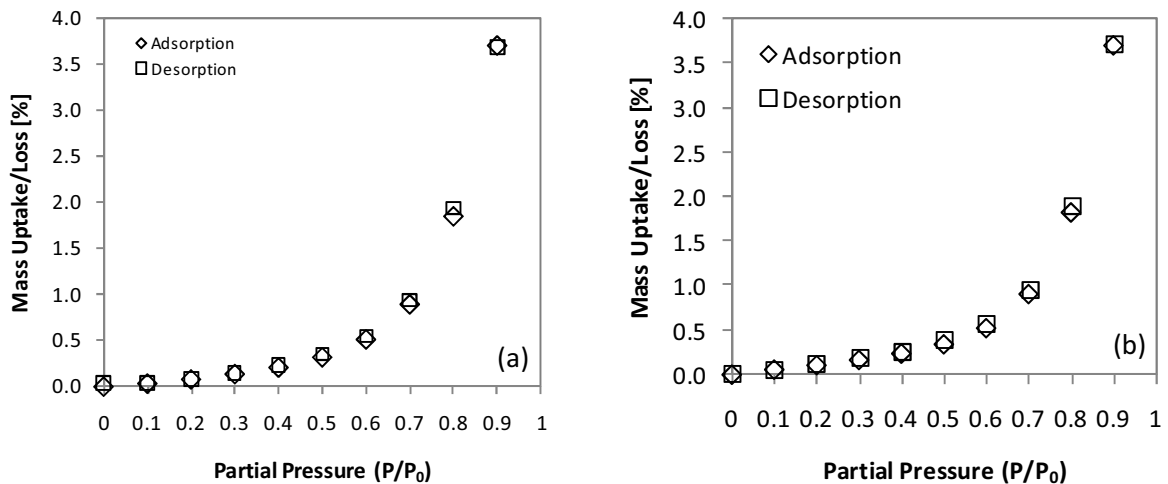
Figure 5.23: Equilibrium sorption and desorption isotherms of p(Sty-co-BA) polymer stabilized with (a) SDBS and (b) OPE

The solubility coefficients for p(Sty-co-BA) stabilized with conventional surfactants (SDBS and OPE) exhibited a similar variation across the water vapour partial pressure range investigated (see Figure 5.24). An initial reduction in the solubility coefficient was observed for P/P_0=0.1-0.4, reaching a minimum value at P/P_0=0.4 before the solubility coefficient increased significantly towards higher water vapour partial pressures. A maximum solubility coefficient was reached for both latex films stabilized with conventional surfactants SDBS and OPE at P/P_0=0.9.
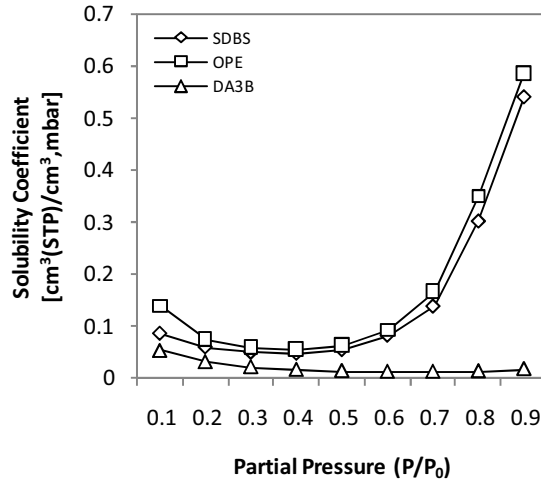
Figure 5.24: Solubility coefficients versus water vapour partial pressure for *p*(Sty-*co*-BA) latex films stabilized with SDBS, OPE and DA3B respectively

This trend can be explained in terms of the relative position of the surfactant in the latex film. The exudation of surfactant to the film-air and film-substrate interface seen with SDBS and OPE create polar domains close to the surface of the film, increasing the affinity of the latex film to water vapour at initial low water vapour partial pressures. As water vapour is sorbed into the film, the surfactant migrates with the diffusing water molecules deeper into the film, reducing the polar domains close to the surface of the film and therefore also reducing the ease with which water vapour is dissolved in the film (refer to Section 5.4.3.1 where it was shown that SDBS diffused into the film with increasing amounts of water being absorbed by the film). At higher water vapour partial pressures (where $P/P_0 \geq 0.4$) a critical water vapour concentration is exceeded in the latex film, facilitating clustering of the penetrant molecules instead of having water vapour molecules diffusing through the film as individual molecules. This behaviour is in line with the penetrant-penetrant interactions predicted by the Flory-Huggins model.

5.5.6.2 Reactive surfactant: DA3B

Contrary to the OPE and SDBS stabilized films, the DA3B stabilized film absorbed very little water vapour over the entire partial pressure range evaluated, with a total mass increase at $P/P_0=0.9$ of only 0.32% of the original dry sample mass, which corresponds to less than 10% of the mass uptake of the SDBS and OPE stabilized latex films for equivalent water vapour partial pressure (see Figure

5.25). This significant difference could be attributed to the difference in mobility, and therefore relative position, of the surfactant within the polymer matrix, as well as the relative lower polarity of the polar head of DA3B due to its reactive organic counterion. As no clustering of the DA3B surfactant took place, the hydrophobicity of the film remained constant throughout the film volume, resulting in limited interaction between the penetrant and the polymer matrix throughout the entire film and diffusion of individual water vapour molecules through the polymer matrix. Penetrant-penetrant interaction was also limited due to the lack of clustering of surfactant, resulting in a significantly lower equilibrium sorption of the water vapour.
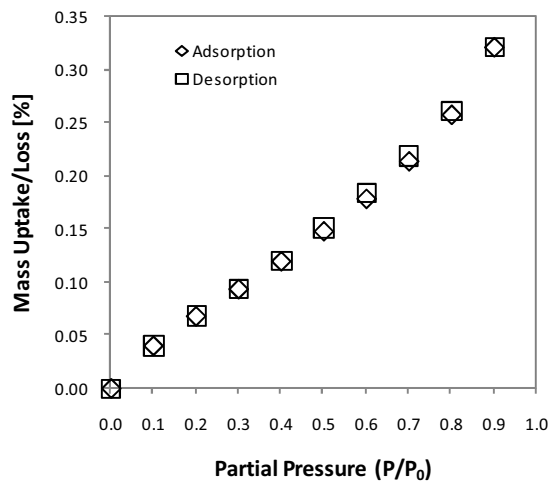
Figure 5.25: Equilibrium adsorption and desorption isotherm of *p*(Sty-*co*-BA) polymer stabilized with DA3B

p(Sty-*co*-BA) stabilized with DA3B exhibited completely different thermodynamic behaviour compared to the same polymer stabilized with the conventional surfactants SDBS and OPE. From $P/P_0=0.2$ to $P/P_0=0.7$ the isotherm showed a linear increase in mass uptake for the DA3B stabilized latex film with an increase in partial pressure, in line with Henry's Law. The amount of water vapour in the film is therefore only dependent on the partial pressure of the water vapour, and is not due to any interaction between the water vapour and polymer or due to penetrant-penerant interactions. A slight exponential increase in % mass uptake (in line with Flory-Huggins type behaviour) was only observed at high partial pressures where $P/P_0>0.7$.

The solubility coefficient of *p*(Sty-*co*-BA) latex film at increasing water vapour partial pressures differed significantly from that seen for the same polymer stabilized with conventional surfactants SDBS and OPE respectively. It was significantly lower and decreased from $P/P_0=0.1$ to $P/P_0=0.7$, after

which there was a slight increase in the solubility coefficient (see Figure 5.24 and Figure 5.26). The initial decrease in the solubility coefficient corresponds to the linear region of the isotherm, while the slight increase in the solubility coefficient reflects the portion of the isotherm which appeared to be following the Flory-Huggins model due to penetrant-penetrant interactions.

As the solubility coefficient is determined by the ratio of the concentration of water vapour sorbed to the actual water vapour pressure, it follows that the solubility coefficient would decrease across the water vapour partial pressure range if the amount of water vapour absorbed did not increase at a similar level to the increase in the water vapour pressure. In this case, the amount of water vapour sorbed remained constant at approximately 0.2% of the original dry sample mass for P/P_0=0.1-0.7, while the water vapour pressure increased at a faster rate. This low affinity of the latex film to water vapour can be attributed to the hydrophobicity of the polymer matrix, as well as the relative position and hydrophobicity of DA3B surfactant in the latex film. The hydrophobicity of the latex film was also reflected in the water absorption evaluation (refer to Section 5.3) where the polymer latex film containing DA3B absorbed significantly less water than the latex films stabilized with SDBS or OPE. The amount of water vapour absorbed by the polymer increased for P/P_0>0.7 as a result of penetrant-penetrant interactions (refer to the isotherm in Figure 5.25). This resulted in a slight increase in the solubility coefficient.
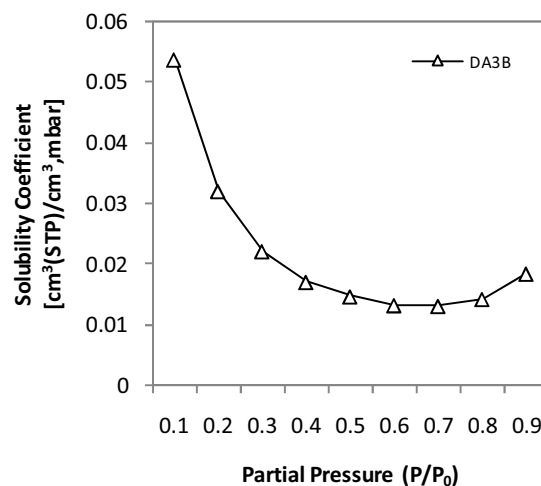
Figure 5.26: Solubility coefficient versus water vapour partial pressure for *p*(Sty-*co*-BA) latex film stabilized with DA3B

140

5.5.7 Permeability of *p*(Sty-*co*-BA) latex films stabilized with different surfactants

Permeability coefficients (P) were determined for *p*(Sty-*co*-BA) latex films stabilized with SDBS, OPE and DA3B respectively. This was done using equation 2.1, P being equal to the product of the diffusion coefficient D and the solubility coefficient S, as determined at a specific water vapour partial pressure. Figure 5.27 depicts the permeability coefficient as a function of the water vapour partial pressure.

The permeability coefficients decreased with increasing water vapour partial pressure, and apart from the permeability coefficients at $P/P_0=0.1$, the permeability coefficients for the three latex films evaluated were found to be very similar. This result is significant if one considers the considerable difference in the diffusion and solubility coefficients of the latex films stabilized with conventional surfactants compared to the polymer stabilized with the reactive surfactant. The low diffusion coefficients of *p*(Sty-*co*-BA) stabilized with conventional surfactants SDBS and OPE, combined with the high solubility coefficients therefore resulted in similar permeability behaviour as the polymer latex film stabilized with DA3B where the immobilized surfactant resulted in high diffusion rates in combination with extremely low solubility behaviour.
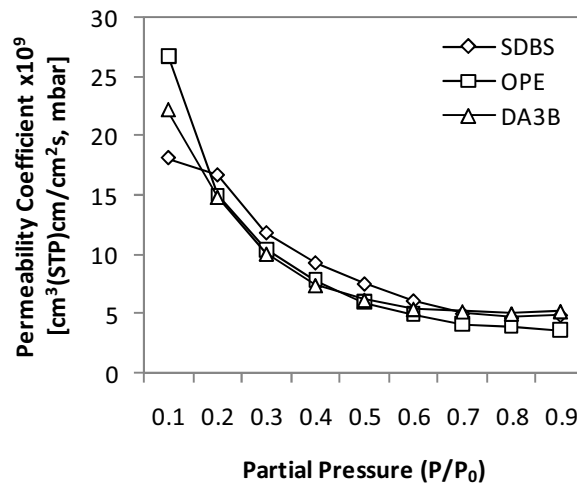
Figure 5.27: Permeability coefficients of *p*(Sty-*co*-BA) latex films stabilized with SDBS, OPE and DA3B respectively

The variation in permeability coefficients for $P/P_0=0.1$ could be attributed to the combined impact of the anomalous diffusion behaviour (described in Section 5.5.5) at $P/P_0=0.1$ compared to $P/P_0=0.2$ for

141

all three films evaluated and the impact of the surfactant at the surface of the film for the latex films stabilized with conventional surfactants.

5.5.8 Kinetic behaviour of different film thicknesses

The impact of film thickness on the water vapour sorption properties of p(Sty-co-BA) stabilized with SDBS or DA3B was evaluated. Two film thicknesses of each type of surfactant stabilized film were evaluated: a 420 µm and 173 µm film for the SDBS stabilized film, and a 365 µm and 160 µm film for the DA3B stabilized film. Sorption isotherms were determined across a partial pressure range of 0.1 to 0.9 in increments of 0.1. The reduced sorption curves and diffusion coefficients of the respective films are depicted in Figure 5.28 and the equilibrium mass uptake per cm^3 is shown in Figure 5.29.

The reduced sorption curves in Figure 5.28(a) indicated that water vapour sorption in p(Sty-co-BA) followed Sigmoidal kinetic sorption behaviour irrespective of the type of surfactant used to stabilize the polymer or the film thickness of the respective polymers. The key difference was that, for the DA3B stabilized film, the thicker film resulted in a faster rate of sorption compared to the thinner film; while the opposite was found for the SDBS stabilized film. For both types of films there was a reduction in the diffusion coefficient with increasing water vapour partial pressures for both thin and thick films (see Figure 5.28(b). For the SDBS stabilized film the diffusion coefficients for the thin and thick films were similar from P/P$_0$=0.5-0.9. A significant difference was however noted for the diffusion coefficients of the DA3B stabilized film over the same water vapour partial pressure range.
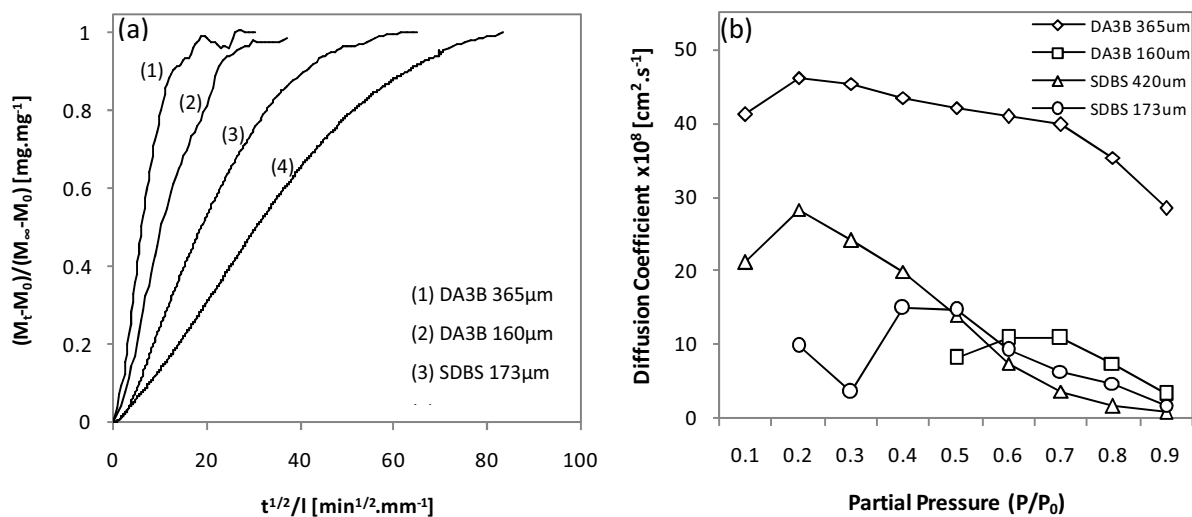
Figure 5.28: Kinetic sorption data at P/P$_0$=0.9 for p(Sty-co-BA) stabilized with DA3B or SDBS: (a) Reduced sorption curve; and (b) diffusion coefficients
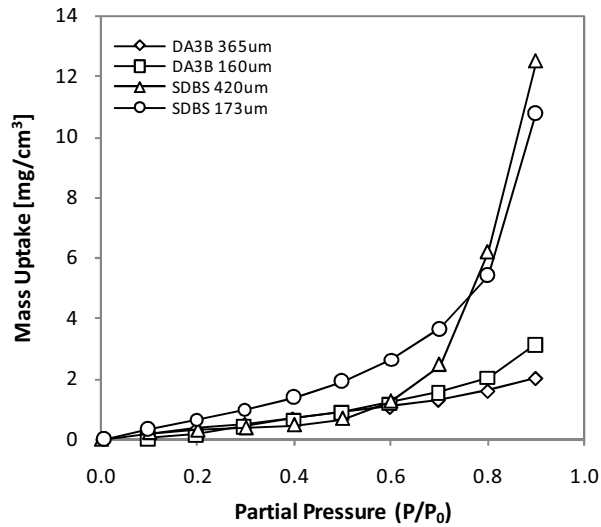
Figure 5.29: Mass Uptake of *p*(Sty-*co*-BA) films of different thicknesses, stabilized with SDBS or DA3B

The equilibrium sorption isotherm, expressed in terms of the mass uptake per cm^3 of film, for the DA3B stabilized film showed no significant difference between the thin film and the thick film over most of the water vapour partial pressure range evaluated (see Figure 5.29). This could be attributed to the absence of interaction between the water vapour molecules and the polymer matrix. It was only at P/P$_0$=0.8-0.9 that a difference was noted between the sorption behaviour of the two film thicknesses, where the thin DA3B stabilized film appeared to absorb more water vapour per cm^3 compared to the thick film. This significance of this variance in sorption capacity of the two thickness films was however not established in this study.

Different thermodynamic behaviour was seen for the thin and thick films of *p*(Sty-*co*-BA) stabilized with SDBS for water vapour partial pressures of 0.1-0.8 (see Figure 5.29), where the water vapour sorption capacity of the thicker film appeared to be lower than that of the thinner film. The reason for this phenomenon is not known. The overall trend of the isotherms followed in the Flory-Huggins model for both film thicknesses evaluated.

5.6 Conclusions

The type of surfactant used to stabilize latexes plays a critical role in determining the type of water vapour sorption behaviour of the resultant latex film. This is due to the mobility of conventional surfactants compared to reactive surfactants, with conventional surfactants resulting in surfactant exudation to the film-air and film-substrate interfaces, creating sites for water vapour clustering during diffusion through the latex film. During the sorption of water vapour into the film it was also

shown that conventional surfactants will have a tendency to diffuse with the water vapour back into the bulk of the film. Reactive surfactants, on the contrary, are distributed and immobilized throughout the bulk of the latex film, resulting in significantly different sorption behaviour of the latex film.

The choice of surfactant impacted on the water vapour sorption kinetics of p(Sty-co-BA) films. The time required to reach equilibrium for p(Sty-co-BA) latex films stabilized with SDBS or OPE (conventional surfactants) was significantly longer than for the same polymer stabilized with DA3B (a reactive surfactant). The high diffusion coefficients for the DA3B stabilized latex film could be attributed to the relative position of the reactive surfactant in the latex film, where the immobilization of the reactive surfactant in the bulk of the film resulted in a pathway for the water vapour through the polymer film. Exudation of the conventional surfactants to the film-air and film-substrate interfaces resulted in significantly lower diffusion coefficients due to surfactant-penetrant interactions as well as clustering of water vapour in the region where surfactant is present in high concentrations.

Typical Flory-Huggins sorption behaviour was observed for p(Sty-co-BA) latex films stabilized with the conventional surfactants. Both the anionic SDBS surfactant and the polymeric non-ionic OPE surfactant exhibited similar sorption behaviour despite the difference in molecular size and structure of the molecules. The DA3B stabilized latex film exhibited sorption behaviour typical of Henry's Law, where the sorption was only dependent on the water vapour partial pressure and no penetrant-polymer interactions took place. At water vapour partial pressures greater than 0.7 a slight deviation from Henry's Law was evident, in line with Dual Mode sorption behaviour. This could be attributed to the diffusion of two populations of water vapour molecules through the polymer matrix.

Despite the significant difference in the diffusion and solubility coefficients of p(Sty-co-BA) stabilized with conventional surfactants SDBS and OPE compared to the reactive surfactant DA3B, similar permeability coefficients were obtained across the water vapour partial pressure range investigated, with the exception of P/P_0=0.1.

The water vapour sorption behaviour of p(Sty-co-BA)/Na-MMT PCNs are discussed in the next chapter.

144

References

1.   Extrand, C.W., *A Thermodynamic Model for Contact Angle Hysteresis.* Journal of Colloid and Interface Science, 1998. **207**: p. 11-19.

2.   Extrand, C.W. and Kumagai, Y., *An Experimental Study of Contact Angle Hysteresis.* Journal of Colloid and Interface Science, 1997. **191**: p. 378-383.

3.   Heldmann, C., Cabrera, R.I., Momper, B., Kuropka, R., and Zimmerschied, K., *Influence of nonionic emulsifiers on the properties of vinyl acetate/VeoVa10 and vinyl acetate/ethylene emulsions and paints.* Progress in Organic Coatings, 1999. **35**(1-4): p. 69-77.

4.   Niu, B.-J. and Urban, M.W., *Recent Advances in Stratification and Film Formation of Latex Films; Attenuated Total Reflection and Step-Scan Photoacoustic FTIR Spectroscopic Studies.* Journal of Applied Polymer Science, 1998. **70**: p. 1321-1348.

5.   Tzitzinou, A., Jenneson, P.M., Clough, A.S., Keddie, J.L., Lu, J.R., Zhdan, P., Treacher, K.E., and Satguru, R., *Surfactant concentration and morphology at the surfaces of acrylic latex films.* Progress in Organic Coatings, 1999. **35**(1-4): p. 89-99.

6.   Zhao, Y. and Urban, M.W., *Phase Separation and Surfactant Stratification in Styrene/n-Butyl Acrylate Copolymer and Latex Blend Films. 17. A Spectroscopic Study.* Macromolecules, 2000. **33**: p. 2184-2191.

7.   Huang, J. and Urban, M.W., *Novel Approach to Quantitative Depth Profiling of Surfaces Using ATR/FT-IR Measurements.* Applied Spectroscopy, 1993. **47**(7): p. 973-981.

8.   Cole, K.C., Thomas, Y., Pellerin, E., Dumoulin, M.M., and Paroli, R.M., *New Approach to Quantitative Analysis of Two-Component Polymer Systems by Infrared Spectroscopy.* Applied Spectroscopy, 1996. **50**(6): p. 774-780.

9.   Kumar, A., Commereuc, S., Gonon, L., and Verney, V., *Depth-profile of photo-oxidation of polyoctenamer.* Polymer Degradation and Stability, 2002. **75**: p. 509-516.

10.   Chen, J. and Gardella Jr., J.A., *Quantitative ATR FT-IR Analysis of Surface Segregation of Polymer Blends of Polystyrene/Poly(dimethylsiloxane)-co-polystyrene.* Applied Spectroscopy, 1998. **52**(3).

11.   Shick, R.A., Koenig, J.L., and Ishida, H., *Depth Profiling of Stratified Layers Using Variable-Angle ATR.* Applied Spectroscopy, 1996. **50**(8): p. 1082-1088.

12.   Shick, R.A., Koenig, J.L., and Ishida, H., *Theoretical Development for Depth Profiling of Stratified Layers Using Variable-Angle ATR.* Applied Spectroscopy, 1993. **47**(8): p. 1237-1244.

13.   Keddie, J.L. and Routh, A.F., *Fundamentals of Latex Film Formation*. 2010, Dordrecht, The Netherlands: Springer.

14.   Pasto, D.J. and Johnson, C.R., *Organic Structure Determination*. 1969, New York: Prentice-Hall Inc.

15.   Pavia, D.L., Lampman, G.M., and Kriz, G.S., *Introduction to Spectroscopy: A Guide for students of organic chemistry*. Third ed. 2001: Brooks Cole Publishing Company.

16.   McMurry, J., *Organic Chemistry*. 3rd ed. 1992, Belmont: Wadsworth Inc.

17.   Schoonbrood, H.A.S., Unzué, M.J., Amalvy, J.I., and Asua, J.M., *Reactive Surfactants in Heterophase Polymerization. VIII. Emulsion Polymerization of Alkyl Sulfopropyl Maleate Polymerizable Surfactants (Surfmers) with Styrene.* Journal of Polymer Science Part A: Polymer Chemistry, 1997. **35**(13): p. 2561-.

18.   Fieldson, G.T. and Barbari, T.A., *The use of FTIR-ATR spectroscopy to characterize penetrant diffusion in polymers.* Polymer, 1993. **34**(6): p. 1146-1153.

19.   Hajatdoost, S., Sammon, C., and Yarwood, J., *FTIR-ATR studies of diffusion and perturbation of water in polyelectrolyte thin films. Part 4. Diffusion, perturbation and swelling processes for ionic solutions in SPEES/PES membranes.* Polymer, 2002. **43**: p. 1821-1827.

20.   Linossier, I., Gaillard, F., Romand, M., and Feller, J.F., *Measuring Water Diffusion in Polymer Films on the Substrate by Internal Reflection Fourier Transform Infrared Spectroscopy.* Journal of Applied Polymer Science, 1997. **66**(2465-2473).

21.   Fieldson, G.T. and Barbari, T.A., *The use of FTi.r.-a.t.r spectroscopy to characterize penetrant diffusion in polymers.* Polymer, 1993. **34**(6): p. 1146-1153.

22.   Mwesigwa, E., Basit, A.W., and Buckton, G., *Moisture Sorption and Permeability Characteristics of Polymer Films: Implications for Their Use as Barrier Coatings for Solid Dosage Forms Containing Hydrolyzable Drug Substances.* Journal of Pharmaceutical Sciences, 2008.

23.   Amalvy, J.I., Unzue, M.J., Schoonbrood, H.A.S., and Asua, J.M., *Reactive Surfactants in Heterophase Polymerization: Colloidal Properties, Film-Water Absorption, and Surfactant*

Exudation. Journal of Polymer Science Part A: Polymer Chemistry, 2002. **40**(17): p. 2994-3000.

CHAPTER 6

Impact of Na-MMT on water vapour sorption properties of polymer clay nanocomposites

Summary: *In this chapter the impact of plate-like clays (sodium montmorillonite, Na-MMT) and small hydrophilic molecules (2-acrylamido-2-methylpropanesulfonic acid, AMPS) on the water vapour sorption properties of* polystyrene-*co*-butyl acrylate (*p(Sty-co-BA))* is discussed. Na-MMT was modified with AMPS to facilitate compatibility between the hydrophilic clay and the hydrophobic polymer. The polymer clay nanocomposite (PCN) was prepared via in situ miniemulsion polymerization.*

Water and water vapour sorption properties of the resultant PCN films were evaluated in terms of their chemical and physical properties, with specific emphasis on the roles of Na-MMT and AMPS on these properties.

This study showed that the PCNs exhibited Sigmoidal kinetic behaviour towards the sorption of water vapour, irrespective of the Na-MMT or AMPS concentration. The equilibrium sorption isotherms showed elements of a dual sorption mode and this was attributed to the presence of Na-MMT in the polymer matrix, restricting the mobility of the polymer chains, thus simulating a polymer in its glassy state even above its T_g. As expected, the plate-like nature of the Na-MMT reduced the diffusion coefficient with increasing Na-MMT concentration, while the hydrophilic nature of the clay resulted in an increase in the solubility coefficient with increasing clay concentration.

6.1   Characterisation of *p*(Sty-*co*-BA) PCNs

Chapter 3 highlighted the theoretical aspects of the impact of various polymer properties, such as chemical composition, glass transition temperature, additive content, etc. on sorption behaviour of polymers towards specific types of penetrants. Accurate interpretation of the sorption behaviour of the PCNs investigated in this study therefore required a thorough understanding of their associated polymer properties. A variety of analytical techniques were employed including ^{1}H NMR spectroscopy to confirm the monomer composition, thermo gravimetrical analysis (TGA) to confirm the clay content, size exclusion chromatography to determine the molar mass of the polymers, small angle X-ray scattering (SAXS) and transmission electron microscopy (TEM) to verify the degree of exfoliation of the clay, Fourier transform infra-red photoacoustic spectroscopy (FTIR-PAS) to evaluate the relative concentration of the clay in the film and positron annihilation lifetime spectroscopy (PALS) to determine the free volume. (Refer to Chapter 4 for the methodologies of these analytical test methods).

6.1.1   Chemical and physical properties of PCNs

Chemical composition and **molar mass** determinations were not possible due to unsuccessful attempts to recover the polymer for ^{1}H NMR spectroscopy or size exclusion chromatography. The PCNs consist of two types of polymer chains, polymer chains bound to the Na-MMT as well as unbound polymer chains. The method proposed by Choi et al. for the recovery of these bound and unbound polymer components were evaluated for the recovery of the *p*(Sty-*co*-BA) polymer component. It was however not possible to extract the polymer using this method.[1] A possible reason for this is physical crosslinking of the PCN via a hydrogen bonding mechanism between the sulphate and amido groups of AMPS and the hydroxyl groups of the octahedral sheets of the clay, rendering it impossible to dissolve the polymer. Due to the relatively high conversions achieved for the synthesis of the PCNs (90-99% monomer incorporation), and the similar hydrophobicity of polystyrene and poly(n-butyl acrylate), it is assumed that, apart from the increasing AMPS concentration, the chemical compositions of the polymers studied here remained the same and would not lead to significant variation in water vapour sorption behaviour.

Although it was not possible to determine the molar mass and the degree of polymerisation in the PCNs, the following general findings from literature give an indication of what could be expected: The research of Greesh et al. indicated that the molar mass of polymers in PCNs prepared via a similar in situ polymerisation is dependent on the concentration of Na-MMT in the PCN.[2, 3] It was found that molar mass decreases with an increase in clay concentration as the clay particles hinder polymer chain growth.

Wang et al. also compared bulk, solution, suspension and emulsion polymerisation and melt blending techniques for the preparation of polystyrene/Na-MMT and poly(methyl methacrylate)/Na-MMT nanocomposites and found that there was a significant reduction in molar mass of the PCNs compared to the virgin polymers, with PCNs prepared using emulsion polymerisation showing the greatest reduction in molar mass (60-90% lower than the virgin polymer). This was attributed to the possibility of the clay acting as an additional micelle during the polymerisation process, thus increasing the number of micelles and consequently decreasing the molar mass of the resultant polymer.[4] The packing density of the clays is a further factor that could influence the degree of polymerisation. Exfoliated or delaminated clays result in the highest degrees of polymerisation.[5] Although SAXS and TEM analyses indicated that the degree of exfoliation was not the same for all polymers synthesized in this study, all the PCNs contained Na-MMT that was largely exfoliated. The degree of polymerisation of the different PCNs is therefore assumed to be comparable.

Clay loading in the PCNs was confirmed using TGA, by determining the % char remaining after decomposition of the PCN.[3, 6, 7] The results are given in Figure 6.1 (example of the obtained thermograms for the PCNs) and Table 6.1.
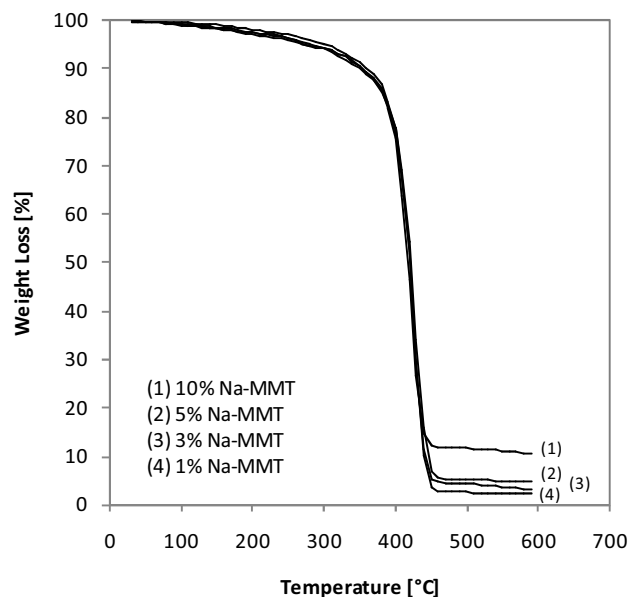
Figure 6.1: Thermograms of *p*(sty-*co*-BA) PCNs containing 4.5% AMPS and different Na-MMT concentrations

A comparison of the theoretical % Na-MMT to the % char after complete decomposition of the PCN at approximately 460 °C indicates that a good correlation exists between the actual amount of Na-MMT originally added during the PCN synthesis and the amount present in the stable emulsion from which the film was cast, confirming that the amount of Na-MMT originally added to the *in situ* polymerization was incorporated fully into the stable emulsion and therefore the PCN structure.

Table 6.1: Residual mass of PCNs as determined by TGA

AMPS [%]	Theoretical Na-MMT [%]	Char at 460°C after PCN decomposition [%]
4.5%	1%	2.310
4.5%	3%	3.142
4.5%	5%	4.614
4.5%	10%	10.60
1.5%	5%	5.586
3.0%	5%	5.220
4.5%	5%	4.614
6.0%	5%	4.953

Glass transition temperatures of the different *p*(Sty-*co*-BA)/Na-MMT PCNs were determined using DSC and the results are summarised in Table 6.2.

Table 6.2: Glass transition temperatures of *p*(Sty-*co*-BA)/Na-MMT PCNs

Na-MMT [%]	AMPS [%]	T_g [°C]
0	4.5	24.0
1	4.5	22.6
3	4.5	22.0
5	4.5	27.0
10	4.5	20.2
5	1.5	30.0
5	3.0	24.0
5	4.5	27.0
5	6.0	25.0

These results show no correlation between the amount of Na-MMT incorporated in the PCN and the T_g value measured. This is in contrast to findings from other researchers where it was shown that the PCN had a higher T_g compared to the virgin polymer and that increasing clay concentrations resulted in an increase in the T_g. This type of behaviour is largely attributed to the plate-like clays inhibiting the movement of polymer chains.[3, 8]

Free volume was determined for p(Sty-co-BA)/Na-MMT PCNs containing increasing amounts of Na-MMT. The experimental data was resolved into four lifetimes and the free volume results for τ_3 and τ_4 components are summarised in Table 6.3.

Table 6.3: Free volume of p(Sty-co-BA) PCNs containing 4.5% AMPS

Na-MMT	τ_3 component: crystalline and interfacial regions							
[%]	τ_3	$\Delta\tau_3$	I_3	ΔI_3	R	ΔR	ffv	Δffv
	[ns]	[ns]	[%]	[ns]	[Å]	[Å]	[%]	[%]
0%[1]	2.0000	0.0000	8	3	2.8554	0.0000	1.5	0.5
1%	2.0000	0.0000	7	2	2.8554	0.0000	1.3	0.3
3%	2.0000	0.0000	9	2	2.8554	0.0000	1.7	0.3
5%	2.0000	0.0000	14	1	2.8554	0.0000	2.4	0.2
10%	2.0000	0.0000	10	1	3.47923	0.0000	1.8	0.2
Na-MMT	τ_4 component: amorphous regions							
[%]	τ_4	$\Delta\tau_4$	I_4	ΔI_4	R	ΔR	ffv	Δffv
	[ns]	[ns]	[%]	[%]	[Å]	[Å]	[%]	[%]
0%[2]	2.50	0.08	17	3	3.28	0.05	4.6	1.0
1%	2.61	0.05	22	2	3.36	0.02	6.3	0.6
3%	2.68	0.05	19	2	3.41	0.03	5.7	0.6
5%	2.84	0.05	15.6	0.9	3.53	0.02	5.2	0.4
10%	2.77	0.04	19	1	3.48	0.02	6.1	0.5

Apart from a small increase in the hole concentration in the regions of complex morphology where Na-MMT is present, no trend was observed in terms of the hole size or concentration in the amorphous (τ_4) regions or the more complex morphological regions containing Na-MMT (τ_3).

---

[1] 0% Na-MMT and 1.5% AMPS

[2] 0% Na-MMT and 1.5% AMPS

6.1.2 Exfoliation of Na-MMT in *p*(Sty-*co*-BA) PCNs

p(Sty-*co*-BA) and a microcomposite of Na-MMT and *p*(Sty-*co*-BA), where Na-MMT was blended with the polymer latex after the polymer was synthesized, were compared to PCNs where polymerization of the styrene and *n*-butyl acrylate monomers took place in the presence of swollen, organically modified Na-MMT. The degree of exfoliation of Na-MMT was monitored quantitatively by SAXS and qualitatively by TEM measurements. The results are depicted in Figure 6.2 and Figure 6.3.
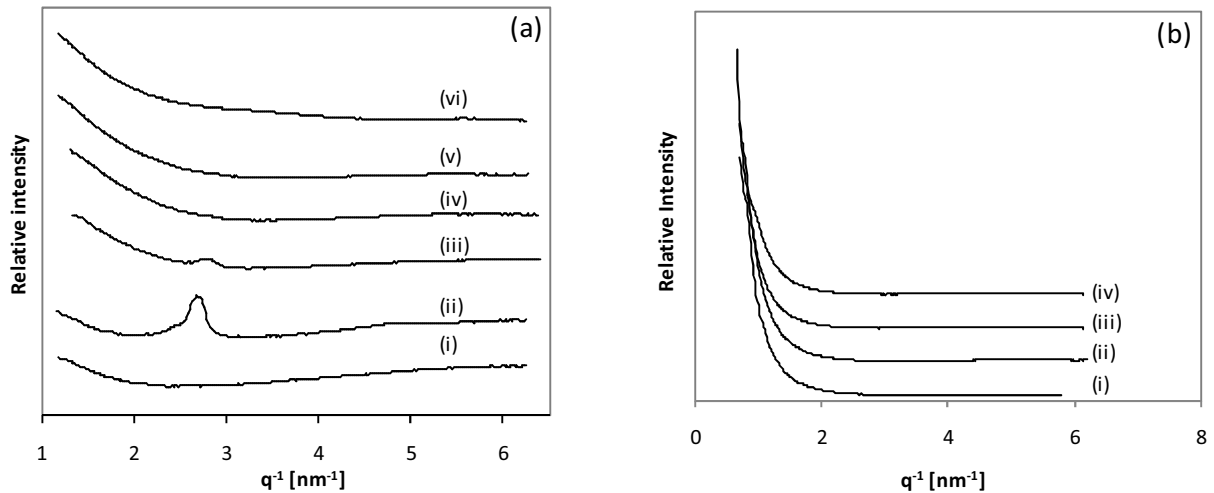
Figure 6.2: SAXS patterns of (a) *p*(Sty-*co*-BA) containing 4.5% AMPS and varying amounts of Na-MMT: (i) with 0% Na-MMT; (ii) microcomposite with 1% Na-MMT; (iii) PCN with 1% Na-MMT; (iv) PCN with 3% Na-MMT; (v) PCN with 5% Na-MMT; and (vi) PCN with 10% Na-MMT; and (b) *p*(Sty-*co*-BA) containing 5%Na-MMT and varying amounts of AMPS: (i) 1.5% AMPS, (ii) 3.0% AMPS, (iii) 4.5% AMPS and (iv) 6.0% AMPS

| (a) 1% Na-MMT | (b) 3% Na-MMT | (c) 5% Na-MMT | (d) 10% Na-MMT |
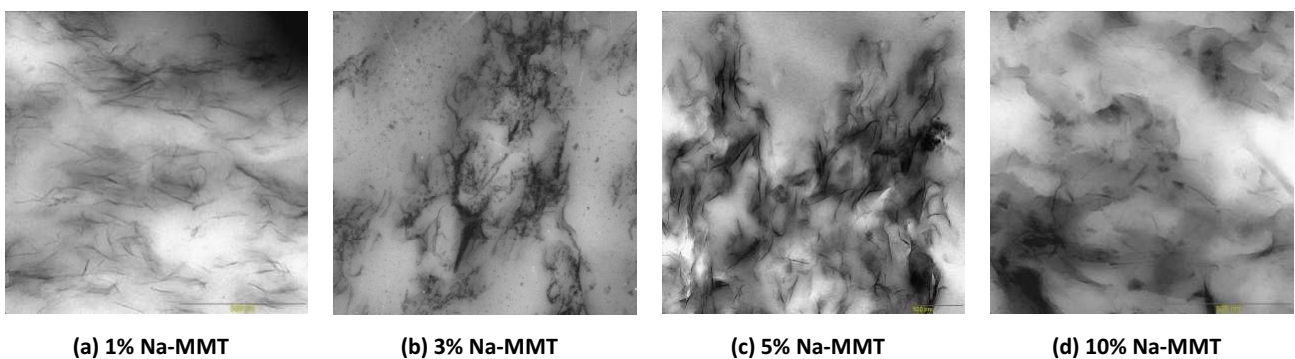
Figure 6.3: TEM images of styrene-co-butyl acrylate copolymers with 4.5% AMPS and varying Na-MMT content

153

A SAXS diffraction peak, representing an average interlamellar distance around 2.18 nm for Na-MMT in the microcomposite is evident. (Refer to Figure 6.2, plot (a)). As the interlamellar gallery thickness of Na-MMT is 0.79 nm, and that of hydrated Na-MMT is 1.45 nm, the interlamellar gallery spacing obtained for the microcomposite is indicative of an intercalative structure.[9] The interlamellar gallery thickness for the 1% Na-MMT PCN increased to 2.28 nm indicating a slight increase in the interlamellar gallery distance in comparison to that of the microcomposite. In situ polymerisation of organically modified Na-MMT therefore allowed for greater penetration of the polymer in between the clay sheets. A reduction in the relative intensity of the diffraction peak also indicates the presence of both intercalative and exfoliated clay structures. At 3% Na-MMT the PCN had an extremely small diffraction peak at 2.26 nm. The low intensity is indicative of a small amount of clay having an intercalative structure, with the bulk of the Na-MMT being exfoliated completely. No diffraction peak was visible for the PCNs containing 5% and 10% Na-MMT. It is therefore showing that complete exfoliation of the clay was achieved for these PCNs. This was unexpected as an increase in the amount of clay would suggest a reduction in the degree of exfoliation achieved. These results however correspond to the find of Greesh and co-workers.[2]

The variation in degree of exfoliation of the 1% Na-MMT PCN compared to the PCNs containing higher concentrations of Na-MMT was unexpected. Despite the same concentration of AMPS being used to modify the interlamellar gallery clay surface, different degrees of interaction between the clay and polymer may be observed, resulting in the different degrees of exfoliation. It is therefore evident that factors other than the ratio of organophilic modifier to clay should be considered when explaining the exfoliation of clay.

It was initially proposed that AMPS interaction with Na-MMT is based on a cation exchange mechanism.[8, 10] Greesh at al. however found that, due to the very low pKa value of the amido groups of AMPS, it is unlikely that the amido group would become protonated in water in neutral pH conditions. Their research found that AMPS may adsorb onto the edge of the Na-MMT platelets due to hydrogen bonding between the sulphate and amido groups of the AMPS molecules with the hydroxyl groups from the octahedral sheet of the clay.[11] It was also demonstrated that AMPS could adsorb onto the clay surface in the interlamellar gallery in one of two ways: (1) the formation of hydrogen bonds between the amido group of AMPS and the water molecules surrounding the exchangeable cation, and (2) the formation of ion-dipole interactions between the sulfonate and group of AMPS and the cation exchangeable groups.[11]

6.1.3 Distribution of Na-MMT in *p*(Sty-*co*-BA) PCNs

p(Sty-*co*-BA) containing 1.5% AMPS and 5% Na-MMT was used to demonstrate the relative position of Na-MMT throughout the PCN film. FTIR-PAS was used to analyze the sample at increasing depths of penetration into the sample. The presence of Na-MMT was monitored using the absorption band at 3638 cm^{-1} (refer to Appendix E). The spectra were normalized using the aromatic carbon-hydrogen stretching vibrations in the 3111-2805 cm^{-1} wavenumber region. The resultant spectra are shown in Figure 6.4.
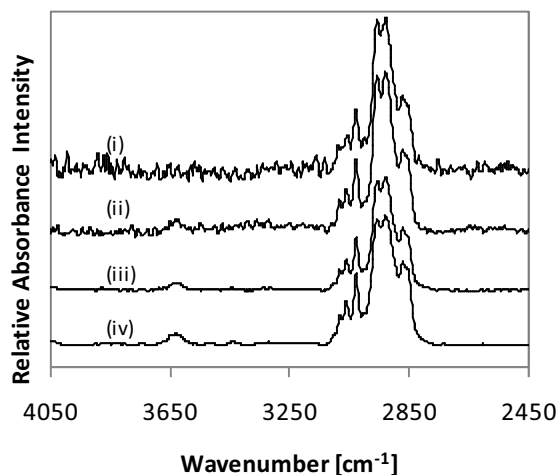
Figure 6.4: FTIR-PAS spectra of *p*(Sty-*co*-BA) polymer containing 1.5% AMPS and 5% Na-MMT at 4 depths of penetration: (i) 2.4 μm, (ii) 3.8 μm, (iii) 5.4 μm and (iv) 9.4 μm

From these results it is evident that the intensity of the hydroxyl stretching vibration at 3638 cm^{-1}, due to structural water in the Na-MMT, increases with increasing depth, indicating that the clay is embedded in the bulk of the polymer film. This is expected as the compatibilisation of Na-MMT with the organic monomers via AMPS would result in the immobilisation of the clay platelets within the latex particles, thus preventing it from migrating to the surface during film formation.[12] The high aspect ratio of the clays can be viewed as a secondary constraining factor, preventing migration to the film-air or film-substrate interface.

6.2 Liquid water sorption properties of PCNs

p(Sty-*co*-BA) PCN films containing 4.5% AMPS and increasing amounts of Na-MMT were immersed in water and their affinity for water determined at set time intervals. The results are depicted in Figure 6.5.

All films evaluated, except for the PCN containing 10% Na-MMT, exhibited Fickian behaviour where the sorption behaviour was characterised by fast uptake of water until equilibrium is reached. The kinetics for the PCN film containing 10% Na-MMT differed in that it appeared to follow the two-stage sorption kinetics rather than Fickian sorption kinetics, i.e. fast Fickian absorption followed by slower non-Fickian sorption before equilibrium is reached. This different kinetic behaviour could be attributed to the higher clay loading in the PCN, where the Na-MMT could act as sites for clustering of water, thus slowing down the diffusion of the water further into the film.
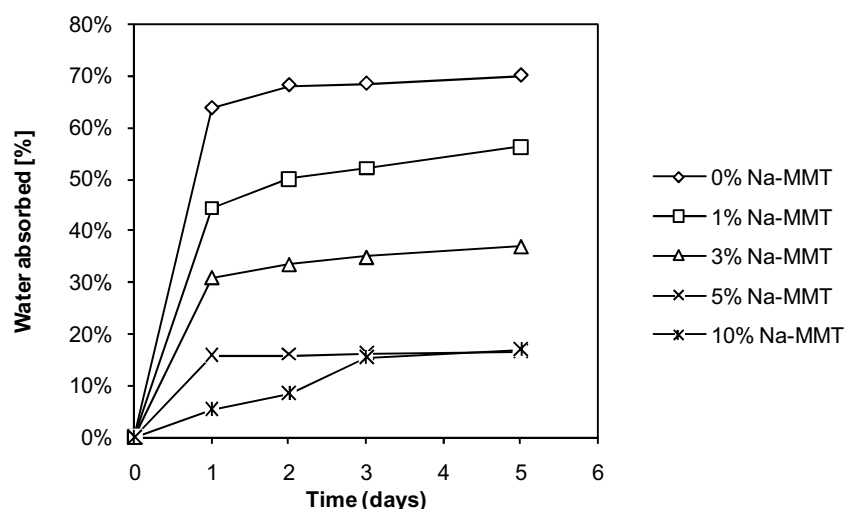
Figure 6.5: Water absorption of PCNs containing 4.5% AMPS and different concentrations of Na-MMT

6.3   Gravimetric determination of water vapour sorption properties of *p*(Sty-*co*-BA)/Na-MMT PCNs

This section focuses on the determination of water vapour sorption properties of two series of *p*(Sty-*co*-BA)/Na-MMT PCNs according to the gravimetric method described in Chapter 4: (i) *p*(Sty-*co*-BA)/Na-MMT PCNs containing 4.5% AMPS and increasing concentrations of Na-MMT; and (ii) *p*(Sty-*co*-BA)/Na-MMT PCNs containing 5% Na-MMT and increasing concentrations of AMPS. Films (size: 1.5 cm x 1.5 cm; thickness: ± 300 µm) were exposed to increasing water vapour partial pressures at 30 °C using the Intelligent Gravimetric Analyzer. The analyses were therefore performed above the T_g of the polymers. Table 6.4 summarises the T_g and film thickness values of the films prepared from the *p*(Sty-*co*-BA)/Na-MMT PCN latexes and has been repeated for the reader's convenience.

These *p*(Sty-*co*-BA)/Na-MMT PCNs were characterised in terms of their kinetic behaviour when exposed to increasing water vapour partial pressures. Their equilibrium mass sorption isotherms were also considered

to elucidate more on the potential penetrant and polymer interactions. The diffusion coefficient, solubility coefficient and permeability coefficient were determined for the different PCNs at increasing water vapour partial pressures and the trends obtained were analyzed. Lastly, the impact of temperature on the water vapour sorption properties of the *p*(Sty-*co*-BA)/Na-MMT nanocomposite containing 4.5% AMPS and 5% Na-MMT was determined, with sorption properties compared at 10 °C, 20 °C and 30 °C.

Table 6.4: *p*(Sty-*co*-BA) Na-MMT nanocomposite films used in this analysis

Sample Nr	% AMPS	% Na-MMT	T_g [°C]	Film thickness [µm]
1	4.5%	0%	24.0	260
2	4.5%	1%	22.6	170
3	4.5%	3%	22.0	400
4	4.5%	5%	27.0	350
5	4.5%	10%	20.2	300
6	1.5%	5%	30.0	260
7	3.0%	5%	24.0	360
8	4.5%	5%	27.0	350
9	6.0%	5%	25.0	350

6.3.1 Water vapour sorption kinetic behaviour of *p*(Sty-*co*-BA)/Na-MMT nanocomposites

The kinetic behaviour of the *p*(Sty-*co*-BA)/Na-MMT PCNs was evaluated over the water vapour partial pressure range from 0.1 to 0.9. This was done for both the PCN series with increasing Na-MMT content and the series with increasing AMPS concentration. Similar mass sorption curves were obtained for the two series. Typical examples of the mass sorption and reduced mass sorption curves are given in Figure 6.6. From these curves it is evident that, for increasing water vapour partial pressures, the PCNs evaluated absorbed increasing amounts of water vapour while the time required to reach equilibrium increased from approximately 100 minutes to 300 minutes.

The reduced mass sorption curves demonstrated typical Sigmoidal patterns, indicating initial slow water vapour uptake, followed by fast Fickian sorption. This could be attributed to the presence of SDBS surfactant at the film-air interface due to migration of these unbound compounds to the surface of the film during the initial film formation as discussed in more detail in Chapter 5.

The rate of diffusion of the water molecules into the PCN films varied as a function of partial pressure. This is illustrated in terms of the diffusion coefficients as determined by equation 4.11 using the software of the Intelligent Gravimetric Analyzer (see Figure 6.7). Similar trends were observed for the *p*(Sty-*co*-BA)/Na-

157

MMT PCNs of the two series evaluated. The diffusion coefficients for the p(Sty-co-BA)/Na-MMT PCNs containing lowest AMPS and Na-MMT concentrations increased with increasing water vapour partial pressure up to P/P_0=0.8, after which a sudden drop in the diffusion coefficient was seen. The reason for this is unclear. For the other AMPS and Na-MMT concentrations, the two series also showed great similarity with the diffusion coefficient increasing to an initial maximum value at P/P_0=0.2-0.3, followed by a drop in the diffusion coefficient to reach a minimum value at P/P_0=0.4-0.5. Thereafter a steady increase in the diffusion coefficient was observed, reaching a maximum value at P/P_0=0.9.
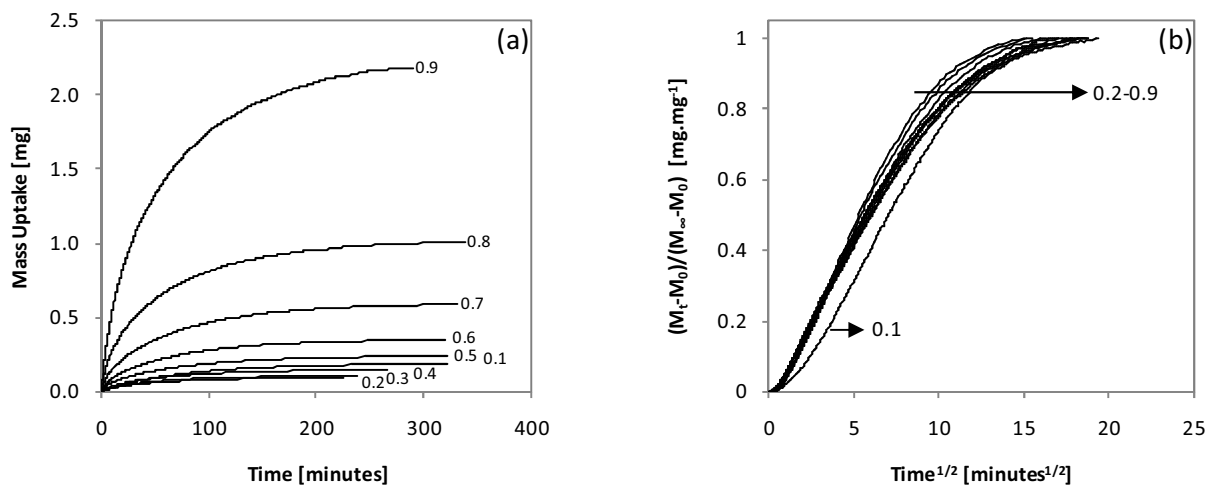
Figure 6.6: p(Sty-co-BA)/Na-MMT PCN containing 4.5% AMPS and 3% Na-MMT: (a) mass sorption curve; and (b) reduced mass sorption curve

These diffusion coefficient trends differ significantly from the trends observed for the random p(Sty-co-BA) polymer containing SDBS (refer to Figure 5.19, Chapter 5), where after an initial small increase in the diffusion coefficient from P/P_0=0.1-0.2, a steady decrease was observed in the diffusion coefficient. The absolute magnitude of the diffusion coefficient is also significantly lower for the PCNs compared to the random p(Sty-co-BA) polymer.
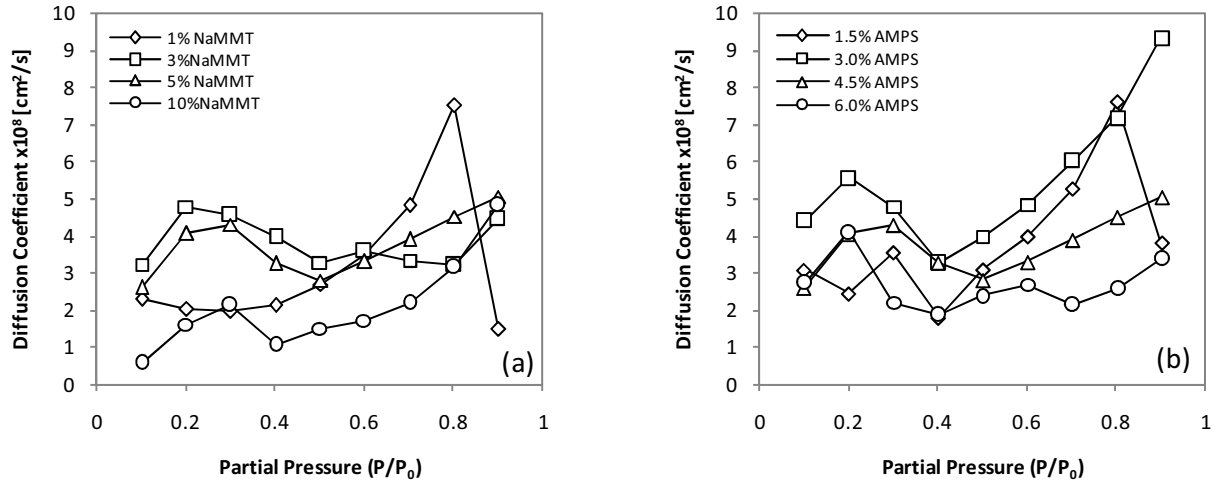
Figure 6.7: Diffusion coefficients for the adsorption of water vapour into *p*(Sty-*co*-BA)/Na-MMT PCNs: (a) the Na-MMT series with 4.5% AMPS and increasing Na-MMT conc., and (b) the AMPS series with 5% Na-MMT and increasing AMPS conc.

The following four factors should be considered to gain better understanding of the difference in diffusion behaviour: (1) the surface polarity of the PCN film; (2) the polarity of the bulk of the PCN film; (3) the tortuosity of the pathway through the PCN film; and (4) the relative mobility of the polymer chains in the PCN film. These factors are considered in terms of the additives of the PCNs that could potentially influence these properties. A summary of the relative impact of these factors is given in Table 6.5.

Table 6.5: Relative impact of PCN properties on diffusion of water vapour

Factors	Na-MMT	AMPS	SDBS	H_2O
Surface polarity of PCN film	-	-	+++	-
Polarity of bulk of PCN film	+++	+++	+	-
Tortuosity of pathway	+++	-	-	-
Chain mobility of polymer	++	-	-	+++

+++ significant impact; ++ moderate impact; + low impact; - no impact

Surface polarity of the PCN film: As was shown in Chapter 5, the presence of SDBS at the film-air interface will increase the surface polarity of the PCN film relative to the polarity of the bulk of the film. This could be the reason for the slight Sigmoidal kinetic behaviour seen with the reduced mass sorption curves.

Polarity of the bulk of the PCN film: Although the copolymer was synthesized using two hydrophobic monomers styrene and n-butyl acrylate, the presence of hydrophilic additives such as Na-MMT, AMPS and SDBS, would have a significant impact on the polarity of the bulk of the PCN film. It was shown in Figure 6.4,

159

using FTIR-PAS, that Na-MMT was immobilized in the bulk of the PCN film. Since AMPS adsorbed onto the Na-MMT surface via hydrogen bonding it can also be assumed that the AMPS is distributed throughout the polymer film. Due to the migration of SDBS to the film-air interface of the PCN film, the SDBS will however have a lesser effect on the polarity of the bulk of the PCN film. Na-MMT and AMPS will therefore significantly increase the polarity of the bulk of the PCN film compared to the polarity of the p(Sty-co-BA) polymer film where SDBS was the only polar additive.

Tortuosity of the pathway: 5% Na-MMT was used in the PCN series containing increasing amounts of AMPS. As complete exfoliation of the Na-MMT was confirmed using SAXS, the degree of tortuosity due to the presence of Na-MMT in the PCN films containing increasing amounts of AMPS, is assumed to be the same for all samples. The rate of diffusion of water vapour through these PCN films should therefore not be influenced by variations in the tortuosity of the pathway. The Na-MMT concentration and the degree of exfoliation of the Na-MMT however varied for the Na-MMT series. As a result, the tortuosity of the pathway for the water vapour molecules also varied. For P/P_0 = 0.1-0.6 the diffusion coefficient decreased for an increase in the Na-MMT concentration from 3% to 10%. This was expected given the increase in the tortuosity of the pathway. The diffusion coefficient for the PCN containing 1% Na-MMT did however not follow this trend. This deviation from the trend could be attributed to the combination of intercalated and exfoliated clay structures found in the PCN. Water vapour may exhibit a preference for the inter gallery space in the intercalated structures, resulting in a reduced diffusion coefficient compared to the diffusion coefficients for the completely exfoliated PCNs. As shown in previous studies, the orientation of plate-like clays to the sorption direction of the penetrant plays a key role in determining the tortuosity of the pathway and therefore the rate at which sorption of the penetrant would occur.[13] Although the orientation of Na-MMT in the p(Sty-co-BA) polymer matrix was not determined in the current study, it was assumed that this would remain constant as the same film preparation procedure was used throughout for the preparation of all the PCN films.

Chain mobility of the polymer: The mass sorption curves for the p(Sty-co-BA)/Na-MMT PCNs indicated that, for an increase in the water vapour partial pressure, there was an increase in the amount of water vapour absorbed. This increase in concentration of water vapour in the film could result in significant plasticization of the PCN film, reducing the T_g and increasing the polymer chain mobility significantly at a set temperature. At $P/P_0 > 0.5$ it is therefore suggested that, due to the relatively high concentration of water in the PCN film, there is a reduction in the T_g of the film, resulting in greater chain mobility and

therefore faster polymer relaxation during the migration of water vapour through the film. This would be reflected in an increase in the diffusion coefficient as seen in Figure 6.7. These findings correlate well with the findings of Sun and Lee where they studied the sorption properties of water vapour in poly(2-hydroxyethyl methacrylate) and found that for increasing water vapour content in the polymer matrix, there was an decrease in the T_g of the polymer.[14]

Based on the above, it can be concluded that the diffusion coefficient trends observed in Figure 6.7 compared to that seen in Chapter 5 for the SDBS stabilized *p*(Sty-*co*-BA) polymer, could be attributed to the significantly higher polarity of the bulk of the PCN film which resulted in significant absorption of water vapour and this consequently lead to plasticization of the PCN film.

6.3.2 Thermodynamic behaviour of *p*(Sty-*co*-BA)/Na-MMT nanocomposites

The equilibrium sorption isotherms of the *p*(Sty-*co*-BA)/Na-MMT PCNs containing increasing amounts of Na-MMT and AMPS are discussed in terms of the type of model that would be the most appropriate to predict the thermodynamic behaviour seen experimentally. Explanations are offered for the equilibrium sorption isotherm trends observed. The impact of the AMPS and Na-MMT concentrations on the solubility coefficients is also discussed.
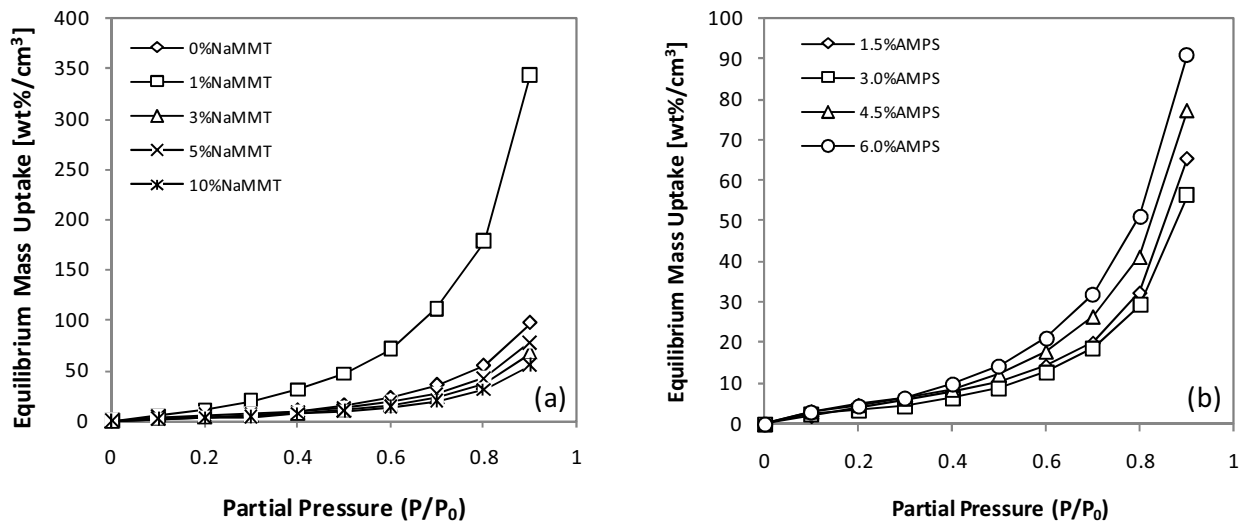
Figure 6.8: Equilibrium sorption isotherms of p(Sty-co-BA)/Na-MMT PCNs: (a) the Na-MMT series containing 4.5% AMPS and increasing concentrations of Na-MMT; and (b) the AMPS series containing 5% Na-MMT and increasing concentrations of AMPS

At first glance the equilibrium sorption isotherms of the *p*(Sty-*co*-BA)/Na-MMT PCNs appear to follow the Flory-Huggins model for hydrophobic polymers where penetrant-penetrant interactions are dominant (see Figure 6.8). Upon closer analysis of these isotherms, a small inflection point is however noted at low water vapour partial pressures, in line with typical BET (type II) behaviour, which is a combination of the Langmuir and Flory-Huggins sorption models. This type of behaviour is typical of a combination of penetrant-penetrant and penetrant-polymer interactions and could be attributed to the presence of Na-MMT, a hydrophilic plate-like clay, distributed in the hydrophobic *p*(Sty-*co*-BA) polymer matrix.

For the purpose of clarity, the assumptions regarding some of the theoretical models described in literature and used in this study, are briefly discussed here. A 2-parameter BET equation was developed to predict this type of sorption behaviour, based on two important assumptions:[15] (1) the number of adsorbed layers of penetrant is assumed to be infinite, and (2) the condensation-evaporation properties of the molecules in the second and higher layers are the same as that of the penetrant molecules in the liquid state. As the BET equation could only accurately describe sorption behaviour for a partial pressure range of 0-0.5, further refining of the model was required. Discarding the first assumption led to an increase in the partial pressure range (0-0.9) for which sorption behaviour could be accurately predicted and resulted in the following equation:

$$C = \frac{ac_p x}{(1-x)} \frac{1-(n+1)x^n+nx^{n+1}}{1+(c_p-1)x-c_p x^{n+1}}$$

(6.1)

C represents the amount of penetrant sorbed, a and c_p are parameters of the BET model, x is the penetrant partial pressure and n is the number of sorbed layers of penetrant.

Another model that could also be considered to explain the sorption behaviour of water vapour into the PCN films is the Dual Mode Sorption (DMS) model developed by Feng for sorption of vapours in glassy polymers, based on a multilayer sorption theory.[16] This model is given by equation 6.2 and is based on the following 4 assumptions: (1) two types of sorption sites exist in glassy polymers, the polymer matrix region and the microvoid region; (2) the penetrant molecules in the matrix region have the same partition functions; (3) the GAB model describes sorption in the microvoid region; and (4) penetrant molecules beyond the first adsorption layer have the same partition function as the penetrant molecules in the matrix region.

$$c = \overline{C}_p \frac{k\prime a}{1-k\prime a} + \overline{C}_p \frac{(A'-1)k\prime a}{1+(A'-1)k\prime a} \qquad\qquad (6.2)$$

Here c is the amount of water vapour sorbed at equilibrium, $\overline{C}_p$ is the weighted mean value of the sorption capacity of the PCN to water vapour, k' is the ratio of the partition function of molecules sorbed in the multilayer to that of molecules in the bulk liquid based on $\overline{C}_p$, A' is the ratio of the partition function of the first molecule sorbed on a site to that of molecules sorbed beyond the first molecules in the multilayer based on $\overline{C}_p$, and a is the water vapour partial pressure. The first term in the equation is also referred to as C1 and refers to sorption in the matrix region of the polymer, while the second term is referred to as C2 and represents sorption in the microvoid region.

Although the sorption analyses of the PCNs were done above their T$_g$, the DMS model was also considered here as the presence of plate-like clays in the polymer matrix could lead to microvoids and also restrict polymer chain mobility, therefore introducing elements of restricted polymer motion typically associated with polymers in their glassy state. To explain the observed sorption behaviour, 4 different models were evaluated using a regression fitting application for nonlinear functions: the BET 3-parameter model, the GAB model, the DMS model and the ENSIC model (an extension of the Flory-Huggins model). Of the models evaluated, the BET 3-parameter model and the DMS model gave the best fits and are therefore discussed further.

6.3.2.1 BET 3-parameter model

The BET 3-parameter model regression fit parameters are given in Table 6.6. The BET model fitted the experimental data of both the Na-MMT and the AMPS series very well, resulting in R^2 > 0.999. For the Na-MMT series specific trends were not identified in terms of the BET parameters relative to the Na-MMT concentration. It was however noted that, for 1% Na-MMT where the greatest amount of water vapour was absorbed, the a parameter was significantly higher than for the other Na-MMT concentrations. The parameters determined for the AMPS series showed definite trends relative to the AMPS concentration: a increased with increasing AMPS concentration, while c_p and n were inversely proportional to the AMPS concentration.

Table 6.6: BET 3-parameter model nonlinear regression fit parameters for *p*(Sty-*co*-BA)/Na-MMT PCNs

Na-MMT [%]	*a* Value	*a* Std Error	c_p Value	c_p Std Error	n Value	n Std Error	Statistics R²
0	13.3	0.4	1.5	0.2	24	1	0.9993
1	45	1	1.2	0.1	29	1	0.9997
3	8.7	0.2	1.9	0.2	26	1	0.9994
5	9.3	0.2	2.3	0.3	31	2	0.9993
10	7.00	0.07	2.2	0.1	27.6	0.6	0.9999
AMPS [%]	*a* Value	*a* Std Error	c_p Value	c_p Std Error	n Value	n Std Error	Statistics R²
1.5	6.95	0.04	3.1	0.1	51	3	0.9999
3.0	6.5	0.1	2.5	0.3	35	2	0.9996
4.5	9.3	0.2	2.3	0.3	31	2	0.9993
6.0	12.3	0.3	1.5	0.1	24.5	1.0	0.9996

6.3.2.2 DMS Model

The water vapour equilibrium mass uptake per cm³ was used for these calculations in order to compare the data from different films with different film thicknesses. The DMS model regression fit parameters for both the Na-MMT and the AMPS *p*(Sty-*co*-BA)/Na-MMT PCN series are given in Table 6.7. Despite the fact that the sorption behaviour for water vapour was determined in PCNs which were in their rubbery state while the model was originally developed for polymers in their glassy state, very good correlation was achieved between the experimental values and the values predicted by the DMS model, giving a $R^2 > 0.999$ for both the Na-MMT and AMPS series. Substituting the parameters c_p, k' and A' into equation 6.2, it was also possible to calculate the sorption in the rubbery (C1) and glassy (C2) components of the PCNs (See Figure 6.9 and Figure 6.10).

From the calculated DMS model parameters, and excluding the 0% Na-MMT data, it can be deduced that the sorption capacity (c_p) of the PCNs containing increasing Na-MMT concentrations for water vapour is inversely proportional to the Na-MMT concentration, i.e. the sorption capacity increases with a decrease in Na-MMT concentration. The opposite trend is observed for the PCNs containing increasing amounts of AMPS. These trends can be explained as follows: An increase in the Na-MMT concentration reduces the polymer volume component relative to the total PCN volume, therefore leaving a smaller volume of the polymer for the absorption of water vapour with increasing Na-MMT concentration. This will result in a reduction in the amount of water vapour sorbed for increasing Na-MMT concentrations. Contrary to this,

164

Stellenbosch University http://scholar.sun.ac.za

an increase in the AMPS concentration increases the polarity of the polymer volume, while the volume available to absorb the water vapour remains constant, resulting in an increase in water vapour with an increase in the AMPS concentration. For both series evaluated, the k' parameter was less than 1, with k' decreasing slightly with an increase in AMPS concentration, while remaining approximately constant with changing Na-MMT concentration. Contrary to this, A' increases within increasing Na-MMT concentration (except for 10% Na-MMT), while it decreases with increasing AMPS concentration. Feng showed that for $A' = 1$ the film is in its rubbery state, while $A' > 1$ was indicative of microvoid regions.[16] According to these regression fit results $A' \neq 1$, i.e. A' was either greater than 1 or less than 1 for all PCNs considered. The model proposed by Feng did not provide for A' values less than 1.

Table 6.7: DMS model fit parameters for *p*(Sty-*co*-BA)/Na-MMT PCNs

NaMMT	C_p		k'		A'		Statistics
[%]	Value	Std Error	Value	Std Error	Value	Std Error	R^2
0%	20	2	0.92	0.01	0.87	0.01	0.9995
1%	61	2	0.95	0.00	0.77	0.05	0.9999
3%	11	1	0.95	0.01	1.2	0.3	0.9989
5%	10.8	0.7	0.97	0.01	1.7	0.3	0.9991
10%	8.7	0.4	0.96	0.01	1.6	0.2	0.9996
AMPS	C_p		k'		A'		Statistics
[%]	Value	Std Error	Value	Std Error	Value	Std Error	R^2
1.5	7.1	0.1	1.00	0.00	3.0	0.2	0.9999
3.0	7.2	0.3	0.99	0.00	2.0	0.3	0.9994
4.5	10.8	0.7	0.97	0.01	1.7	0.3	0.9991
6.0	18	2	0.93	0.01	0.9	0.1	0.9995

For the Na-MMT series the amount of water vapour absorbed into the rubbery section of the polymer volume decreases with increasing Na-MMT concentration (see Figure 6.9(a)). This correlates with the trend seen for the water vapour sorption capacity of the polymer as predicted by the parameter c_p. Due to $A' < 1$ for the Na-MMT series of PCNs containing 0% Na-MMT and 1% Na-MMT, equation 6.2 predicted a negative amount of water vapour to be absorbed in the microvoid region, becoming more negative for increasing partial pressures (see Figure 6.9(b)). As it is not possible for a negative amount of water vapour to be absorbed in the microvoid region of the PCN, it can be deduced that the model proposed by Feng is unable to predict the sorption behaviour for these two PCNs. One or more of the assumptions for the DMS model is therefore not met.
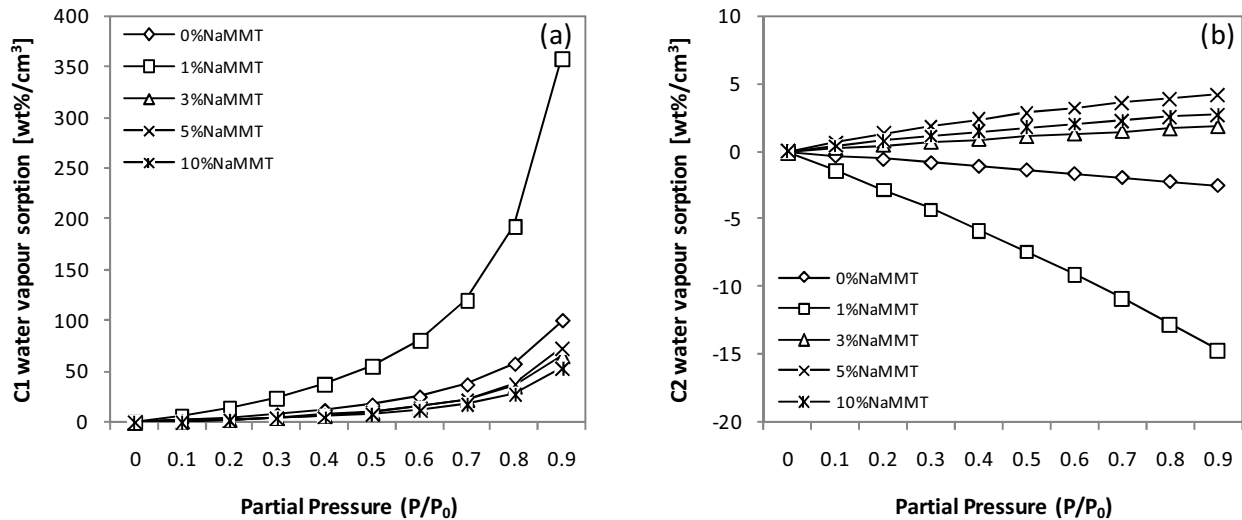
Figure 6.9: Water vapour sorption curves for *p*(Sty-*co*-BA)/Na-MMT PCNs containing 4.5% AMPS and increasing Na-MMT concentrations based on the DMS model: (a) C1 component for equilibrium sorption in the matrix region; and (b) C2 component for equilibrium sorption in the microvoid region

Water vapour was predominantly absorbed in the rubbery region of the PCNs from the AMPS series, with the amount of water vapour absorbed increasing with increasing concentration of AMPS (see Figure 6.10(a)). Water vapour sorption in the glassy or microvoid regions represented by the polymer region in close proximity to the plate-like Na-MMT clays where the mobility of the polymer chains may be restricted, was significantly lower, contributing less than 5% of the total amount of water absorbed by the PCN (see Figure 6.10(b)). The C2 component of equation 6.2 representing sorption of the penetrant in the microvoid region, was negative for the 6% AMPS PCN, suggesting that, for this PCN, one or more of the four assumptions for the DMS model have not been met. As the Na-MMT concentration and degree of exfoliation were the same for all PCN films from the AMPS series, it is assumed that the microvoid region would be comparable for these films. Although the reason for the failure of the DMS model for the 6% AMPS PCN was not considered further, the consistent nature of the Na-MMT in the PCN films containing different AMPS concentrations suggest that the failure was not due to a variation in the types of sorption sites available in the PCN. Variances in the partition function for water vapour may be a more probable cause for failure of the DMS model to predict the sorption behaviour.
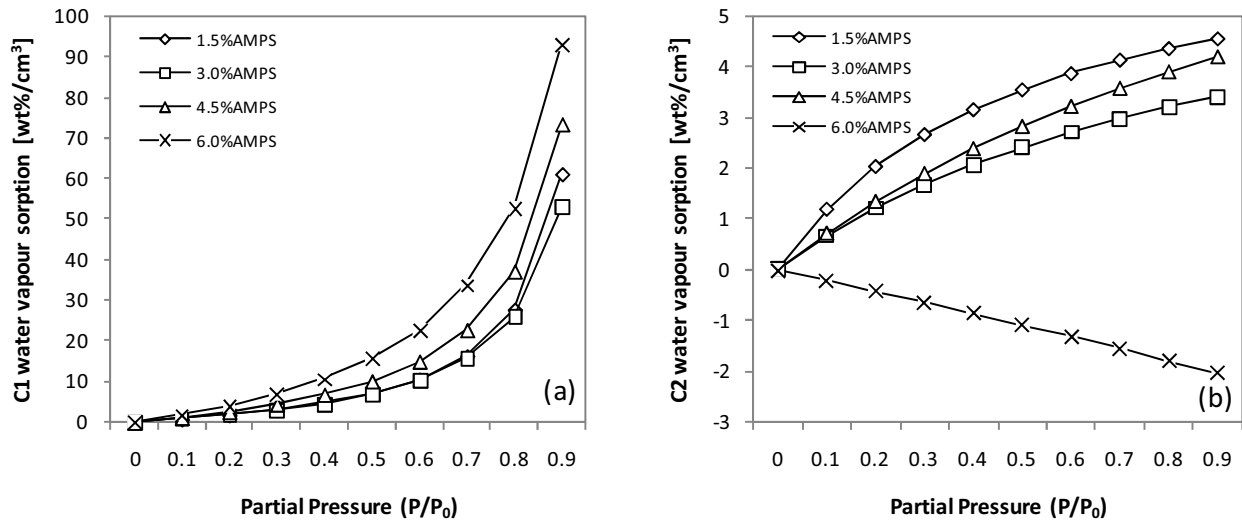
Figure 6.10: Water vapour sorption curves for p(Sty-co-BA)/Na-MMT PCNs containing 5% Na-MMT and increasing AMPS concentrations based on the DMS model: (a) C1 component for equilibrium sorption in the matrix region; and (b) C2 component for equilibrium sorption in the microvoid region

6.3.2.3 Impact of Na-MMT and AMPS on the sorption behaviour

The equilibrium mass sorption isotherms indicated that, apart from the 1% Na-MMT PCN, the relative mass uptake for the Na-MMT PCN series per specific volume of PCN film was similar to that observed for the AMPS series, (see Figure 6.8).

When measured as a function of % Na-MMT, the equilibrium mass uptake for the Na-MMT PCN series suggests that a maximum amount of water vapour is absorbed for the 4.5% AMPS and 1% Na-MMT *p*(Sty-*co*-BA)/Na-MMT PCN, after which it decreases to achieve a minimum amount of water vapour sorbed for the *p*(Sty-*co*-BA)/Na-MMT PCN containing 4.5% AMPS and 10% Na-MMT. This trend is visible at all partial pressures from 0.1 to 0.9 (refer to Figure 6.11(a)). As the clay component of a PCN is viewed as being impermeable, it is generally accepted that the polymer component of the PCN determines the degree of solubility of the penetrant into the PCN matrix.[13] For a constant PCN film volume and constant polymer polarity, the amount of penetrant absorbed by the PCN should therefore decrease with an increase in the clay component as the relative volume of the polymer component in the PCN is reduced. To gain a better understanding of the reason for the maximum water vapour absorption seen for the PCN containing 1% Na-MMT (refer to Figure 6.11(a)), the amounts of water vapour sorbed relative to the available polymer volume were expressed as a function of Na-MMT concentration (see Figure 6.12). Contrary to what was

167

expected, the 1% Na-MMT PCN which had the smallest polymer volume component absorbed the most water vapour, thus indicating that other factors apart from the polymer volume must be contributing to the sorption phenomenon seen for the PCN series.
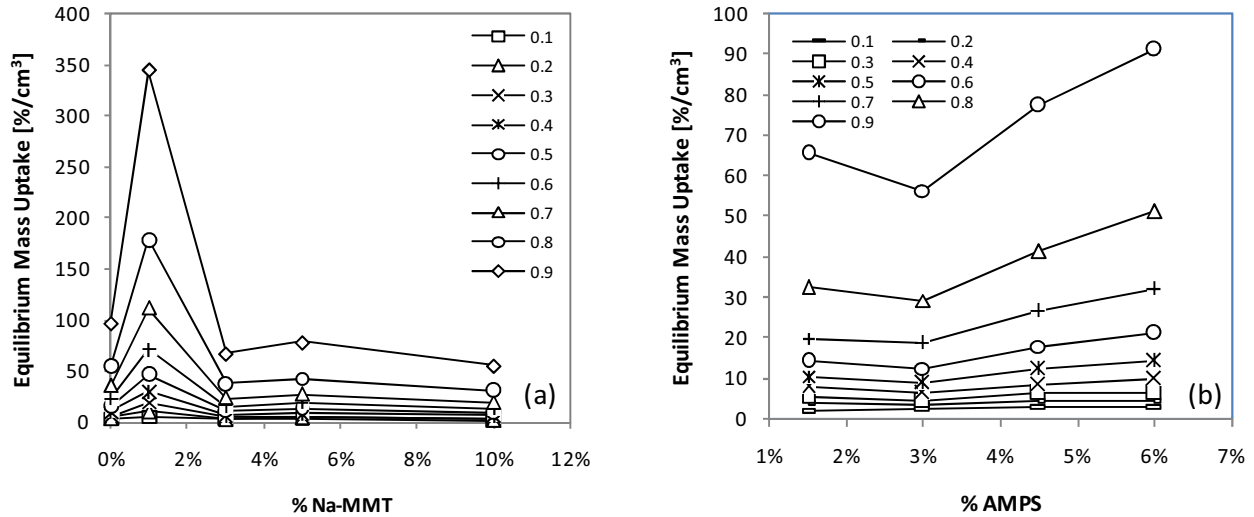
Figure 6.11: Equilibrium mass sorption uptake (corrected for variation in film thickness) of *p*(Sty-*co*-BA)/Na-MMT PCNs as a function of: (a) the Na-MMT series; and (b) the AMPS series

Comparing the degree of exfoliation of the Na-MMT in the PCNs with the amount of water vapour absorbed by the PCNs, it was found that PCNs containing partially exfoliated Na-MMT resulted in the absorption of more water vapour than PCNs with completely exfoliated Na-MMT (see Figure 6.2 and Figure 6.12). The 1% Na-MMT PCN, where only partial exfoliation was achieved, has a combination of intercalated and exfoliated clay platelets. The intercalated structures contain water molecules that are associated with the exchangeable cation in the inter gallery space. These water molecules create regions for potentially strong association with water vapour penetrant molecules through penetrant-Na-MMT and penetrant-penetrant interactions. In the PCNs containing completely exfoliated Na-MMT, these hydrophilic sites are not available to water vapour penetrant molecules, resulting in a reduction of the overall bulk polarity of the PCN and therefore its ability to absorb water vapour.
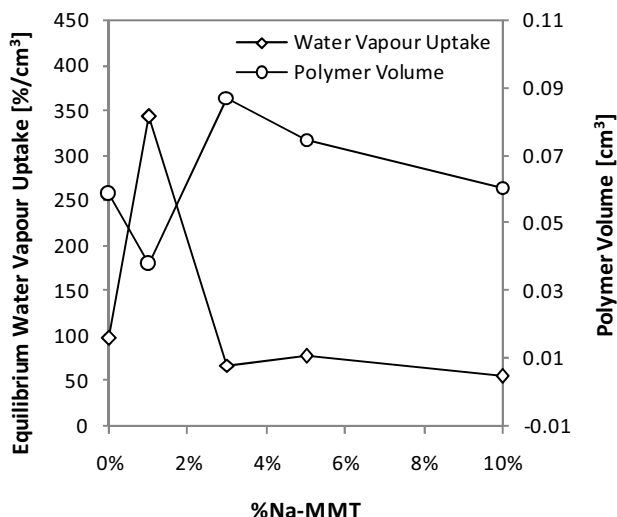
Figure 6.12: Equilibrium water vapour sorption of PCNs containing increasing Na-MMT concentrations, relative to its polymer volume, as a function of Na-MMT concentration

An increase in the equilibrium water vapour concentration is observed for increasing AMPS concentration with a constant Na-MMT concentration (see Figure 6.8(b) and Figure 6.11(b)). This could be attributed to a relative increase in the polarity of the polymer component of the PCN due to increased concentrations of AMPS.

6.3.2.4 *Solubility coefficients for the AMPS and Na-MMT series*

The solubility coefficients for *p*(Sty-*co*-BA)/Na-MMT PCNs containing increasing amounts of Na-MMT and AMPS are shown in Figure 6.13(a) and (b) respectively. The variation in the solubility coefficient across the water vapour partial pressure range 0.1-0.9 is similar for the two series evaluated, characterised by an initial decrease in the solubility coefficient from P/P_0=0.1-0.2, followed by a slow increase up to P/P_0=0.8 and finally a sharp increase from P/P_0=0.8-0.9. This trend is as a result of the Flory-Huggins type isotherm that characterises the equilibrium water vapour sorption behaviour for these two series of PCNs.

The absolute value of the solubility coefficients for the two series of PCNs evaluated is also comparable, except for the solubility coefficients of the *p*(Sty-*co*-BA)/Na-MMT PCN containing 1% Na-MMT and 4.5% AMPS (see Figure 6.13(a)) which is higher than the other solubility coefficients across the entire water vapour partial pressure range evaluated. This deviation was expected given the significantly higher water sorption capacity due to the presence of intercalated Na-MMT in the PCN.

169
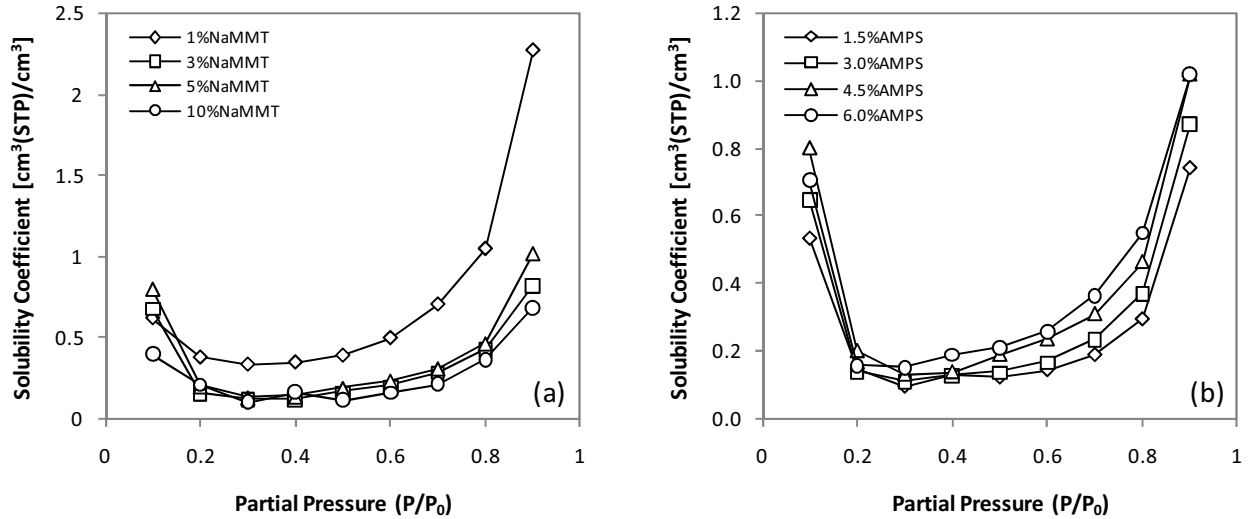
Figure 6.13: Solubility coefficients versus partial pressure: (a) S for increasing Na-MMT concentration; and (b) S for increasing AMPS concentration

6.3.3 Temperature dependence of the sorption mechanism

6.3.3.1 Kinetic behaviour

The impact of temperature on the sorption behaviour of *p*(Sty-*co*-BA)/Na-MMT PCN containing 4.5% AMPS and 5% Na-MMT, with a T_g of 27 °C, were investigated. Sorption isotherms were recorded at 10 °C, 20 °C and 30 °C, and across a partial pressure range from 0.1 to 0.9 at 0.1 increments. For illustrative purposes the mass sorption curve and reduced mass sorption curves at P/P_0 are given in Figure 6.14 and Figure 6.15, and the permeability coefficient, diffusion coefficient and solubility coefficient for P/P_0=0.5 are summarised in Table 6.8 (Also refer to Appendix K for detailed results). From these results it is evident that, for increasing temperatures, the amount of water vapour absorbed by the PCN increases, while the time required for equilibrium decreases (see Figure 6.14). These phenomena can be attributed to a higher water vapour pressure at increasing temperatures for the same partial pressure, resulting in more water vapour being available for absorption, while the increase in the rate of diffusion is as a result of higher polymer chain mobility at increased temperatures.
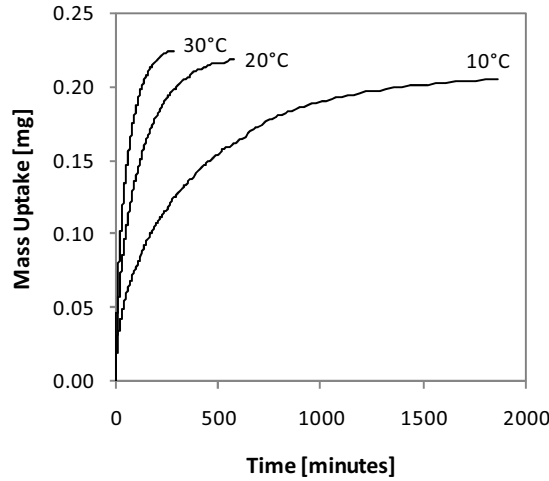
Figure 6.14: Mass sorption curve at P/P$_0$=0.5: Comparison of 10 °C, 20 °C and 30 °C kinetic curves

Sigmoidal kinetic behaviour was noted for sorption of water vapour by the *p*(Sty-*co*-BA)/Na-MMT nanocomposite at all temperatures investigated (refer to Figure 6.15). This slower surface equilibrium phenomenon was only observed at very short times, i.e. at the start of the kinetic curve, after which the kinetics for the absorption of water vapour followed Fickian behaviour. The reason for this kinetic behaviour was not investigated in greater detail here.
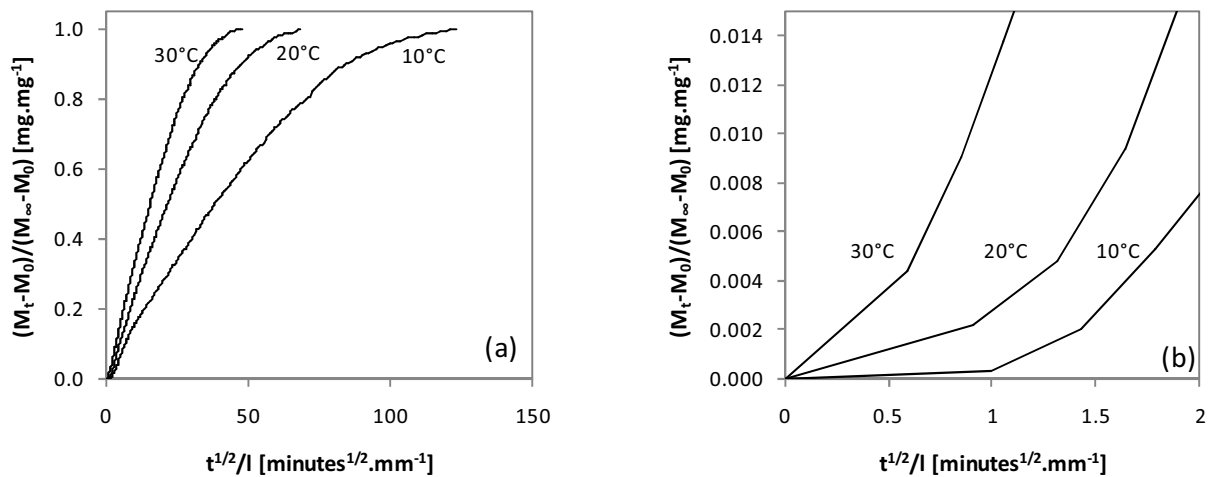
Figure 6.15: Reduced sorption curve of *p*(Sty-*co*-BA) PCN at 10 °C, 20 °C and 30 °C for P/P$_0$=0.5: (a) the entire reduced sorption curve; and (b) the reduced sorption curve at short times only highlighting the Sigmoidal behaviour

171

Based on the Arrhenius equation, it can be expected that the diffusion coefficient increases with an increase in temperature as the free volume in the polymer matrix increases with an increase in temperature due to greater mobility of the polymer chains. The solubility coefficient, on the other hand, should decrease with an increase in temperature for water vapour as the heat of solution is negative and is governed by the molar heat of condensation of water vapour. These trends are evident for the diffusion and solubility coefficients observed here (see Table 6.8 and Section 3.2 where the Arrhenius equations are discussed). The permeability coefficient, which is the product of the diffusion and solubility coefficients, increases with an increase in temperature.

Table 6.8: Diffusion, solubility and permeability coefficients at $P/P_0=0.5$

Temp. [°C]	Pressure [mbar]	Equilibrium water vapour mass uptake [%]	$D \times 10^8$ [cm^2/s]	S [$cm^3(STP)/cm^3 mbar$]	$P \times 10^9$ [$cm^3(STP)cm/cm^2 s$, mbar]
10°C	11.090	0.87	0.427	0.55	2.35
20°C	21.107	0.97	1.43	0.31	4.45
30°C	38.270	1.05	2.82	0.19	5.38

D: diffusion coefficient; S: solubility coefficient; P: permeability coefficient

6.3.3.2 Thermodynamic behaviour

An increase in the equilibrium mass uptake of the PCNs was observed for increasing temperatures from 10 °C to 30 °C (refer to Figure 6.16). For example, at $P/P_0=0.5$ the increase in mass due to the absorption of water vapour was 0.87% at 10 °C, 0.97% at 20 °C and 1.05% at 30 °C. This is due to an increase in the molar heat of condensation of water vapour as a function of temperature. Although one would expect that an increase in the equilibrium water vapour mass uptake would result in an increase in the solubility coefficient, the opposite was observed here. This phenomenon can be explained in terms of the relatively low increase in water vapour mass uptake compared to the increase in water vapour pressure at the three temperatures investigated here. As the solubility coefficient is calculated as the ratio of the penetrant concentration in the polymer film to the penetrant vapour pressure surrounding the polymer film, this would result in a reduction in the solubility coefficient (refer to equation 4.13 and Table 6.8).

At lower temperatures the isotherms showed a hysteresis effect. This was the most prominent for the 10 °C isotherm and can be seen as the difference in the % increase in sample mass from the original dry sample for the adsorption and desorption curves, at a specific partial pressure and temperature. This phenomenon can be attributed to strong interaction between water vapour molecules trapped in voids in the polymer

172

matrix due to the presence of hydrophilic Na-MMT. Minimal hysteresis was observed for the 30 °C isotherm. As the isotherm temperature was above the T_g of the polymer (T_g=27 °C), the polymer chains were able to rearrange faster than the rate of diffusion of the water vapour molecules, thus facilitating the release of water vapour molecules from free volume cavities in the polymer matrix. At isotherm temperatures below the T_g of the polymer, the water molecules could remain trapped in the voids in the polymer matrix, as much higher activation energies would be required to assist the water vapour molecules to jump from one free volume hole to another.
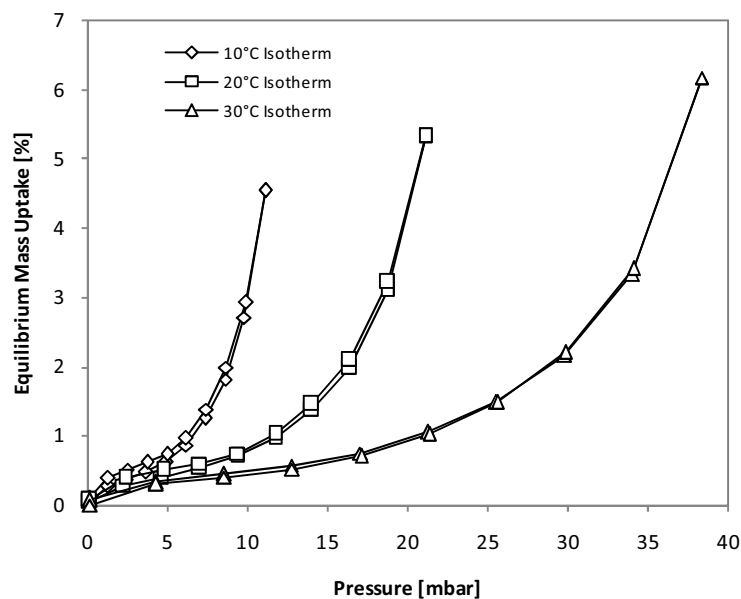
Figure 6.16: Isotherms at different temperatures for *p*(Sty-*co*-BA) PCN containing 5% Na-MMT and 4.5% AMPS

6.3.3.3 Modelling of water vapour sorption in PCNs

Similar to previous classification of the equilibrium sorption isotherms of *p*(Sty-*co*-BA)/Na-MMT PCNs from this study, the equilibrium water vapour isotherms at the three temperatures exhibit typical BET (type II) behaviour, which is a combination of the Langmuir and Flory-Huggins sorption models (Refer to Figure 6.16 and Appendix K). This type of behaviour is typical of hydrophilic polymers and could be attributed to the presence of Na-MMT, a hydrophilic plate-like clay, distributed in the hydrophobic *p*(Sty-*co*-BA) polymer matrix. To explain the observed sorption behaviour, 4 different models were evaluated using a regression fitting application for nonlinear functions: the BET 3-parameter model, the GAB model, the DMS model and the ENSIC model. Of the models evaluated, the BET 3-parameter model and the DMS model gave the best fit and are therefore discussed further.

173

BET 3-Parameter model

The sorption parameters for the BET model are summarised in Table 6.9. The 3-parameter BET model gave a very good prediction based on the experimental data, with $R^2 \approx 0.999$. According to the parameters obtained, the number of layers of sorbed water vapour increases with an increase in temperature. This correlates with the increase in equilibrium water vapour mass uptake for a specific water vapour partial pressure, with increasing temperature. a increased slightly with increasing temperature, while the variation in c_p could not be correlated to a change in temperature.

Table 6.9: Influence of temperature on water sorption parameters for the BET 3-parameter model

Temp [°C]	a		c_p		n		Statistics
	Value	Std Error	Value	Std Error	Value	Std Error	R^2
10	0.60	0.02	3.1	0.6	23	1	0.9986
20	0.68	0.02	3.0	0.5	26	1	0.9990
30	0.72	0.02	3.3	0.6	32	3	0.9987

Dual Mode Sorption model

The water vapour sorption isotherms were also evaluated in terms of equation 6.2 and the 3 parameters (C_p, k' and A') determined. The parameters obtained are summarised in Table 6.10 and sorption in the matrix and microvoid regions of the polymer are depicted in Figure 6.17. Based on the R^2 value it can be said that the experimental data fit the DMS model very well.

Figure 6.17 indicated that for increasing temperatures water vapour sorption via the polymer matrix (component C1 of equation 6.2) increased, while water vapour sorption via microvoids in the polymer (component C2 of equation 6.2) decreased. This correlated well with an increase in the relative mobility of the polymer chains as a result of an increase in the experimental temperature relative to the T_g of the polymer.

Feng showed that for A'=1 the sorption behaviour is typical of a polymer in its rubbery state.[16] The results obtained in this case indicated that the sorption behaviour was typical of a polymer in its glassy state at all three temperatures evaluated, even though the measured T_g of the polymer was 27 °C, suggesting that the polymer should be in its rubbery state for the isotherm at 30 °C. Figure 6.20(b) also confirmed that at 30 °C component C2 (representing sorption in the microvoid region resulting from the

174

glassy nature of the polymer) still contributed approximately 0.1 wt% of the total amount of water vapour sorbed at P/P_0=0.9. This behaviour could be attributed to the presence of Na-MMT in the polymer, resulting in restricted movement of the polymer chains, thus simulating behaviour of glassy polymers.
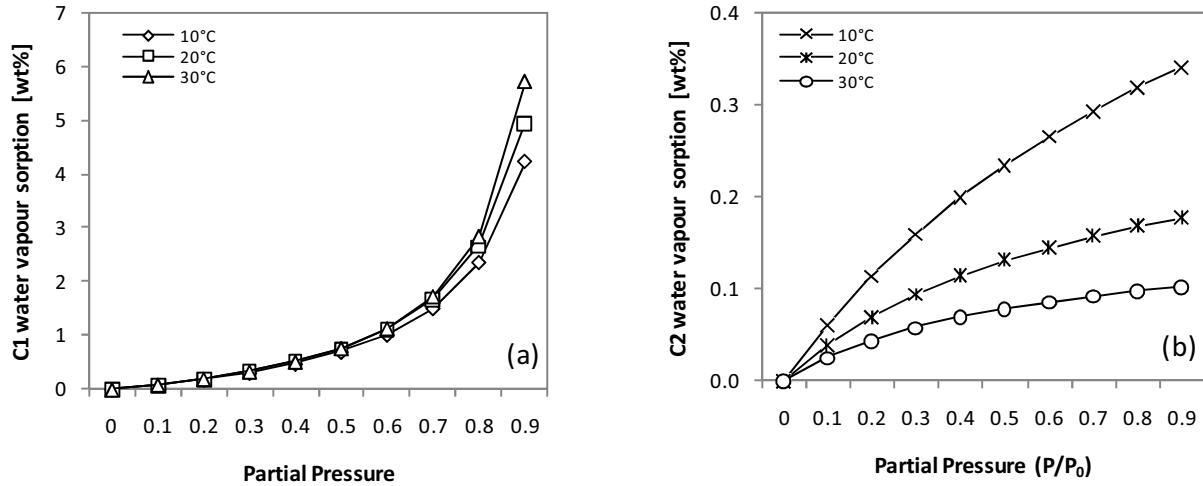
Figure 6.17: Water vapour sorption curves of glassy polymers: (a) C1 component for the matrix region; and (b) C2 component for the microvoid region

Feng found that larger k' values predicted greater interaction between the penetrant and the polymer.[16] The k' parameter determined for the isotherms in this study indicated a slight increase in the penetrant-polymer interactions relative to the penetrant-penetrant interactions with an increase in temperature. This may be as a result of greater polymer chain mobility allowing the water vapour molecules to migrate to the polar interfaces on the NaMMT clay surface thus facilitating penetrant-polymer interactions. At lower temperatures the restricted mobility of polymer chains would result in clustering of water vapour molecules, thus increasing the penetrant-penetrant interaction.

Table 6.10: Parameters determined using the DMS model

Temp	C_p		k'		A'		Statistics
[°C]	Value	Std Error	Value	Std Error	Value	Std Error	R^2
10	0.79	0.09	0.94	0.01	1.9	0.5	0.9978
20	0.84	0.08	0.95	0.01	2.0	0.5	0.9979
30	0.81	0.05	0.97	0.01	2.6	0.6	0.9983

175

6.4   Conclusions

The *p*(Sty-*co*-BA)/Na-MMT PCNs containing different Na-MMT and AMPS concentrations used in this study exhibited similar kinetic trends for the sorption of water vapour, absorbing increasing amounts of water vapour at increasing partial pressures, while requiring longer periods of time to reach equilibrium at these higher water vapour partial pressures. The diffusion coefficients for these PCNs are very different to the diffusions coefficients determined for *p*(Sty-*co*-BA) stabilized with SDBS. It was suggested that the significant increase in the polarity of the bulk of the PCN due to the presence of Na-MMT attributed to significantly higher concentrations of water vapour being absorbed, resulting in plasticization of the PCN films and therefore an increase in the diffusion coefficients.

It was shown that partially exfoliated Na-MMT in *p*(Sty-*co*-BA)/Na-MMT PCNs resulted in significantly higher equilibrium water vapour uptake compared to the same PCNs containing completely exfoliated Na-MMT. The increase in the amount of absorbed water was attributed to the inter gallery space in the intercalated clay structures that promoted clustering of water.

Despite being in its rubbery state, it was possible to predict the water vapour sorption behaviour of the *p*(Sty-*co*-BA)/Na-MMT PCNs using sorption models such as the 3-parameter BET model and the DMS model even though these models have been developed specifically to predict sorption behaviour in glassy polymers. This was deemed possible due to the presence of Na-MMT in the polymer matrix which may result in restricted movement of the polymer chains and therefore regions of varying polymer mobility in the PCN volume that would result in differential penetrant mobility in the polymer matrix.

It was lastly shown that the temperature at which the sorption evaluation is done is critical in determining the kinetic and thermodynamic behaviour of the PCN film. As predicted by the Arrhenius equations, an increase in temperature resulted in an increase in the diffusion coefficient and a decrease in the solubility coefficient. For $P/P_0=0.5$ this translated in a reduction in the permeability coefficient with an increase in temperature despite the relatively high polarity of these PCNs.

The water vapour sorption behaviour of p(MMA-co-ODA) are discussed in the next chapter.

References

1.   Choi, Y.S., Choi, M.H., Wang, K.H., Kim, S.O., Kim, Y.K., Chung, I.J., *Synthesis of Exfoliated PMMA/Na-MMT Nanocomposites via Soap-Free Emulsion Polymerization.* Macromolecules, 2001. **34**: p. 8978-8985.

2.   Greesh, N., Hartmann, P.C., Cloete, V., and Sanderson, R.D., *Impact of the Clay Organic Modifier on the Morphology of Polymer–Clay Nanocomposites Prepared by In Situ Free-Radical Polymerization in Emulsion.* Journal of Polymer Science Part A: Polymer Chemistry, 2008. **46**(11): p. 3619-3628.

3.   Greesh, N., *Preparation of polymer-clay nanocomposites using emulsion polymerisation: Influence of clay modifiers on the final nanocomposites morphology*, Degree of Masters of Science, Stellenbosch University, 2006

4.   Wang, D., Zhu, J., Yao, Q., and Wilkie, C.A., *A Comparison of Various Methods for the Preparation of Polystyrene and Poly(methyl methacrylate) Clay Nanocomposites.* Chemistry of Materials, 2002. **14**: p. 3837-3843.

5.   Bergaya, F. and Lagaly, G., *Surface modification of clay minerals.* Applied Clay Science, 2001. **19**: p. 1-3.

6.   Alexandre, M. and Dubois, P., *Polymer-layered silicate nanocomposites: preparation, properties and uses of a new class of materials.* Materials Science and Engineering, 2000. **28**: p. 1-63.

7.   Ray, S.S. and Okamoto, M., *Polymer/layered silicate nanocomposites: a review from preparation to processing.* Progress in Polymer Science, 2003. **28**: p. 1539-1641.

8.   Xu, M., Choi, Y.S., Kim, Y.K., Wang, K.H., and Chung, I.J., *Synthesis and characterization of exfoliated poly(styrene-co-methyl methacrylate)/ clay nanocomposites via emulsion polymerization with AMPS.* Polymer, 2003. **44**: p. 6387-6395.

9.   Utracki, L.A., *Clay-Containing Polymeric Nanocomposites*. Vol. Volume 1. 2004, Shawbury, UK: Rapra Technology Limited.

10.   Choi, Y.S., Ham, H.T., and Chung, I.J., *Polymer/silicate nanocomposites synthesized with potassium persulfate at room temperature: polymerization mechanism, characterization, and mechanical properties of the nanocomposites.* Polymer, 2003. **44**: p. 8147-8154.

11.   Greesh, N., Hartmann, P.C., Cloete, V., and Sanderson, R.D., *Adsorption of 2-acrylamido-2-methyl-1-propanesulfonic acid (AMPS) and related compounds onto montmorillonite clay.* Journal of Colloid and Interface Science, 2008. **319**(1): p. 2-11.

12.   Keddie, J.L. and Routh, A.F., *Fundamentals of Latex Film Formation*. 2010, New York: Springer.

13.   Choudalakis, G. and Gotsis, A.D., *Permeability of polymer/clay nanocomposites: A review.* Europeaan Polymer Journal, 2009. **45**(4): p. 967-984.

14.   Sun, Y.-M. and Lee, H.-L., *Sorption/desorption properties of water vapour in poly(2-hydroxyethyl methacrylate): 1. Experimental and preliminary results.* Polymer, 1996. **37**(17): p. 3915-3919.

15.   Jonquières, A. and Fane, A., *Modified BET Models for Modeling Water Vapor Sorption in Hydrophilic Glassy Polymers and Systems Deviating Strongly from Ideality.* Journal of Applied Polymer Science, 1998. **67**(8): p. 1415-1430.

16.   Feng, H., *Modeling of vapor sorption in glassy polymers using a new dual mode sorption model based on multilayer sorption theory.* Polymer, 2007. **48**: p. 2988-3002.

CHAPTER 7

Impact of crystallinity on water vapour sorption properties

Summary: *In this chapter the impact of the crystallinity of semi crystalline polymers on the water vapour sorption properties is discussed. Poly(methyl methacrylate) (PMMA), poly(octadecyl acrylate) (PODA) and random copolymers of poly(methyl methacrylate-co-octadecylacrylate) (p(MMA-co-ODA)) were synthesized for this study using solvent batch polymerization.*

The synthesized polymers were characterized in terms of their chemical composition, melting temperature, degree of crystallinity, lamellar structure and free volume. The liquid water and water vapour sorption properties of the resultant films were determined and discussed in terms of their chemical and physical properties.

This study showed that although crystallinity reduced the diffusion of water vapour through the films, the presence of a methyl group on the α-carbon of the vinyl group of the polymer building blocks had a more pronounced effect on the rate of diffusion as well as the activation energy of diffusion. Polymers containing methacrylate building blocks had lower rates of water vapour diffusion due to the restricted mobility of the polymer backbone.

7.1 Characterization of PMMA and PODA and *p*(MMA-*co*-ODA) polymers

The impact of various polymer properties such as chemical composition, glass transition temperature and crystallinity on the sorption behaviour of polymer films has been highlighted in Chapter 3. To understand the impact of side-chain crystallinity of *p*(MMA-*co*-ODA) polymers on the water vapour sorption behaviour of the polymers, detailed characterization of the copolymers is required in terms of their chemical, physical and structural properties. ^{1}H NMR, SEC, DSC, XRD and SAXS were used to determine the chemical composition, molar mass, melting temperature, degree of crystallinity and fine structural properties of the *p*(MMA-*co*-ODA) random copolymers, respectively.

7.1.1 Chemical and physical properties

The **chemical composition** of *p*(MMA-*co*-ODA) polymers as determined by ^{1}H NMR spectroscopy is summarized in Table 7.1 below in terms of the MMA and ODA concentrations (Also refer to Appendix A). Based on the integration of the ^{1}H NMR spectra, the following mol% of ODA was achieved: 0%, 20%, 53%, 71% and 100%. The slightly lower ODA content (20% and 71%) compared to the theoretical value could be attributed to the impact of the reactivity ratios and the changing monomer concentrations.

Table 7.1: Chemical composition

%ODA (Theoretical mol %)	Mol %		Weight %	
	MMA	ODA	MMA	ODA
0	100	0	100	0
25	80	20	55	45
50	47	53	21	79
75	29	71	11	89
100	0	100	0	100

Batch polymerization has the tendency of producing copolymers with a drifting chemical composition due to the difference in reactivity ratios of the monomers. This may impact on the physical properties of the final copolymer. O'Leary and Paul [1] evaluated the poly(*n*-alkyl acrylate) copolymer reactivity ratios for various *n*-alkyl acrylates, with the alkyl side chains ranging from C6-C22 and found that the reactivity

of these monomers resulted in ideal copolymerization [1]reactions. The reactivity ratios of the copolymerization of styrene with dodecyl methacrylate and octadecyl methacrylate also indicated a tendency for ideal copolymerization.[2] This indicated that the relatively small size of the styrene monomer compared to the *n*-alkyl acrylates evaluated in the study of O'Leary and Paul, did not impact on the overall reactivity of the monomer when polymerized with a large monomer such as octadecyl methacrylate. Contrary to what is indicated above, MMA and ODA do not result in ideal copolymerization.[3, 4] The reactivity ratios, where ODA is monomer 1 and MMA is monomer 2, were determined to be:

$$r_1 = \frac{k_{11}}{k_{12}} = 0.464$$

$$r_2 = \frac{k_{22}}{k_{21}} = 2.477$$

It can therefore be said that, for a growing polymer chain containing an ODA radical, approximately 1 ODA monomer are incorporated for every 2 MMA monomers incorporated. Conversely, 5 MMA monomers are incorporated into a growing polymer chain containing a MMA radical at the end of the chain for every 2 ODA monomers being incorporated. MMA rich polymers will therefore be dominant at the beginning of the polymerization reaction, while ODA rich polymers will be synthesized towards the latter part of the polymerization reaction. The product of the two reactivity ratios are equal to 1.149 indicating that, although ideal copolymerization is not achieved, it is not far from an ideal random copolymer structure.[5] An increase in viscosity towards the end of the polymerization could however restrict the movement of the ODA monomer, resulting in a slightly lower incorporation of this bulky monomer.

---

[1] Ideal copolymerization: Copolymerization is classified as ideal when $r_1r_2=1$. This signifies the scenario where both propagating species have the same tendency to copolymerize.

The **molar masses** of the copolymers were determined by SEC (Also refer to Chapter 4 for the methodology). The number average molar mass (Mn), weight average molar mass (Mw) and polydispersity (PDI) are given in Table 7.2 while the SEC traces are given in Figure 7.1.

Table 7.2: Molar mass[2] of PMMA, PODA and *p*(MMA-*co*-ODA) polymers

Mol% ODA	Mn [g/mol]	Mw [g/mol]	PDI
0% ODA	126,000	665,000	5.3
25% ODA	39,000	89,000	2.3
50% ODA	39,000	131,000	3.3
75% ODA	37,000	118,000	3.2
100% ODA	51,000	193,000	3.7
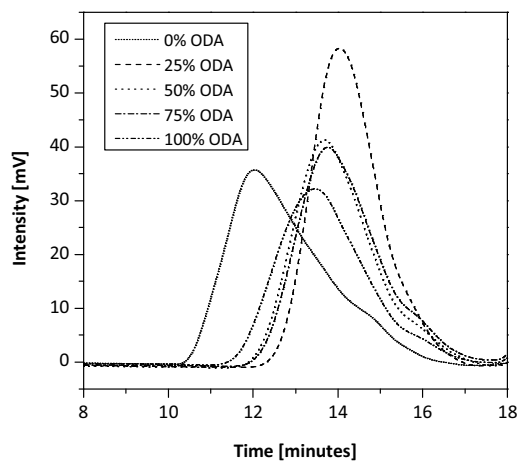
Figure 7.1: SEC plots for polymers containing different concentrations of ODA

---

[2] Relative to polystyrene

PMMA had a significantly higher molar mass compared to the *p*(MMA-*co*-ODA) and PODA. This could be attributed to the relative mobility and reactivity of the small MMA monomer relative to the bulky ODA monomer and the relative ease with which it could diffuse to the site of propagation. A high polydispersity index was also obtained for the PMMA relative to the *p*(MMA-*co*-ODA) polymers and the PODA. The polydispersity of *p*(MMA-*co*-ODA) increased with increasing ODA content, with PODA having the highest polydispersity of the polymers containing ODA. This could be attributed to the relatively slow diffusion of ODA to the site of chain propagation due to its relatively large size. This trend is also reflected in the SEC traces in terms of the broadening of the peak. The peaks of all the polymers are asymmetric and have a tail to the right which is indicative a relatively higher concentration of lower molar mass polymers.

The **thermal properties** of the polymer series were determined using DSC. PODA has a T_g of -100 °C. Due to limitations in the minimum temperature that the DSC could achieve, it was not possible to determine the T_g of all the copolymers. The T_g of the synthesized polymers are therefore reported here. The melting temperature was however determined using DSC (Refer to Table 7.3). As was expected, the melting temperature increased with increasing ODA concentration, reaching a maximum temperature of 50.3 °C for PODA.

Table 7.3: Melting temperature and crystallinity of PMMA, PODA and *p*(MMA-*co*-ODA) polymers

Mol% ODA	T_{onset} [°C]	T_m [°C]	ΔH_f [J.g^{-1}]	x_c	% Crystallinity
0% ODA	-	-	-	0	0
25% ODA	32.91	37.40	5.23	0.024	2.4
50% ODA	33.74	43.39	48.92	0.223	22.3
75% ODA	39.94	46.03	64.96	0.296	29.6
100% ODA	48.02	50.34	82.45	0.375	37.5

7.1.2 Structural properties

The structural properties of the PMMA, PODA and the *p*(MMA-*co*-ODA) polymers were determined in terms of degree of crystallinity, lamellar structure and free volume. Differential scanning calorimetry (DSC), X-ray diffraction (XRD), small angle X-ray scattering (SAXS) and positron annihilation lifetime spectroscopy (PALS) techniques were used for these determinations.

7.1.2.1 Degree of crystallinity

The degree of crystallinity of the *p*(MMA-*co*-ODA) polymer series was determined using DSC and XRD. The percentage crystallinity was calculated from the DSC results by expressing the enthalpy of fusion (ΔH_f) as a fraction of the enthalpy of fusion of a crystal for alkyl side-chain polymers (ΔH_{f0} = 219.807 J.g^{-1}), [6-9] while the diffraction peaks from the XRD pattern were integrated to confirm the degree of crystallinity. Refer to Table 7.3 and Figure 7.2 for the results and to Appendix H for the integration methodology.
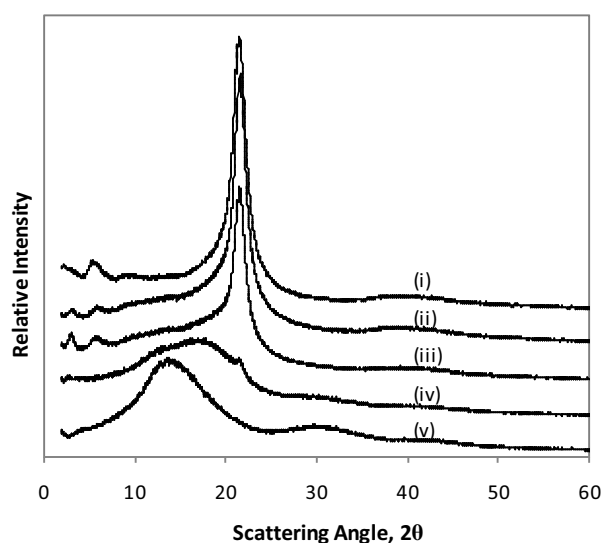
Figure 7.2: X-ray diffraction patterns of (i) 100% ODA, (ii) 75% ODA, (iii) 50% ODA, (iv) 25% ODA and (v) 0% ODA (also referred to as PMMA)

As was expected, an increase in the amount of ODA resulted in an increase in the degree of crystallinity. The T_m and x_c values for PODA correlated well with the findings of Mogri and Paul.[7] A slight variation in these values was however observed for the copolymers compared to the work from Jordan et al.[10] This variation could be attributed to a variation in the degree of polymerization.

The XRD diffraction patterns were resolved into the amorphous halo and the diffraction peaks from the crystalline phase (Refer to Figure 7.2 and Appendix H). Peaks in the higher 2θ region are indicative of

small structural properties such as crystalline regions within the polymer, where the alkyl side chains are packed in an ordered manner. Due to the relatively large size of the peak at 2θ=22 ° compared to the other peaks, it was decided to use only this peak in the integration and determination of the crystallinity of the polymer samples. A relative comparison was therefore made between the peak area at 2θ=22 ° in the XRD patterns and the degree of crystallinity as determined by DSC. Good correlation was achieved between the two methods used (Refer to Figure 7.3).

The slight deviation of the XRD peak areas could be attributed to the overlapping peaks and the assumptions made in terms of the integration parameters. The peak disappeared completely for PMMA (0% ODA pattern) as no long alkyl side chains were present that could contribute to the crystallinity of the polymer. In the 2θ region directly to the left of the sharp peak a broad peak appeared and its intensity increased with increasing MMA concentration in the copolymer. This broad peak can be attributed to the amorphous nature of MMA.
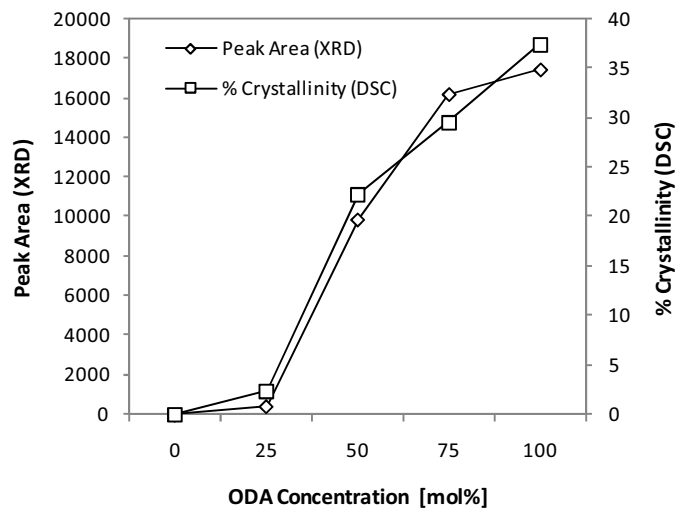
Figure 7.3: Correlation between XRD and DSC crystallinity analyses

185

7.1.2.2 Lamellar structure

At small 2θ angles the XRD scattering patterns indicate larger structural properties such as lamellar structures within a polymer. SAXS was used to determine the wave vector q for these larger structural properties. Figure 7.4 below shows the SAXS scattering patterns at low wave vector values.

The 0% ODA diffraction pattern for PMMA shows no peaks in this region which is expected for an amorphous structure. The p(MMA-co-ODA) polymers and PODA had peaks in the low wave vector region which was indicative of larger structural properties and could be attributed to the distance between crystalline regions in the polymer matrix. The distance between these lamellar structures for the p(MMA-co-ODA) random copolymers decreased slightly with increasing ODA concentration. At 25 mol% ODA the inter-lamellar distance is given as q^{-1}=0.58 nm, decreasing to 0.51 nm and 0.47 nm for the 50 mol% and 75 mol% ODA copolymers respectively. This slight reduction in the distance could be attributed to greater rotational flexibility around the polymer backbone as a result of a reduction in methacrylate content, thus enabling better association and alignment of the C18 alkyl side chains of the acrylate and therefore higher levels of crystallization. PODA had the smallest distance between the lamellar structures with a reciprocal wave vector value q^{-1}=0.24 nm.
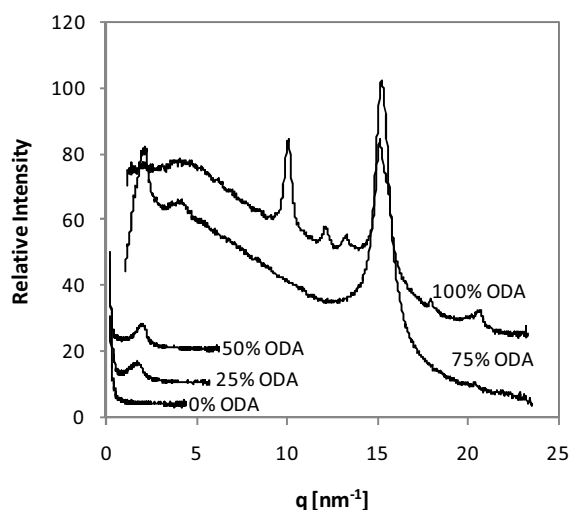
Figure 7.4: Diffraction patterns as determined by SAXS: PMMA, PODA and p(MMA-co-ODA) containing 25 mol%, 50 mol% and 75 mol% ODA respectively

7.1.2.3 Free volume

The free volume of the different polymers was determined using PALS (Refer to Chapter 4 for the methodology). The lifetime spectrum for 0% ODA could only be resolved into three components (τ_3) as no crystalline regions were present. The lifetime spectra of the other polymers containing 25%-100% ODA were resolved into 4 lifetime components, confirming the presence of both amorphous (τ_4) and crystalline (τ_3) components. Refer to Figure 7.5 and Table 7.4 for the results.

PMMA had a significantly higher overall free volume concentration (I_3) compared to the overall free volume concentration (I_4) in the amorphous regions of PODA, while the p(MMA-co-ODA) polymers containing 25% ODA, 50% ODA and 75% ODA had similar overall free volume concentrations, only slightly higher than that of PODA. The overall free volume concentration (I_3) in the crystalline regions of the polymers containing ODA was significantly lower than in the amorphous regions. These trends can be explained in terms of the ease with which the molecular segments are able to rotate and pack in the polymer backbone. The methyl group on the α-carbon of MMA restricts the rotation ability of the atoms in the polymer backbone. This results in inefficient packing and therefore the tendency of a relatively high free volume concentration. The absence of the methyl group on the α-carbon of ODA makes rotation of the side chains around the polymer backbone relatively easier, resulting in more efficient packing of polymer chains. As a result the overall free volume concentration will be lower.

Table 7.4: PALS results for PMMA, PODA and p(MMA-co-ODA) polymers:

%ODA	τ_3 component							
	τ_3 [ns]	$\Delta\tau_3$ [ns]	I_3 [%]	ΔI_3 [%]	R [Å]	ΔR [Å]	%ffv [%]	Δ%ffv [%]
0%	1.94	0.01	26.0	0.2	2.800	0.009	4.31	0.07
25%	1.2	0.3	6	1	2.0	0.4	0.3	0.3
50%	0.98	0.1	8.2	0.3	1.5	0.3	0.2	0.1
75%	1.2	0.2	7	1	1.9	0.3	0.4	0.3
100%	1.1	0.4	3.8	0.8	1.9	0.6	0.2	0.2
%ODA	τ_4 component							
	τ_4 [ns]	$\Delta\tau_4$ [ns]	I_4 [%]	ΔI_4 [%]	R [Å]	ΔR [Å]	%ffv [%]	Δ%ffv [%]
0%	-	-	-	-	-	-	-	-
25%	2.66	0.09	17	2	3.40	0.05	4.9	0.7
50%	2.59	0.05	16.8	0.7	3.35	0.03	4.7	0.3
75%	2.58	0.10	15	2	3.33	0.05	4.2	0.7
100%	2.64	0.10	13	1	3.38	0.05	3.9	0.6

The average size of free volume holes of PMMA (τ_3) was significantly smaller than the average size of the free volume holes of the polymers containing ODA (τ_4), with no significant difference in the average hole size of the ODA-containing polymers. A similar trend was seen for the hole radius sizes of the polymers analyzed.

Taking the standard deviation of the fractional free volume results for PMMA, PODA and the *p*(MMA-*co*-ODA) polymers into consideration, it is evident that there is no significant difference in the fractional free volume of these polymers (See Table 7.4 and Figure 7.5).
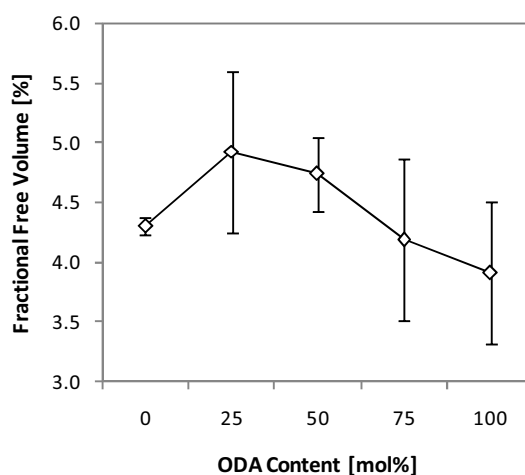
Figure 7.5: Free volume results for PMMA, PODA and *p*(MMA-*co*-ODA) polymers

7.2   Water sorption of *p*(MMA-*co*-ODA), PMMA and PODA

All polymers (refer to Table 7.1) were cast from toluene onto aluminium foil and allowed to cure at room temperature for a period of 7 days. Films of 2 cm x 2 cm (±300 µm thickness) were used for the evaluation. The water uptake was determined by immersing the films into water and removing and weighing the samples at 24 hr intervals using a 5-decimal place balance. After 5 days no water uptake

188

was noted for all films. The evaluation was abandoned thereafter and it was assumed that the different copolymers exhibited sufficient hydrophobicity to have zero water uptake at ambient conditions.

7.3 Water vapour sorption properties of *p*(MMA-*co*-ODA) and PODA

The water vapour sorption properties of *p*(MMA-*co*-ODA) containing 50 mol% ODA and PODA were evaluated at P/P_0=0.9 and across a temperature range below their melting temperature (10 °C, 20 °C and 30 °C). In the remainder of this section any reference made to *p*(MMA-*co*-ODA) will refer specifically to *p*(MMA-*co*-ODA) containing 50 mol% ODA and 50 mol% MMA. As free hanging films were used for the sorption evaluation, it was not possible to evaluate these polymer films above their melting temperatures. Other research groups have used porous ceramic membrane discs coated with poly(2,6-dimethyl-1,4-phenylene oxide) successfully as sample supports for the evaluation of permeation properties of semi crystalline polymers below and above their melting temperatures.[11] This was however not available during this investigation. The evaluation of sorption properties was therefore restricted to temperatures below the melting temperatures of the polymers. The basic properties of the films used in the sorption analyses are summarized in Table 7.5 for ease of reference.

Table 7.5: Properties of ODA polymer series used for sorption analyses

Polymer	MMA [mol%]	ODA [mol%]	T_m [°C]	lm thickness [µm]
p(MMA-*co*-ODA)	47	53	43	410
PODA	0	100	50	450

The sorption results obtained for the two polymers were analyzed in terms of the type of sorption kinetics displayed, the diffusion, solubility and permeability coefficients relative to temperature, and the Arrhenius behaviour of these polymer films.

7.3.1 Kinetic behaviour of *p*(MMA-*co*-ODA) and PODA

The sorption and reduced sorption curves are given in Figure 7.6(a) and (b) respectively. The sorption curves illustrate that, at a given temperature, the equilibrium mass uptake of water vapour is approximately 80% more for *p*(MMA-*co*-ODA) compared to PODA. This difference could be attributed to the difference in chemical composition of the two polymers and are discussed further in Section 7.3.2.

The time required to reach equilibrium was similar for the two polymers evaluated. An increase in temperature resulted in a significant reduction in the time required for the water vapour sorption to reach equilibrium for both polymers.

The reduced sorption curves for p(MMA-co-ODA) and PODA exhibit Sigmoidal behaviour across the temperature range evaluated (Refer to Figure 7.6(b)). As the polymers were prepared using solvent batch polymerization in heptane, and the films were cast from solvent, no small molecules with the ability to migrate to the surface of the film, e.g. such as surfactants, were present during the film formation process. No polar groups were therefore present at the surface of the film that could interact and slow down the migration of water vapour through the film. The reason for the initial slow uptake of water vapour is therefore not clear.

Both p(MMA-co-ODA) and PODA exhibited similar kinetic curves at a specific temperature. For a given temperature, the rate of water vapour sorption therefore appears to be independent of the chemical composition of the polymer. This may be as a result of the hydrophobic nature of both the MMA and the ODA. Little interaction between the penetrant and polymer is therefore possible, resulting in the rate of diffusion being largely driven by the penetrant concentration.
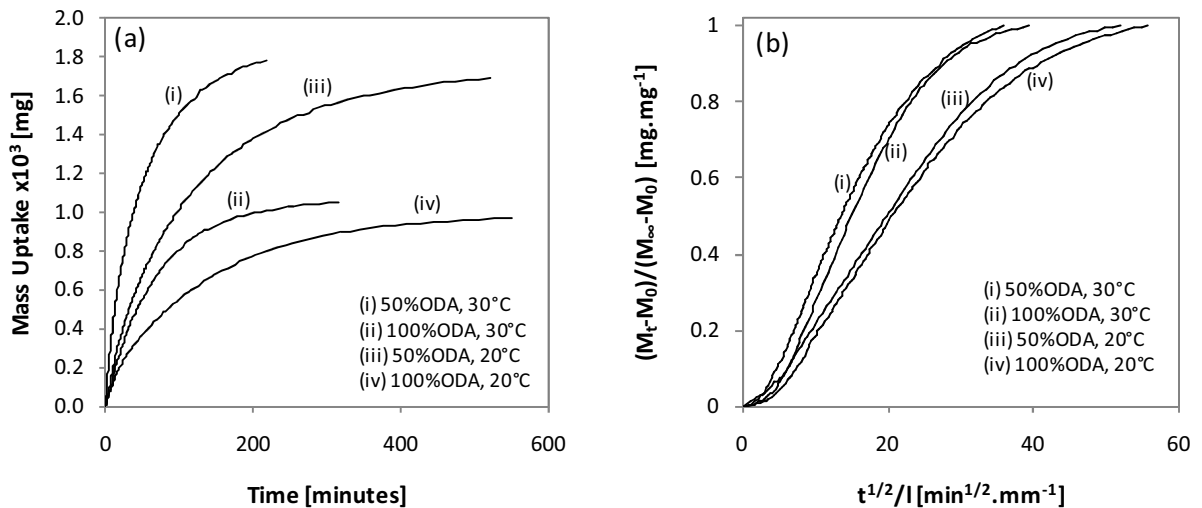
Figure 7.6: (a) Mass sorption curve (mg water vapour sorbed per mg sample); and (b) reduced sorption curves of p(MMA-co-ODA) and PODA films at P/P$_0$=0.9 and temperatures of 20 °C and 30 °C respectively

190

An increase in temperature resulted in an increase in the rate of diffusion of water vapour through the polymer film even though the polymer was still below its melting temperature. This increase in the rate of diffusion could be attributed to an increase in chain mobility, which would in turn result in faster polymer chain relaxation, thus allowing the water vapour molecules to move from one hole to the next.

7.3.2 Isobar behaviour of *p*(MMA-*co*-ODA) and PODA

The water vapour sorption behaviour at a constant water vapour partial pressure of 0.9 and increasing temperatures was evaluated. The equilibrium water vapour uptake as a function of temperature is illustrated in Figure 7.7, while the sorption parameters are summarized in Table 7.6.

It was found that the relative uptake of water vapour increased with an increase in temperature both for *p*(MMA-*co*-ODA) containing 50 mol% ODA and PODA films (Refer to Figure 7.8). This could be attributed to the relative increase water vapour pressure for increasing temperatures to maintain a water vapour partial pressure of 0.9, e.g. at 20 °C a water vapour pressure of 21.107 mbar is required to achieve P/P_0=0.9, while a water vapour pressure of 38.270 mbar is required at 30 °C to achieve the same partial pressure. More water vapour is therefore available to be absorbed by the polymer film at higher temperatures.

The increase in relative mass uptake at increasing temperatures was more significant for *p*(MMA-*co*-ODA) than for PODA. As crystalline regions are normally viewed as being impermeable,[6] this phenomenon could be attributed to the larger amorphous volume which is available for the sorption of water vapour in *p*(MMA-*co*-ODA) having 22.3% crystallinity compared to 37.5% crystallinity of PODA. The difference in degree of solubility of water vapour in the two polymers can also be explained in terms of the alkyl Van der Waals volume of the alkyl side chain of ODA relative to the total Van der Waals volume of the polymer. This method was used by Mogri and Paul to explain the difference in solubility coefficients of CH_4 and CO_2 in PODA and polybehenyl acrylate respectively.[11] The Van der Waals volume of the alkyl side chain component relative to the total Van der Waals volume of the polymer would be larger for PODA than for *p*(MMA-*co*-ODA) as the ODA monomer has a C18 alkyl side chain compared to the C1 alkyl side chain of MMA. The greater the relative volume of the alkyl component,

191

the greater the hydrophobicity of the polymer and the lower the resultant amount of water vapour mass uptake at equilibrium would be.
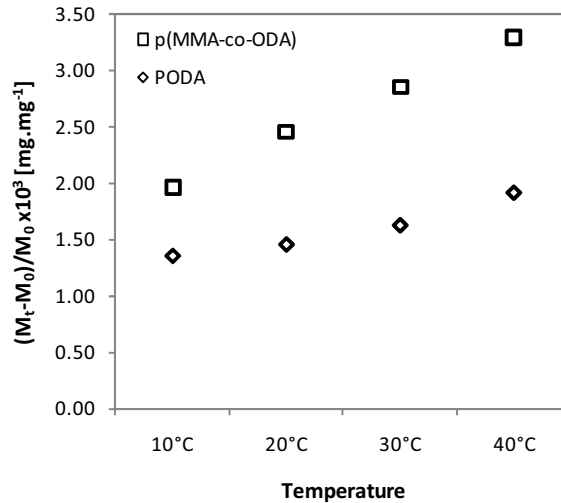
Figure 7.7: Water vapour uptake as a function of temperature for *p*(MMA-*co*-ODA) and PODA polymer films

The solubility coefficient for both polymers evaluated decreases with an increase in temperature, despite the increase in the equilibrium water vapour concentration in the film for increasing temperatures. This phenomenon can be explained in terms of the methodology used to calculate the solubility coefficient (Also refer to equation 4.13). As the solubility coefficient is determined from the ratio of the concentration of equilibrium water vapour absorbed in the polymer film relative to the water vapour pressure, it would follow logically that a relatively small incremental increase in equilibrium water vapour concentration in the film would result in a reduction in the solubility coefficient if the increments whereby the water vapour pressure is increased is significantly larger.

The diffusion coefficient for both polymers increases with increasing temperature, with the diffusion coefficient of *p*(MMA-*co*-ODA) being slightly lower than that for PODA for a given temperature. This was unexpected as it was believed that the higher degree of crystallinity of PODA would result in the lower diffusion coefficient as crystallites are impermeable (therefore increasing the tortuosity of the penetrant path length) and it reduces the chain mobility in the surrounding amorphous phase.[7, 12] Previous

research showed that, for the same side chain length, methacrylate polymers exhibited a lower permeability to a given penetrant compared to the acrylate polymer when in the completely amorphous state.[7] This behaviour was attributed to the relatively high backbone stiffness of methacrylate polymers compared to acrylate polymers as a result of the methyl group on the α-carbon of the vinyl group. The slightly lower diffusion coefficient of p(MMA-co-ODA) compared to PODA can therefore be attributed to difference in backbone stiffness as a result of the methyl group on the α-carbon of the vinyl group in MMA. The higher backbone stiffness of the copolymer would result in reduced polymer chain mobility compared to PODA and this would result in a lower diffusion coefficient.

Table 7.6: Sorption parameters D, S and P

Polymer	Temperature [°C]	D x 10^8 [cm^2.s^{-1}]	S x 10^5 [cm^3(STP)cm^3 Hg]	P x 10^{12} [cm^3(STP)cm/cm^{2}s cm Hg]
P(MMA-co-ODA)	10°C	0.80	21.02	1.68
	20°C	1.94	13.86	2.68
	30°C	4.92	8.89	4.37
PODA	10°C	1.06	12.8	1.36
	20°C	2.17	7.23	1.57
	30°C	4.65	4.47	2.08

The relatively high solubility coefficient of p(MMA-co-ODA) relative to PODA, resulted in p(MMA-co-ODA) having a higher permeability coefficient compared to PODA at the three temperatures evaluated despite the high stiffness of the polymer backbone due to the presence of the methacrylate component. To achieve minimal water vapour permeability a high alkyl Van der Waals volume fraction compared to the acrylate Van der Waals volume fraction is therefore the most important factor.

7.3.3 Activation energy and heats of solution of p(MMA-co-ODA) and PODA

The Arrhenius relationships for the transport parameters P, D and S were used to calculate the activation energies (E_P and E_D) and the heat of solution (ΔH_S) for the permeation, diffusion and solubility coefficients respectively (Also refer to Chapter 3, Section 3.2). These energies were determined by expressing the Arrhenius relationships in terms of a natural logarithm, thus obtaining a straight line equation. By plotting for example $\ln D$ against $\frac{1}{RT}$ the diffusion activation energy could be determined

from the gradient, while D_0 could be determined from the y-intercept. The results are summarized in Figure 7.8 (including the equations for the trendlines) and Table 7.7 respectively.

Example:

$$D = D_0 exp\left(-\frac{E_D}{RT}\right)$$

$$\ln D = -E_D \frac{1}{RT} + \ln D_0$$

These results indicate that the heats of solution for the two polymers were very similar with ΔH_S for p(MMA-co-ODA) being slightly lower than for PODA, while the activation energy for diffusion differed significantly for the two polymers evaluated, with p(MMA-co-ODA) requiring a higher activation energy compared to PODA. This variation is also reflected in the activation energy of permeation as it is the sum of the heat of solution and activation energy of diffusion for a specific polymer.

Table 7.7: Activation energy, heats of solution and pre-exponential factors of P, D and S

Polymer	E_D [kcal.mol^{-1}]	D_0 [cm^2.s^{-1}]	ΔH_S [kcal.mol^{-1}]	S_0 [cm^3(STP)cm^3 Hg]	E_P [kcal.mol^{-1}]	P_0 [cm^3(STP)cm/cm^{2}s cm Hg]
p(MMA-co-ODA)	15.50	7266.28	-7.336	4.65E-10	8.167	3.37E-06
PODA	12.56	52.67	-8.975	1.50E-11	3.593	7.89E-10

Various factors could contribute to the difference in activation energy of diffusion for p(MMA-co-ODA) compared to PODA, e.g. the chain mobility of these polymers, their crystallinity, melting temperature and free volume properties. Taking into consideration that PODA has a higher degree of crystallinity and a higher melting temperature compared to p(MMA-co-ODA), one would expect that these factors would result in low polymer chain mobility and that PODA would therefore have a higher diffusion activation energy compared to p(MMA-co-ODA). Contrary to this, the experimental data indicated higher activation energy for the p(MMA-co-ODA) film containing 50 mol% ODA.

The difference in diffusion activation energy for p(MMA-co-ODA) compared to PODA will be explained in light of the work of Mogri and Paul where the permeation properties of PODA was compared to that of polyoctadecyl methacrylate (PODM).[7] Although the hydrophobicity of these two polymers is similar, their overall permeability in the amorphous state differed significantly, with PODM having a lower

permeability activation energy and permeation coefficient compared to PODA. This phenomenon was explained in terms of the higher backbone stiffness due to the methyl group on the α-carbon of the vinyl group of the PODM polymer which resulted in limited chain mobility. This finding showed that a higher degree of crystallinity of a polymer may not be the main contributing factor to a low diffusion coefficient in the polymer film, but that high stiffness of the polymer backbone could be the dominant factor.
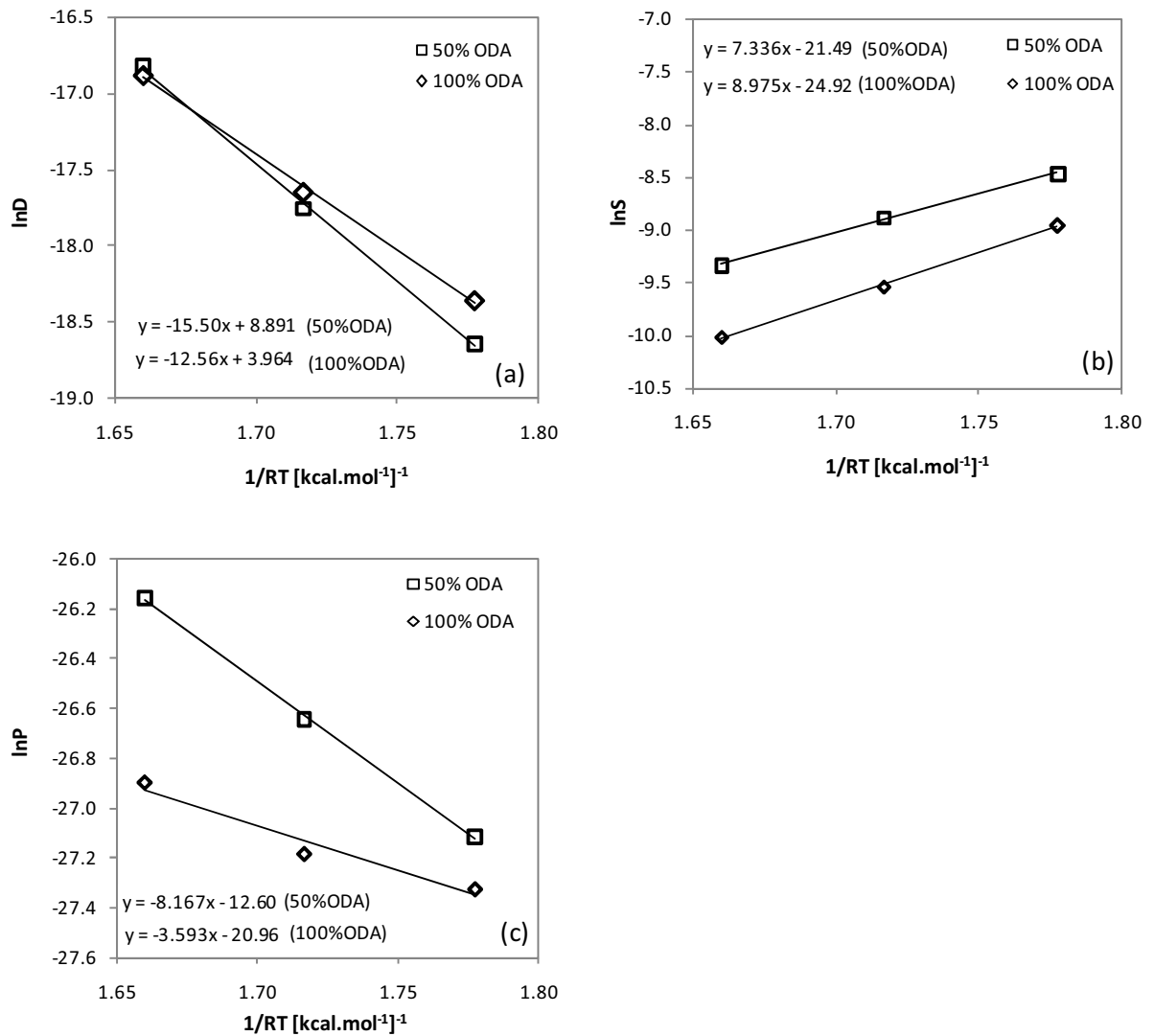
Figure 7.8: Arrhenius plots of the sorption parameters versus the reciprocal of RT (a) diffusion coefficient; (b) solubility coefficient; and (c) permeability coefficient.

Based on the findings of Mogri and Paul, it is suggested that the MMA introduces a significant degree of polymer backbone stiffness to the *p*(MMA-*co*-ODA) random copolymer that was evaluated in this study. Although *p*(MMA-*co*-ODA) only has 22.3% crystallinity compared to 27.5% crystallinity of PODA, and one would expect that PODA would require a higher activation energy for diffusion, the high backbone stiffness resulting from the methacrylate in the polymer backbone appears to be the dominant factor in restricting polymer chain mobility.

7.4 Conclusions

Side chain crystallinity was effectively introduced through the random copolymerization of ODA with MMA, with excellent correlation seen between the degree of crystallization as determined by DSC and XRD.

The rate of diffusion of water vapour through *p*(MMA-*co*-ODA) and PODA appeared to be largely independent of the chemical composition of the polymers for a given temperature, as the mass sorption curves for these polymers very quite similar. The solubility coefficient of the copolymer was however larger than that of PODA and this could be attributed to the larger amorphous component of the co-polymer compared to PODA, as well as a smaller alkyl Van der Waals volume compared to that of PODA.

The sorption properties of both *p*(MMA-*co*-ODA) and PODA at different temperatures were in line with typical sorption behaviour for vapours, with the diffusion coefficient increasing with increasing temperatures, largely due to increasing chain mobility, while the solubility coefficient decreases.

Although it was thought that side chain crystallinity would be the main contributing factor resulting in a reduction in the diffusion coefficient, it was shown that the methyl group on the α-carbon of the vinyl group reduced the diffusion to a greater extent through the increased stiffness of the polymer backbone. This was also reflected in *p*(MMA-*co*-ODA) having a greater activation energy for diffusion compared to PODA.

The conclusions and recommendations are discussed in the next chapter.

References

1. O'Leary, K. and Paul, D.R., *Copolymers of poly(n-alkyl acrylates): synthesis, characterisation, and monomer reactivity ratios.* Polymer, 2004. **45**(19): p. 6575-6585.

2. Vidovic, E., Saric, K., and Janovic, Z., *Copolymerization of Styrene with Dodecyl Methacrylate and Octadecyl Methacrylate.* Croatica Chemica Acta, 2002. **75**(3): p. 769-782.

3. Jordan Jr., E.F., Bennett, R., Shuman, A.C., and Wrigley, A.N., *Reactivity ratios and copolymerization parameters for copolymers incorporating n-octadecyl acrylate and N-n-octadecylacrylamide* Journal of Polymer Science: Part A: Polymer Chemistry, 1970. **8**(11): p. 3113-3121.

4. Brandrup, J., Immergut, E.H., and Grulke, E.A., eds. *Polymer Handbook*. Vol. 2. 1999, John Wiley & Sons: Hoboken, New Jersey.

5. Hagiopol, C., *Copolymerization: Towards a Systematic Approach*. 1999, New York: Kluwer Academic/Plenum Publishers.

6. Mogri, Z., Paul, D.R., *Gas sorption and transport in side-chain crystalline and molten poly(octadecyl acrylate).* Polymer, 2001. **42**: p. 2531-2542.

7. Mogri, Z., Paul, D.R., *Gas sorption and transport in poly (alkyl (meth)acrylate)s. I. Permeation properties.* Polymer, 2001. **42**: p. 7765-7780.

8. Platé, N.A. and Shibaev, V.P., *Comb-Like Polymers. Structures and Properties.* Journal of Polymer Science: Macromolecular Reviews, 1974. **8**: p. 117-253.

9. Jordan, E.F., Feldeisen, D.W., and Wrigley, A.N., *Side-Chain Crystallinity. I. Heats of Fusion and Melting Transitions on Selected Homopolymers Having Long Side Chains.* Journal of Polymer Science: Part A-1, 1971. **9**: p. 1835-1852.

10. Jordan, E.F., Artymyshyn, B., Speca, A., and Wrigley, A.N., *Side-Chain Crystalinity. II. Heats of Fusion and Melting Transitions on Selected Copolymers Incorporating n-Octadecyl Acrylate or Vinyl Stearate.* Journal of Polymer Science: Part A: Polymer Chemistry, 1971. **9**: p. 3349-3365.

11.   Mogri, Z. and Paul, D.R., *Gas sorption and transport in poly (alkyl (meth)acrylate)s: II. Sorption and diffusion properties.* Polymer, 2001. **42**: p. 7781-7789.

12.   Weinkauf, D.H. and Paul, D.R., *Effects of Structural Order on Barrier Properties*, in *Barrier Polymers and Structures*, W.J. Koros, Editor. 1993, American Chemical Society: Washington, DC.

CHAPTER 8

Conclusions and Recommendations

8.1 Conclusions

Water vapour sorption behaviour of the model random copolymer *p*(Sty-*co*-BA) stabilized with different types of surfactants was evaluated. Although the conventional surfactants SDBS and OPE exuded to the surface during film formation, FTIR-ATR spectroscopy showed that these surfactants migrated back into the bulk of the film when the film was exposed to high water vapour partial pressures. Contrary to this, the reactive surfactant DA3B was immobilized throughout the bulk of the polymer film and its relative position in the film was unaffected by changes to the water vapour partial pressure in the atmosphere surrounding the latex film. The relative position of the surfactant in the film affected the rate of migration of water vapour, with the DA3B having a significantly higher diffusion coefficient compared to SDBS and OPE due to the pathway created by this surfactant throughout the polymer film. The solubility of water vapour in the latex film was significantly higher for the conventional surfactants and could be attributed to the polarity of these molecules. Overall SDBS and OPE stabilized films exhibited Flory-Huggins sorption behaviour, while the DA3B stabilized latex film followed Henry's Law. Despite the significantly different thermodynamic behaviour of these films, it was found that the overall permeability coefficient of the latex film stabilized with different surfactants did not differ noticeably.

The impact of Na-MMT and AMPS on the water vapour sorption properties of *p*(Sty-*co*-BA) random copolymers was evaluated. It was found that the addition of Na-MMT and AMPS to the model polymer *p*(Sty-*co*-BA) used in the initial surfactant investigation resulted in a significant change in the water vapour sorption properties of the resultant latex films. The presence of AMPS and Na-MMT throughout the bulk of the latex film increased the overall hydrophilicity of the film significantly, resulting in faster migration of

199

water vapour through the film and as a result, shorter times to reach equilibrium. The reduced sorption curves of the p(Sty-co-BA)/Na-MMT PCNs containing SDBS were therefore similar to that of p(Sty-co-BA) stabilized with DA3B. It was also found that complete exfoliation of Na-MMT was critical to ensure low water vapour sorption in the p(Sty-co-BA)/Na-MMT model polymer. Partial exfoliation resulted in significantly higher levels of water vapour being absorbed in the latex film, probably due to clustering of water vapour in the inter gallery spaces of the clay. The isotherm obtained for p(Sty-co-BA)/Na-MMT showed a slightly convex curve at low water vapour partial pressures, indicating BET(II) thermodynamic behaviour. Using a least squares regression fit, a good correlation was obtained with the DMS model which was designed for films in their glassy state, even though the PCNs analysed were above their glass transition temperature. The presence of Na-MMT in the polymer matrix resulted in restricted polymer chain mobility at the interface between the clay platelets and the bulk of the polymer. This limitation in polymer chain mobility was suggested to be the reason for the similarity in thermodynamic behaviour to glassy polymers.

The impact of side-chain crystallinity on the water vapour sorption properties of p(MMA-co-ODA) was evaluated. An increase in the degree of crystallinity in the polymer matrix did not significantly change the rate of diffusion of water vapour through the polymer film as PODA showed similar kinetic behaviour to p(MMA-co-ODA). The slightly lower diffusion coefficient of p(MMA-co-ODA) actually suggested that the restriction in polymer backbone mobility due to the methyl group on the α-carbon of the methacrylate group of MMA played a more significant role in reducing the rate of diffusion of water vapour through the polymer matrix.

8.2 Recommendations

- The sigmoidal kinetic behaviour of SDBS and OPE stabilized p(Sty-co-BA) random copolymers should be studied further utilizing a liquid cell and FTIR-ATR spectroscopy. This will enable the evaluation of the penetration of water molecules close to the surface of the polymer film at short time intervals, therefore overcoming the limitations in terms of the method used in this study.
- The impact of film thickness of p(Sty-co-BA) random copolymers stabilized with SDBS and DA3B respectively on the water vapour sorption properties should be studied further to determine why the kinetic behaviour differs for the two types of surfactants used.
- The suitability of using the DMS model to predict sorption behaviour of PCNs should be explored further.

- The impact of water vapour sorption on the T_g of PCNs should be explored further utilising an analytical method such as dynamic mechanical analysis.

- The feasibility of incorporating a methacrylate monomer into the backbone of the model random copolymer p(Sty-co-BA) stabilized with DA3B should be explored with the aim of determining whether the introduction of higher backbone stiffness would reduce the high diffusion coefficient which resulted from the pathway that was created throughout the bulk of the polymer by the presence of DA3B.

- The impact of utilizing miniemulsion polymerisation, as opposed to solvent polymerisation, on the water vapour sorption properties of p(MMA-co-ODA) should be investigated to allow for direct comparison of sorption behaviour of these polymer films with those prepared for the surfactant study described in Chapter 5 and the crystallinity study described in Chapter 7.

APPENDIX A

Integration of ^{1}H NMR spectra of polymer synthesized

1.   **^{1}H NMR integration of *p*(Sty-*co*-BA) polymers**

Peaks at the following chemical shifts were used to determine the composition of the *p*(Sty-*co*-BA) polymer in terms of mol % and weight %:

Table 1: Chemical shifts used for integration of ^{1}H NMR spectra

Monomer	*Molecular weight (g.mol^{-1})*	*Functional group*	*Functional group code*	*No. of H atoms*	*Chemical shift*
Styrene	104.15	Styrenic H(a)	A	5	7.0-7.5
n-Butyl acrylate	128.17	Methylene H(d) (-O-CH$_2$-)	B	2	3.8-4.5

Taking the number of protons per integrated area into consideration, the polymer composition was determined as follows:

Component	Proton Integration	Mol %	Weight %
Styrene	$I_A = \dfrac{I_{Sty}}{5}$	$\dfrac{I_A}{(I_{A+B})}$	$\dfrac{Sty\ Mol\% \times MW_{Sty}}{\left(Sty\ Mol\% \times MW_{Sty}\right) + \left(BA\ Mol\% \times MW_{BA}\right)}$
n-Butyl Acrylate	$I_B = \dfrac{I_{BA}}{2}$	$\dfrac{I_B}{(I_A + I_B)}$	$\dfrac{BA\ Mol\% \times MW_{BA}}{\left(Sty\ Mol\% \times MW_{Sty}\right) + \left(BA\ Mol\% \times MW_{BA}\right)}$

The integrated areas were incorporated into equations for the calculation of Mol% and Weight%.

2. ^{1}H NMR integration of p(MMA-co-ODA) polymers

Peaks at the following chemical shifts were used to determine the composition of the *p*(MMA-*co*-ODA) polymer in terms of mol % and weight %:

Table 2: Chemical shifts used for integration of ^{1}H NMR spectra

Monomer	Molecular weight (g.mol^1)	Functional group	Functional group code	No. of H atoms	Chemical shift
MMA	100.12	Methyl H(d) (-O-CH$_3$)	A	3	3.75
ODA	324.55	Methylene H(d) (-O-CH$_2$-)	B	2	4.1-4.2

Taking the number of protons per integrated area into consideration, the polymer composition was determined as follows:

Component	Proton Integration	Mol %	Weight %
MMA	$I_A = \dfrac{I_{MMA}}{3}$	$\dfrac{I_A}{(I_{A}+I_B)} \times 100$	$\dfrac{MMA\,Mol\% \times MW_{MMA}}{(MMA\,Mol\% \times MW_{MMA}) + (ODA\,Mol\% \times MW_{ODA})} \times 100$
ODA	$I_B = \dfrac{I_{ODA}}{2}$	$\dfrac{I_B}{(I_A + I_B)} \times 100$	$\dfrac{ODA\,Mol\% \times MW_{ODA}}{(ODA\,Mol\% \times MW_{ODA}) + (MMA\,Mol\% \times MW_{MMA})} \times 100$

The integrated areas were incorporated into equations for the calculation of Mol% and Weight%.

3. ^{1}H NMR results of polymers synthesized

Table 3: Surfactant Series (Chapter 5): *p*(Sty-*co*-BA) polymer composition

p(Sty-co-BA) Surfactant type	Theoretical content				Actual content			
	Mol %		Weight %		Mol %		Weight %	
	Sty	*BA*	*Sty*	*BA*	*Sty*	*BA*	*Sty*	*BA*
2% SDBS	60%	40%	55%	45%	63%	37%	58%	42%
2% DA3B	60%	40%	55%	45%	63%	37%	58%	42%
6% OPE	60%	40%	55%	45%	64%	36%	59%	41%

Table 4: ODA Series (Chapter 7): *p*(MMA-*co*-ODA) polymer composition

p(MMA-co-ODA) ODA Conc. [Mol %]	Theoretical content				Actual content			
	Mol %		Weight %		Mol %		Weight %	
	MMA	*ODA*	*MMA*	*ODA*	*MMA*	*ODA*	*MMA*	*ODA*
0%	100	0	100%	0%	100	0	100	0
25%	85	15	60%	40%	80	20	55	45
50%	55	45	25%	75%	47	53	21	79
75%	40	60	16%	845	29	71	11	89
100%	25	75	8%	92%	0	100	0	100

APPENDIX B

Sampling depth of FTIR-PAS measurements

FTIR-PAS was used to characterize the *p*(Sty-*co*-BA) polymer films containing different surfactants (Chapter 4), as well as to determine the relative position of Na-MMT in *p*(Sty-*co*-BA)polymers (Chapter 6).

The sampling depth is dependent on both the mirror velocity and the wavenumber of the infrared radiation.[1] Equations (3.3-3.5) were used to calculate the sampling depth or thermal diffusivity for a specific mirror velocity and wavenumber. For polymeric materials at can be assumed that the thermal diffusivity is equal to 0.01×10^{-5} m^2/s.[2]

The table below contains the modulation frequencies and sampling depths for polymers analysed using mirror velocity settings of 0.05 cm.s^{-1}, 0.15 cm.s^{-1}, 0.30 cm.s^{-1} and 0.75 cm.s^{-1}.

Table 5: Sampling depths at different wavenumbers and mirror velocities for polymers

Wavenumber [cm^{-1}]	Mirror Velocity [cm.s^{-1}]			
	0.05	0.15	0.30	0.75
	Sampling Depth [µm]			
1012	17.7	10.2	7.2	4.6
1043	17.5	10.1	7.1	4.5
1493	14.6	8.4	6.0	3.8
1601	14.1	8.1	5.8	3.6
2184	12.1	7.0	4.9	3.1
3638	9.4	5.4	3.8	2.4

---

[1] Jurdana, L.E., et al., *Application of FT-IR Step-Scan Photoacoustic Phase Modulation Methods to Keratin Fibers.* Applied Spectroscopy, 1995. **49**(3): p. 361-366.

[2] Zhang, W.R., Lowe, C., and Smith, R., *Depth profiling of coil coating using step-scan photoacoustic FTIR.* Progress in Organic Coatings, 2009. **65**: p. 469-476.

APPENDIX C

FTIR Spectra of Surfactants

FTIR spectroscopy was used to identify unique surfactant bands for the 3 surfactants evaluated in Chapter 4. These bands are used to confirm the presence of the surfactant in the polymer at specific depths of analysis.

(1)   Sodium dodecyl benzene sulfonate (SDBS)

FTIR spectra of five compounds were used to identify the unique infrared bands that can be used to identify SDBS in the p(Sty-co-BA) latex films. These were: (a) p(Sty-co-BA) containing 10% SDBS; (b) p(Sty-co-BA) containing 6% SDBS; (c) p(Sty-co-BA) containing 1% SDBS; (d) p(Sty-co-BA) without any SDBS; and (e) SDBS.
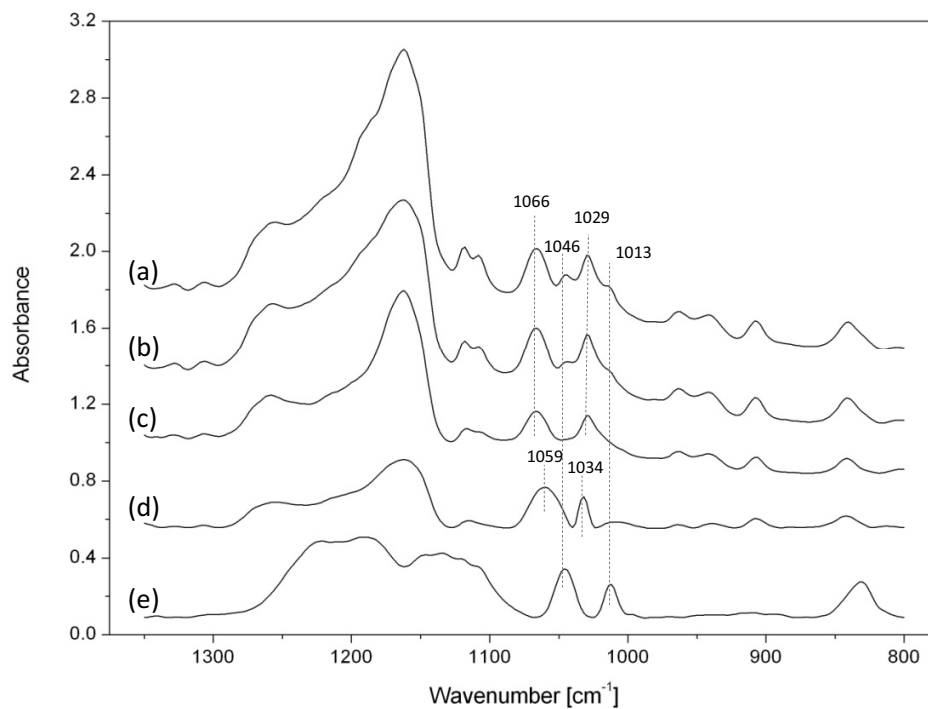
Figure 1: FTIR spectra of (a) p(Sty-co-BA) containing 10% SDBS; (b) p(Sty-co-BA) containing 6% SDBS; (c) p(Sty-co-BA) containing 1% SDBS; (d) p(Sty-co-BA) containing no SDBS; and (e) SDBS

The ester group of p(Sty-co-BA) is unique, i.e. it is not present in the surfactant SDBS. The –C-O-C-structure within this group exhibits two characteristic bands in the region of 1300-1030 cm^{-1} which can be attributed to the symmetric and asymmetric absorption bands of –C-O-C-[3]. Two unique bands corresponding to this wavelength region at 1034 cm^{-1} and 1059 cm^{-1} can be attributed to these vibrations (Refer to spectrum (d) in Figure 1).

SDBS has two distinct infra-red bands at 1046 cm^{-1} and 1013 cm^{-1} representing S-O symmetric stretching vibrations (Refer to spectrum (e) in Figure 1). These bands normally have a strong intensity and are used for structural assignment[4]. Based on this, these bands were used to identify the presence of SDBS in the polymer films prepared in this study.

When comparing spectra (d) and (e) to the two spectra containing both the polymer and the surfactant (spectra (a), (b) and (c)), the SDBS stretching vibrations are visible as a shoulder to the right of the asymmetric and symmetric absorption bands of –C-O-C-.The intensity of these bands increase with an increase in the SDBS concentration.

Based on these results, the infrared bands at 1046 cm^{-1} and 1013 cm^{-1} can therefore be used effectively to confirm the presence of SDBS in the p(Sty-co-BA) latex film.

(2)   Dodecylammonium-3-butenoate (DA3B)

FTIR spectra of p(Sty-co-BA) containing DA3B, p(Sty-co-BA) without surfactant and DA3B were compared to identify the unique bands whereby the presence of DA3B could be confirmed (Refer to Figure 2 below).

The primary ammonium cation group of DA3B is unique to the surfactant as it is not present in p(Sty-co-BA) and was therefore used to indentify DA3B in the infrared spectra of the polymer latex film. The typical wavenumber region for the asymmetric and symmetric bending deformations of primary ammonium cations[5] are 1600-1575 cm^{-1} and 1490 cm^{-1} respectively. Infrared absorption bands at 1540 cm^{-1} and 1472 cm^{-1} were identified that correspond well to the asymmetric and symmetric bending deformations of N^+-H_3 (Refer to spectrum (c) in Figure 2 below).

The styrene functionality are unique to p(Sty-co-BA) as it is not present in the DA3B surfactant. In-plane skeletal vibrations of the aromatic C=C functional groups[6] can be found at approximately 1600 cm^{-1}, 1580 cm^{-1}, 1500 cm^{-1} and 1450 cm^{-1} and the carbonyl group of the carboxylic ester at 1735 cm^{-1}. The following bands were identified as corresponding to these vibrational bands: 1735 cm^{-1} for the carbonyl group, 1601 cm^{-1} and 1452 cm^{-1} for the C=C group (Refer to spectra (a) and (b) in Figure 2 below).

---

[3] Pasto, D.J. and Johnson, C.R., Organic Structure Determination. Prentice-Hall Inc., UK and Eire, 1969, p.127.

[4] Pasto, D.J. and Johnson, C.R., Organic Structure Determination. Prentice-Hall Inc., UK and Eire, 1969, p.132.

[5] Pasto, D.J. and Johnson, C.R., Organic Structure Determination. Prentice-Hall Inc., UK and Eire, 1969, p.121.

[6] Pasto, D.J. and Johnson, C.R., Organic Structure Determination. Prentice-Hall Inc., UK and Eire, 1969, p.123.

The low DA3B concentration relative to the *p*(Sty-*co*-BA) polymer has largely resulted in quenching of the primary ammonium bands, making it difficult to use this technique to determine the presence of DA3B at the air-film and film-substrate interfaces.
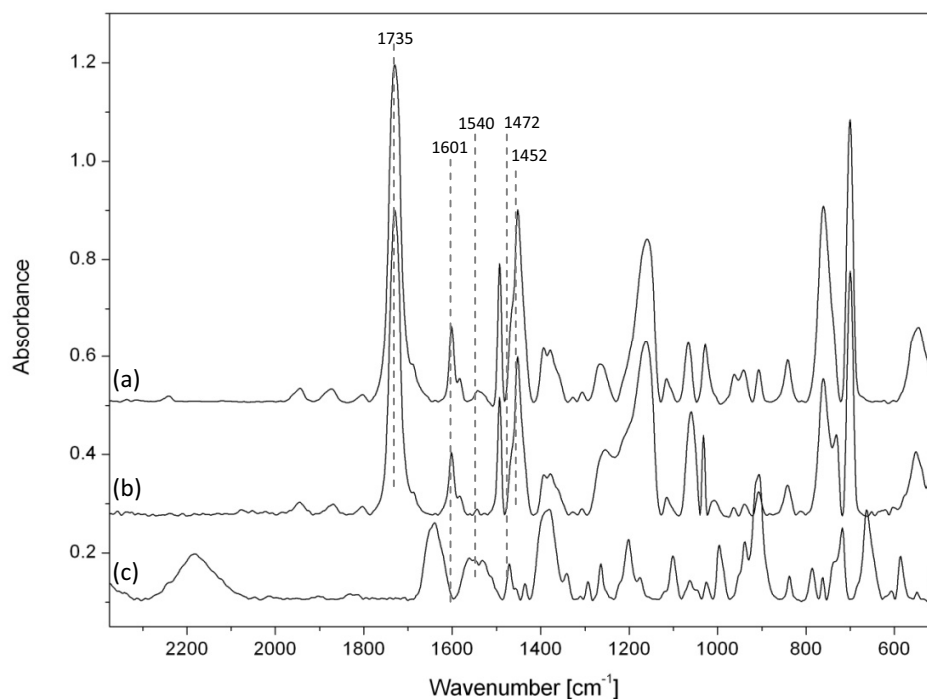
Figure 2: FTIR PAS spectra of (a) *p*(Sty-*co*-BA) polymer containing DA3B; (b) *p*(Sty-*co*-BA) polymer without DA3B; and (c) DA3B

(3)   Octyl Phenol Ethoxylate (OPE)

The OPE surfactant contain a primary C-O-H group and acyclic ether groups (C-O-C) which are unique to the surfactant. These C-O single bond alcohol and ether absorption bands are found in the 1250-1000 cm^{-1} wavenumber region, with C-O-H at 1050 cm^{-1} and strong C-O-C asymmetric stretching absorption bands at 1150-1070 cm^{-1} and 1270-1200 cm^{-1} and symmetric absorption bands at 1070-1020 cm^{-1} respectively.[7] From Figure 3 the following absorption bands were identified: 1280 cm^{-1} and 1240 cm^{-1} for the C-O-C stretching absorption bands, and 1062 cm^{-1} for the C-O-H absorption band.

The *p*(Sty-*co*-BA) polymer contains aromatic C=C groups as well as carboxylic ester groups with vibrational bands in the wavenumber region 1600 cm^{-1}, 1580 cm^{-1}, 1500 cm^{-1} and 1450 cm^{-1} for the

---

[7] Pasto, D.J. and Johnson, C.R., Organic Structure Determination. Prentice-Hall Inc., UK and Eire, 1969, p.124-126.

aromatic carbon double bonds and 1735 cm^{-1} and 1300-1050 cm^{-1} for the carboxylic ester groups respectively. The following bands were identified in Figure 3 below: 1730 cm^{-1} and 1160 cm^{-1} for the carboxylic ester absorption bands and 1601 cm^{-1}, 1496 cm^{-1} and 1452 cm^{-1} for the aromatic C=C absorption bands.
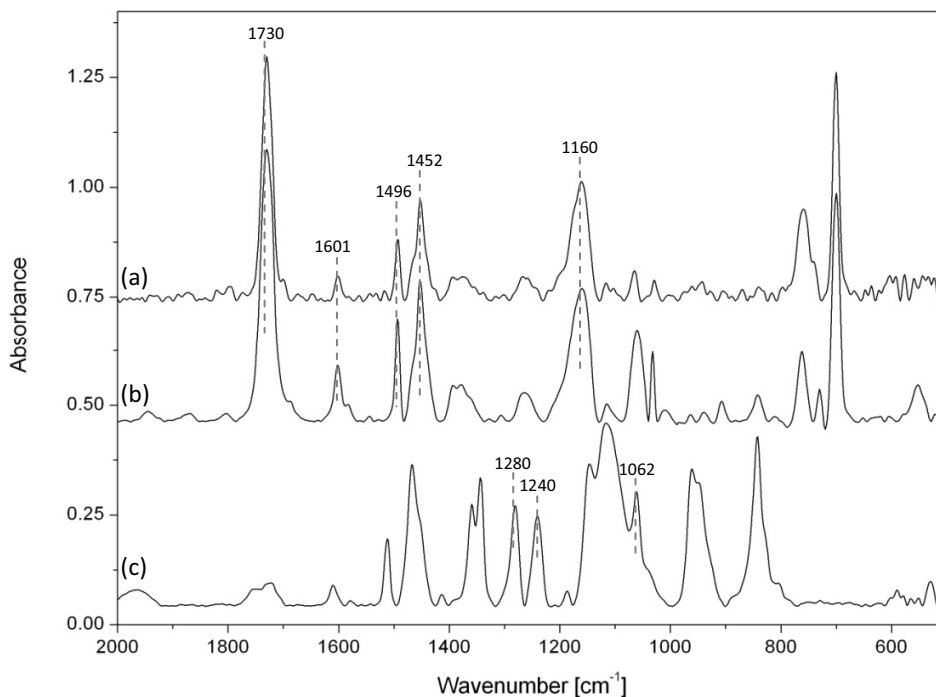
Figure 3: FTIR spectra of (a) *p*(Sty-*co*-BA) polymer containing 6% OPE; (b) *p*(Sty-*co*-BA) polymer containing no OPE; and (c) OPE

From the above spectra it was clear that, due to the overlap of the vibrational bands of the C-O groups of the OPE surfactant with the vibrational bands of the carboxylic ester and C=C functional groups of *p*(Sty-*co*-BA) polymer, it was not possible to confirm whether OPE exude to the film-air or film-substrate interfaces.

APPENDIX D

Integration of FTIR-ATR spectra

The reproducibility of the FTIR-ATR spectroscopy method used to determine the degree of migration of free water and SDBS into the p(Sty-co-BA) latex film are illustrated here. Baseline correction was done for each spectrum, followed by normalization of the spectrum relative to the vibrational band of the carbonyl group at 1735 cm^{-1}. Thereafter the free water band at 3450 cm^{-1} and the S-O symmetric stretching vibrations at 1043cm^{-1} and 1013cm^{-1} were integrated and the areas obtained were used to determine the relative concentration of free water and surfactant at a penetration depth of 0.61μm and ±2μm respectively. The results below are based on an average value of three measurements.

The following areas were obtained for the p(Sty-co-BA) latex film stabilized with SDBS:

Time [min]	Free water @ 3450 cm^{-1}			SDBS @ 1043 cm^{-1}		
	Band Area	Std. Dev.	Conc. [%]	Band Area	Std. Dev.	Conc. [%]
0	13	2	0%	1.2	0.5	100%
5	18	5	12%	0.3	0.3	24%
10	38	2	58%	1.0	0.5	82%
15	34	4	50%	0.9	0.1	73%
20	34	12	50%	0.90	0.08	73%
30	34	5	49%	0.8	0.3	65%
40	44	6	73%	0.56	0.10	45%
50	43	3	69%	0.8	0.4	62%
60	48	6	83%	0.77	0.08	63%
90	58	14	104	0.6	0.2	51%
120	56	4	100%	0.8	0.2	68%

The high standard deviations obtained indicate that the method used is not accurate. It does however give an indication of relative change of concentration of the two components monitored. An FTIR-ATR flow-through liquid cell would eliminate a significant amount of variation due to experimental variability and should be explored for further research on this topic.

APPENDIX E

Infrared spectra of Na-MMT and p(Sty-co-BA)

Transmission FTIR spectra of the p(Sty-co-BA) and Na-MMT were used to determine a unique band for Na-MMT that could be used in FTIR-PAS to determine the relative concentration of the Na-MMT to the polymer matrix at different depths of analysis.

Three absorption regions of montmorillonite can be used in infrared spectroscopy: 3,000-3,800 cm^{-1}, 1,300-1,800 cm^{-1} and 500-1,200 cm^{-1}.[1] Due to the overlap of absorption bands of p(Sty-co-BA) and Na-MMT, only the 3,000-3,800 cm^{-1} region appeared to be suitable for the identification of unique Na-MMT bands for depth profiling. The band at 3638 cm^{-1} was found to be unique to the spectrum of Na-MMT and was thus used to identify the clay in the FTIR-PAS spectra of the PCNs. This band can be attributed to the OH stretching vibration of structural hydroxyl groups situation at the inner surface of montmorillonite.
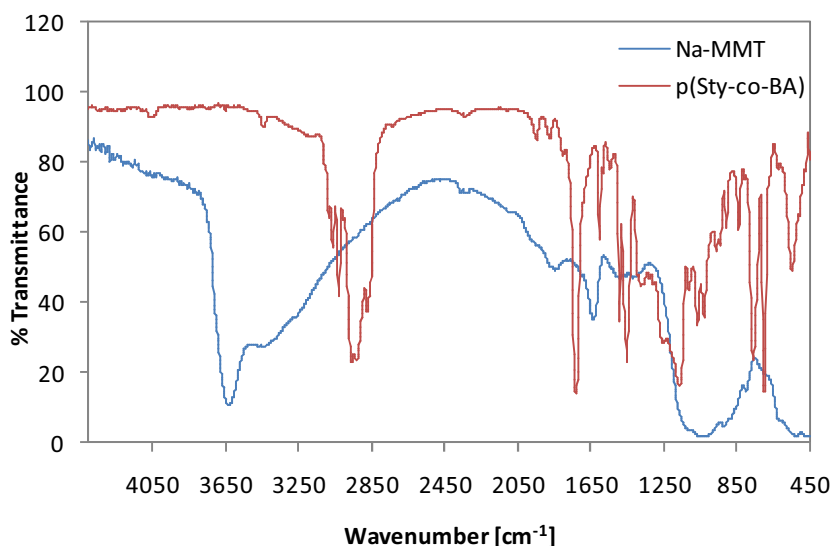
Figure 4: FTIR spectra of Na-MMT clay and p(Sty-co-BA) polymer

APPENDIX F

Refractive index determinations of polystyrene and styrene-co-butyl acrylate polymers

Polystyrene with known refractive index (n_D=1.5894) were used to evaluate the accuracy of the mechanism used to determine the refractive index of the styrene-*co*-butyl acrylate polymers. Different concentrations of polystyrene were prepared in THF (n_D=1.4072) and the refractive index of the dissolved polymer measured. The plot of the refractive index of the polystyrene solutions versus the concentration of polystyrene (weight %) resulted in a linear relationship. Using the equation for a straight line, the refractive index of 100% polystyrene was calculated.

n_D (polystyrene - literature): 1.59-1.592 @ 20°C[8]
n_D (polystyrene – calculated): 1.5949

Table 6: Refractive index value of polystyrene

Wt.% THF	Wt.% p-Sty	Measured n_D	Calculated n_D	Literature n_D	st dev
100	0	1.4050		1.4072 @ 20 °C	
98.5	1.5	1.4075			
97.2	2.8	1.4102			
0	100		1.5949	1.5894	0.003889
				1.5915 @ 20 °C	0.003889

Reference: Polystyrene in THF

y = 0.001x + 1.404

---
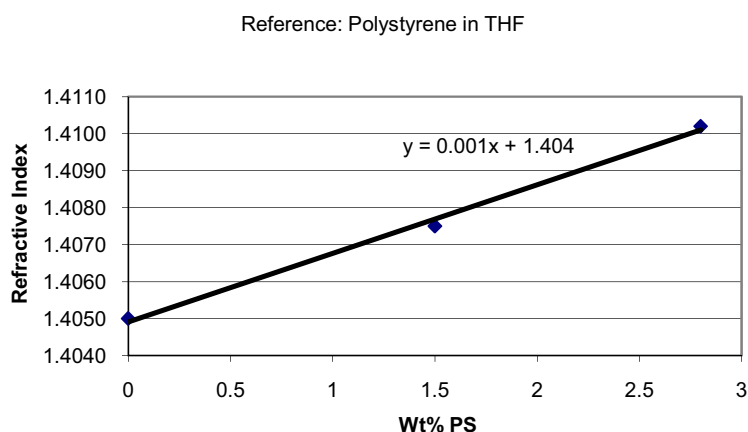
[8] Polymer Handbook 4th Edition, Volume 2, p.VI/581

The same method was applied to calculate the refractive index of the p(Sty-co-BA) polymers synthesized with different surfactant systems. The measured refractive indexes for different concentrations of the polymer dissolved in acetone (n_D=1.3561) are summarized in the table below.

Table 7: Refractive index values of p(Sty-co-BA) polymers stabilized with different surfactants

Wt.% Acetone	Wt.% Sty-BA-1%SDBS	Measured n_D	Calculated n_D	Literature n_D[9]
100	0	1.3561		1.3586 @ 20 ℃
96.6	3.4	1.362		
93.4	6.6	1.367		
0	100		1.5262	

Wt.% Acetone	Wt.% Sty-BA-1%DA3B	Measured n_D	Calculated n_D	Literature n_D
100	0	1.3561		1.3586 @ 20 ℃
98.5	1.5	1.3581		
97.4	2.6	1.3602		
96	4	1.3625		
0	100		1.5159	

Wt.% Acetone	Wt.% Sty-BA-6%Igepal	Measured n_D	Calculated n_D	Literature n_D
100	0	1.3561		1.3586 @ 20 ℃
97.6	2.4	1.3602		
96.5	3.5	1.3618		
95.4	4.6	1.3628		
0	100		1.5063	

---

[9] http://macro.lsu.edu/howto/solvents/Refractive%20Index.htm

APPENDIX G

Surface Energy Analysis of *p*(Sty-*co*-BA) polymer films containing surfactants

Table 8: Surface roughness measurements

Surfactant	Film Thickness [μ]	Area Roughness [nm]	Average Roughness [nm]	Std Deviation
1% SDBS	430	165.98 162.41	164.20	2.52
1% SDBS	173	337.30 146.70 140.49 144.00	192.12	96.82
1% DA3B	365	252.88 190.18 281.66 225.15	237.47	39.07
1% DA3B	160	37.31 227.91 58.40 337.33	165.24	142.97
6% OPE	378	47.33 7.33 17.40 31.09	25.79	17.35
6% OPE	148	10.13 14.46 16.56	13.72	3.28

Table 9: Contact angle hysteresis results

Surfactant	Film thickness [μm]	Advancing angle [°]	Receding angle [°]	Hysteresis	Film thickness [μm]	Advancing angle [°]	Receding angle [°]	Hysteresis
SDBS	173	71.6	43.9	27.8	430	59.6	39.0	20.6
	173	78.1	61.2	16.8	430	68.5	25.5	43.0
	173	69.5	56.2	13.4	430	71.1	34.8	36.3
	173	88.1	44.9	43.2	430	80.3	44.3	36.1
	173	78.5	38.1	40.5	430	44.5	34.2	10.3
DA3B	160	50.8	39.6	11.1	365	99.3	50.3	49.1
	160	42.7	34.9	7.7	365	83.8	57.3	26.5
	160	43.1	45.7	2.3	365	80.6	46.8	33.8
	160	46.5	32.2	14.4	365	78.6	56.0	22.6
OPE	148	65.3	87.5	22.22	378	99.3	50.3	49.1
	148	58.4	33.8	24.6	378	75.3	36.7	38.7
	148	84.8	51.4	33.4	378	75.4	57.2	18.2
	148	78.3	63.7	14.6	378	68.7	39.0	29.3
	148	80.2	55.3	25.0	378	82.9	57.6	25.3
	148	78.8	53.6	25.3	-	-	-	-

APPENDIX H

XRD Integration

A trapezium is defined as a 4-sided geometric shape with one pair of parallel sides. The area of a trapezoid is calculated as follows:
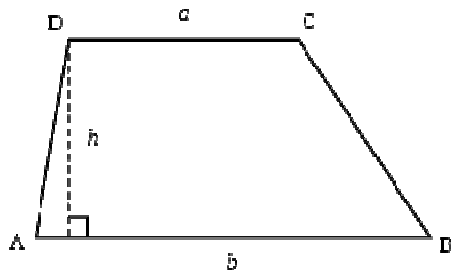
In mathematics the trapezium rule (also called the trapezoidal rule) is an approximation technique for calculating the definite integral   . This rule works by approximating the region under the graph of the function   as a trapezium and calculating its area. The smaller the intervals on the x-axis, the more accurate the integration of the peak in question.
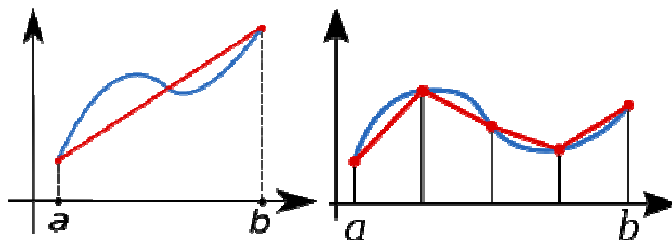
Peak areas of the crystalline peak at 2θ=22 ° were calculated by subdividing the area into small trapeziums and using the standard equation for the surface area of a trapezium to calculate to area. The parameters for the area equation (see above) were therefore selected as follows:

h: 0.016711 (step size setting during XRD analysis)
a,b: Intensity of each consecutive step size

The amorphous peak (refer to figure below – 0% ODA line, peak between 2θ=5 and 25) overlaps with the crystalline peak (refer to figure below – 100% ODA line, peak between 2θ=15 and 30).As deconvolution software was not available to isolate the crystalline peak effectively, it was decided to rather select a narrow scattering angle range, thereby minimizing the impact of the amorphous peak on the surface area of the crystalline peak. The scattering angle range for the determination of the peak area was therefore selected from 2θ=20-25.
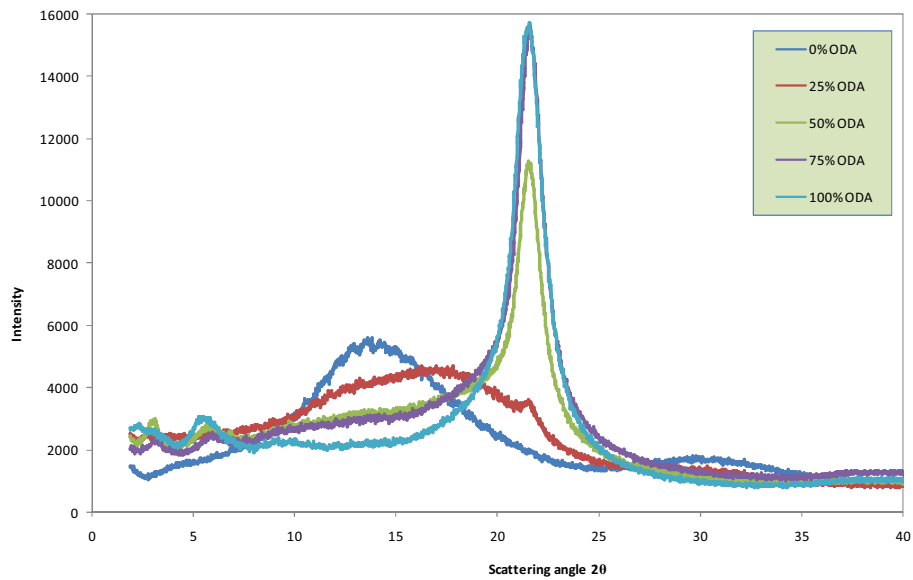
Baseline corrections were done by utilizing the same methodology, i.e. the trapezoidal rule. The initial area approximation calculated the area from the x-axis, i.e. the white area as well as the grey area (See Figure below). The baseline correction was done by calculating the area for the white region and deducting it from the original area (white + grey regions).
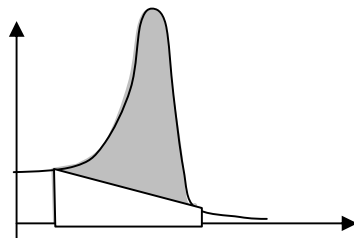
Source: Wikipedia (Keywords: trapezium, trapezoidal rule)

APPENDIX I

Real-time processing using the IGA for isotherm determinations

The processor requires certain input parameters to control *time origin* when data collection must start, the time that will determine that equilibrium has been reached, the number of data points to be collected, etc. To this end, the following parameters must be set before the isotherm can be determined:

Real-Time Parameters	Definition	Set point for analyses
Mode	The model used for least squares analysis.	F1
Phase	The point at which data collection must start (the time origin).	0.5
Min Time	Minimum data collection time.	2hr
Timeout	Maximum data collection time.	50hr
Wait Until		98.5%
RTP Min.	Minimum increase in weight	5µg
RTP Tolerance	Allowed deviation of actual data from trajectory of model used	2µg
Acquisition Min.	Data logging interval.	1µg

a) The Time Origin

The diagram below simulates the change in pressure to go from one pressure set point (P0) to the next (P1) as a function of time (green line). Data collection for the new isotherm point can start anywhere between these two pressure settings and are determined by the phase setting (ranging between 0.5 and 0.99). It is determined by the following equation:

$$P = P_0 + Phase(P_1 - P_0)$$

A phase setting of 0.5 allows for collection of the most data points and is normally used when there may be some interaction between the sample and the penetrant. A setting closer to 1 is sued for samples where no interaction is expected. The two blue lines indicate the region in which data collection can start.
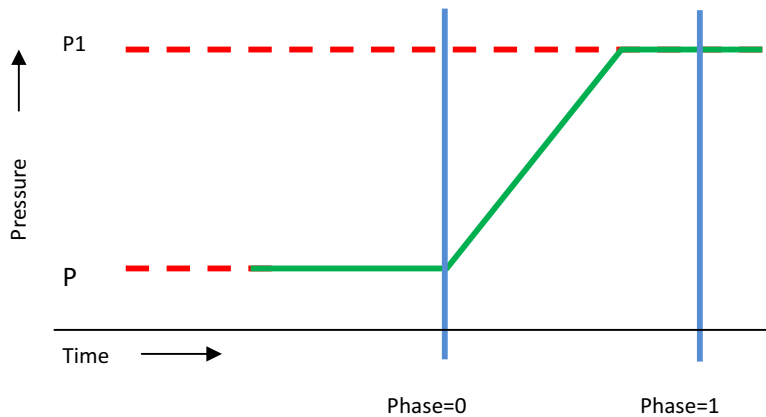
b) Timing Parameters

The *data logging interval* (Acquisition Min) is defined as the value in micrograms (µg) and this is set as the data-logging interval. Data will therefore only be logged when the weight change exceeds the acquisition min. All analyses were done at a setting of 1 µg.

The *minimum data collection time* (Min Time) is the minimum for the total data collection time during mass relaxation. This parameter was set at 15 minutes for all analyses.

The maximum data collection time (Timeout) represents the maximum amount of data for data collection during mass relaxation. It may happen that the timeout value is too short and that equilibrium is not reached. The timeout value was set to 480 minutes for all analyses.

c) RTP Tolerance and Minimum

These two parameters determine whether the current trend analysis is acceptable.

RTP Tolerance sets the acceptance threshold both in terms of the deviation of the last logged reading from the fit trajectory together with the average deviation of the fit trajectory from the data between the time original and the current time. Typical values would be a few micrograms with a recommended minimum of 1 µg. A value of 2 µ was used for all analyses.

The *RTP Min* sets a threshold on the minimum change in uptake before real-time analysis can be attempted. A typical value of 10 µg is recommended. As the polymer systems for this evaluation was fairly hydrophobic, this level was reduced to 5 µg.

d) Real-Time Analysis Models

Two mathematical models are used in the IGA software for the least squares analysis of the kinetic curves.

Model 1: The Linear Driving Force (LDF) Model
The LDF model of the relaxation $u(t)$ is,

$$F1: u(t) = u_0 + \Delta u\big(1 - exp(-[t - t_0']^x/k)\big)$$

where u_0 is the uptake at the arbitrary time origin t_0,, k is the exponential time constant and Δu is the change in uptake. The asymptotic uptake is then equal to $u_0 + \Delta u$.

This model has the following advantages:
  • This behaviour is identical with the response of the microbalance control system.
  • It is the simplest of all possible models in that there are a minimum of process dependent variables. In practice we refine both u_0 and Δu separately and so there are three model parameters. The co-variance between u_0 and Δu is generally not high and can still be accounted in the error analysis for the asymptote.
  • It is applicable to a range of processes; both those completely described by the LDF model, and those governed by the LDF model in the final approach to equilibrium providing t_0' is advanced to suit. This is true for diffusive processes, which become single exponential-like in the long time limit.

The LDF model conforms to all our ground rules: Initial estimates of model parameters are straight forward since the time constant can be expressed in terms of the normalised change in gradient $\delta u/\delta t$. The stability of this calculation in comparing the current rate with earlier values provides a criteria to set t_0' and this is further advanced if the fit is unsuccessful (e.g., if the refinement matrix is not well-conditioned).

Model 2: The Avrami's Model
Avrami's model of the relaxation $u(t)$ is,

$$F2: u(t) = u_0 + \Delta u\big(1 - exp(-[t - t_0']^x/k)\big)$$

where u_0 is the uptake at the arbitrary time origin t_0, k is the time constant, x is a variable power (see below) and Δu is the change in uptake. The asymptotic uptake is then equal to $u_0 + \Delta u$. This semi-empirical model was originally developed to describe the kinetics of metal recrystallisation where x is greater than 1 and the kinetics exhibit the sigmoidal shape indicated below. This type of curve is typical of phase transitions (processes of nucleation and growth) and therefore Avrami's model adapts well (x>1) to the observed sorption-time curves of, for example, hydride and hydrate transitions. There is another family of curves produced by this model which are equally relevant to sorption-time analysis when x<1 (see below). By observation, these solutions are an excellent approximation to many (non-LDF) sorption curves. For example the kinetics of water sorption during pore-filling of meso-porous glass are in near perfect agreement with Avrami's model when x ~ 0.7. This is probably coincidental in that the stretching power produces a shape similar to the sum of exponentials in solutions to the diffusion equation. We cannot offer a mathematical proof but this is certainly the case by many observations.

This model then has the following advantages:
  • The behaviour is identical with the response of the microbalance control system when x=1.
  • Four adjustable parameters (u_0 , Δu, k and x) yield many types of observed sorption-time curves.

219

e) Real-Time Analysis Modes

The model for the least squares analysis is selected in the Real-Time parameters setup. The following modes are available:

OFF	Real-time analysis is not used; The *Min Time* parameter defines the data collection time.
F1	The LDF model is used for real-time analysis.
AF1	The LDF model is used for real-time analysis. It will however move automatically to the next isotherm point if the change in uptake between the initial uptake and the current reading is less than the *RTP Min* setting at the elapsed time defined by *Min Time*.
F2	Avrami's model is used for real-time analysis.
AF2	Avrami's model is used for real-time analysis. It will however move automatically to the next isotherm point if the change in uptake between the initial uptake and the current reading is less than the *RTP Min* setting at the elapsed time defined by *Min Time*.
MAN	Real-time analysis is not used. Data is collected indefinitely until the override option is manually selected.

f) Temperature and Pressure Parameters

The following temperature parameters were used:

Temperature Parameters	*Pressure Parameters*
Temperature stability 0.1° C/min Temperature rate 1° C/min Scans 2	Regulation ON Pressure Ramp Time 10 mbar/min

APPENDIX J

Reproducibility evaluation of IGA results using poly-Sty-co-BA polymer

Although the purpose of this study was not to optimize the reproducibility of the gravimetric sorption analysis method using the Intelligent Gravimetric Analyzer, it was deemed necessary to understand the potential variance in the results as a result of variability in the control of experimental parameters, or variability due to variability in the sample composition. The reproducibility of the sorption behaviour of the films were therefore evaluated by (1) evaluating the sorption behavior of a single film prepared from the 1% SDBS stabilized Sty-BA latex when analyzed three consecutive times under the same conditions, and (2) analyzing the sorption behaviour of 3 different films prepared from the 1% SDBS stabilized Sty-BA latex. These analyses indicated that there was insignificant variance between the different films. As a result, a single film was analyzed for the sorption evaluations in this investigation.

The reproducibility of the gravimetric water vapour sorption experiments was evaluated using the Intelligent Gravimetric Analyzer Model IGA002 from Hiden Isochema. The sorption and desorption of water vapour was evaluation at a low and a high P/P_0 value using two approaches:

- **Reproducibility of the test method:** The same p(Sty-co-BA) polymer film containing 1% SDBS was analyzed three consecutive times to evaluate the reproducibility of the analysis methodology for a specific film in terms of the diffusion, solubility and permeation coefficients.

- **Reproducibility of film properties:** Three different films of p(Sty-co-BA) polymer containing 1% SDBS were evaluated to determine the impact of film variation on the diffusion, solubility and permeation coefficients.

a) Reproducibility of the test method

Partial pressure (P/P₀)		Ads/Des[10]	D [cm²/s x 10⁻⁸]		S [cm³(STP)/cm³ cm Hg x 10⁻²]		P [cm³(STP)cm/cm² s cm Hg x 10⁻⁹]	
Start	Finish		Average	Std Dev	Average	Std Dev	Average	Std Dev
0.3	0.4	Ads	17.53	0.25	47.9	0.06	8.40	0.02
0.7	0.8	Ads	1.56	0.03	29.75	0.30	4.65	0.04
0.8	0.7	Des	1.67	0.19	33.41	2.27	5.59	1.03
0.4	0.3	Des	14.00	1.31	8.14	0.47	11.36	0.41

The adsorption coefficients for diffusion, solubility and permeation show better reproducibility than the desorption coefficients.

b) Reproducibility of the film properties

---

[10] Ads/Des: Acronym for Adsorption/Desorption

Partial pressure (P/P$_0$)		Ads/Des	D [cm^2/s x 10^{-8}]		S [cm^3(STP)/cm^3 cm Hg x 10^{-2}]		P [cm^3(STP)cm/cm^2 s cm Hg x 10^{-9}]	
Start	Finish		Average	Std Dev	Average	Std Dev	Average	Std Dev
0.3	0.4	Ads	11.93	2.82	4.72	0.41	5.56	0.80
0.7	0.8	Ads	2.83	1.76	10.27	1.41	2.74	1.26
0.8	0.7	Des	3.50	1.25	11.63	2.08	3.99	1.24
0.4	0.3	Des	10.44	0.99	5.46	1.64	5.74	1.95

Similarly to the reproducibility evaluation of the test method, the reproducibility evaluation of the film properties indicate that better reproducibility was achieved for the adsorption of water vapour than for the desorption.

Based on the results summarized in the above two tables, it can be concluded that both the test method and the sample preparation method and therefore sample homogeneity give reproducible results. Sorption results obtained from a single evaluation should therefore result in accurate results and it is deemed unnecessary to do these evaluations in triplicate.

APPENDIX K

Water vapour sorption results

1. *p*(Sty-*co*-BA) polymers: SDBS, OPE and DA3B surfactants (Chapter 5)

Table 10: Equilibrium adsorption isotherm at 25 °C for *p*(Sty-*co*-BA) polymer stabilized with different surfactants

P/P$_0$	Pressure [mbar]	Equilibrium sample mass increase [%]						
		1% SDBS (173 µm)	1% SDBS (420 µm)	1% DA3B (160 µm)	1% DA3B (365 µm)	2% DA3B (290 µm)	6% OPE (378 µm)	No surfactant (200 µm)
0.0	0	0.000065	0.001117	0.002110	0.000006	0.011678	0.000007	
0.1	3.18	0.039475	0.034146	0.000060	0.040061	0.035314	0.056786	0.000014
0.2	6.36	0.077111	0.079807	0.020925	0.067836	0.053341	0.106270	0.033926
0.3	9.54	0.117541	0.137105	0.081046	0.093295	0.077169	0.165332	0.038445
0.4	12.72	0.169987	0.207900	0.129766	0.119417	0.102238	0.238066	0.085830
0.5	15.90	0.233446	0.318392	0.174060	0.147600	0.129901	0.342292	0.121568
0.6	19.08	0.314680	0.512240	0.239183	0.178128	0.160896	0.523795	0.147023
0.7	22.26	0.439791	0.893002	0.307849	0.213341	0.196379	0.907527	0.176438
0.8	25.44	0.652157	1.846401	0.412419	0.256986	0.243026	1.825457	0.213842
0.9	28.62	0.298060	3.696654	0.637652	0.320403	0.312892	3.704895	0.260976

Table 11: Equilibrium desorption isotherm at 25 °C for *p*(Sty-*co*-BA) polymer stabilized with different surfactants

P/P$_0$	Pressure [mbar]	Equilibrium sample mass decrease [%]						
		1% SDBS (173 µm)	1% SDBS (420 µm)	1% DA3B (160 µm)	1% DA3B (365 µm)	2% DA3B (290 µm)	6% OPE (378 µm)	No surfactant (200 µm)
0.9	28.62	1.298060	3.696654	0.637652	0.320403	0.312892	3.704895	0.260976
0.8	25.44	0.811379	1.948132	0.433072	0.260474	0.246557	1.891339	0.212350
0.7	22.26	0.573273	0.948903	0.324097	0.218725	0.200566	0.952933	0.170568
0.6	19.08	0.377560	0.552915	0.249853	0.183229	0.162975	0.569084	0.136132
0.5	15.90	0.250126	0.359157	0.191459	0.150782	0.129654	0.381616	0.104533
0.4	12.72	0.177050	0.242967	0.154137	0.119972	0.098742	0.264371	0.083586
0.3	9.54	0.120025	0.156796	0.122063	0.093341	0.070925	0.178786	0.056628
0.2	6.36	0.079281	0.091738	0.080470	0.067897	0.045187	0.113383	0.038198
0.1	3.18	0.038236	0.040492	0.053265	0.039755	0.012514	0.059316	0.021302
0	0	0.000002	0.000000	0.000300	0.000006	0.000001	0.010216	0.023515

Table 12: Adsorption diffusion coefficients for *p*(Sty-*co*-BA) polymer films stabilized with different surfactants

Surfactant	Thickness	Temp.	Diffusion coefficients at different partial pressures x 10^8 [cm^2/s]								
	[µm]	[°C]	0.1	0.2	0.3	0.4	0.5	0.6	0.7	0.8	0.9
1% SDBS	173	25	NA	9.81	3.62	15.0	14.7	9.32	6.39	4.74	1.74
1% SDBS	420	25	21.2	28.3	24.1	199	14.0	7.50	3.69	1.56	0.912
1% DA3B	160	25	NA	NA	NA	NA	8.17	10.8	10.9	7.47	3.36
1% DA3B	365	25	41.2	46.2	45.4	43.5	42.1	41.0	39.8	35.4	28.5
2% DA3B	290	25	34.7	40.0	37.1	37.0	36.5	31.8	30.1	24.9	17.5
6% OPE	378	25	19.2	20.0	17.5	14.3	9.52	5.49	2.51	1.14	0.628

Table 13: Desorption diffusion coefficients for *p*(Sty-*co*-BA) polymer films stabilized with different surfactants

Surfactant	Thickness	Temp.	Diffusion coefficients at different partial pressures x 10^8 [cm^2/s]								
	[µm]	[°C]	0.8	0.7	0.6	0.5	0.4	0.3	0.2	0.1
1% SDBS	173	25	3.72	4.99	4.89	7.44	0.112	0.116	0.132	NA
1% SDBS	420	25	1.08	2.09	4.48	8.76	14.2	19.8	23.7	28.2
1% DA3B	160	25	5.45	7.21	9.35	13.7	NA	NA	NA	NA
1% DA3B	365	25	31.8	38.7	39.1	39.9	42.4	43.7	45.5	42.7
2% DA3B	290	25	20.6	25.3	30.5	29.8	30.9	32.8	32.6	33.6
6% OPE	378	25	0.754	1.39	3.18	6.18	9.77	13.1	16.6	19.8

Table 14: Adsorption solubility coefficients for *p*(Sty-*co*-BA) polymer films stabilized with different surfactants

Surfactant	Thickness	Temp.	Solubility coefficients at different partial pressures [cm^3(STP)/cm^3]								
	[µm]	[°C]	0.1	0.2	0.3	0.4	0.5	0.6	0.7	0.8	0.9
1% SDBS	173	25	12.87	6.13	4.39	4.27	4.12	1.38	1.82	2.70	23.38
1% SDBS	420	25	8.57	5.92	4.93	4.69	5.41	6.23	10.49	22.98	54.28
1% DA3B	160	25	0.17	0.77	0.83	0.68	0.65	0.61	0.72	0.96	1.83
1% DA3B	365	25	5.38	3.12	2.22	1.72	1.48	1.33	1.32	1.44	1.85
2% DA3B	290	25	7.20	3.45	2.42	1.92	1.69	1.58	1.55	1.78	2.38
6% OPE	378	25	13.94	7.55	6.01	5.56	6.37	9.25	16.77	35.11	58.79

Table 15: Desorption solubility coefficients for *p*(Sty-*co*-BA) polymer films stabilized with different surfactants

Surfactant	Thickness	Temp.	Solubility coefficients at different partial pressures [cm³(STP)/cm³]							
	[μm]	[°C]	0.8	0.7	0.6	0.5	0.4	0.3	0.2	0.1
1% SDBS	173	25	19.82	11.09	10.62	8.30	5.96	6.20	6.64	10.86
1% SDBS	420	25	57.75	32.42	16.75	9.83	7.36	7.28	8.24	12.96
1% DA3B	160	25	1.87	1.14	0.90	0.75	0.87	0.91	1.28	1.99
1% DA3B	365	25	1.97	1.57	1.56	1.71	2.03	2.34	3.34	6.34
2% DA3B	290	25	2.54	2.01	1.92	2.04	2.35	2.84	3.93	7.20
6% OPE	378	25	69.37	41.02	19.57	11.47	8.96	8.71	9.99	16.52

Table 16: Adsorption permeability of *p*(Sty-*co*-BA) polymer films stabilized with different surfactants

Surfactant	Thickness	Temp.	Permeability at different partial pressures x 10⁷ [cm³(STP)cm/cm²s, mbar]								
	[μm]	[°C]	0.1	0.2	0.3	0.4	0.5	0.6	0.7	0.8	0.9
1% SDBS	173	25	NA	6.02	1.59	6.42	6.07	1.29	1.16	1.28	4.07
1% SDBS	420	25	18.2	16.7	11.9	9.35	7.58	4.67	3.87	3.59	4.95
1% DA3B	160	25	NA	NA	NA	NA	0.528	0.658	0.777	0.715	0.614
1% DA3B	365	25	22.2	14.4	10.1	7.46	6.22	5.47	5.26	5.08	5.28
2% DA3B	290	25	25.0	13.8	8.98	7.11	6.18	5.03	4.66	4.45	4.16
6% OPE	378	25	26.8	15.1	10.5	7.94	6.06	5.08	4.20	3.99	3.69

Table 17: Desorption permeability of *p*(Sty-*co*-BA) polymer films stabilized with different surfactants

Surfactant	Thickness	Temp.	Permeability at different partial pressures x 10⁷ [cm³(STP)cm/cm²s, mbar]							
	[μm]	[°C]	0.8	0.7	0.6	0.5	0.4	0.3	0.2	0.1
1% SDBS	173	25	7.37	5.54	5.19	6.18	6.68	7.18	8.78	NA
1% SDBS	420	25	6.24	6.76	7.51	8.61	10.4	14.4	19.6	36.6
1% DA3B	160	25	1.02	0.819	0.846	1.04	0.917	NA	NA	NA
1% DA3B	365	25	6.27	6.07	6.08	6.81	8.58	10.2	15.2	27.1
2% DA3B	290	25	5.23	5.09	5.85	6.07	7.27	9.32	12.8	24.2
6% OPE	378	25	5.23	5.70	6.23	7.09	8.75	11.4	16.5	32.8

2.   p(Sty-co-BA) PCNs containing Na-MMT (Chapter 6)

Table 18: Equilibrium adsorption isotherm at 30 °C for *p*(Sty-*co*-BA) PCN containing 4.5% AMPS and different Na-MMT concentrations

P/P$_0$	Pressure [mbar]	Equilibrium sample mass [%]				
		0% Na-MMT	1% Na-MMT	3% Na-MMT	5% Na-MMT	10% Na-MMT
0.0	0.182	0	0	0	0.076302	0
0.1	4.231	0.179920	0.194932	0.24603	0.327037	0.108189
0.2	8.505	0.280674	0.433772	0.361893	0.453075	0.222094
0.3	12.718	0.395947	0.750385	0.495276	0.577379	0.304188
0.4	17.016	0.623473	1.189899	0.680825	0.751136	0.483172
0.5	21.222	0.912364	1.804062	0.986762	1.048527	0.641026
0.6	25.514	1.341341	2.740314	1.429268	1.490327	0.903020
0.7	29.733	2.100029	4.280111	2.157911	2.16877	1.309130
0.8	33.999	3.208354	6.835855	3.411289	3.326752	2.097831
0.9	38.284	5.687845	13.16479	6.080974	6.17457	3.763874

Table 19: Equilibrium desorption isotherm at 30 °C for *p*(Sty-*co*-BA) PCN containing 4.5% AMPS and different Na-MMT concentrations

P/P$_0$	Pressure [mbar]	Equilibrium sample mass [%]				
		0% Na-MMT	1% Na-MMT	3% Na-MMT	5% Na-MMT	10% Na-MMT
0.9	38.284	5.690000	13.16479	6.080974	6.174527	3.763874
0.8	33.999	3.220000	6.953181	3.423469	3.411240	2.273640
0.7	29.733	2.130000	4.389591	2.231506	2.208241	1.557092
0.6	25.514	1.460939	2.908551	1.512134	1.488561	1.097370
0.5	21.222	0.999772	1.918832	1.028940	1.020192	0.798731
0.4	17.016	0.674774	1.238432	0.701000	0.707981	0.610990
0.3	12.718	0.440652	0.734838	0.507384	0.523384	0.481257
0.2	8.505	0.290961	0.421785	0.385532	0.407537	0.386675
0.1	4.231	0.198292	0.223151	0.266714	0.300840	0.286921
0	0.182	0	0	0	0	0

Table 20: Equilibrium adsorption isotherms for *p*(Sty-*co*-BA) PCN containing 4.5% AMPS and 5% Na-MMT

P/P_0	10 °C Isotherm		20 °C Isotherm		30 °C Isotherm	
	Pressure [mbar]	Mass [%]	Pressure [mbar]	Mass [%]	Pressure [mbar]	Mass [%]
0.0	0.190	0.007271	0.187	0.049967	0.182	0.076302
0.1	1.241	0.266813	2.297	0.284196	4.231	0.327037
0.2	2.422	0.370137	4.635	0.407898	8.505	0.453075
0.3	3.648	0.470469	6.997	0.540375	12.718	0.577379
0.4	4.890	0.6199438	9.336	0.707561	17.016	0.751136
0.5	6.114	0.867701	11.702	0.974938	21.222	1.048527
0.6	7.342	1.250186	14.012	1.363837	25.514	1.490327
0.7	8.598	1.815983	16.369	1.986853	29.733	2.16877
0.8	9.802	2.716224	18.699	3.109487	33.999	3.326752
0.9	11.059	4.554707	21.048	5.32426	38.284	6.17457

Table 21: Equilibrium desorption isotherm for *p*(Sty-*co*-BA) PCN containing 4.5% AMPS and 5% Na-MMT

P/P_0	10 °C Isotherm		20 °C Isotherm		30 °C Isotherm	
	Pressure [mbar]	Mass [%]	Pressure [mbar]	Mass [%]	Pressure [mbar]	Mass [%]
0.9	11.059	4.554770	21.048	5.324260	38.284	6.174527
0.8	9.802	2.934771	18.699	3.228046	33.999	3.411240
0.7	8.598	1.989719	16.369	2.096979	29.733	2.208241
0.6	7.342	1.383671	14.012	1.450786	25.514	1.488561
0.5	6.114	0.971366	11.702	1.023944	21.222	1.020192
0.4	4.890	0.734972	9.336	0.748808	17.016	0.707981
0.3	3.648	0.613241	6.997	0.605954	12.718	0.523384
0.2	2.422	0.517475	4.635	0.501303	8.505	0.407537
0.1	1.241	0.395600	2.297	0.394034	4.231	0.300840
0.0	0.190	0.104479	0.187	0.077403	0.182	0.000013

Table 22: Adsorption diffusion coefficient for *p*(Sty-*co*-BA) PCNs containing 4.5% AMPS

% Na-MMT	Thickness	T_g	Temp.	Diffusion coefficients at different partial pressures x 10^8 [cm^2/s]								
	[μm]	[°C]	[°C]	0.1	0.2	0.3	0.4	0.5	0.6	0.7	0.8	0.9
0%	260	24.0	30	5.49	8.13	5.84	3.47	3.34	2.41	1.45	1.11	0.454
1%	170	22.6	30	2.31	2.05	1.97	2.15	2.70	3.51	4.82	7.52	1.48
3%	400	22.0	30	3.24	4.81	4.56	3.97	3.30	3.60	3.35	3.23	4.46
5%	350	23.2	10	0.455	0.764	0.725	0.423	0.427	0.555	0.848	1.57	2.11
5%	350	23.2	20	1.20	1.54	1.47	1.40	1.43	1.69	2.17	2.52	4.64
5%	350	23.2	30	2.61	4.07	4.32	3.29	2.82	3.31	3.91	4.53	5.07
10%	300	20.2	30	0.589	1.63	2.15	1.06	1.52	1.74	2.19	3.17	4.85

Table 23: Desorption diffusion coefficients for *p*(Sty-*co*-BA) PCNs containing 4.5% AMPS

% Na-MMT	Thickness	T_g	Temp.	Diffusion coefficients at different partial pressures x 10^8 [cm^2/s]								
	[μm]	[°C]	[°C]	0.8	0.7	0.6	0.5	0.4	0.3	0.2	0.1	0
0%	260	24.0	30	0.771	1.42	2.06	2.61	3.23	3.89	5.32	6.69	NA
1%	170	22.6	30	2.63	3.09	2.40	2.39	2.17	1.79	1.93	2.26	NA
3%	400	22.0	30	4.96	2.97	2.96	3.16	3.29	3.97	5.45	4.48	NA
5%	350	23.2	10	1.30	0.807	0.681	0.497	0.607	0.782	0.959	0.461	0.144
5%	350	23.2	20	2.77	2.32	1.39	1.02	1.24	1.64	1.95	1.40	0.133
5%	350	23.2	30	3.69	3.55	3.09	2.45	2.52	3.33	4.22	4.11	0.316
10%	300	20.2	30	5.27	3.42	1.79	1.57	1.51	1.65	1.87	1.43	NA

Table 24: Adsorption solubility coefficients for *p*(Sty-*co*-BA) PCNs containing 4.5% AMPS

% Na-MMT	Thickness	T_g	Temp.	Solubility coefficients at different partial pressures [cm^3(STP)/cm^3]								
	[μm]	[°C]	[°C]	0.1	0.2	0.3	0.4	0.5	0.6	0.7	0.8	0.9
0%	260	24.0	30	52.11	14.61	11.17	16.53	16.80	20.80	31.56	40.34	80.25
1%	170	22.6	30	62.72	38.53	34.15	35.48	39.70	50.46	71.16	105.38	227.55
3%	400	22.0	30	68.16	16.07	12.37	12.89	17.00	20.52	28.97	43.62	82.61
5%	350	23.2	10	288.99	56.48	37.01	41.24	55.05	70.69	89.71	124.89	226.54
5%	350	23.2	20	136.70	36.01	25.70	24.31	31.12	37.78	51.87	81.83	143.40
5%	350	23.2	30	80.19	20.18	13.30	13.92	19.08	23.64	31.14	46.52	102.04
10%	300	20.2	30	40.24	21.25	10.23	16.71	11.80	16.33	21.71	36.91	69.33

Table 25: Desorption solubility coefficients for *p*(Sty-*co*-BA) PCNs containing 4.5% AMPS

% Na-MMT	Thickness [μm]	T_g [°C]	Temp. [°C]	Solubility coefficients at different partial pressures [cm³(STP)/cm³]							
				0.8	0.7	0.6	0.5	0.4	0.3	0.2	0.1
0%	260	24.0	30	89.90	45.45	32.24	26.83	23.62	22.73	21.72	26.83
1%	170	22.6	30	251.19	118.47	79.82	63.98	54.94	54.11	50.85	63.94
3%	400	22.0	30	92.50	47.41	33.37	26.88	22.78	17.97	16.91	32.87
5%	350	23.2	10	224.75	149.85	112.02	91.44	64.75	44.89	53.02	134.9
5%	350	23.2	20	152.80	94.18	62.79	49.70	40.03	27.70	30.46	62.45
5%	350	23.2	30	111.01	55.22	38.53	30.07	25.04	19.77	18.55	34.09
10%	300	20.2	30	69.75	38.32	28.67	22.33	17.53	16.18	17.64	37.09

Table 26: Adsorption permeability coefficients for *p*(Sty-*co*-BA) PCNs containing 4.5% AMPS

% Na-MMT	Thickness [μm]	T_g [°C]	Temp. [°C]	Permeability coefficients at different partial pressures x 10⁷ [cm³(STP)cm/cm²s, mbar]								
				0.1	0.2	0.3	0.4	0.5	0.6	0.7	0.8	0.9
0%	260	24.0	30	28.6	11.9	6.53	5.73	5.61	5.01	4.59	4.50	3.64
1%	170	22.6	30	14.5	7.88	6.73	7.61	10.73	17.74	34.30	79.20	32.50
3%	400	22.0	30	22.1	7.73	5.64	5.11	5.62	7.38	9.71	14.1	36.9
5%	350	23.2	10	13.1	4.31	2.68	1.74	2.35	3.92	7.61	19.6	47.7
5%	350	23.2	20	16.3	5.54	3.77	3.40	4.45	6.39	11.3	20.7	66.6
5%	350	23.2	30	21.0	8.22	5.74	4.59	5.38	7.83	12.2	21.1	51.7
10%	300	20.2	30	2.37	3.46	2.20	1.77	1.79	2.83	4.76	11.69	33.62

Table 27: Desorption permeability coefficients for *p*(Sty-*co*-BA) PCNs containing 4.5% AMPS

% Na-MMT	Thickness [μm]	T_g [°C]	Temp. [°C]	Permeability coefficients at different partial pressures x 10⁷ [cm³(STP)cm/cm²s, mbar]								
				0.8	0.7	0.6	0.5	0.4	0.3	0.2	0.1	
0%	260	24.0	30	6.93	6.43	6.63	7.00	7.64	8.84	11.5	17.9	
1%	170	22.6	30	66.10	36.58	19.13	15.27	11.95	9.68	9.83	14.44	
3%	400	22.0	30	45.8	14.1	9.86	8.51	7.50	7.14	9.22	14.7	
5%	350	23.2	10	29.1	12.1	7.63	4.55	3.93	3.51	5.08	6.23	
5%	350	23.2	20	42.4	21.8	8.74	5.09	4.96	4.55	5.94	8.72	
5%	350	23.2	30	40.9	19.6	11.9	7.36	6.30	6.58	7.83	14.0	
10%	300	20.2	30	36.8	13.1	5.14	3.51	2.65	2.67	3.30	5.32	

Table 28: Equilibrium adsorption isotherm at 30 °C for *p*(St-*co*-BA) PCNs containing 5% Na-MMT

P/P$_0$	Pressure [mbar]	Equilibrium sample mass [%]			
		1.5% AMPS	3% AMPS	4.5% AMPS	6% AMPS
0.0	0.182	0.000000	0.000002	0.076302	0.000001
0.1	4.231	0.121947	0.190598	0.327037	0.241928
0.2	8.505	0.227921	0.272167	0.453075	0.350440
0.3	12.718	0.332812	0.370666	0.577379	0.507218
0.4	17.016	0.457585	0.523694	0.751136	0.769198
0.5	21.222	0.619026	0.728786	1.048527	1.130607
0.6	25.514	0.841164	1.026031	1.490327	1.664362
0.7	29.733	1.172345	1.511859	2.168770	2.534403
0.8	33.999	1.894270	2.380321	3.326752	4.041003
0.9	38.284	3.832087	4.564027	6.174527	7.174478

Table 29: Adsorption diffusion coefficient for *p*(Sty-*co*-BA) PCNs containing 5% Na-MMT

% AMPS	Thickness [μm]	T$_g$ [°C]	Temp. [°C]	Diffusion coefficients at different partial pressures x 10^8 [cm^2/s]								
				0.1	0.2	0.3	0.4	0.5	0.6	0.7	0.8	0.9
1.5%	260	30	30	3.08	2.45	3.56	1.80	3.10	3.99	5.27	7.61	3.82
3.0%	360	24	30	4.43	5.58	4.80	3.31	3.99	4.84	6.05	7.19	9.34
4.5%	350	27	30	2.61	4.07	4.32	3.29	2.82	3.31	3.91	4.53	5.07
6.0%	350	25	30	2.76	4.14	2.20	1.90	2.41	2.69	2.18	2.60	3.41

Table 30: Adsorption solubility coefficients for *p*(Sty-*co*-BA) PCNs containing 5% Na-MMT

% AMPS	Thickness [μm]	T$_g$ [°C]	Temp. [°C]	Solubility coefficients at different partial pressures [cm^3(STP)/cm^3]								
				0.1	0.2	0.3	0.4	0.5	0.6	0.7	0.8	0.9
1.5%	260	30	30	53.50	14.99	9.69	13.26	12.37	14.58	19.04	29.62	74.36
3.0%	360	24	30	64.88	13.89	11.21	13.05	14.01	16.93	23.74	37.14	87.60
4.5%	350	27	30	80.19	20.18	13.20	13.92	19.08	23.64	31.14	46.52	102.04
6.0%	350	25	30	70.43	15.80	15.28	19.12	21.12	26.01	36.35	55.09	101.88

Table 31: Adsorption permeability coefficients for *p*(Sty-*co*-BA) PCNs containing 5% Na-MMT

% AMPS	Thickness [μm]	T$_g$ [°C]	Temp. [°C]	Permeability coefficients at different partial pressures x 10^7 [cm^3(STP)cm/cm^{2}s, mbar]								
				0.1	0.2	0.3	0.4	0.5	0.6	0.7	0.8	0.9
1.5%	260	30	30	16.50	3.68	3.45	2.39	3.83	5.82	10.00	22.50	28.40
3.0%	360	24	30	28.75	7.75	5.38	4.31	5.58	8.20	14.40	26.70	81.90
4.5%	350	27	30	21.0	8.22	5.74	4.59	5.38	7.83	12.2	21.1	51.7
6.0%	350	25	30	19.4	6.54	3.36	3.63	5.09	7.00	7.91	14.3	34.8

3.   *p*(ODA-*co*-MMA) polymers: 50% and 100% ODA (Chapter 7)

Table 32: Equilibrium adsorption at P/P$_0$=0.9 and different temperatures (10 °C, 20 °C, 30 °C and 40 °C)

P/P$_0$	Pressure	Temp	Equilibrium sample mass [%]	
	[mbar]	[°C]	50% ODA	100% ODA
0.9	11.090	10	0.195477	0.134949
0.9	21.107	20	0.245255	0.145228
0.9	38.270	30	0.285216	0.162662
0.9	160.733	40	0.330237	0.192051

Table 33: Adsorption diffusion, solubility and permeability coefficients at 10°C, 20°C, 30°C and 40°C

P/P$_0$	Pressure	Temp	50% ODA			100% ODA		
	[mbar]	[°C]	$Dx10^8$	$Sx10^3$	$Px10^{10}$	$Dx10^8$	$Sx10^3$	$Px10^{10}$
0.9	11.090	10	0.798	21.0	1.68	1.06	12.8	1.36
0.9	21.107	20	1.94	13.9	2.68	2.17	7.23	1.57
0.9	38.270	30	4.92	8.89	4.37	4.65	4.47	2.08
0.9	160.733	40	NA	5.48	NA	NA	3.03	NA

APPENDIX L

Kinetics of miniemulsion polymerisations

Surfactant impact on polymerisation kinetics

It was found that increased levels of surfactant resulted in a reduction in particle size of the monomer droplets and therefore the size of the resultant polymer particle (see Table 34). This resulted in an increased overall monomer droplet surface area that increased the probability of nucleation within each droplet. Higher rates of conversion were achieved with smaller droplet sizes (refer to Figure 5). Although a variation in the sonication energy may also contribute to a variation in monomer droplet size for a particular surfactant, it was shown in this study that surfactant concentration variation was the main contributing factor.

Table 34: Polymer particle size as a function of surfactant type and concentration, determined by DLS.

Surfactant Conc. (%)	Average particle size (nm) and polydispersity index (PDI)					
	SDBS		OPE		DA3B	
	Particle size	PDI	Particle size	PDI	Particle size	PDI
0.5%	171.7	0.039	-	-	-	-
1.0%	80.1	0.052	-	-	211.0	0.024
2.0%	58.8	0.032	618.5	0.332	171.0	0.128
4.0%	-	-	370.5	0.152	-	-
6.0%	-	-	238.0	0.084	-	-

The type of surfactant also played a significant role in the polymerisation kinetics (see Figure 5). A marked difference in the monomer incorporation rate was observed when comparing the two conventional surfactant systems, i.e. SDBS and OPE, confirming the findings of Landfester et al., who investigated the impact of different types of surfactant stabilization systems on the kinetics of miniemulsion systems.[2] The conversion rate of miniemulsion systems stabilized with nonionic surfactant systems is significantly lower than that stabilized with anionic surfactant systems. This can be attributed to the relatively large droplet size of monomers stabilized through a steric hindrance mechanism with nonionic surfactants in miniemulsion systems resulting in a relatively low surface area for nucleation, compared to the smaller monomer droplet size miniemulsions stabilized through an

electrostatic stabilization mechanism with a higher surface area for nucleation (See Table 34). The low conversion rate of the OPE stabilized emulsion can therefore be attributed to lower nucleation rates as a result of relatively large monomer droplet sizes.

The reactive surfactant (DA3B) showed similar conversion rates to the anionic surfactant (SDBS), with almost 97.5% conversion after300 minutes for 1% DA3B. This was interesting when taking into consideration that a significant particle size increase was observed for the DA3B stabilized latex after polymerisation was completed (see Table 35). The reason for this is unknown, although it is suspected that agglomeration of particles could have taken place, resulting in the perception of larger particle sizes. Particle size analysis using TEM could shed more light on this phenomenon. These results are however not available.

Table 35: Sonication and polymerization details of final polymer latexes

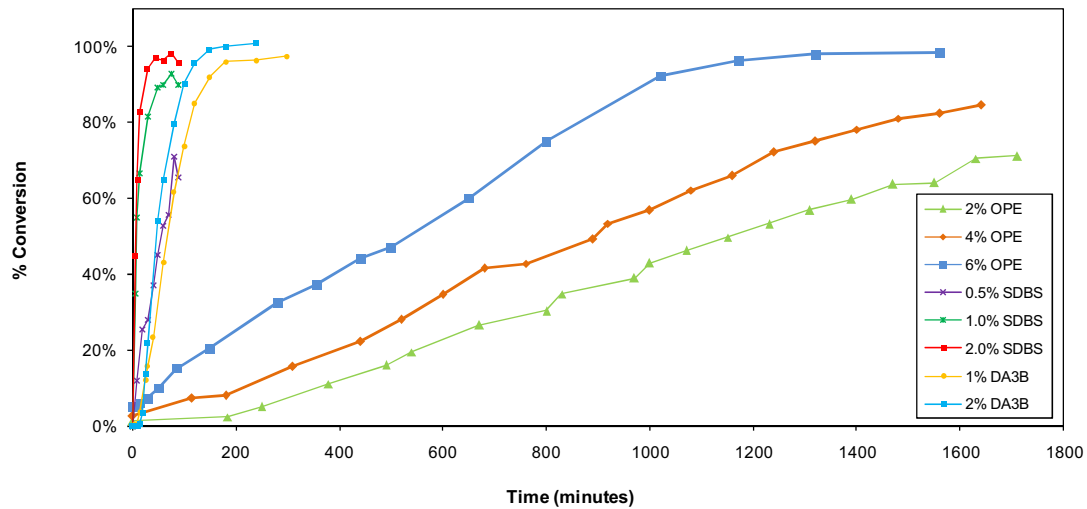| Properties	*p*-Sty-*co*-BA polymers		
	SDBS	DA3B	OPE
Surfactant conc.	1%	1%	6%
Sonication energy	35 848 J	54 403 J	43 241 J
Conversion	98% after 250 min	98.5% after 2500 min	97.5% after 300 min
Particle size			
• Monomer droplet	173 nm ± 0.054 nm	166 nm ± 0.116 nm	294 nm ± 0.233 nm
• Polymer particle	138 nm ± 0.016 nm	437 nm±0.676 nm	232 nm ± 0.057 nm

Figure 5: Conversion curves of SDBS, DA3B and OPE stabilized miniemulsions

Kinetics of Polymer Clay Nanocomposites

The slight leveling off of the percentage monomer incorporation for the PCN series containing 4.5% AMPS and increasing amounts of Na-MMT indicate phase III kinetics of the miniemulsion polymerization process where the initial amount of monomer added into the reactor charge have largely been incorporated into the polymer backbone. The addition of the remainder of the monomer mix 1 hour after the initiation of the polymerization therefore took place only after this phase. The amount of Na-MMT in the miniemulsion did not impact on the rate of monomer incorporation as similar kinetic trends were observed for the Na-MMT concentration range investigated.

234
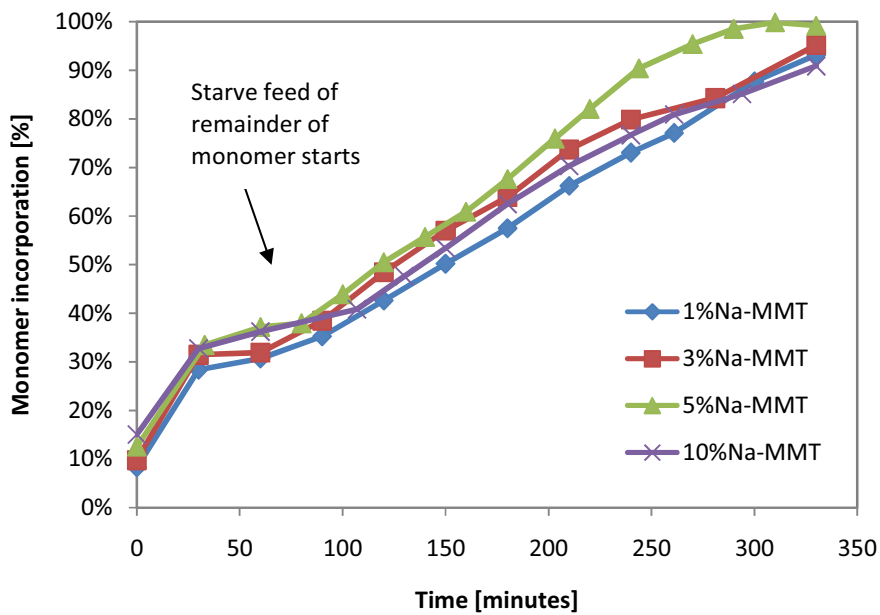
Figure 6: Monomer incorporation for PCN synthesis using 4.5% AMPS and increasing amounts of Na-MMT clay

Monomer incorporation of 90-99% was obtained in 5 hours 30 minutes for the PCN series containing 4.5% AMPS and increasing amounts of Na-MMT. No significant difference was noted in terms of the kinetics of the monomer incorporation for different concentrations of Na-MMT.

References

1.   Du, C., Zhou, G., Wang, H., Chen, X., and Zhou, J., *Depth profiling of clay - xanthan complexes using step-scan mid-infrared photoacoustic spectroscopy.* Journal of Soil Sediments, 2010. **10**: p. 855-862.

2.   Landfester, K., Bechthold, N., Tiarks, F., and Antonietti, M., *Miniemulsion Polymerization with Cationic and Nonionic Surfactants: A Very Efficient Use of Surfactants for Heterophase Polymerization.* Macromolecules, 1999. **32**: p. 2679-2683.